15. SITE 683[1]

Shipboard Scientific Party[2]

HOLE 683A

Date occupied: 0715 L, 15 November 1986

Date departed: 1715 L, 18 November 1986

Time on hole: 82 hr

Position: 9°01.69′S, 80°24.40′W

Water depth (sea level; corrected m, echo-sounding): 3071.8

Water depth (rig floor; corrected m, echo-sounding): 3082.3

Bottom felt (m, drill pipe): 3086.6

Penetration (m): 419.2

Number of cores: 45

Total length of cored section (m): 419.2

Total core recovered (m): 219.17

Core recovery (%): 52.3

Oldest sediment cored
Depth (mbsf): 419.2
Nature: diatomaceous mudstone
Age: middle Miocene
Measured velocity (km/s): 1.65

HOLE 683B

Date occupied: 1715 L, 18 November 1986

Date departed: 1800 L, 20 November 1986

Time on hole: 72 hr 45 min

Position: 9°01.59′S, 80°24.26′W

Water depth (sea level; corrected m, echo-sounding): 3071.5

Water depth (rig floor; corrected m, echo-sounding): 3082.0

Bottom felt (m, drill pipe): 3076.6

Penetration (m): 488

Number of cores: 9

Total length of cored section (m): 85.5

Total core recovered (m): 30.67

Core recovery (%): 35.7

Oldest sediment cored:
Depth (mbsf): 35.7
Nature: mudstone
Age: middle Eocene
Measured velocity (km/s): ~1.7

Principal results: Site 683 was chosen to investigate the history of vertical tectonic movement of the Peruvian continental margin along the northern of two transects. Two objectives at this site were to recover metamorphic basement at a estimated depth of 600 mbsf and to extend the stratigraphy of industry wells Ballena and Delphin to the seaward flank of the Yaquina Basin. Extending the published ages assigned to sediments in these wells to Site 683 indicated a thin Neogene sequence to a depth corresponding to 0.2 s two-way traveltime and underlain by dipping irregular reflectors of inferred Eocene age, extending from 0.2–0.5 s. The location appeared ideal for recovering samples of metamorphic basement unconformably overlain by sediment recording vertical tectonic movement.

Drilling showed that these age assignments for the Yaquina Basin sediments were incorrect. The sequence recovered is mostly of Neogene age, and the top of the basement reflections corresponds to middle Eocene mudstone. The hiatus that separates these stratigraphic units encompasses the upper Eocene, Oligocene, and lower Miocene. These revised ages provide a history of events for the northern transect that is similar to the southern transect.

The sedimentary sequence recovered at Site 683 consists of three units: (1) Quaternary–Pliocene diatomaceous mud with minor calcareous mud and turbidites, (2) poorly indurated middle Miocene diatomaceous mudstone and volcanic ash, and (3) well-indurated middle Eocene mudstone with minor volcanic ash, dolomite, and limestone. The boundary between the upper and middle units is marked by a middle Pliocene to middle Miocene hiatus, and the boundary between the middle and lower units is the major biostratigraphic hiatus between middle Miocene and middle Eocene. Continuous hemipelagic sedimentation was broken during the last 1 m.y. by numerous turbidites, with almost continuous volcanic activity peaking during the middle Miocene. Repeated cycles of upwelling-related sedimentation, alternating with more terrigenous sedimentation, are recog-

[1] Suess, E., von Huene, R., et al., 1988. *Proc. ODP, Init. Repts.*, 112: College Station, TX (Ocean Drilling Program).

[2] Erwin Suess (Co-Chief Scientist), Oregon State University, College of Oceanography, Corvallis, OR 97331; Roland von Huene (Co-Chief Scientist), U.S. Geological Survey, Branch of Pacific Marine Geology, 345 Middlefield Rd. M/S 999, Menlo Park, CA 94025; Kay-Christian Emeis (ODP Staff Scientist), Ocean Drilling Program, Texas A&M University, College Station, TX 77843; Jacques Bourgois, Département de Géotectonique, Université Pierre et Marie Curie, 4 Place Jussieu, 75230 Paris Cedex 05, France; José del C. Cruzado Castañeda, Petroleos del Peru S. A., Paseo de la Republica 3361, San Isidro, Lima, Peru; Patrick De Wever, CNRS, Laboratoire de Stratigraphie, Université Pierre et Marie Curie, 4 Place Jussieu, 75230 Paris Cedex 05, France; Geoffrey Eglinton, University of Bristol, School of Chemistry, Cantock's Close, Bristol BS8 1TS, England; Robert Garrison, University of California, Earth Sciences, Applied Sciences Building, Santa Cruz, CA 95064; Matt Greenberg, Lamont-Doherty Geological Observatory, Columbia University, Palisades, NY 10964; Elard Herrera Paz, Petroleos del Peru, S. A., Paseo de la Republica 3361, San Isidro, Lima, Peru; Phillip Hill, Atlantic Geoscience Centre, Bedford Institute of Oceanography, Box 1006, Dartmouth, Nova Scotia B2Y 4A2, Canada; Masako Ibaraki, Geoscience Institute, Faculty of Science, Shizuoka University, Shizuoka 422, Japan; Miriam Kastner, Scripps Institution of Oceanography, SVH, A-102, La Jolla, CA 92093; Alan E. S. Kemp, Department of Oceanography, The University, Southampton SO9 5NH, England; Keith Kvenvolden, U.S. Geological Survey, Branch of Pacific Marine Geology, 345 Middlefield Rd., M/S 999, Menlo Park, CA 94025; Robert Langridge, Department of Geological Sciences, Queen's University at Kingston, Ontario K7L 3A2, Canada; Nancy Lindsley-Griffin, University of Nebraska, Department of Geology, 214 Bessey Hall, Lincoln, NE 68588-0340; Janice Marsters, Department of Oceanography, Dalhousie University, Halifax, Nova Scotia B3H 4J1, Canada; Erlend Martini, Geologisch-Paläontologisches Institut der Universität Frankfurt, Senckenberg-Anlage 32-34, D-6000, Frankfurt/Main, Federal Republic of Germany; Robert McCabe, Department of Geophysics, Texas A&M University, College Station, TX 77843; Leonidas Ocola, Laboratorio Central, Instituto Geofisico del Peru, Lima, Peru; Johanna Resig, Department of Geology and Geophysics, University of Hawaii, Honolulu, HI 96822; Agapito Wilfredo Sanchez Fernandez, Instituto Geologico Minero y Metalurgico, Pablo Bermudez 211, Lima, Peru; Hans-Joachim Schrader, College of Oceanography, Oregon State University, Corvallis, OR 97331 (currently at Department of Geology, University of Bergen, N-5000 Bergen, Norway); Todd Thornburg, College of Oceanography, Oregon State University, Corvallis, OR 97331; Gerold Wefer, Universität Bremen, Fachbereich Geowissenschaften, Postfach 330 440, D-2800 Bremen 33, Federal Republic of Germany; Makoto Yamano, Earthquake Research Institute, University of Tokyo, Bunkyo-ku, Tokyo 113, Japan.

nizable in the upper part of the Quaternary. Moderate to extensive bioturbation throughout the section suggests that bottom waters remained oxic. Structures within the sediments reveal a history of soft-sediment deformation related to downslope creep and slumping, followed by extensional microfaulting and minor compressional microfaulting.

The sediments at Site 683 show all of the early diagenetic processes previously seen at Site 682; however, overall, the reactive zones are more readily discernable and reaction pathways less ambiguous. Gradients of dissolved chemical species are (1) steeper; (2) contain maxima and minima of calcium, magnesium, and alkalinity; (3) indicate carbonate mineral diagenesis; (4) are more pronounced; and (5) indicate more abundant authigenic calcite and dolomite phases. The sulfate-reduction zone is compressed toward the sediment/water interface (<20 mbsf) as is typical for rapidly accumulating organic carbon-rich sediments. Methanogenesis dominates throughout the remainder of the hole. Calcite precipitates first near the base of the sulfate-reduction zone. This causes the Mg^{2+}/Ca^{2+} molar ratio to increase dramatically to around 13, the highest value ever reported for nonevaporitive environments. Consequently, highly favorable conditions for rapid dolomitization prevail. With increasing dolomitization at increasing depth, the Mg^{2+}/Ca^{2+} ratio decreases to a value <2, again favoring calcite formation. Generations of micritic dolomite layers and authigenic calcite cements throughout the sequence support the proposed reaction sequence.

Gas hydrates should form from the high biogenic methane contents generated below the thin sulfate-reduction zone at Site 683. Characteristic dissolved chloride profiles suggest the presence of methane hydrates, although none were observed. We believe a significant chloride maximum around 50 mbsf reflects salt exclusion during the formation of gas hydrates. This chloride maximum advances above the gas-hydrate front by diffusion, as previously suggested at Site 682. Chloride decreases gradually below this maximum to 454 mmol/L (80% of seawater value) at 452 mbsf. This is attributed to freshwater dilution from dissociation of gas hydrates.

Although basement was not reached at Site 683, the overlying sediment is a typical continental sequence displaying a lithostratigraphy and geochemistry not normally found in open-ocean basins. This sediment was deposited before the Neogene (Quechuan) phase of the Andean orogeny, and thus the site is situated on crust attached to the continent rather than an oceanic element tectonically accreted at the front of the Andean convergent margin.

BACKGROUND AND SCIENTIFIC OBJECTIVES

During the Nazca Plate Project, the regional geophysical surveys of the Peruvian margin were complemented by detailed surveys in three corridors across representative areas. The middle corridor was near a latitude of 9°S, about midway between the northern and southern political boundaries of Peru. Along with other geophysical observations, the multichannel seismic-reflection technique was employed to obtain high-quality seismic data. A single line was shot from the upper slope across the trench and onto the oceanic crust. The shelf and slope have a morphology typical of the Peruvian convergent margin without major canyons or other special features. From general morphology and the regional geology, the 9°S area is typical for the entire Peruvian convergent margin (Fig. 1).

Multichannel seismic-reflection line CDP-2 (or Peru-2) was shot 24 times and processed using common-depth-point (CDP) techniques. During processing of the field data, the 24 channels were grouped into 12 channels (Kulm et al., 1981). An accompanying seismic-refraction transect was made that gave needed velocity control (Jones, 1981). From the refraction and gravity data, Jones (1981) concluded that the entire landward slope of the margin was composed of material accreted from the Nazca Plate, despite his observations that the material had a higher acoustic velocity and density than is normal for an accreted complex. From the CDP data, Kulm et al. (1981) concluded that the crystalline and metamorphic rocks of the continental crust extended seaward to between 26 and 115 km of the Peru Trench axis. These authors also proposed a mechanism whereby the process of tectonic accretion would mix oceanic crust and trench sediment in an accretionary complex.

The Nazca Plate Project geophysical data, other CDP seismic-reflection data from industry, and the results from two drill holes on the outer continental shelf and along the transect were subsequently summarized in the Ocean Margin Drilling Project Atlas 6 (Thornburg, 1985). These geophysical data were complete enough to show the basic structure of the forearc basins on the shelf and upper slope. The stratigraphy of the exploratory drill holes was essentially tied to CDP-2, although not specifically indicated in the drawing of the record. The drill holes reached metamorphic basement of continental affinity, which was covered unconformably by Eocene age and younger shelf sediment. CDP-2 also was reprocessed using all 24 channels and modern migration techniques, which greatly clarified the geometry of the reflective sequences and imaged much more structural detail (von Huene et al., 1985; Kulm et al., 1986). The accretion of sediment is clearly imaged beneath the lower slope of the margin but becomes increasingly obscured toward the midslope area. The upper slope is a continuation of the continental sediment sequence and basement of the shelf. This upper slope is broken by numerous small normal faults. That structure also becomes obscured in the midslope area in much the same manner as the lower-slope accretionary structure. Thus, the seismic record shows that the midslope obscured area separates continental from accreted terranes. The zone of crustal transition is about 15 km landward of the trench axis.

Once the transect was selected for drilling, a site survey was conducted by the *Moana Wave* (Hussong et al., this volume; Ballesteros et.al., this volume). That survey included swath-mapping with the SeaMARC II instrument system and CDP seismic-reflection lines. Only three months before Leg 112, a Seabeam and geophysical survey of the area was conducted by the French research vessel *Charcot* (Bourgois et al., this volume). In addition to a Seabeam map (Fig. 2), CDP cross-lines were made to provide a complete suite of seismic data as required for assessment of drilling safety (von Huene and Miller, this volume).

The initial results of the new studies confirmed the previous ones. They amplified the indications of normal faulting on the upper slope and revealed erosion of the slope by multiple rivulets, where it is locally steep. The rivulets end in the ponded sediment cover on the midslope terrace. The terrace is a laterally extensive feature, but its origin and relationship to the division between continental and accreted terranes is still obscure in this corridor. The lower slope is relatively two-dimensional and lacks pronounced local morphological features but does display subtle anastamosing morphological features parallel to the strike, which could be thrust faults.

The tectonic objectives at Sites 683 and 684 were (1) to establish the seaward extent of the continental crust and (2) to establish the landward extent of the accreted complex at the foot of the slope. These boundaries were proposed in earlier studies, based mainly on geophysics and surface samples. On the continental crust, the profound unconformity above the metamorphic basement shows that this surface once existed at shallow depths where a high-energy erosional process could remove sufficient material to unroof a metamorphic complex. The Andean orogeny occurred during convergence of the oceanic and continental lithospheric plates and development of a subduction zone. If the subsidence of the crust is related to plate convergence during the Andean orogeny, then some form of subcrustal erosion in the subduction zone is implied. This would be consistent with the apparent truncation of the Peruvian continental crust in the midslope area. The subsidence history, if related to periods of batholithic intrusion in the Andes, provides constraints on tectonic mechanisms. When related to companion Site 685 (on the accretionary complex), some indication of the time of evolution

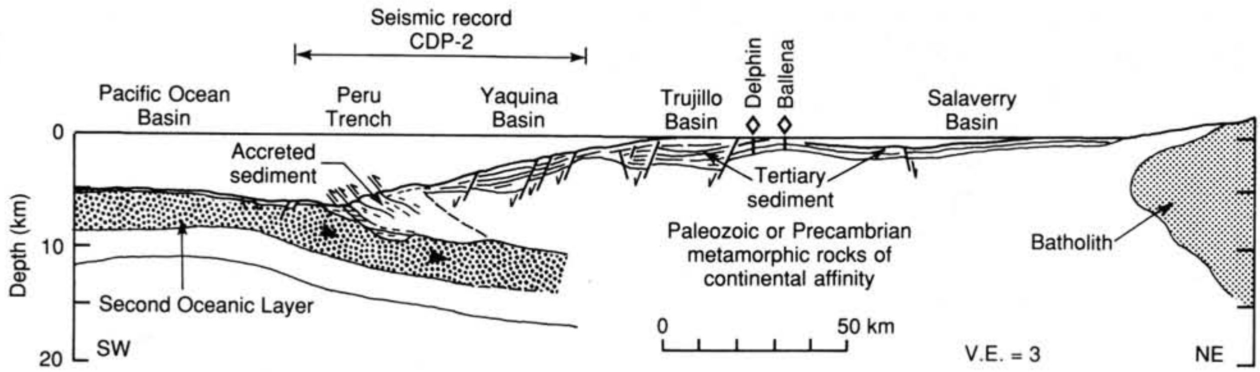

Figure 1. Cross section of the Peruvian convergent margin.

from the erosional convergent margin to the accretionary convergent margin may possibly be established. In turn, this event can be related to the regional geology, which may provide an indication of the basic causes of each tectonic mechanism.

Although this site was selected primarily for tectonic objectives, it also offers an overview of the paleoceanographic conditions upslope. The presence of transported products from upwelling centers and their relative abundance in relation to terrigeneous sediment provides a continuous regional upwelling history, as deposition in deeper water precludes strong erosion.

OPERATIONS

The *Resolution* departed Site 682 at 1715 L on 14 November 1986 and steamed from the southern transect to the northern one at 9°S. The survey to locate Site 683 began about 0540 L (1040 UTC) when the ship intersected the track of seismic line Peru-2, on which the tectonic sites of the northern transect are located (Fig. 3). The location from the global positioning system (GPS) was acquired at 0656 hr, and a beacon was dropped 26 min later when the ship's position and the PDR depth corresponded to those of the site. After the ship had stabilized over the beacon, our position proved to be precisely on target and water depth agreed with the *Charcot* Seabeam survey data.

An APC mudline core was obtained at a water depth of 3086 m and eight other cores were obtained with the APC before the overpull became excessive. XCB coring began at 78.2 m with the typical decrease in core recovery experienced previously during this leg (Table 1). However, after considerable experimentation, recovery improved and the overall average reached 52%. Despite a considerable investment in conditioning, the hole began to deteriorate rapidly after Core 112-683A-44X. Then, to avoid sticking, the drill bit was pulled to the mud line after cutting Core 112-683A-45X (419 m).

Hole 683B was located 320 m upslope toward material that appeared less fractured, based on the character of reflections in seismic record Peru-2. We spent about a day washing down to make two cores overlap with the previously drilled section. The hole conditions remained good to 469 m, after which conditions became worse, requiring a sweep of the hole with drilling mud and a wiper trip. We abandoned the hole at 488 m after it became too unstable for another core. We considered logging too risky because of the unstable hole conditions. Thus, our third attempt to recover basement ended about 100 m above its estimated depth.

LITHOSTRATIGRAPHY

Lithologic Units

Sediments recovered at Site 683 are divided into three units on the basis of visual core descriptions, smear slides, and biostratigraphy (Table 2 and Fig. 4): (1) an upper unit of diatomaceous mud, (2) a middle unit of diatomaceous mudstone and mud, and (3) a lower unit of well-indurated mudstone. The upper two units are subdivided into four and three subunits, respectively. The units and subunits agree well with results of physical-properties studies (see "Physical Properties" section, this chapter). Units I and II are separated by a hiatus spanning middle Pliocene to middle Miocene, and Units II and III are separated by a hiatus ranging from middle Miocene to middle Eocene.

Unit I

Cores 112-683A-1H through 112-683A-27X-1; depth, 0–240 mbsf; age, middle Pliocene to Quaternary.

Unit I consists of unlithified diatomaceous mud with variable amounts of calcareous microfossils and clastic sediment. The unit is divided into four subunits (Table 2 and Fig. 4). Subunit IA consists of Quaternary bioturbated diatomaceous muds and extends to a depth of 43 mbsf, where it grades over a short interval into the more calcareous diatomaceous muds of Quaternary Subunit IB. The base of Subunit IB at 63 mbsf grades into the sandy and silty diatomaceous muds of Quaternary Subunit IC. The clastic interbeds of Subunit IC are interpreted as turbidites. At a depth of 107 mbsf, a sudden decrease in turbidite interbeds marks the top of Subunit ID. The diatomaceous muds of Subunit ID span the Quaternary–Pliocene boundary at about 170 mbsf with no obvious lithologic break.

Subunit IA (0–43 mbsf; Core 112-683A-1H to Sample 112-683A-6H-2, 145 cm)

Subunit IA consists of diatomaceous mud, typically a homogeneous olive gray with regular cycles of subtle but distinct color changes. These color changes are gradational over an interval of a few centimeters and are repeated at intervals of 10–40 cm. The color changes reflect slight variations in the relative proportions of diatoms, calcareous microfossils, and terrigenous clastics. The unit is moderately to extensively bioturbated (Fig. 5). Burrows identified on board the ship include *Cylindrichnus* (Section 112-683A-1H-1) and *Chondrites* (Section 112-683A-4H-3). The unit grades downward into more calcareous, foraminifer-bearing diatomaceous mud near its base.

Subunit IA is homogeneous, with randomly scattered mottlings of slightly lighter (olive gray) or darker (black) mud, which either fills or borders individual burrows (Fig. 5). Very dark gray to black patches of pyrite-rich mud about 1–2 mm in diameter are common, as are small peloidal concentrations of white sponge spicules. Rare shell fragments are preserved, as are rare laminae and faint bedding defined by subtle color changes. Sparsely distributed silt and sandy silt beds within the unit contain somewhat higher concentrations of terrigenous quartz, feldspar, and rock fragments relative to biogenic material; their sharp bases and graded bedding suggest a turbidite origin.

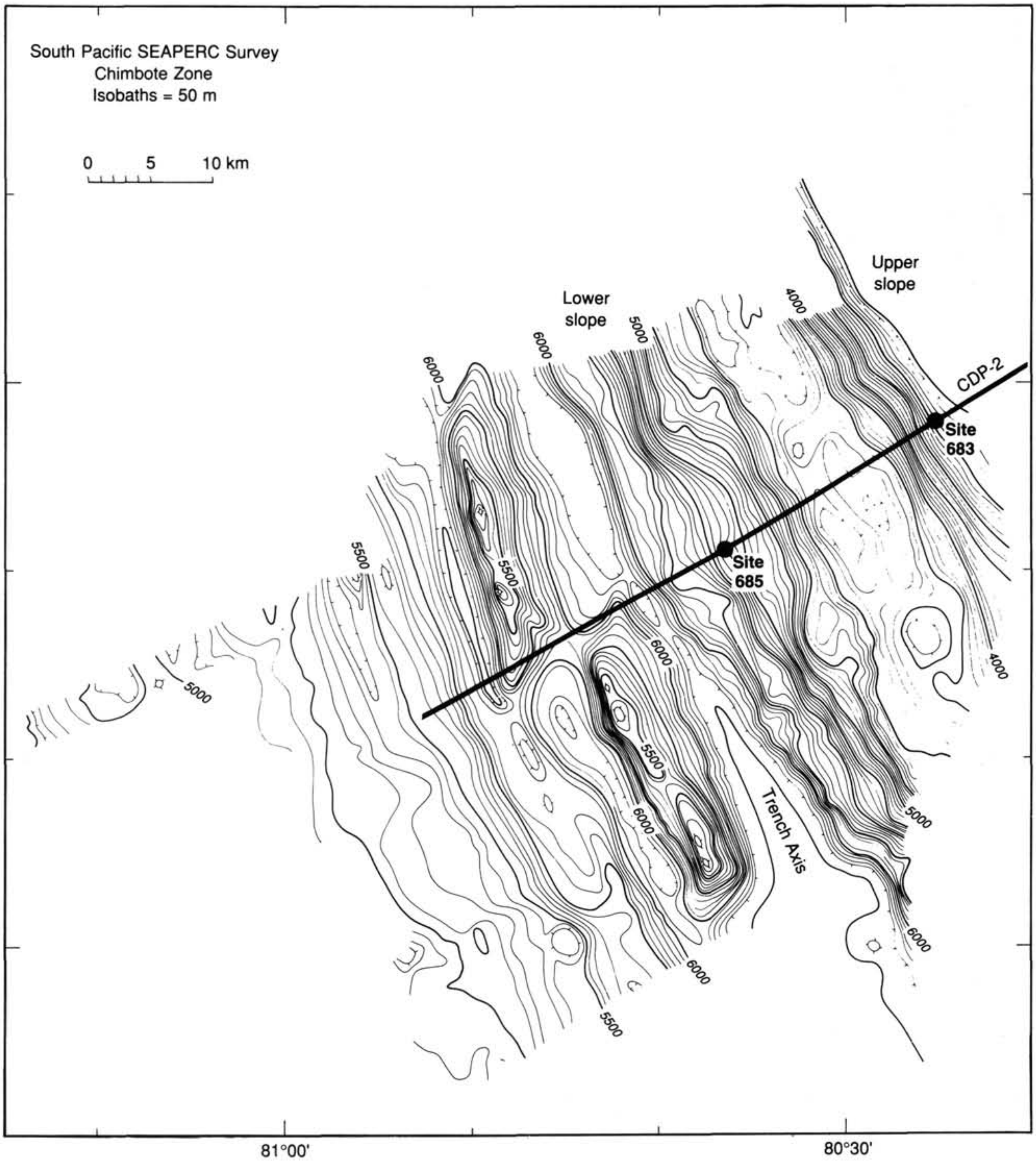

Figure 2. Seabeam bathymetric map of the lower slope, the trench axis, and the seaward slope showing location of seismic record CDP-2 and Sites 683 and 685 (from Bourgois et al., in press).

Minor lithologies in Subunit IA include several intervals rich in calcareous microfossils (to 20%); their bases are indistinct and gradational, with underlying units. A bed of volcanic ash (60%) at Sample 112-683A-4H-3, 131 cm, is rich in diatoms and sponge spicules and contains minor amounts of feldspar. Traces (1%–5%) of volcanic glass are present in nearly all cores in Subunit IA.

Except for minor interbeds and laminae where foraminifers or nannofossils are concentrated, only trace amounts of $CaCO_3$ occur in the upper part of Subunit IA. However, the amount of $CaCO_3$ increases steadily downward as Subunit IA grades into Subunit IB and increases sharply at the boundary.

Subunit IB (43–63 mbsf; Samples 112-683A-6H-2, 145 cm, to 112-683A-8H-3, 45 cm)

Subunit IB consists of olive gray to dark olive gray calcareous diatomaceous mud containing up to 30% foraminifers, 50% nannofossils, and 20% authigenic carbonate. Total carbonate

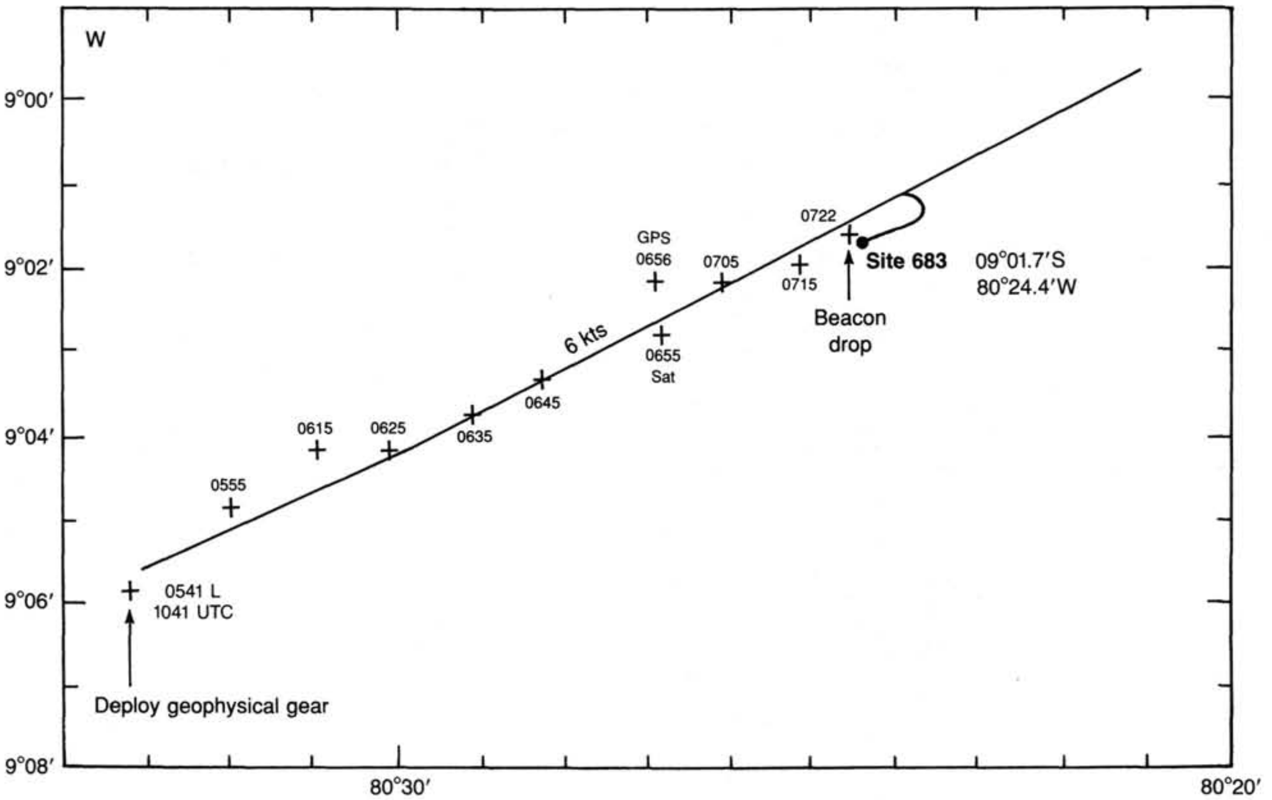

Figure 3. Track chart of approach to Site 683 location with GPS control.

content estimated from smear slides typically ranges from 30% to 60% throughout this interval, representing a sharp increase over Subunit IA, which typically has less than 15% calcareous microfossils and authigenic carbonate combined (Table 3).

Subunit IB is massive and has moderate to extensive bioturbation. Small worms were found in Sample 112-683A-6H-6, 35 cm, at a depth of 48 mbsf. About 2-3 mm in diameter and between 1 and 2 cm long, these worms consist of well-preserved translucent organic tissue. The preservation of original organic tissue suggests that these worms inhabited the sediment at this depth below the seafloor. Contamination from the upper part of the hole is unlikely because drilling would have destroyed the delicate tissue structure if the worms were not protected by intact sediment.

Cyclic, light-to-dark color changes similar to those in Subunit IA appear to represent variations in the relative proportions of calcareous, siliceous, and terrigenous components. Volcanic glass is present in trace amounts (1%-5%) throughout Subunit IB.

Subunit IC (63-107 mbsf; Sample 112-683A-8H-3, 45 cm, to Section 112-683A-12X, CC)

Subunit IC consists of dark gray to olive diatomaceous mud interbedded with dark to very dark gray diatom-bearing mud and terrigenous silt or sandy silt turbidite beds. This subunit is distinct from Subunits IA and IB not only for its higher terrigenous content but also because of its low carbonate content (Table 3) and generally lower diatom content. Much of the terrigenous material is disseminated throughout the unit in the form of higher clay contents and generally higher contents of silt- to sand-sized grains of feldspar, quartz, and lithic fragments. The sharply based, graded turbidite beds consist of dark gray to black sand and sandy silt and, in some cases, exhibit laminated tops. The sharp basal contacts of many of these beds are cut by microfaults (Fig. 6), and the lighter colored tops are typically diffuse and highly burrowed. Bioturbation is moderate to extensive throughout most of the unit. Present in minor amounts are thin laminae or beds of nannofossil ooze, foraminifer-rich silt, or calcareous mud with authigenic calcite. Volcanic glass is ubiquitous in small amounts (1%-5%).

Subunit ID (107-240 mbsf; Sections 112-683A-13X-1 to 112-683A-27X-1)

Subunit ID consists of very dark gray to dark olive gray diatom-bearing to diatomaceous mud, which becomes darker, more pyrite-rich, and somewhat fissile toward the base. The subunit is distinguished from the overlying Subunit IC by a sharp decrease in the number of sandy turbidite interbeds. Although some sharply based, graded turbidite interbeds are present in Subunit ID, they are much finer-grained and consist typically of black silty mud grading upward into more clay-rich, diatom-rich mud. The tops of these turbidite beds are intensely burrowed. The degree of induration in Subunit ID is slightly greater than in the overlying units because the mud exhibits incipient fissility, which is enhanced by drilling disturbance and probably contributes to the poor recovery in parts of this unit. Volcanic glass occurs throughout the unit, ranging from trace amounts to 5%, but is disseminated rather than concentrated in distinct beds. Both biogenic and authigenic carbonate are present in trace amounts; however, these are only important in rare interbeds. Authigenic pyrite is present throughout the unit in small amounts (1%-5%), but it increases toward the base of the unit, where it makes up to 60% of minor black interbeds.

Bioturbated structures (including *Chondrites*) are common throughout the unit, as are shell fragments, peloidal accumulations of sponge spicules, and collapsed sponges. The collapsed sponges are of particular interest. These are concentrated in lay-

Table 1. Coring summary for Site 683.

Core/section	Date (November 1986)	Time (L)	Depth (mbsf)	Length cored (m)	Length recovered (m)	Recovery (%)
112-683A-1H	15	1625	0-2.2	2.2	2.20	100.0
2H	15	1715	2.2-11.7	9.5	7.03	74.0
3H	15	1750	11.7-21.2	9.5	7.69	80.9
4H	15	1830	21.2-30.7	9.5	9.91	104.0
5H	15	1925	30.7-40.2	9.5	4.92	51.8
6H	15	2020	40.2-49.7	9.5	10.57	111.2
7H	15	2100	49.7-59.2	9.5	9.70	102.0
8H	15	2145	59.2-68.7	9.5	10.26	108.0
9H	15	2300	68.7-78.2	9.5	9.99	105.0
10X	16	0145	78.2-87.7	9.5	1.74	18.3
11X	16	0245	87.7-97.2	9.5	1.18	12.4
12X	16	0348	97.2-106.7	9.5	9.47	99.7
13X	16	0450	106.7-116.2	9.5	1.00	10.5
14X	16	0550	116.2-125.7	9.5	1.24	13.0
15X	16	0700	125.7-135.2	9.5	9.32	98.1
16X	16	0830	135.2-144.7	9.5	1.95	20.5
17X	16	0945	144.7-154.2	9.5	1.17	12.3
18X	16	1050	154.2-163.7	9.5	6.95	73.1
19X	16	1200	163.7-173.2	9.5	1.05	11.0
20X	16	1315	173.2-182.7	9.5	0.65	6.8
21X	16	1430	182.7-192.2	9.5	2.84	29.9
22X	16	1545	192.2-201.7	9.5	0.84	8.8
23X	16	1700	201.7-211.2	9.5	1.51	15.9
24X	16	1830	211.2-220.7	9.5	0.92	9.7
25X	16	2125	220.7-230.2	9.5	7.88	82.9
26X	17	0035	230.2-239.7	9.5	0.64	6.7
27X	17	0210	239.7-249.2	9.5	1.53	16.1
28X	17	0400	249.2-258.7	9.5	3.11	32.7
29X	17	0605	258.7-268.2	9.5	1.49	15.7
30X	17	0735	268.2-277.7	9.5	2.57	27.0
31X	17	0845	277.7-287.2	9.5	1.89	19.9
32X	17	1000	287.2-296.7	9.5	1.20	12.6
33X	17	1105	296.7-306.2	9.5	8.90	93.7
34X	17	1215	306.2-315.7	9.5	6.06	63.8
35X	17	1335	315.7-325.2	9.5	4.30	45.2
36X	17	1500	325.2-334.7	9.5	6.58	69.2
37X	17	1620	334.7-344.2	9.5	6.20	65.2
38X	17	2020	344.2-353.7	9.5	3.21	33.8
39X	17	2135	353.7-363.2	9.5	7.08	74.5
40X	18	0125	363.2-372.7	9.5	10.26	108.0
41X	18	0300	372.7-381.2	8.5	9.47	111.0
42X	18	0410	381.2-390.7	9.5	0.94	9.9
43X	18	0530	390.7-400.2	9.5	4.03	42.2
44X	18	0715	400.2-409.7	9.5	8.95	94.2
45X	18	1700	409.7-419.2	9.5	8.78	92.4
112-683B-1X	19	1055	402.5-412.0	9.5	1.36	14.3
2X	19	1215	412.0-421.5	9.5	4.39	46.2
3X	19	1350	421.5-431.0	9.5	3.29	34.6
4X	19	1530	431.0-440.5	9.5	0.65	6.8
5X	19	1730	440.5-450.0	9.5	3.71	39.0
6X	19	1935	450.0-459.5	9.5	3.42	36.0
7X	19	2140	459.5-469.0	9.5	3.66	38.5
8X	20	0340	469.0-478.5	9.5	9.81	103.0
9X	20	0710	478.5-488.0	9.5	0.38	4.0

H = hydraulic piston; X = extended-core barrel.

ers (Fig. 7) and scattered throughout the sediments between Sections 112-683A-17X-1 and 112-683A-27X-1 (base of the unit). The sponges consist of flattened oblate rings having an average diameter of about 0.5 cm and a maximum diameter of 2 cm. Sponge spicules are randomly oriented within a wall 0.5 mm thick around a mud-filled interior. In some cases, the interiors of the sponges contain concentrations of carbon-rich mud or pyrite. The presence of numerous sponges in turbidite layers (Fig. 8) suggests that these were transported from much shallower depths.

We first observed dewatering pipes near the base of Subunit ID (Section 112-683A-23X-1); these may occur higher in the sediment column but we did not observe any because of poor recovery and drilling disturbance.

Subunit ID was deposited in an environment of oxic bottom waters that received both pelagic and terrigenous sediments (including volcanic ash) from middle Pliocene into early Pleistocene time. Cyclic alternations between more- and less-biogenic sediments were not recognized in this unit.

Table 2. Lithologic units at Site 683.

Lith. unit	Lithology	Core/section interval (cm)	Depth (mbsf)
Pliocene-Quaternary			
I	Diatomaceous mud, calcareous diatom mud, turbidites	112-683A-1H to 27X-1	0-240
IA	Diatomaceous mud	112-683A-1H to 6H-2, 145	0-43
IB	Calcareous diatomaceous mud	112-683A-6H-2, 145 to -8H-3, 45	43-63
IC	Sandy-silty turbidites in diatomaceous mud	112-683A-8H-3, 45 to -12X	63-107
ID	Diatomaceous mud and laminated pyrite-rich diatom mud	112-683A-13X-1 to 27X-1	107-240
middle Miocene			
II	Diatomaceous mud and mudstone	112-683A-27X to -45X 112-683B-1X to -6X	240-418 402.5-453
IIA	Diatomaceous mudstone to mud	112-683A-27X-1 to -33X-5, 85	240-303.6
IIB	Volcanic ash and ashy diatomaceous mud and mudstone	112-683A-33X-5, 85 to -41X-1, 50	303.6-373.2
IIC	Diatomaceous to diatom-bearing mudstone and laminated mudstone; dolomite; limestone	112-683A-41X to -45X 112-683B-1X to -6X	373.2-418 402.5-453
Eocene			
III	Mudstone with minor ash, dolomicrite, limestone breccia	112-683B-7X to -9X	459.5-479

Unit II

Cores 112-683A-27X to 112-683A-45X; 112-683B-1X to 112-683B-6X; depth, 240–418 mbsf in Hole 683A and 402.5–453 mbsf in Hole 683B; age, middle Miocene.

Unit II consists of diatomaceous mudstone interbedded with diatomaceous mud and is divided into three subunits in Hole 683A. In Hole 683B, recovery was so poor that we could not correlate samples with confidence. However, the top two cores from Hole 683B were similar in lithology to Subunit IIC, suggesting that at least that much overlap occurs between the two holes.

Subunit IIA (240–303.6 mbsf; Section 112-683A-27X-1 to Sample 112-683A-33X-5, 85 cm)

Subunit IIA consists of partially indurated diatomaceous mudstone, dark olive gray to black, interbedded with olive to dark olive gray or black diatomaceous mud. Nannofossil-diatom ooze is present as disseminated sparse interbeds containing 20%–50% nannofossils; sponge spicules and foraminifers are common. Volcanic glass is ubiquitous in small amounts (1%–5%), in several interbeds, 20%–40% glass is present. A single, nearly pure, ash bed occurs in Sample 112-683A-29X-1, 43 cm, and pumice clasts 0.5–1.0 cm in diameter occur in Section 112-683A-31X-2 (Fig. 9). Rare, olive-colored dolomite nodules are present, and a hard fragment of dolomicrite breccia was recovered in Section 112-683A-27X, CC.

Because of its greater degree of induration, Subunit IIA often fractured during drilling, and recovery was uniformly poor. Structures other than drilling disturbance are difficult to observe. Burrows are common within drilling biscuits that are not fractured too much. This suggests that most of the sediments were subjected to moderate bioturbation. In general, sediments of Subunit IIA were deposited in a region of hemipelagic sedimentation, probably above the carbonate compensation depth

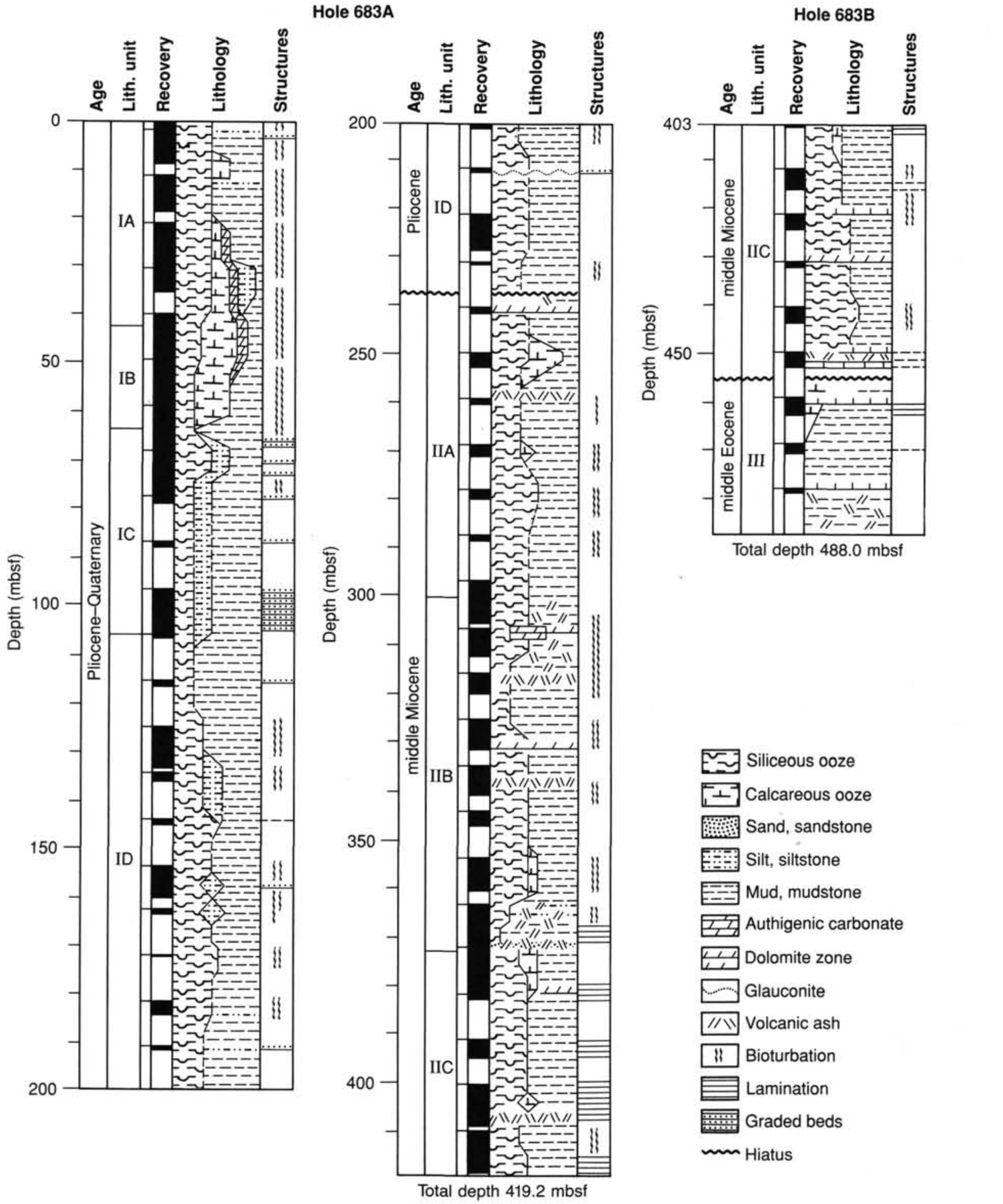

Figure 4. Lithostratigraphic sections for Site 683.

(CCD), where sparse, graded, terrigenous-rich layers may have been deposited as turbidites.

Subunit IIB (303.6–373.2 mbsf; Samples 112-683A-33X-5, 85 cm, to 112-683A-41X-1, 50 cm)

Subunit IIB consists of light to dark olive gray diatomaceous mud and mudstone rich in volcanic ash. The upper contact of Subunit IIB is marked by a sharp increase in disseminated volcanic glass from less than 5% to about 5%–15%, with some layers containing 40%–75% volcanic glass (Fig. 10). The lower contact with Subunit IIC was placed at the lowest ash bed we observed. Subunit IIB is locally dolomitic and ranges from olive gray dolomitic mud to well-indurated, olive-colored dolomite (Sections 112-683A-34X-1 and 112-683A-36X, CC, [30 cm]). Au-

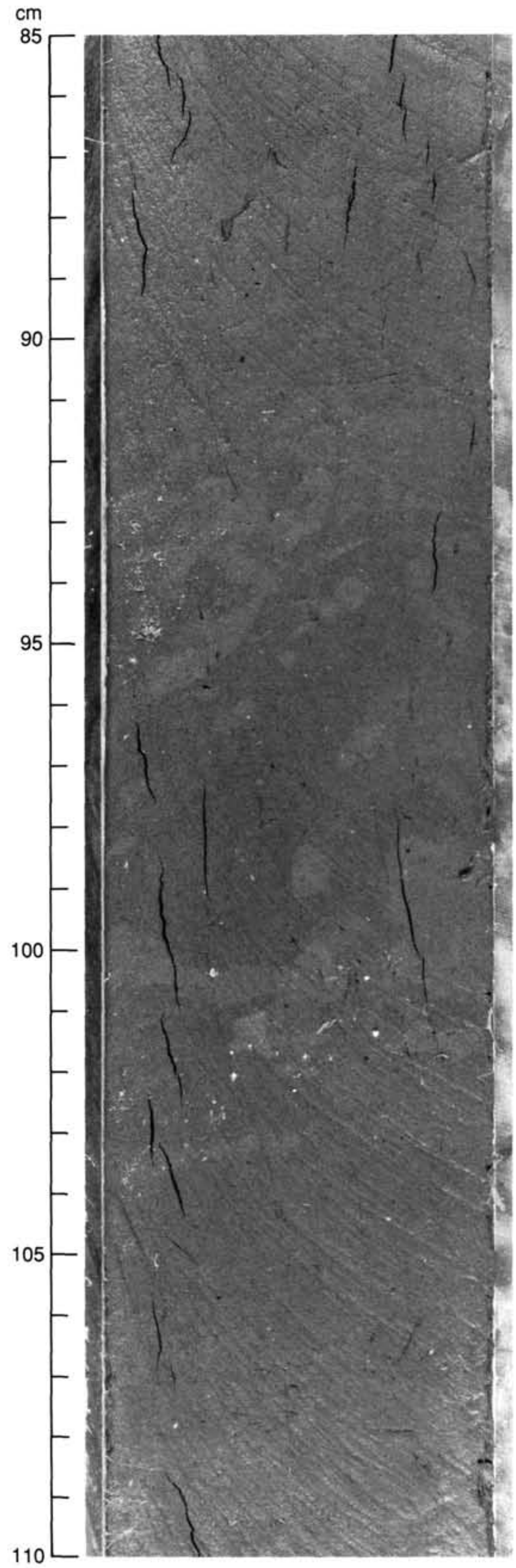

Figure 5. Burrows in diatomaceous mud of Subunit IA. Burrows filled with lighter mud are offset by extensional microfaults filled with veins of darker mud (Sample 112-683A-4H-4, 85–110 cm).

Table 3. Calcium carbonate contents, Hole 638A.

Sample interval (cm)	Depth (mbsf)	Carbonate (%)
112-638A-1H-1, 58–60	0.58	7.41
1H-1, 79–81	0.79	6.08
2H-1, 91–93	3.11	6.08
2H-2, 9–11	3.79	4.83
2H-2, 90–92	4.60	5.17
2H-3, 9–10	5.29	8.33
2H-3, 101–102	6.21	9.41
2H-4, 17–19	6.87	10.00
2H-5, 37–39	8.57	26.41
3H-1, 117–118	12.87	5.17
3H-2, 48–50	13.68	3.67
3H-3, 9–10	14.79	7.00
3H-3, 63–65	15.33	7.91
3H-4, 69–71	16.89	10.83
3H-5, 118–120	18.88	16.16
4H-1, 114–116	22.34	10.25
4H-2, 79–81	23.49	11.58
4H-3, 72–74	24.92	2.58
4H-4, 98–100	26.68	5.08
4H-5, 47–49	27.67	6.91
5H-1, 63–65	31.33	6.76
5H-1, 85–87	31.55	8.92
5H-1, 110–112	31.80	5.34
5H-2, 54–56	32.74	5.50
5H-3, 54–56	34.24	2.17
6H-1, 54–56	40.74	14.26
6H-1, 108–110	41.28	9.51
6H-3, 108–111	44.28	13.76
6H-5, 78–81	45.73	9.59
7H-2, 113–115	52.33	22.10
7H-3, 13–15	52.83	22.02
7H-4, 84–86	55.04	20.16
7H-5, 113–115	56.83	12.26
7H-6, 113–115	58.33	8.01
7H-7, 40–42	59.10	5.25
8H-1, 124–126	60.44	21.68
8H-2, 124–126	61.94	14.09
8H-4, 124–126	64.94	3.59
8H-5, 124–126	66.44	2.50
8H-6, 49–51	67.19	11.33
8H-6, 124–126	67.94	3.50
9H-1, 118–120	69.88	3.25
9H-2, 113–115	71.33	5.09
9H-4, 110–112	72.80	13.01
9H-4, 110–112	74.30	1.75
9H-5, 110–112	75.80	2.00
10X-1, 20–21	78.40	2.17
10X-1, 43–45	78.63	1.25
11X-1, 39–40	88.09	1.00
11X-1, 59–60	88.29	3.67
12X-1, 101–103	98.21	4.25
12X-2, 98–100	99.88	1.08
12X-2, 111–113	99.81	1.92
12X-3, 111–112	101.31	0.83
12X-4, 80–82	102.50	3.25
12X-6, 84–86	105.54	0.83
13X-1, 53–54	107.23	2.50
13X-1, 55–57	107.25	2.92
14X-1, 46–47	116.66	3.08
14X-1, 85–87	117.05	3.59
15X-1, 65–66	126.35	2.00
15X-1, 82–84	126.52	0.50
15X-4, 93–95	131.13	0.58
18X-4, 21–23	158.91	0.75
20X-1, 36–37	173.56	0.58
21X-1, 117–118	183.87	0.25
22X-1, 41–42	192.61	0.42
23X-1, 68–69	202.38	0.42
24X-1, 42–43	211.62	1.42
26X-1, 44–45	230.64	4.50
27X-1, 94–95	240.64	0.25
29X-1, 65–66	259.35	1.17
30X-1, 57–58	268.77	1.08
31X-1, 120–121	278.90	1.17
32X-1, 91–92	288.11	1.58
33X-6, 45–46	304.65	0.83
34X-2, 105–106	308.75	0.83
35X, CC, 20–21	319.88	0.08
36X-1, 6–7	325.26	0.08
37X-2, 45–46	336.65	0.25
38X, CC, 7–8	347.27	0.92
39X-3, 27–28	356.97	4.42
40X-5, 80–81	370.00	4.67
42X-1, 14–15	381.34	0.08
43X-3, 32–33	394.02	6.75

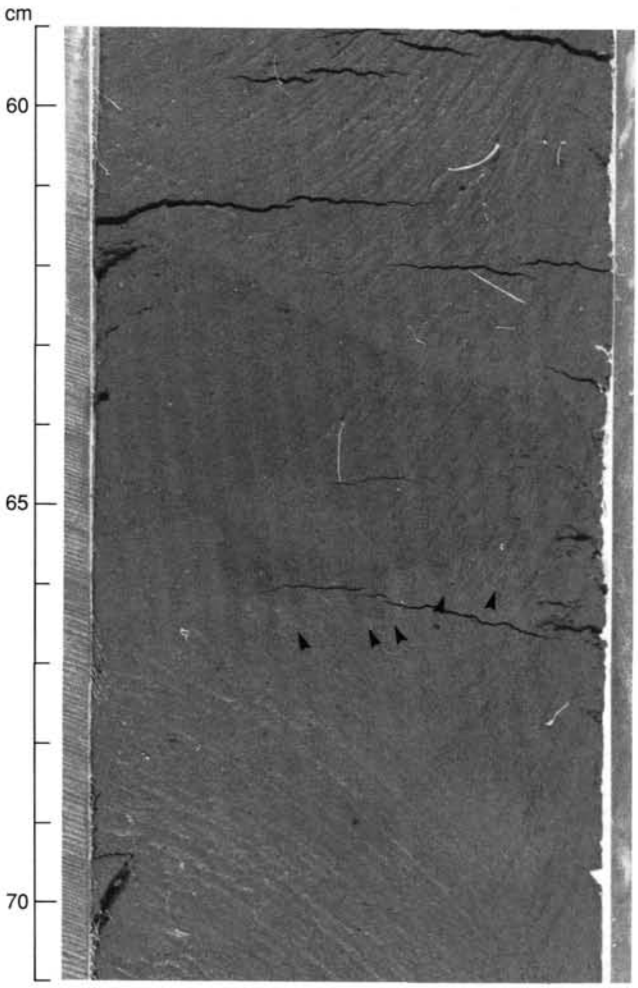

Figure 6. Graded turbidite bed in Subunit IC. Base of bed is offset by small extensional faults (arrows) (Sample 112-683A-9H-6, 59–71 cm).

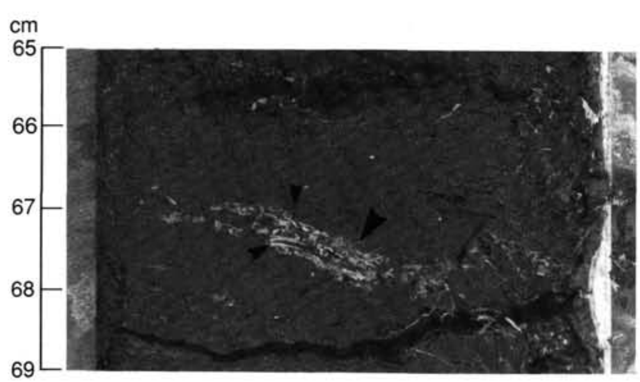

Figure 7. Collapsed sponges concentrated in a layer 0.5-cm-thick in diatomaceous mud of Subunit ID (large arrow). Some of the ovoid shapes are filled with mud enriched with organic matter or pyrite (small arrows) (Sample 112-683A-18X-2, 65–69 cm).

thigenic pyrite is present throughout the unit in amounts ranging from trace to 10% and somtimes 15%–20%. Some layers are also rich in nannofossils and foraminifers. Bioturbation ranges from sparse to moderate (including small burrows of *Chondrites*).

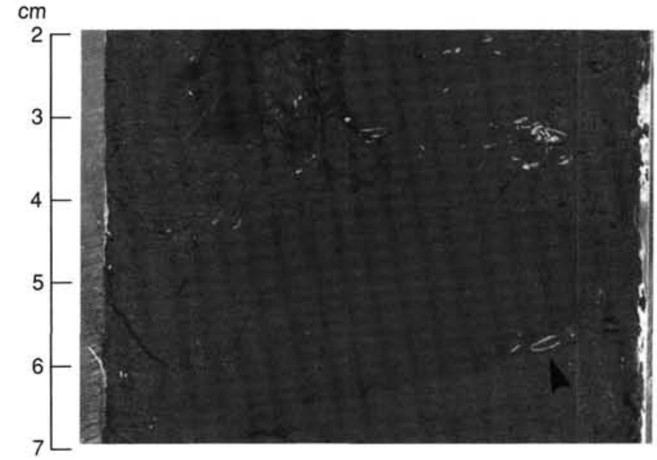

Figure 8. Collapsed sponges in diatomaceous mud of Subunit ID. Arrow marks sharp base of graded turbidite bed, which contains a nearly intact sponge 0.45 cm long (Sample 112-683A-18X-4, 2–7 cm).

Subunit IIB contains fewer diatoms and much more sand, terrigenous clasts, and volcanic ash, which suggests deposition during a period of greater volcanic activity. We believe that deposition of the clastic sediments was partly turbiditic, but drilling disruption was so severe that most primary sedimentary structures were concealed. Higher contents of authigenic dolomite and pyrite indicate that diagenesis has proceeded further than in the overlying units.

Subunit IIC (373.2–418 mbsf in Hole 683A; 402.5–453 mbsf in Hole 683B; Cores 112-683A-41X to 112-683A-45X and 112-683B-1X to 112-683B-6X)

Subunit IIC consists of well-indurated, dark gray to dark olive gray or black diatomaceous to diatom-bearing mudstone, interbedded with minor laminated mud and mudstone. Nannofossils are common in some parts of the unit, and the sediment is an olive gray nannofossil ooze in some places. Smear-slide descriptions from this unit show a higher proportion of clay relative to diatoms from those in overlying units. The clay-sized fraction in this unit probably includes crushed and fragmented diatoms that cannot be distinguished under a microscope. Quartz, feldspar, and lithic fragments are present throughout this unit and the overlying units, and volcanic glass is present in small amounts (1%–10%). A bed containing 40% volcanic glass occurs in Sample 112-683B-6X-3, 10-15 cm, and small volcanic glass-rich pebbles occur in Section 112-683A-41X-4. Authigenic pyrite increases downsection in Hole 683A and is locally rich in the upper part of Hole 683B, where it reaches concentrations of 10%–15% in some beds.

Bioturbation is minor to locally moderate throughout Subunit IIC (Fig. 11), and the lower part of the unit is typically laminated in 683A (Fig. 12). Laminations are not as well preserved in Hole 683B, but bioturbation is more intense. Because of the degree of induration, drilling disturbance was extensive, with much of the recovered material consisting of brecciated fragments of mudstone in a slurry of disaggregated mud. Near the base of each core (where drilling disturbance was minimal), evidence of soft-sediment deformation can be seen in the stretching, necking, and ductile bending of the laminae (Fig. 12). Microfaults and a scaly fabric are overprinted on these features (discussed in detail next).

Correlation of the lower section of Hole 683A with at least the upper two cores of Hole 683B is supported by similarities in composition and induration, pyrite content, laminae, and bio-

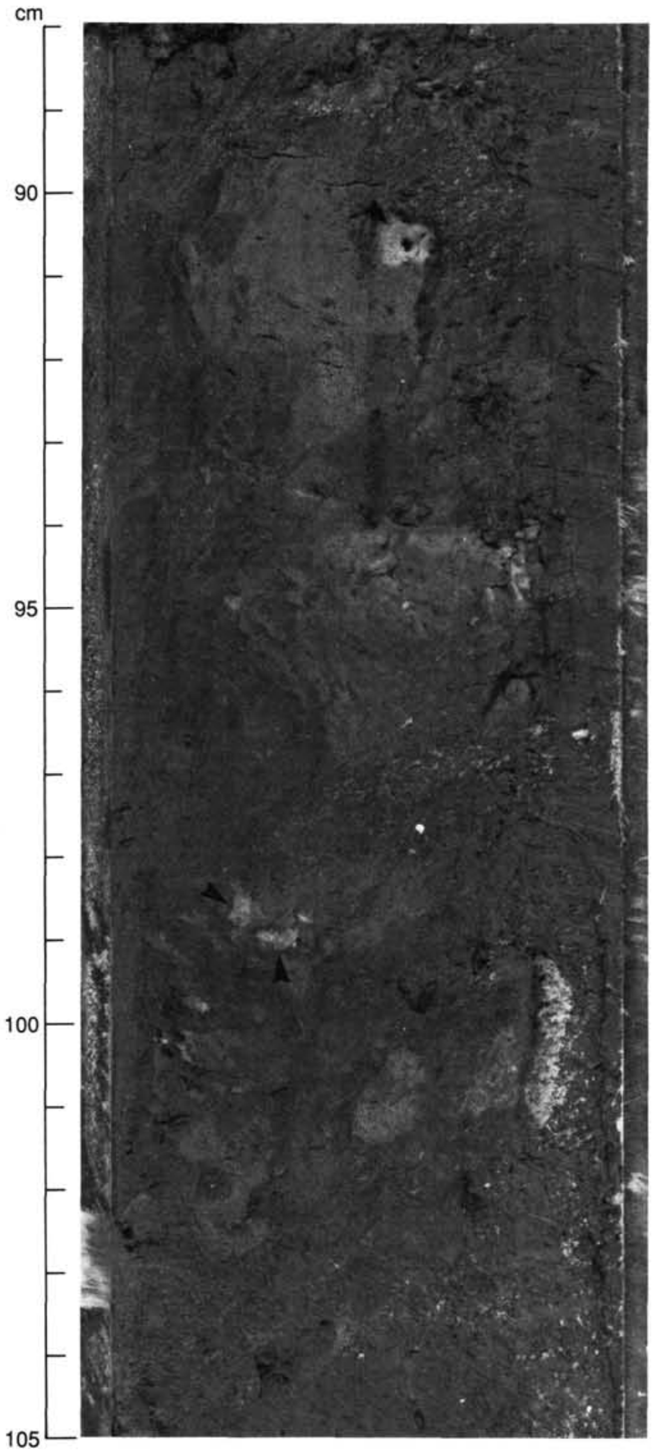

Figure 9. Pumice clasts (arrows) in burrowed diatomaceous mudstone of Subunit IIA. Microfaults within the well-defined drilling biscuits cross-cut both burrows and laminae (Sample 112-683A-31X-2, 88–105 cm).

stratigraphy. Cores 112-683B-1X and 112-683B-2X overlap the laminated mudstone recovered from Hole 683A. Below Core 112-683B-2X, the pyrite content decreases, and the mudstone begins to lose its laminated character as bioturbation increases. Near the base of Subunit IIC, recovery included hard fragments of limestone and dolomite, including olive gray micritic limestone (Samples 112-683B-3X-1, 9–12 cm, and 112-683B-3X, CC

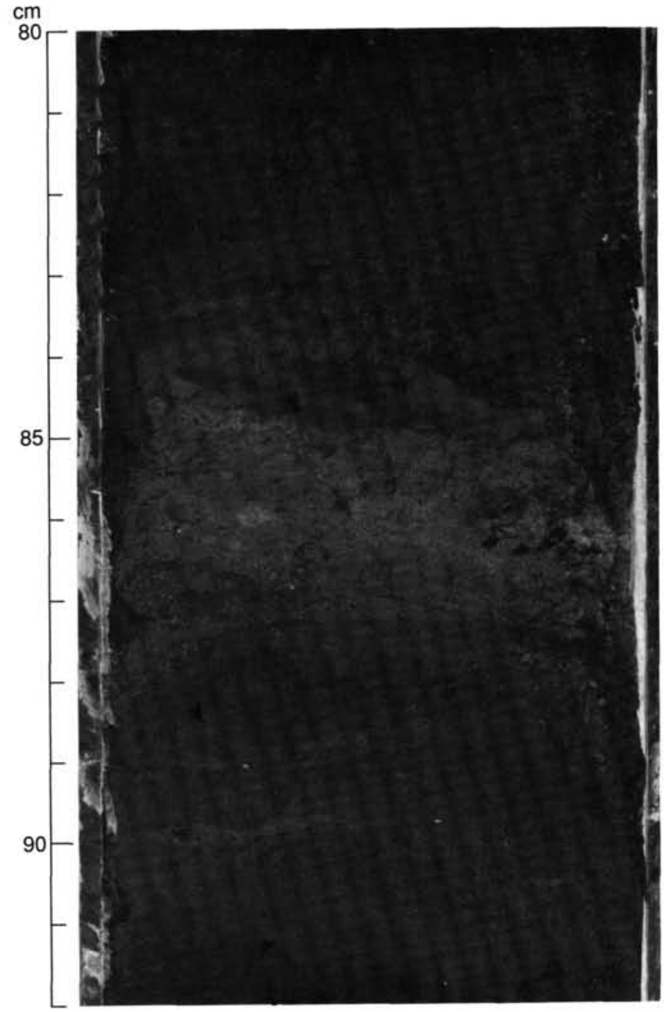

Figure 10. Layer of volcanic ash-rich mudstone, Subunit IIB. Some of the mud-filled microfaults may represent dewatering pipes (arrows), (Sample 112-683A-34X-4, 80–92 cm).

[15 cm]), olive dolomicrite (Sample 112-683B-4X-1, 0–7 cm), black dolomicritic limestone (Sample 112-683B-6X-1, 0–5 cm), and greenish-gray micritic limestone breccia with white calcite veins (Section 112-683B-6X, CC; Fig. 13).

Unit III

Cores 112-683B-7X to 112-683B-9X; depth, 459.5–479 mbsf; age, middle Eocene.

Unit III is marked by a biostratigraphic hiatus (see "Biostratigraphy" section, this chapter) and a stepwise increase in bulk density (see "Physical Properties" section, this chapter), as well as by a sudden lithologic change to well-indurated mudstone. Unit III is further distinguished by an absence of diatoms below Core 112-683B-7X and an increased proportion of sand-sized terrigenous grains, especially feldspar and rock fragments. Volcanic glass occurs throughout Unit III in trace amounts, and a single bed containing 40% glass occurs in Section 112-683B-9X, CC. Pinkish-gray and olive dolomicrite (Sections 112-683B-7X-1 and 112-683B-9X, CC) and micritic limestone breccia (Section 112-683B-8X, CC) also were recovered.

Unit III is well-indurated mudstone with good fissility. Drilling disturbance, fracturing, and brecciation are common, but some bedding and laminations are preserved (Fig. 14). Biotur-

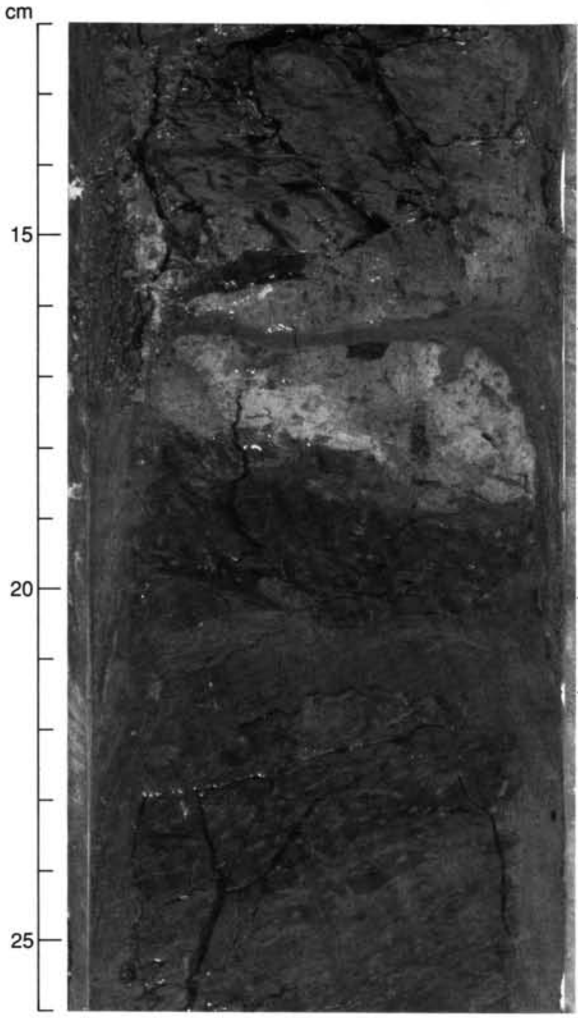

Figure 11. Burrowed, ashy, laminated diatomaceous mudstones of Subunit IIC. Arrows indicate boundaries of drilling biscuits (Sample 112-683A-44X-6, 12–26 cm).

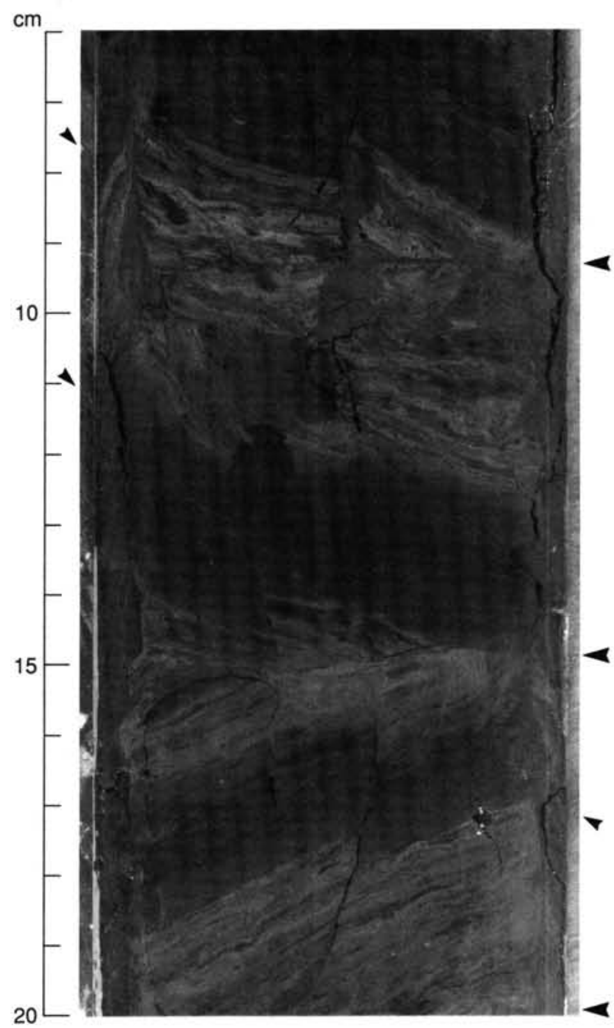

Figure 12. Laminated, diatomaceous mudstone typical of lower part of Subunit IIC. Boundaries between the three drilling biscuits are indicated by large arrows. Extent of drilling disturbance is shown by the mixed and homogenized areas near the sides of the core (small arrows) as well as by rotation of biscuits to produce apparent contrasting dips. Authentic structures preserved in biscuits include distended and necked beds, overprinted by compressional microfaults and small folds (Sample 112-683A-44X-5, 6–20 cm).

bation is minor. Microfaults and fluid-escape structures are preserved in some drilling biscuits. The environment of deposition was probably lower-bathyal hemipelagic.

Carbonate Contents

Measurements of carbonate from samples in Hole 683A generally agree with observations from core descriptions and smear slides. As shown in Figure 15, carbonate values in Subunit IA average between 5% and 10%, whereas for Subunit IB these carbonate values increase to between 10% and 25%. In terms of carbonate content, the boundary between Subunits IB and IC is gradational, when carbonate values decrease to less than 5% in the lower two-thirds of Subunit IC. Subunits ID, IIA, IIB, and IIC typically contain less than 3% carbonate, with minor fluctuations caused by dolomitic or limy interbeds.

Diagenesis

Phosphate

As at Site 682, phosphates are rare at Site 683, perhaps because extensive burrowing prevented buildup of dissolved phosphate in the pore waters of shallowly buried sediments. A thin sand layer in Sample 112-683A-2H-1, 16–17 cm, contains 5% reworked phosphatic peloids, and trace amounts of phosphatic peloids occur in diatomaceous mud in Sample 112-683B-2X-1, 90 cm. A distinctive growth form of apatite occurs sporadically and in generally small to moderate amounts (trace to 10%) between about 410 and 460 mbsf (Cores 112-683A-45X to 112-683B-7X). Referred to as "unidentified" in many of the original smear-slide descriptions, this form of apatite commonly occurs as twin crystal aggregations that radiate from a nucleus (often a pyrite framboid) to form small rosettes 20 to 30 μm in diameter. X-ray diffraction confirms that this mineral is apatite (Fig. 16). Its occurrence only in deeply buried sediments may indicate that, in contrast to the F- and D-phosphates at other sites, this unusual apatite forms relatively late during burial diagenesis. For a detailed definition of F- and D-phosphates, see "Lithostratigraphy" section, Site 679 chapter (this volume).

Authigenic Carbonates

Authigenic calcite and dolomite are comparatively sparse at Site 683 and occur only sporadically in Holes 683A and 683B. We were able to recognize three zones of carbonate diagenesis.

Carbonate diagenetic zone 1 extends from the seafloor to about 159 mbsf (Cores 112-683A-1H through 112-683A-18X-3)

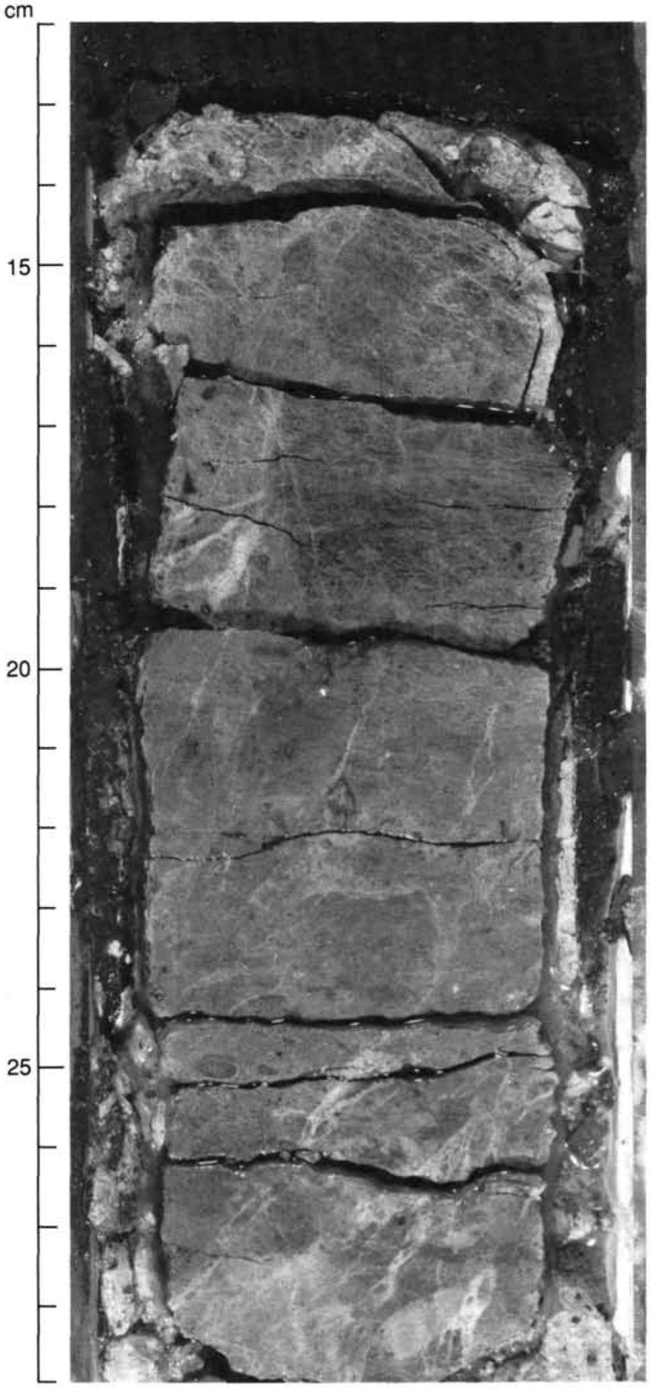

Figure 13. Micritic limestone breccia cut by several generations of calcite veins, Subunit IIC. As discussed in "Diagenesis" subsection, this chapter, this is a unique type of diagenetic limestone. Dark layer at the top is diatomaceous mudstone (Sample 112-683B-6X, CC, 12–29 cm).

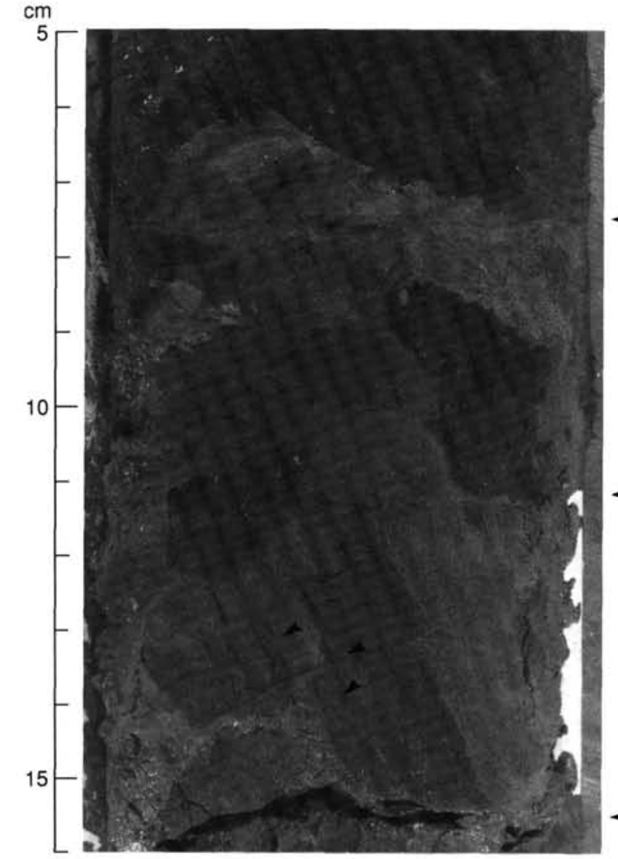

Figure 14. Laminated mudstone of Unit III showing microfaults (small arrows). Large arrows indicate boundaries of drilling biscuits (Section 112-683B-8X, CC).

and includes all except the lower 80 m of Unit I. The authigenic carbonate in this zone mainly consists of small anhedral calcite crystals ("micrite"), but at least a small percentage of dolomite rhombs also are typically present. Figure 17 is an X-ray diffractogram from this zone. Smear-slide estimates of the amounts of authigenic carbonates in zone 1 vary between 2% and 20% (the latter values occur at Samples 112-683A-5H-4, 6 cm, and 112-683A-7H-1, 21 cm). The higher values tend to coincide with layers containing abundant nannofossils and/or foraminifers. Carbonate determinations show total carbonate values between 1% and 26% within zone 1 (Fig. 15). As discussed in the "Inorganic Geochemistry" section (this chapter), the calcium concentration in pore waters decreases from the seafloor to a depth of about 75 mbsf, a trend consistent with calcite precipitation. At this point the trend reverses, and calcium concentrations rise to the base of zone 1 while magnesium concentrations fall, which suggests that calcite replaces dolomite. Authigenic carbonate minerals in this lower part of zone 1 are generally a mixture of about two-thirds anhedral crystals (probably calcite) and one-third dolomite rhombs.

Carbonate diagenetic zone 2 lies between about 159 and 421 mbsf (Cores 112-683A-18X-3 through 112-683B-2X) and encompasses the lower part of Subunit ID and all of Unit II. Authigenic carbonates are rare to absent in this zone, and total carbonate values are generally low but vary unevenly (Fig. 15). The only significant authigenic carbonates in zone 2 occur in a 60-cm-thick layer of unlithified, olive, dolomitic mud containing 55% dolomite rhombs, 15% diatoms, and 20% clay minerals (Sample 112-683A-34X-1, 0–60 cm). A thin unlithified layer having 70% dolomite rhombs occurs in Sample 112-683A-34X-1, 78–82 cm. These layers contain the first abundant dolomite found at Site 683 and occur at about 306 mbsf.

Carbonate diagenetic zone 3, which lies between 459 and 488 mbsf (Cores 112-683B-3X through 112-683B-9X), contains both authigenic calcite and dolomite as well as the first lithified carbonate beds. The shallowest lithified bed is a micritic limestone at about 422 mbsf (Sample 112-683B-3X-1, 10–13 cm), which constitutes a unique type of fine-grained limestone that hereto-

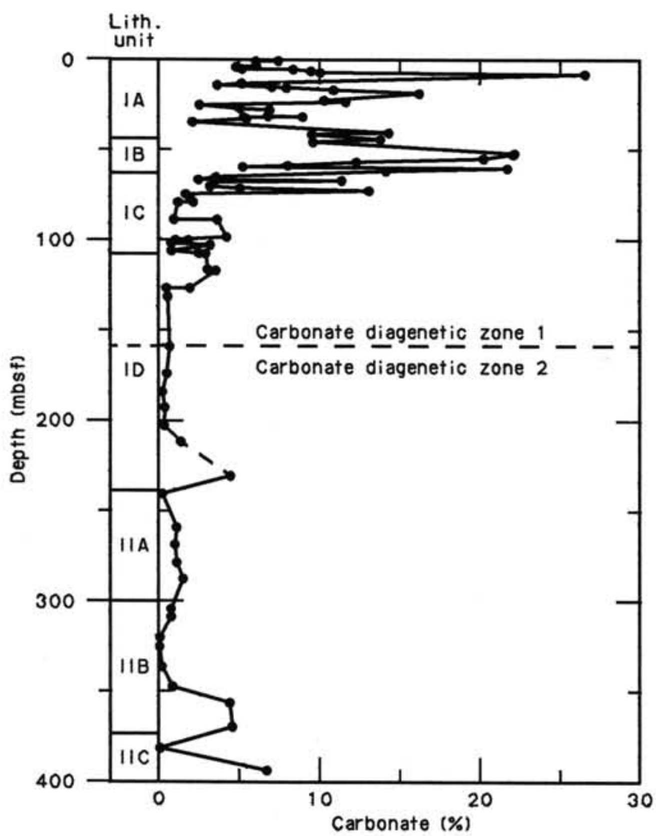

Figure 15. Carbonate content in Hole 683A.

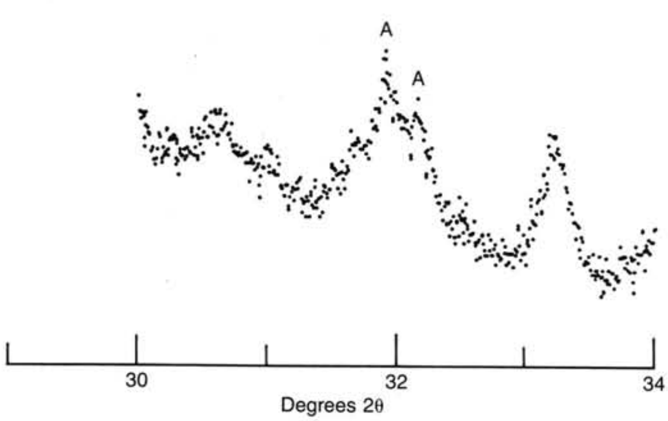

Figure 16. X-ray diffractogram (slow scan) of Sample 112-683A-45X-1, 86 cm, showing characteristic twin apatite peaks at 31.90 and 32.17° 2θ. This identifies the occurrence of an unusual form of authigenic apatite.

fore has not been well documented by carbonate sedimentologists. Below this point, beds containing mostly calcite and those having mostly dolomite occur more or less randomly within a sequence of diatomaceous mud and mudstone layers. Major occurrences of authigenic carbonates are summarized in Table 4.

In summary, carbonate diagenesis at Site 683 is similar to that at Site 682 in that (1) overall, much less authigenic carbonate is produced than at Sites 679 through 681; (2) both authigenic calcite and dolomite formed, but calcite predominates (in contrast to Sites 679 through 681; where dolomite dominates), (3) the first lithified carbonate layers occur at comparatively deep levels (422 mbsf at Site 683 and 108 mbsf at Site 682); (4) there is a tendency for authigenic carbonate minerals, both calcite and dolomite, to be most abundant in layers with high primary calcite content, especially those layers with abundant nannofossils; and (5) variable pore-water chemistries (see "Inorganic Geochemistry" section, this chapter) probably determine whether calcite or dolomite forms.

Pyrite

Pyrite occurs in at least trace amounts in nearly every smear slide examined. Values of 2% to 5% are typical, and in one instance a diatomaceous mud contains 60% small pyrite framboids (Sample 112-683A-18X-3, 105 cm).

Glauconite

Like phosphate, glauconite is rare at Site 683, and that which does occur appears to have been transported from shallow water, as relatively high concentrations occur in the turbidite interbeds. Glauconite peloids occur sporadically and in small amounts (trace to 5%) in the coarse-grained basal parts of thin turbidite layers in Cores 112-683A-1H, 112-683A-2H, and 112-683A-8H through 112-683A-24X; the latter core contains a thin sand layer with 60% glauconite (Sample 112-683A-24X-1, 45–46 cm).

Silicates

Trace amounts of a zeolite (probably clinoptilolite) were observed in one sample (112-683A-25X-6, 10 cm). Starting with Core 112-683A-45X (409.7 mbsf), the matrix in many muds and mudstones has a recrystallized appearance that seems to coincide with increasing consolidation of the sediments. A single X-ray diffractogram from this interval did not reveal any unusual phases, such as opal-CT, but we believe this phenomenon warrants further investigation.

Depositional Environment

All sediments recovered at Site 683 were deposited in lower-bathyal depths, based on benthic foraminifers (see "Biostratigraphy" section, this chapter). The moderate to extensive bioturbation of Unit I and Subunit IIA (late Pliocene–Quaternary) suggests that they were deposited well below the oxygen-minimum zone, whereas the more sparsely bioturbated and laminated sediments of Subunits IIb and IIC and Unit III (middle Miocene–middle Eocene) were probably deposited in oxygen-deficient waters. The subtle color changes in Unit I that result from variations in biogenic silica, biogenic calcite, and terrigenous debris may reflect climatic cycles, with the slightly lighter and more diatom-rich intervals having formed during upwelling phases, and the slightly darker and more clastic-rich intervals having formed during periods of slower biogenic sedimentation.

The low carbonate content of Subunit ID and Unit II (Fig. 15) suggests that they were deposited below the CCD. Isolated higher values of carbonate from these units are either from interbeds of dolomite or limestone, or from concentrations of transported foraminifers in turbidites.

Silt and sandy silt interbeds found throughout the stratigraphic column at Site 683 (especially within Subunit IC) are interpreted as turbidites because of their sharp basal contacts, which in many cases have eroded into the underlying beds, and their higher proportion (60%–90%) of terrigenous clastic debris relative to biogenic components. Some beds exhibit laminated tops, although the tops of most are extensively burrowed. These burrows decrease downward, further supporting the interpretation that these beds were deposited rapidly.

Sparsely disseminated volcanic glass occurs throughout the stratigraphic column at Site 683, suggesting a steady input of fresh or reworked volcanic ash. Rare interbeds of more concentrated ash include both primary ashfall and reworked volcanic ash in probable turbidites. Beds consisting of nearly pure unaltered glass shards with minor euhedral to subhedral quartz and feldspar grains (e.g., Sample 112-683A-29X-1, 43 cm) were in-

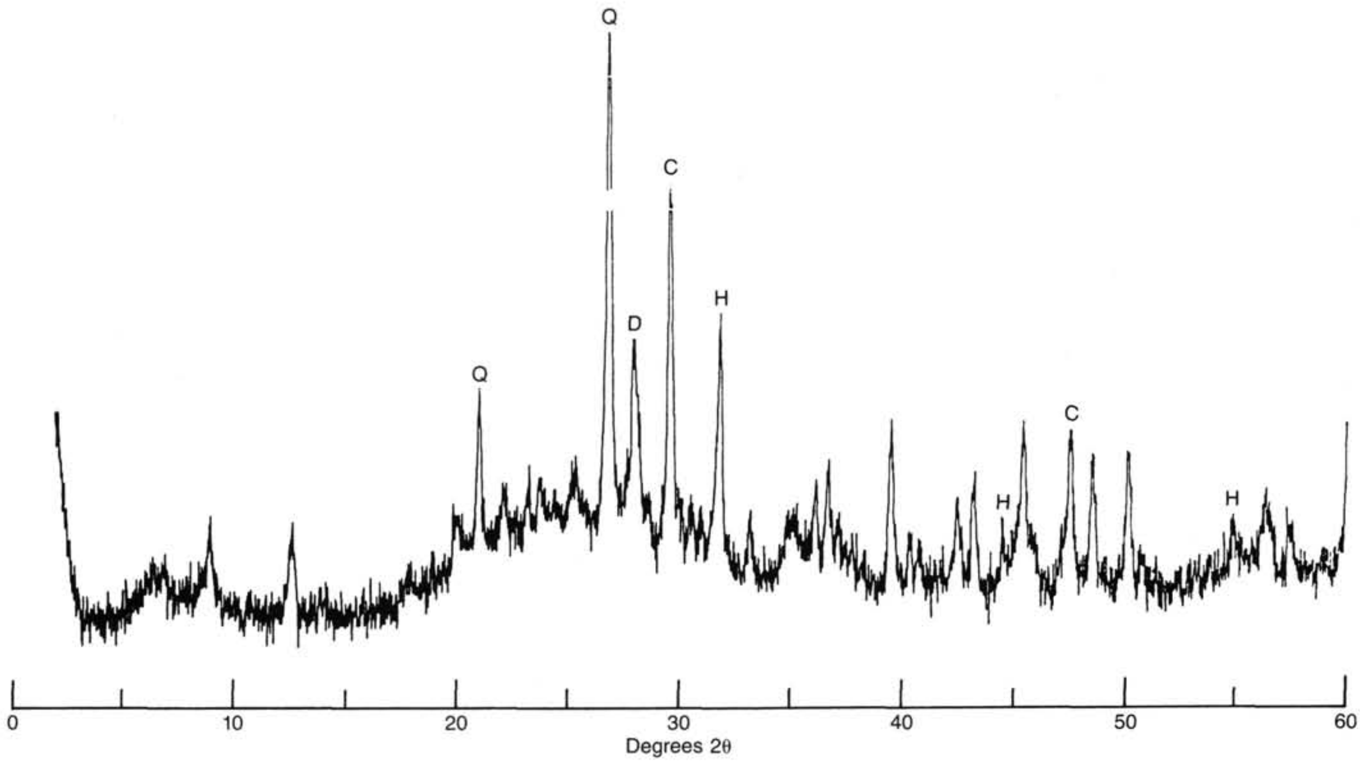

Figure 17. X-ray diffractogram of a sample with abundant authigenic carbonate minerals, from carbonate diagenetic zone 1 (Sample 112-683A-5H-4, 5 cm). Major labelled peaks are Q = quartz, P = plagioclase, C = calcite, and H = halite (an artifact).

Table 4. Authigenic carbonates at Site 683.

Core/section interval (cm)	Depth (mbsf)	Description
112-683B-4X-1, 0–7	431.1	7-cm layer of olive dolomicrite (90% euhedral rhombs, 10% well-preserved diatoms); this dolomite, which is slightly lithified, apparently replaced a diatomaceous mud.
112-683B-6X-1, 2–5	450.0	Thin, micritic limestone layer with 5%–10% dolomite rhombs.
112-683B-6X, CC, 13–33	453.0	20-cm bed of greenish gray micritic limestone (100% very fine-grained anhedral calcite crystals) traversed by fractures filled with calcite (see Fig. 13).
112-683B-7X-1, 45–47 and 80–82	459.9 and 460.3	Two thin layers of unlithified dolomitic micrite (75% anhedral calcite, 10% dolomite rhombs, 15% nannofossils).
112-683B-8X, CC and -683B-9X, CC	478.3 and 478.5	Both core-catcher samples contain broken fragments of olive dolomite.

terpreted as primary ashfall. Beds containing brown, devitrified glass shards mixed with clear shards, rounded mineral and rock fragments of probably clastic origin, or biogenic grains were interpreted as reworked volcanic ash (e.g., Samples 112-683A-4H-3, 131 cm, and 112-683B-6X-3, 10–15 cm). Angular pebbles of volcanic ash contained within intervals of diatomaceous mud also were interpreted as reworked (e.g., Sample 112-683A-41X-4H, 6–107 cm).

Structure

Drilling-Induced Structures

Almost all the XCB cores recovered exhibit moderate to extensive drilling disturbance, which typically consists of a homogenized drilling slurry around the outside of the core. Penetration of somewhat harder sediments produces "drilling biscuits," defined by veins and fractures along which the peripheral drilling slurry has penetrated (Figs. 11 and 12). Only structures within the drilling biscuits are authentic. In the laminated mudstones of Subunit IIC, rotation of individual drilling biscuits relative to each other produced features resembling recumbent chevron folds (Fig. 18).

As the degree of lithification increases and the mudstones develop fissility (Fig. 19), fracturing caused by drilling becomes more and more extensive. Biscuits become progressively smaller (Fig. 20), until it is no longer clear how much of the brecciation is an authentic predrilling structure. One must use extreme caution when interpreting such features. The shipboard scientific party did not always agree on a common interpretation.

Deformational Structures

Slump Folds and Soft-Sediment Deformation

Bedding that was inclined at angles of 15°–75° relative to the vertical axis of the core occurred in Sample 112-683A-3H-5, 102–108 cm, and Sections 112-683A-4H-1 to 112-683A-4H-3. Because these inclined beds lie within sequences of horizontal beds and are clearly discordant, we interpreted them as resulting from slumping. A single fold nose interpreted as a probable slump fold occurs in Sample 112-683A-42X, CC, 5–15 cm, and small slump folds and convolute bedding occur throughout the finely laminated mudstones of Subunit IIC (Figs. 11 and 12). Contorted, necked, and boudinaged beds are common wherever bedding and lamination are not destroyed by bioturbation or drilling disturbance. We interpreted these features as representing extension while the sediments were still soft.

Dewatering Structures

In a few cores, subvertical fractures filled with mud cut across this bedding. These filled fractures are typically located in fine muds just above somewhat coarser beds of sandy or silty muds. We interpreted these features as dewatering veins. We observed

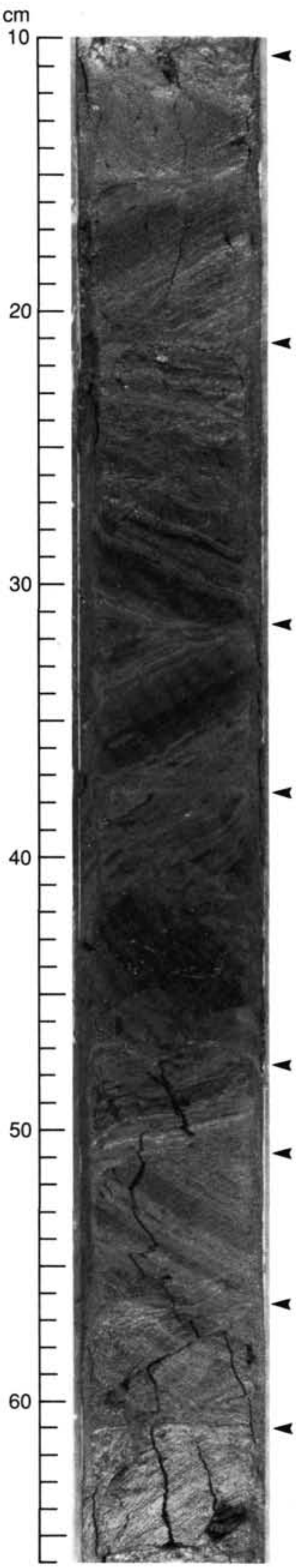

Figure 18. Rotation of drilling biscuits in laminated mudstones of Subunit IIC produced features resembling recumbent chevron folds. Only the structural relationships in biscuits are authentic. Biscuit boundaries are indicated by arrows (Sample 112-683A-44X-5, 10–66 cm).

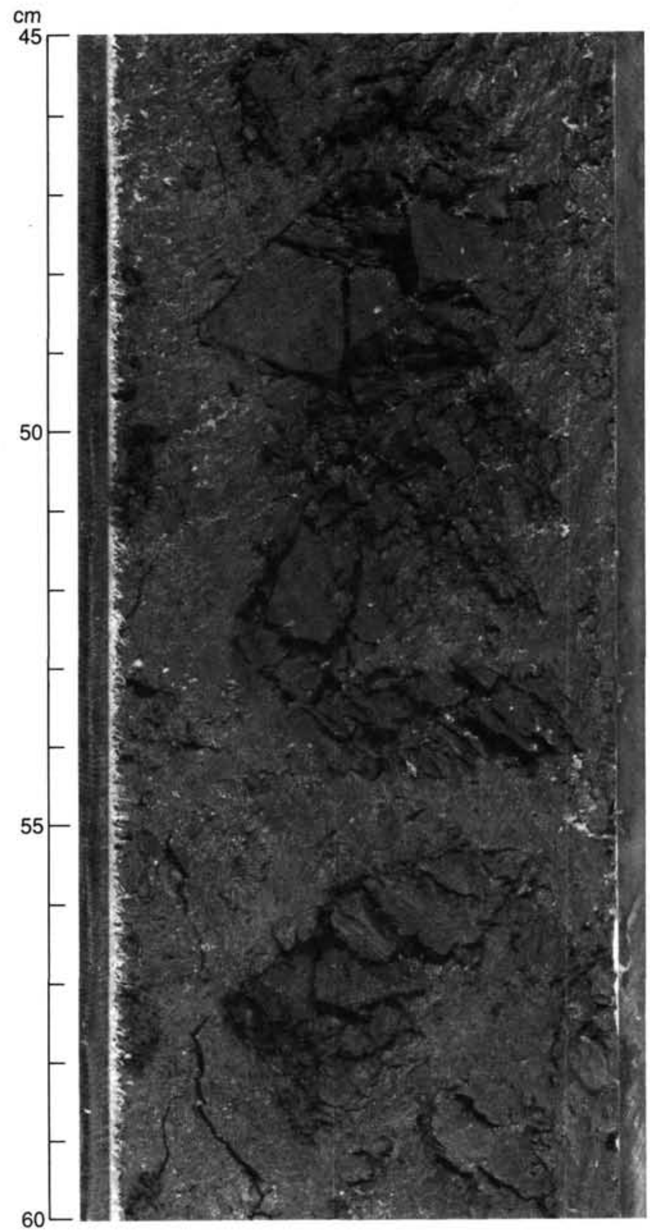

Figure 19. Fissile mudstone within drilling biscuits, Subunit IIB, with fractures resulting from drilling disturbance (Sample 112-683A-37X-3, 45–60 cm).

them at depths ranging from 202 (Core 112-683A-23X-1) to 478 mbsf (Section 112-683B-8X, CC), but because of the extensive bioturbation (especially in Unit I) we could not determine their actual extent. In addition, many of the extensional and compressional microfaults discussed next seem to localize mud-filled veins. These also represent probable dewatering veins (Figs. 9, 10, and 14).

Microfaults

Numerous microfaults occur throughout Holes 683A and 683B, although these are difficult to see because of the generally homogeneous nature of the sediments. Once the cores dry out, fine structural details are almost impossible to see unless they cut across strongly contrasting lithologic boundaries, such as burrows filled with a different color of mud (Fig. 5) or the base of a turbidite bed (Fig. 6). Both extensional and compressional

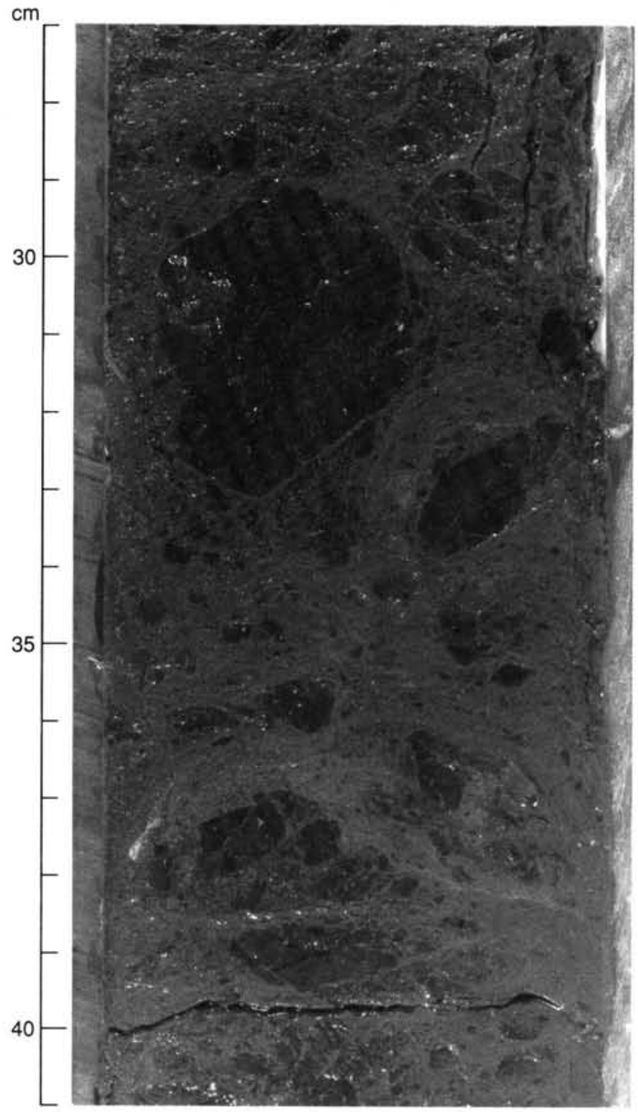

Figure 20. Breccia composed of dolomicrite fragments in dolomicritic diatomaceous mud. Most, if not all, of this brecciation is probably due to drilling disturbance (Sample 112-683B-7X-1, 27–41 cm).

microfaults are present, as well as faults perpendicular to bedding (Figs. 5, 9, 12, and 14). The extensional microfaults typically occur where extension by soft-sediment deformation occurred. These microfaults are commonly filled with mud, as if they were serving as dewatering conduits and fine material was being transported along them. Although relationships are not always clearcut, in at least one case the compressional microfaults offset the extensional features (Fig. 12) and therefore are younger.

Fissility and Fracturing

As the muds become progressively more indurated and make the transition into mudstone, they begin to develop an incipient fissility or parting that is roughly parallel to bedding. As seen in Figure 19, individual sheets of mudstone 1 to 2 mm thick tend to break along conjugate fractures that cut across the fissility at angles of 45° to 60°, producing small broken chips. This fissility is distinct from scaly foliation in that the ends of the fragments are blunt rather than pointed and are wedge-shaped or blocky rather than lenticular in cross sections. Furthermore, the fracture surfaces are not polished, grooved, or slickensided, suggesting that no movement has occurred along them. Fissility begins to appear at a depth of about 42 m in Sections 112-683A-6H-7 and 112-683A-6H-8, but is best developed below depths of about 240 m.

Scaly Cleavage

We did not observe well-developed scaly cleavage in Site 683 cores, but in some cases (e.g., Section 112-683A-45X-1), the pervasive fissility begins to resemble scaly foliation. Individual chips of mudstone exhibit a slight polish and rare slickenlines on some, but not all, surfaces. However, we did not observe transport along these surfaces nor offset of bedding by these surfaces, suggesting that these surfaces do not represent a true scaly foliation.

BIOSTRATIGRAPHY

Two holes were drilled at Site 683 that penetrated hemipelagic middle- to lower-bathyal diatomaceous muds. Holocene to early Miocene age to 419.2 mbsf in Hole 683A and to 459.5 mbsf in Hole 683B. Hole 638B terminated at 488.0 mbsf in middle Eocene, upper- to upper-middle bathyal sediments (Figs. 21 and 22).

Two hiatuses were found at approximately 250 and 360 mbsf, separated by a middle to lower Miocene slump deposit. We found a third hiatus in which most of the Oligocene and upper Eocene were missing at 470 mbsf.

Diatoms are abundant and well preserved to a depth of 419.2 mbsf. Other microfossil groups occurred sporadically throughout the section. Their preservation ranged from poor to good.

Benthic foraminifers indicate a lower-bathyal environment throughout Hole 683A.

Sedimentation rates are plotted in Figure 22 and detail the high resolution in a complete Quaternary to upper Pliocene section of hemipelagic sediments. Radiolarians and diatoms reveal an identical sequence of events (Fig. 23) at this site and at sites from the equatorial Pacific, DSDP Leg 85 (Nigrini, 1977; Baldauf, 1985).

Diatoms and Silicoflagellates

Diatoms were abundant and well preserved in all core-catcher samples studied from Hole 683A to 419.2 mbsf; they were abundant and well preserved in Sections 112-683B-1X, CC through 112-683B-6X, CC (403.7–452.9 mbsf) in Hole 683B. No recognizable diatom frustules were found in core-catcher samples of Cores 112-683B-7X and 112-683B-9X. A middle to early Miocene assemblage that we thought represented downhole contamination occurred in Section 112-683B-8X, CC (478.3 mbsf) .

An undisturbed, diatom-rich, Quaternary to upper Pliocene hemipelagic section revealed several diatom events in high resolution. These were described by Barron (1985), Baldauf (1985), Burckle (1977), and Koizumi (1986) from equatorial and northern Pacific deep-sea sections and included *Rhizosolenia matuyama*, *Rhizosolenia praebergonii* Zone (Subzone C), *Thalassiosira convexa* LAD, *Rhizosolenia praebergonii* Zone (Subzone B), and *Rossiella tatsunokuchiensis* LAD. All these events and zonal boundary definitions agreed well with Baldauf's (1985) data from high-resolution, APC sites in the eastern equatorial Pacific.

Based on these well-dated datums and zones, we inferred a Quaternary to late Pliocene sedimentation rate of 100 m/m.y. for the interval from 0 to 246 mbsf, spanning the last 2.5 m.y. (Fig. 22).

The assemblages of this interval consist of a mixture of oceanic and near-shore coastal upwelling members (Schuette and Schrader, 1979, 1981), which indicates constant transporting of near-shore sediment material to this site. This also is supported by a noticeably increased silt and sand content (see "Lithostratigraphy" section, this chapter). The amount of displaced shallow-water benthic diatoms was noticeable over this interval.

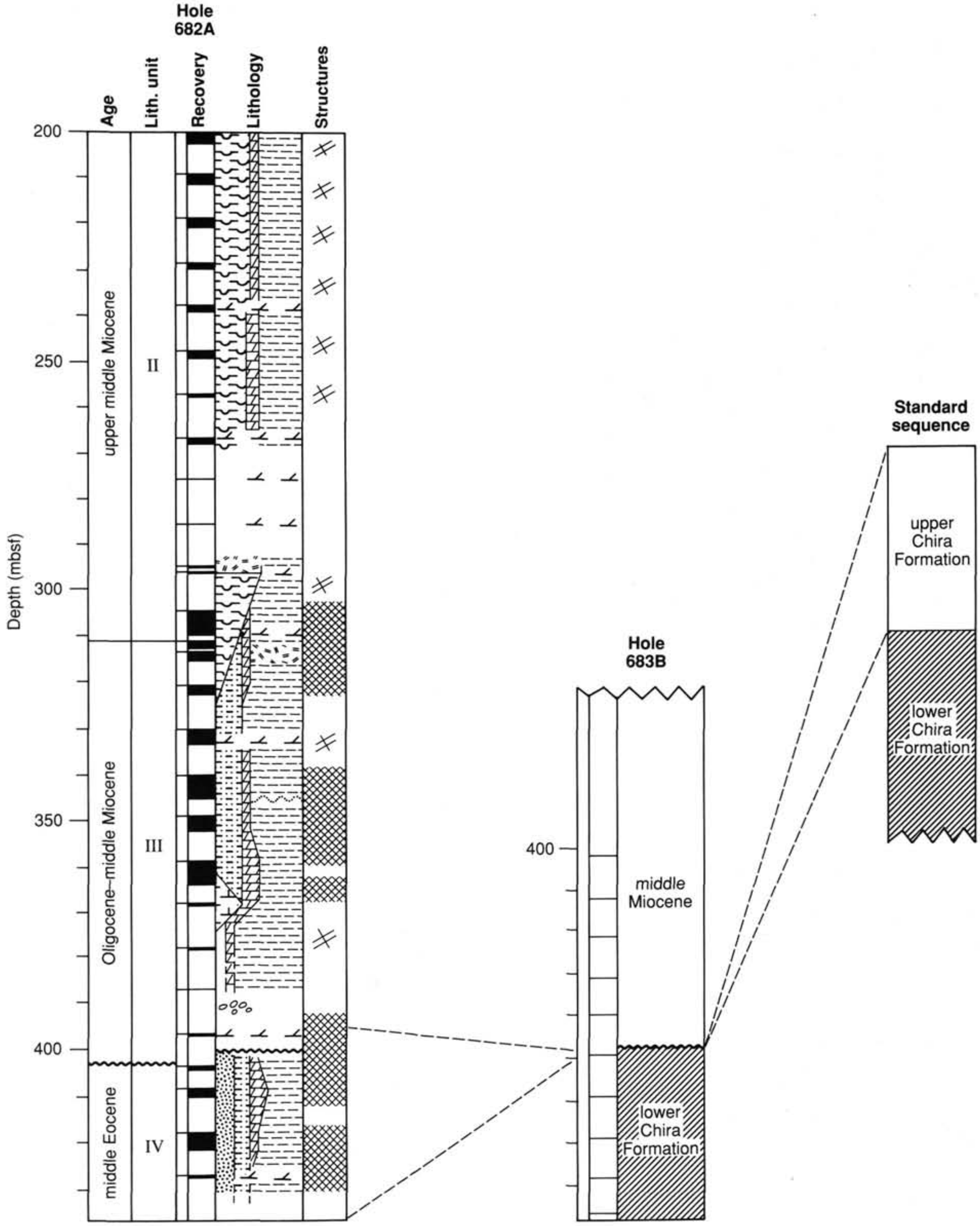

Figure 21. Correlation of the lower parts of Holes 682A and 683B with the onshore Standard Peruvian sequence. Lower Chira Formation was penetrated only in Hole 683A. Upper Chira Formation is missing from Hole 683B.

The Pleistocene/Pliocene contact in Core 112-683A-17X (144.7–145.6 mbsf) is characterized by the scarcity of *Pseudoeunotia doliolus* and relative abundance of *Nitzschia fossilis*.

Mesocena quadrangula ranges slightly above the *Rhizosolenia matuyama* LAD and first appears slightly above the first occurrence of *R. matuyama*. This species is a useful Quaternary biostratigraphic indicator whenever the more temperate species *Rhizosolenia matuyama* is absent. *Distephanus pulchra* occurred sporadically in Cores 112-683A-1H through 112-683A-13X, ranging below the first Pleistocene occurrence of *Mesocena quadrangula*.

Diatom floras below Core 112-683A-27X (241 mbsf) indicate mass slumping of lower upper Miocene to lower Miocene strata.

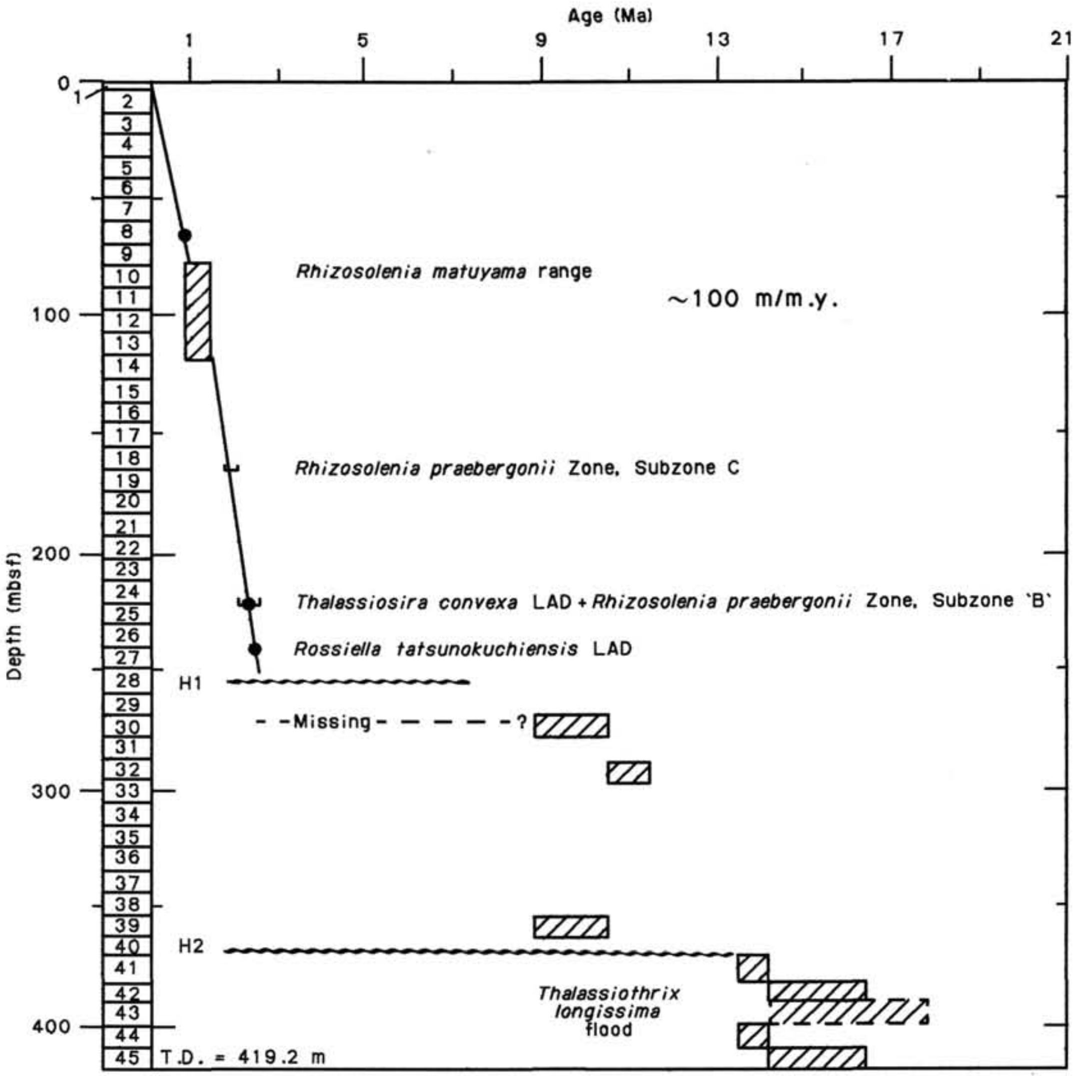

Figure 22. Age vs. depth plot of diatom data and zones. Note hiatuses 1 (H-1) and 2 (H-2). Sedimentation rate for the upper 100 m is around 100 m/m.y. Slumped material occurs between Cores 112-683A-28X to 112-683A-45X. The *Thalassiothrix longissima* flood interval extends from Cores 112-683A-41X to 112-683A-45X.

Zones recognized include the *Craspedodiscus coscinodiscus* Zone, *Actinocyclus moronensis* Zone, *Coscinodiscus lewisianus* Zone, and *Denticulopsis nicobarica* Zone.

A hiatus (H-1 in Fig. 22) occurs between Sections 112-683A-27X, CC and 112-683A-28X, CC, which removed part of the lower Pliocene and most of the upper Miocene sections and produced a gap of approximately 7 m.y.

A second hiatus (H-2 in Fig. 22) may be present in Core 112-683A-38X (344–347 mbsf), separating the *Thalassiothrix longissima* flood assemblage in Cores 112-683A-39X through 112-683A-44X (353.7–409 mbsf) from the more diverse assemblages above (Core 112-683A-39X) and below (Core 112-683A-45X) this event.

The "needle" assemblage of middle Miocene age represents cold and stress conditions and corresponds to the cold event that we previously recognized in Cores 112-682A-29X through 112-682A-30X (266–276 mbsf). One difference is that at Site 682 this assemblage was characterized by increased numbers of *Coscinodiscus marginatus* and was thought to have occurred at about 13 to 14.2 Ma. At Site 683 this event cannot be dated more precisely owing to the general lack of good biostratigraphic marker species. This assemblage is *not* characteristic of coastal upwelling but is associated with cold-water current systems. We found an identical assemblage in Core 112-683B-6X (450–453 mbsf) that allowed us to correlate the two holes; this unit is compressed to one core in Hole 683B, compared with five cores in Hole 683A.

Hiatus H-1 occurs in Hole 683A at about 250 mbsf with a jump from middle Pliocene to middle Miocene assemblages; it may correspond to the hiatus found at Site 682, where the break occurred at around 110 mbsf (Core 112-682A-13X) with a jump from the lower Pliocene to the upper Miocene.

Diatom assemblages from the middle portions of both the Ballena and Delfin industrial wells clearly reveal a middle Miocene age, contrary to published biostratigraphic age determinations of the Oligocene (Schrader and Cruzado, 1987). The diatom assemblages in the Ballena well are exceptionally well preserved and give true indications of strong coastal upwelling conditions during the late early Miocene through the early late Miocene.

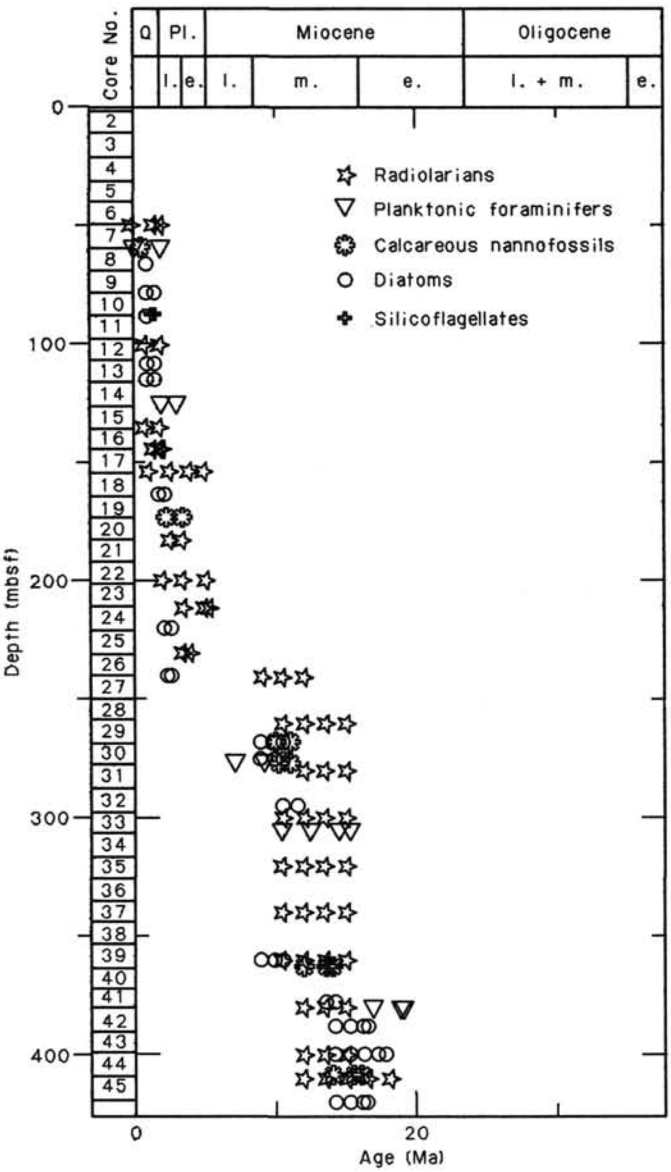

Figure 23. Occurrences and ranges of microfossil data in the Miocene–Holocene interval at Hole 683A.

Silicoflagellates

All core-catcher samples (along with a few additional samples) were studied for silicoflagellates in Hole 683A. Preliminary data show that silicoflagellates are present from the top of the hole down to Core 112-683A-45X (418 mbsf), covering part of the Neogene and the Quaternary.

The Pliocene and Quaternary intervals (Cores 112-683A-1H to 112-683A-25X, 0–228.3 mbsf) show close similarities with Sites 680 to 682. *Dictyocha messanensis aculeata* was found only in Section 112-683A-7H, CC (59.2 mbsf), but *Mesocena quadrangula* and *Distephanus bioctonarius bioctonarius* were observed in several samples. The lowest occurrence of *D. bioctonarius bioctonarius* was noted in Section 112-683A-10X, CC (79.7 mbsf) within the range of *Mesocena quadrangula*, which occurs between Sections 112-683A-9H, CC and 112-683A-12X, CC (78.5–106.5 mbsf). Between Cores 112-683A-16X and 112-683A-21X (137.1–185.3 mbsf), *Distephanus speculum speculum* f. *pentagona* was a frequently found constituent. *Dictyocha messanensis stapedia* and related forms having a vertical apical bar were found down to Core 112-683A-25X (228.3 mbsf).

Below Core 112-683A-25X, the true ranges of silicoflagellate species are obscured because of slumped material, which is indicated by the erratic occurrence of *Corbisema triacantha*, at least in Cores 112-683A-27X, 112-683A-31X, and 112-683A-33X, as well as *Distephanus stauracanthus* f. *octogonus* in Section 112-683A-27X, CC (241 mbsf). Dictyoid forms having a horizontal apical bar (most of which belong to *Dictyocha varia*) are present in varying frequencies from Core 112-683A-27X down to the base of the hole. The occurrence of *Corbisema triacantha* in Core 112-683A-35X and below is considered autochthonous, also the rather common occurrence of *Distephanus stauracanthus* f. *octagonus* in Cores 112-683A-31X to 112-683A-33X may be *in-situ*, although most of the interval between Core 112-683A-27X and the terminal Core 112-683A-45X is represented by badly disturbed, slumped material, with only a few sections in continuous sequence. The most common forms in this part of the sequence are those of the *Distephanus crux* group. Part of the sequence seems to be missing at about Cores 112-683A-26X and 112-683A-27X (part of the lowest Pliocene and most of the upper Miocene).

Silicoflagellates were noted in Cores 112-683B-1X to 112-683B-6X in Hole 683B and include *Dictyocha varia* and members of the *Distephanus* group, which indicates a middle Miocene age. Only a few displaced Miocene species were found in Cores 112-683B-8X and 112-683B-9X, and these may represent downhole contamination during coring. The Eocene section in Cores 112-683B-7X through 112-683B-9X contains no silicoflagellates.

Actiniscidians and ebridians were observed in various samples throughout Hole 683A and in Cores 112-683B-1H to 112-683B-6X of Hole 683B, with *Actiniscus pentasterias* being the most common species. *Actiniscus (?) elongatus* was noted only between Cores 112-683A-19X and 112-683A-39X in Hole 683A, and *Parathranium clathratum*, *Ammodochium serotinum* as well as *Hermesinella conata* occur sporadically in the slumped material below Core 112-683A-25X in Hole 683A and down to Core 112-683B-6X in Hole 683B.

Calcareous Nannoplankton

Quaternary calcareous nannoplankton were found in Hole 683A in rather monotonous assemblages down to Core 112-683A-9H, with boundaries between Zones NN20 (*Gephyrocapsa oceanica* Zone) and NN21 (*Emiliania huxleyi* Zone) in Core 112-683A-1H and between Zone NN19 (*Pseudoemiliania lacunosa* Zone) and NN20 (*G. oceanica* Zone) in Core 112-683A-7X. These assemblages are dominated by *Gephyrocapsa* species, all other species such as *Helicosphaera carteri*, *Cyclococcolithus leptoporus*, and *Coccolithus pelagicus* are only minor constituents. Occasional blooms were noted; the most obvious ones occurred in Samples 112-683A-9H-5, 2 cm (74.7 mbsf) and 112-683A-15X-1, 2 cm (125.7 mbsf), with the latter probably of Pliocene age.

The interval between Cores 112-683A-10X and 112-683A-26X is barren of calcareous nannoplankton, with the exception of the previously mentioned bloom in Core 112-683A-15X and part of Core 112-683A-19X, where a rather insignificant nannoplankton assemblage was observed. The assemblage includes common *Gephyrocapsa* species, rare to few *Coccolithus pelagicus*, *C. miopelagicus*, *Cyclococcolithus leptoporus*, rare specimens of *Cyclococcolithus macintyrei*, and *Discoaster brouweri*. Since *Reticulofenestra pseudoumbilica* could not be found, this assemblage indicates late Pliocene age and may represent nannoplankton Zone NN18 (*Discoaster brouweri* Zone).

From Core 112-683A-27X to Core 112-683A-45X at 419.2 mbsf, calcareous nannoplankton are present in chaotic assemblages representing slumped material from middle Miocene strata, except in a barren interval between Cores 112-683A-34X and 112-683A-38X. The upper Miocene was not recognized and is probably missing. Even though most samples indicate badly mixed assemblages, some levels seem to represent larger blocks of undisturbed material that allow us to recognize zones. Core 112-683A-30X was placed in the middle Miocene nannoplankton Zone NN8 (*Catinaster coalitus* Zone), based on the presence of the nominate species in several samples within Core 112-683A-30X. Part of Core 112-683A-39X represents nannoplankton Zone NN6 (*Discoaster exilis* Zone), with rather common *Cyclococcolithus floridanus* and *Discoaster exilis*. In Core 112-683A-40X, nannoplankton Zones NN4 (*Helicosphaera ampliaperta* Zone) to NN6 (*D. exilis* Zone) were identified, although in reversed order. In Core 112-683A-44X, nannoplankton Zone NN5 (*Sphenolithus heteromorphus* Zone) was recognized by the frequent presence of *Sphenolithus heteromorphus* without additional *Helicosphaera ampliaperta* throughout the core. The assemblage is contaminated with younger, slumped material.

Preservation is good to moderate in the Quaternary part of the sequence and only moderate to poor in the slumped material, depending on the grade of disturbance and sorting of the assemblages. A nearly pure, discoaster-bearing layer was found in Section 112-683A-42X, CC (381.9 mbsf). It is associated with abundant and concentrated diatoms of the genus *Thalassiothrix* and a flood of slightly rounded dolomite rhombs.

In Hole 683B, Cores 112-683B-1X to 112-683B-6X contained middle Miocene calcareous-nannoplankton assemblages. Nannoplankton Zone NN5 (*Sphenolithus heteromorphus* Zone) was identified in Cores 112-683B-1X, 112-683B-4X, and 112-683B-5X, based on the presence of *Sphenolithus heteromorphus* and the absence of *Helicosphaera ampliaperta*. Core 112-683B-3X and Sample 112-683B-4X-1, 8–9 cm, were placed in nannoplankton Zone NN6 (*Discoaster exilis* Zone). Several samples from Cores 112-683B-2X and 112-683B-6X contain only meager middle Miocene assemblages and cannot be confined to a certain nannoplankton zone. Cores 112-683B-1X and 112-683B-2X are from the same level as Cores 112-683A-44X and 112-683A-45X.

We observed moderately preserved, middle Eocene calcareous nannoplankton in Core 112-683B-7X. This observation signifies a prominent hiatus between Cores 112-683B-6X and 112-683B-7X, with the lower Miocene, Oligocene, and upper Eocene missing. Thus, this hiatus covers a time interval of about 26 m.y. The upper part of Core 112-683B-7X down to Sample 112-683B-7X-2, 98–99 cm (462 mbsf) was placed in nannoplankton Zone NP17 (*Discoaster saipanensis* Zone) with the nominate species present in fair numbers. In Sample 112-683B-7X-2, 30 cm, and below, we found *Chiamolithus solitus*. The last occurrence of this species indicates the top of nannoplankton Zone NP16 (*Discoaster tani nodifer* Zone). Accordingly, this sample marks Zone NP16, which extends down to the base of Hole 638B (total depth of 488 mbsf). However, Sections 112-683B-7X, CC and 112-683B-8X, CC (30 cm) had to be placed in nannoplankton Zone NP17 and probably represent downhole contamination.

Cores 112-683B-8X and 112-683B-9X were greatly disturbed by drilling and contained Eocene sediments together with displaced Miocene material from above. Miocene contamination was recognized in Sections 112-683B-8X, CC (10 cm), 112-683B-8X, CC, 112-683B-9X-CC (2 cm) (nannoplankton Zone NN5), and 112-683B-9X, CC.

"Shallow-water" species such as *Zygrhablithus bijugatus*, *Braarudosphaera bigelowi*, *Micrantholithus* sp., and *Discolithina* species were found in the Eocene part of Hole 683B, although in lesser numbers than at Site 682.

Radiolarians

We postulated that two hiatuses occur at Site 683 as no upper Miocene nor lower Miocene to upper Eocene faunas could be found. This thick, middle Miocene sequence was similar to that encountered in Hole 682A but contained much better preserved radiolarians. These are well preserved and abundant from the Holocene to Miocene and are poorly to moderately preserved in the Eocene. To separate radiolarians from Eocene samples, we had to employ techniques used for Mesozoic rocks (De Wever et al., 1979; De Wever, 1982).

Hole 683A

Radiolarians were present in all core-catcher samples from this hole. Their preservation was generally good.

Cycladophora davisiana, *Dictyophimus infabrictus*, *Stichopylium bicorne*, *Eucyrtidium hexagonatum*, *Lamprocyclas maritalis*, *Polysolenia arktios*, and *Carpocanium papillosum* were found in Sections 112-683A-1H, CC to 112-683A-6H, CC (2–50 mbsf). *Lamprocyrtis nigriniae* was generally common; this species first appears near the base of the *Anthocyrtidium angulare* Zone (Quaternary). We did not find any *Collosphaera* species. We list only species of stratigraphic importance in the following discussion.

Lamprocyrtis nigriniae was absent in Core 112-683A-7H, but a few *L. neoheteroporos* did occur. *L. nigriniae* was rare in Sections 112-683A-8H, CC to 112-683A-15X, CC, coexisting with its ancestor *L. neoheteroporos*. *Lamprocyrtis neoheteroporos* becomes common from Sections 112-683A-11X, CC to 112-683A-17X, CC (88.9–145.7 mbsf). This assemblage indicates the early Quaternary period (1.3 to 1.8 Ma).

L. nigriniae was absent in Section 112-683A-16X, CC (137.1 mbsf), but *Theocorythium trachelium* was still present. This species appears at the base of the Quaternary (the most basal part of the *A. angulare* Zone). *L. nigriniae* first appears near the base of the *A. angulare* Zone. Consequently, this sample belongs to the base of the *A. angulare* Zone (very early Quaternary).

L. neoheteroporos and *Theocorythium vetulum* were found in Section 112-683A-17X, CC. In the absence of *L. nigriniae*, these species indicate the lowermost *A. angulare* Zone or the *Pterocanium prismatium* Zone (earliest Quaternary or latest Pliocene, 1.5 to 2.0 Ma).

Stichocorys peregrina was first encountered in Section 112-683A-20X, CC (173.6 mbsf), indicating the top of the *Spongaster pentas* Zone (early late Pliocene).

Stichocorys peregrina, *Theocorythium vetulum*, and *Botryostrobus aquilonaris* were found in Sections 112-683A-21X, CC (185.3 mbsf) and 112-683A-22X, CC (192.8 mbsf). These species indicate the upper *S. peregrina* Zone and the *S. pentas* Zone, which represents all but the earliest and latest Pliocene.

Phormostichoartus fistula, *Botryostrobus aquilonaris*, and *Phormostichoartus doliolum* co-occurred in Section 112-683A-23X, CC (202.3 mbsf). These species indicate the lower part of the *Spongaster pentas* Zone to the upper part of the *Stichocorys peregrina* Zone (early Pliocene).

Lamprocyrtis heteroporos was found in Section 112-683A-24X, CC (212 mbsf), which indicates a Pliocene age, according to Kling (1978).

Pterocanium prismatium, *Stichocorys peregrina*, and *Didymocyrtis tetrathalamus* were found in Section 112-683A-25X, CC (228.3 mbsf). These species indicate the upper part of the *Spongaster pentas* Zone (early late Pliocene to late early Pliocene). Taking into account the age assignment of Section 112-683A-23X, CC, this sample was placed in the late early Pliocene.

Diastus petterssoni and *D. antepenultima* were found in Section 112-683A-26X, CC. These indicate the *D. petterssoni* Zone (late middle Miocene). Therefore, a jump in ages exists between Sections 112-683A-25X, CC and 112-683A-26X, CC (228.3–230.7 mbsf). The cause may be a hiatus or a reworked Miocene fauna. No lowest Pliocene or upper Miocene radiolarian species were found.

Stichocorys delmontensis, *S. wolffii*, *Didymocyrtis laticonus*, and *D. hughesi* were found in Sections 112-683A-27X, CC to 112-683A-X, CC (241 mbsf). These indicate the *D. petterssoni* Zone (late middle Miocene).

Didymocyrtis mammifera and *D. laticonus* were found in Sections 112-683A-X, CC to 112-683A-43X, CC (394.4 mbsf). These indicate the upper part of the *Dorcadospyris alata* Zone (middle middle Miocene).

D. mammifera, *Stichocorys wolffii*, and *S. delmontensis* were found in Section 112-683A-44X, CC (409 mbsf). These indicate the *D. petterssoni* Zone to the *Calocycletta costata* Zone (middle Miocene to the late early Miocene).

Hole 683B

Radiolarians were present in all core-catcher samples. Their preservation is good in the Miocene and poor to moderate in the Eocene; they are common to abundant in the Miocene and few to common in the Eocene.

Diartus petterssoni, *D. laticonus*, *D. mammifera*, and *Stichocorys wolffii* were found in Sections 112-683B-1X, CC to 112-683B-6X, CC (403.7–452.9 mbsf). This assemblage indicates the *D. petterssoni* Zone (late middle Miocene).

Dictyoprora ovata, *Sethochytris triconiscus*, *Calocyclas hispida*, *Dictyoprora amphora*, *D. mongolfieri*, *Eusyringium fistuligerum*, *Podocyrtis papalis*, and *Lychnocanomma bellum* were found in Sections 112-683B-7X, CC to 112-683B-9X, CC (462.8–478.5 mbsf). This assemblage indicates a range from the middle part of *Podocyrtis mitra* Zone to the middle part of *Podocyrtis geotheana* Zone, which represents the late middle Eocene to early late Eocene (according to Riedel and Sanfilippo, 1978; Nigrini, 1977; and Kling, 1978).

Planktonic Foraminifers

Hole 683A

All core-catcher samples were examined for planktonic foraminifers. Above Section 112-683A-7H, CC, planktonic foraminifers are abundant and generally well preserved; these represent part of the Pleistocene to Holocene. Below Section 112-683A-8H, CC, samples are barren or contain only rare specimens. Age-diagnostic species were recognized in Sections 112-683A-30X, CC and 112-683A-33X, CC.

Globigerina bulloides, *G. quinqueloba*, *Neogloboquadrina dutertrei*, and *N. pachyderma* were common in Sections 112-683A-1H, CC through 112-683A-7H, CC. These indicate the temperate Peruvian upwelling regime. These samples were placed in the Pleistocene, based on the occurrence of *Hastigerinopsis riedeli* (Poore, 1979). *Globorotalia crassaformis* and *G. inflata* did not occur in other holes in the Lima Basin (Sites 679 through 682). These are known to occur in temperate regions.

Globorotalia inflata occurred in Section 112-683A-14X, CC (117.2 mbsf). The range of this species is from Zone N21 to Holocene, and the first appearance of *Globorotalia inflata* is at 3.0 Ma, according to Berggren et al. (1983). Based on the presence of *Globorotalia inflata*, this sample was placed in the late Pliocene (N21) to Holocene.

Globigerina bulloides, *G. woodi*, *Globigerinoides subquadratus*, and *Globorotalia siakensis* were found in Section 112-683A-30X, CC (270.4 mbsf). The range of *Globorotalia siakensis* is from N2 to N14 (Blow, 1969), and the range of *Glogigerina bulloides* is from N9 to Holocene. Based on planktonic foraminifers, this sample falls into Zone N9–N14 and is of middle Miocene age.

Globorotalia challengeri was found in Section 112-683A-33X, CC (305.3 mbsf); *Globorotalia challengeri* occurs in the middle Miocene, in the *Orbulina suturalis* Zone to *Globorotalia mayeri* Zone of Srinivasan and Kennett (1981). This sample is middle Miocene in age, based on the presence of *Globorotalia challengeri.*

Globorotalia peripheroronda was recognized in Section 112-683A-41X, CC (382 mbsf). The range of *Globorotalia peripheroronda* is from N4B to N10, early Miocene to middle Miocene (Srinivasan and Kennett, 1981). This sample was placed in the early to middle Miocene.

Hole 683B

All core-catcher samples were examined for planktonic foraminifers, which occurred throughout this hole, except for Sections 112-683B-2X, CC, 112-683B-6X, CC, and 112-683B-9X, CC. Although these are not abundant, preservation is good to moderate, except in Section 112-683B-7X, CC. Large-sized specimens occurred in Section 112-683B-7X, CC. However, because these specimens were strongly deformed in shape, they could not be identified. Age-diagnostic species were recognized in Sections 112-683B-5X, CC, and 112-683B-8X, CC (443.8–478.3 mbsf). These indicate a possible early Miocene and middle Eocene age.

Globigerinoides immaturus, *Globorotalia peripheroronda*, and *Globoquadrina altispira altispira* were found in Section 112-683B-1X, CC (403.7 mbsf). The range of *Globorotalia peripheroronda* is from N4B to N10 (early Miocene to middle Miocene). The range of *Globigerinoides immaturus* is from N5 to the Holocene (Srinivasan and Kennett, 1981). This sample was placed in N5 to N10 (early to middle Miocene). *Globorotalia peripheroronda* was also recognized in Section 112-683B-4X, CC (431.3 mbsf).

Globigerinoides trilobus, *G. primordius*, and *Globorotalia peripheroronda* were found in Section 112-683B-5X, CC (443.8 mbsf). The range of *Globigerinoides primordius* is from N4A to N5 (top of Oligocene to early Miocene). *G. primordius* is commonly found in the middle part of N4 (early lower Miocene; Berggren et al., 1983). Based on planktonic foraminifers, this sample was placed in Zones N4B to N5 (early Miocene).

Chiloguembelina cubensis and *Catapsydrax dissimilis* were recognized in Section 112-683B-7X, CC (462.8 mbsf), in association with large-sized planktonic foraminifers. The range of *Chiloguembelina cubensis* is from Zone P13 to Zone P22; the range of *Catapsydrax dissimilis* is from Zone P13 to Zone N6 (Berggren, 1977). The sample was placed in the middle Eocene to Oligocene.

Acarinina pentacamerata, *A. rotundimarginata*, *A. spinuloinflata*, *A. topilensis*, and *Turborotalia centralis* were found in Section 112-683B-8X, CC (478.3 mbsf). The range of *Acarinina spinuloinflata* is from Zone P9 to Zone P14 (early Eocene to middle Eocene), and the range of *T. centralis* is from Zone P12 to Zone P17 (middle Eocene to late Eocene; Berggren, 1977).

Benthic Foraminifers

Hole 683A

Benthic foraminifers from this hole occur in three assemblages that are indicative of lower- to middle-bathyal environments. In the upper 19 cores, in which late Pliocene and Quaternary sediments were recovered, 50% to 90% of the specimens were transported from shallower (mostly shelf) depths. A summary of these assemblages and the abundance and preservation of specimens follows.

Uvigerina senticosa Assemblage. This assemblage, described from Site 682, occurs continuously in the first 14 cores of Hole 683A and occurs sporadically between barren intervals down to Section 112-683A-25X, CC (228.3 mbsf). It indicates lower-bathyal environments. Specimens are few, but well preserved, and are vastly outnumbered by allochthonous species, mostly *Bolivina costata*, derived from the continental shelf.

Uvigerina rustica—U. gallowayi Assemblage. This assemblage, also described from Site 682, occurs in Sections 112-683A-30X, CC through 112-683A-33X, CC (270.5–305.3 mbsf), where specimens are common and moderately well to well preserved. In Sections 112-683A-29X, CC and 112-683A-30X, CC, an influx of small *Bolivina* sp. may indicate transporting of material from the shelf. Section 112-683A-28X, CC (252 mbsf) is similar, but does not contain *U. rustica* and is dominated by *Bulimina alazanensis*. This assemblage indicates middle-bathyal environments and is separated from assemblages above and below by barren samples.

Cibicidoides trinitatensis—Planulina renzi Assemblage. This assemblage, in which specimens are common to abundant and well to moderately well preserved, occurs in Sections 112-683A-40X, CC and 112-683A-41X, CC (373.1–382 mbsf). More restricted species composition occurs in samples above and below. In addition to the nominate species, *Cibicidoides* cf. *mundulus*, *Gyroidina altiformis/zealandica*, and *Oridorsalis umbonatus* are common to abundant and *Osangularia interrupta* are few. These species were reported at DSDP sites in the Pacific Basin (Douglas, 1973) and on the Nazca Plate (Resig, 1976), where backtracking established a paleodepth of about 4000 m for the sediments in which they occurred.

Hole 683B

Benthic foraminifers occurred in two assemblages, proceeding downhole as follows:

Cibicidoides trinitatensis—Planulina renzi Assemblage. This assemblage, which is a continuation of that described in the lower part of Hole 683A, occurred in Sections 112-683B-1X, CC through 112-683B-6X, CC (403.7–452.9 mbsf). The assemblage is well developed, with both nominate species present in Section 112-683B-5X, CC. Foraminifers are common and moderately well preserved, except in Sections 112-683B-2X, CC and 112-683B-6X, CC, where they are few or rare and moderately to poorly preserved. These species indicate a lower-bathyal environment, as previously described.

Bulimina chirana Assemblage. Foraminifers are few and poorly preserved owing to silicification in this assemblage, which occurred in Sections 112-683B-7X, CC through 112-683B-9X, CC (462.8–488 mbsf). Previously, this assemblage was found in Sections 112-682A-46X, CC (409.9 mbsf) and 112-682A-48X, CC (427.5 mbsf), where a middle or late Eocene age and an upper-bathyal to upper-middle-bathyal paleodepth was interpreted.

Correlation of the Lower Parts of Holes 682A and 683B

All core-catcher samples from Hole 683B were examined. We found that only Sections 112-683B-1X, CC, 112-683B-7X, CC, 112-683B-8X, CC, and 112-683B-9X, CC contained a few planktonic foraminifers. The stratigraphic sequence encountered is discussed next.

Early to middle Miocene: Identified in Section 112-683B-1X, CC (403.7 mbsf) and based on the presence of *Globorotalia praescitula*; this form is indicative of the early Miocene–middle Miocene in the tropical areas and ranges from Zones N6 to N10 (Kennett and Srinivasan, 1983).

Early Miocene: This stratigraphic level was found in Section 112-683B-4X, CC (431.3 mbsf), based on the occurrence of *Globorotalia* (*Globoconella*) *zealandica*. This species is indicative of the early Miocene *Globorotalia miozea* Zone (Kennett and Srinivasan, 1983).

Upper Eocene: A gradual change in the faunal regime was observed in Section 112-683B-5X, CC (443.8 mbsf), with the appearance of benthic foraminifers commonly observed in the upper Eocene. The change became abrupt in Section 112-683B-7X, CC (462.8 mbsf), with the presence of planktonic foraminifers diagnostic of the upper Eocene in the inland coastal basins of Peru. The following planktonic foraminifers were persistently present in Sections 112-683B-5X, CC, 112-683B-7X, CC, 112-683B-8X, CC, and 112-683B-9X, CC: *Clavigerinella eocenica*, *C. jarvisi*, and *Globigerina wilsoni*. These were accompanied by the benthic foraminifers *Stichocassidulina thalmanni*, *Cyclammina simiensis*, *Vulvulina chirana*, *Cibicides perlucidus*, *C. martinezensis*, and *Plectofrondicularia garzaensis*.

The occurrence of *Stichocassidulina thalmanni* is particularly significant because currently we consider this form to be restricted to the base of the Chira Formation in the Talara Basin (Stone, 1946). On this basis, we can state that the Eocene section penetrated during drilling of Hole 682A was younger than the one penetrated during drilling of Hole 638B (Fig. 21).

ORGANIC GEOCHEMISTRY

Holes 683A and 683B were drilled in lower-slope sediments of the Peru Continental Margin. The setting was similar to that at Hole 682A, except that the water depth at Site 683 was about 3080 m, whereas at Site 682 it was about 3800 m. We used the same organic geochemical approaches as those used at previous sites. Details of methods and procedures can be found in "Organic Geochemistry" sections, Site 679 and Site 682 chapters (this volume). Instruments used are described in the "Explanatory Notes" (this volume).

Hydrocarbon Gases

Vacutainer Gases

Gas pockets were first observed in Core 112-683A-4H (30.4 mbsf) and formed in almost all cores to the total depth of drilling. The formation of gas pockets in each core provided us an opportunity to obtain a good record of gas compositions through the entire sediment record cored at this site (Table 5). The C_1 concentrations range from about 64% to 95%. The balance of the gas most likely is air and sometimes carbon dioxide. The occurrence of sufficient C_1 to cause gas pockets at such shallow depths was surprising. The presence of these shallow gas pockets can be explained in terms of the sulfate-reduction/methane-generation model (Claypool and Kaplan, 1974). The rapid increase in C_1 with depth is a result of the complete removal of sulfate by sulfate-reducing bacteria, thereby promoting methanogenesis. At this site, sulfate concentrations decrease quickly to 2.5 mmol/L in Core 112-683A-3H (16 mbsf) and to zero at 270 mbsf and continue at this level to the base of the hole (see "Inorganic Geochemistry" section, this chapter).

C_2 concentrations range from 23 to 57 ppm down to 107 mbsf, and then suddenly increase by at least a factor of 3. This abrupt change in concentration corresponds to a lithologic boundary at 107 mbsf between turbiditic diatomaceous mud and diatomaceous mud having only rare turbidites. C_3 also shows an abrupt change in concentration at about 360 mbsf, where the amounts decrease by at least a factor of 2. This change occurs near a lithologic boundary at 373 mbsf between diatomaceous mud and laminated mudstone.

C_1/C_2 ratios of vacutainer gases are listed in Table 5 and described in Figure 24. There is a rapid decrease in this ratio from 27,000 at 30.4 mbsf to 5100 at 126.2 mbsf. At greater depths, the ratio remains more or less the same, usually ranging between 4000 and 8000. This lack of decreasing ratios with depth below 126 mbsf is unusual in that elsewhere in oceanic sediment the C_1/C_2 ratios commonly decrease with depth (Claypool and Kvenvolden, 1983). The change in slope at 126 mbsf corresponds to the depth where salinity begins to decrease steadily from 35 to 27.8 g/kg at 452 mbsf. The chloride content decreases from 512

Table 5. Vacutainer gases at Site 683A.

Core/section interval (cm)	Depth (mbsf)	C_1 (%)	C_2 (ppm)	C_3 (ppm)	C_1/C_2
112-683A-4H-7 (17)	30.4	64.2	24	5.2	27,000
5H-3 (118)	34.9	78.5	35	9.5	22,000
6H-8 (46)	49.0	86.6	38	10	23,000
7H-3 (14)	52.8	75.1	44	14	17,000
8H-6 (97)	68.5	91.2	52	16	18,000
9H-1 (30)	69.0	80.9	50	17	16,000
10X-1 (100)	79.2	79.1	57	21	14,000
12X-6 (30)	106.5	52.2	23	13	23,000
13X-1 (60)	107.3	70.8	44	20	16,000
15X-4 (40)	126.2	79.3	160	16	5100
15X-5 (25)	132.0	79.6	140	14	5700
16X-1 (100)	136.2	86.4	80	33	11,000
17X-1 (76)	145.5	59.9	160	22	3800
18X-4 (110)	159.8	89.9	96	25	9400
19X-1 (26)	164.0	65.0	150	32	4200
21X-1 (130)	184.0	70.0	240	34	2900
25X-5 (118)	227.9	80.2	120	28	6600
27X-1 (80)	240.5	74.8	160	27	4700
28X-1 (78)	250.0	82.4	270	13	3100
29X-1 (50)	259.2	72.1	130	22	5600
30X-1 (88)	269.1	89.6	150	29	5800
31X-1 (28)	278.0	70.5	170	40	4100
32X-1 (56)	287.8	75.4	120	27	6100
34X-3 (106)	310.3	91.5	130	23	7000
35X-2 (104)	318.2	93.4	130	24	7200
36X-4 (140)	331.1	85.6	110	12	8100
37X-2 (138)	337.6	93.0	130	10	7400
39X-4 (130)	359.5	81.2	110	5.2	7400
39X-5 (55)	360.3	88.0	120	5.4	7400
40X-6 (40)	371.1	95.0	130	2.8	7600
41X-5 (90)	379.6	94.5	110	2.4	8800
42X-1 (20)	381.4	11.6	15		7800
43X-1 (100)	391.7	87.8	120	2.7	7100
44X-5 (77)	407.0	87.0	120	3.1	7300
45X-5 (85)	416.6	96.8	130	3.4	7700
112-683B-1X-1 (77)	403.3	79.2	170	9.6	4600
2X-2 (120)	414.7	81.6	140	7.1	5800
3X-2 (78)	423.8	82.6	120	5.9	6900
5X-2 (59)	442.6	82.2	140	5.9	5800
6X-2 (68)	452.2	91.6	190	4.2	4900

Note: units of % and ppm are in volume of gas component per volume of gas mixture. All measurements were performed on the Hach-Carle Gas Chromatograph.

to 454 mmol/L in the same depth interval (see "Inorganic Geochemistry" section, this chapter). The relationship between C_1/C_2 ratios and salinity or chloride content may result from the presence of gas hydrates below 126 mbsf. Gas hydrates are known to be manifest by decreasing salinity and chlorinity of pore waters, as measured using samples of pore water at this site (see "Organic Geochemistry" section, Site 682 chapter for discussion of gas hydrates). We speculate that in this same depth interval the relative concentrations of C_1 and C_2 reflect the composition of the gas hydrate, and thus the C_1/C_2 ratios remain more or less constant.

Figure 25 compares C_1/C_2 ratios of vacutainer gases with drilling rates in Hole 683A. We made this comparison in an attempt to verify our observations about the effects of drilling on hydrocarbon generation made at Site 682 (see "Organic Geochemistry" section, Site 682 chapter). However, at Site 683, we observed no anomalously high gas concentrations or abnormal compositions in any of the cores. There appears to be little correlation between the two parameters, except that at about 260 mbsf, where the drilling rate was lowest, the C_1/C_2 ratios were also low, but not markedly so.

Extracted Gases

Hydrocarbon gases resulting from the headspace and can procedures are shown in Tables 6 and 7, respectively, and the abundances of C_1 extracted from the sediments by both proce-

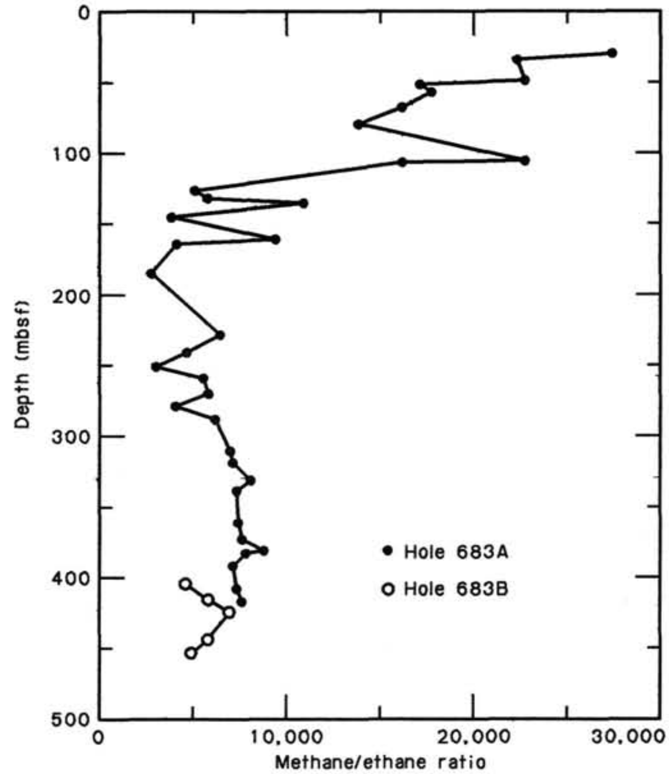

Figure 24. Methane/ethane ratios in gas collected from Holes 683A and 683B using vacutainers.

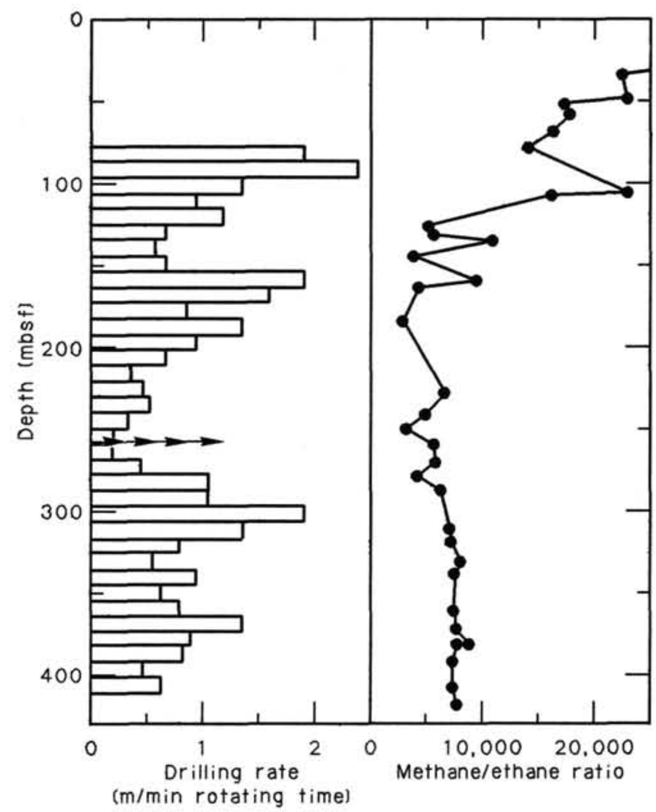

Figure 25. Comparison of methane/ethane ratios and drilling rates (meters per minute of rotating time) at Hole 683A. Arrows indicate a region where slow drilling rates may have slightly affected the methane/ethane ratios.

Table 6. Hydrocarbon gases measured using the headspace procedure at Site 683.

Core/section interval (cm)	Depth (mbsf)	C_1 (μL/L)	C_2 (μL/L)	$C_{2:1}$ (μL/L)	C_3 (μL/L)	C_1/C_2
112-683A-1H-1, 139–140	1.4	60				
2H-3, 0–1	5.2	530				
3H-3, 139–140	16.1	88,000	5.0	2.1	4.5	18000
4H-7, 61–62	27.8	27,000	6.0	2.4	2.9	4400
5H-3, 0–1	33.7	61,000	10	2.7	7.2	6000
6H-2, 139–140	43.1	31,000	7.7	2.3	7.3	4000
7H-3, 0–1	57.2	29,000	7.5	2.0	3.7	3900
8H-6, 0–1	66.7	1200				
9H-4, 66–67	73.9	110,000	11	1.7	8.4	9800
10X-1, 149–150	79.7	18,000	6.4		6.8	2900
11X-1, 117–118	88.9	16,000	15	3.1	21	1100
12X-5, 0–1	103.2	28,000	13		19	2100
13X-1, 85–86	107.6	71,000	22	3.2	25	3200
14X-1, 107–108	117.3	15,000	10		19	1500
15X-1, 114–115	126.9	48,000	17	3.6	25	2900
16X-2, 0–1	136.7	62,000	28		35	2200
17X-1, 96–97	145.7	23,000	20	4.4	35	1200
18X-4, 0–1	158.7	26,000	22	4.8	41	1200
19X-1, 74–75	164.5	14,000	31	5.9	48	450
20X-1, 44–45	173.6	24,000	20	5.0	25	1200
21X-2, 0–1	183.2	24,000	34	3.4	37	700
22X-1, 60–61	192.8	19,000	64	6.8	34	300
23X-1, 0–1	201.7	19,000	28	1.9	30	700
24X-1, 68–69	211.9	39,000	60	7.7	73	650
25X-6, 12–13	228.3	25,000	32	7.6	51	780
26X-1, 49–50	230.7	28,000	80	9.5	100	350
28X-2, 137–138	252.1	190,000	120	9.0	100	1600
29X-1, 129–130	260.0	60,000	32	7.7	38	1900
30X-2, 68–69	270.4	28,000	46	4.5	66	600
31X-2, 17–18	279.4	48,000	56	5.0	69	850
32X-1, 98–99	288.2	26,000	52	7.7	85	500
33X-6, 0–1	304.2	29,000	51	9.9	52	580
34X-3, 0–1	309.2	29,000	30	4.1	29	980
35X-2, 149–150	318.7	21,000	43	6.1	39	490
36X-4, 0–1	329.7	7400	30	5.1	24	250
37X-2, 0–1	336.2	24,000	32			750
39X-3, 0–1	356.7	43,000	34	6.8	8.6	1300
40X-6, 0–1	370.7	14,000	20	4.3	8.5	680
42X-1, 75–76	382.0	26,000	29	6.5	7.5	900
43X-2, 109–110	393.3	33,000	29	2.7	10	1100
44X-5, 149–150	407.7	67,000	36	4.9	8.6	1900
45X-5, 0–1	415.7	8400	22	2.7	8.8	380
112-683B-1X-1, 121–122	403.7	81,000	39	4.4	1.4	2000
2X-3, 0–1	415.0	37,000	51	6.7	12	720
3X-2, 139–140	424.4	29,000	32	3.7	10	900
5X-2, 149–150	443.5	44,000	63	5.9	20	700
6X-3, 0–1	453.0	35,000	62	7.6		570
7X-3, 0–1	462.5	150,000	800		51	190

Note: Units are in microliters of gas component per liter of wet sediment. All measurements were performed on the Hach-Carle Gas Chromatograph.

Table 7. Hydrocarbon gases measured at Site 683 using the canned gas procedure.

Core/section interval (cm)	Depth (mbsf)	C_1 (μL/L)	C_2 (μL/L)	C_3 (μL/L)	C_1/C_2
112-683A-1H-1, 140–145	1.5	18			
3H-3, 140–145	16.2	81,000	5.7	2.2	14,000
6H-3, 140–144	44.6	39,000	5.3	3.4	7300
9H-3, 145–150	73.2	34,000	11	11	3200
12X-4, 145–150	103.2	29,000	8.4	13	3400
18X-3, 140–150	158.7	20,000	11	14	1800
24X-1, 74–79	212.0	26,000	34	41	770
27X-1, 128–133	241.0	7000	33	40	210
30X-2, 69–74	270.4	10,000	28	35	370
36X-3, 135–140	329.6	28,000	30	13	960
43X-2, 135–140	393.6	30,000	17	3.2	1800
112-683B-6X-2, 43–51	452.0	7100	34	5.3	210

Note: Units are in microliters of gas component per liter of wet sediment. All measurements were performed on the Hach-Carle Gas Chromatograph.

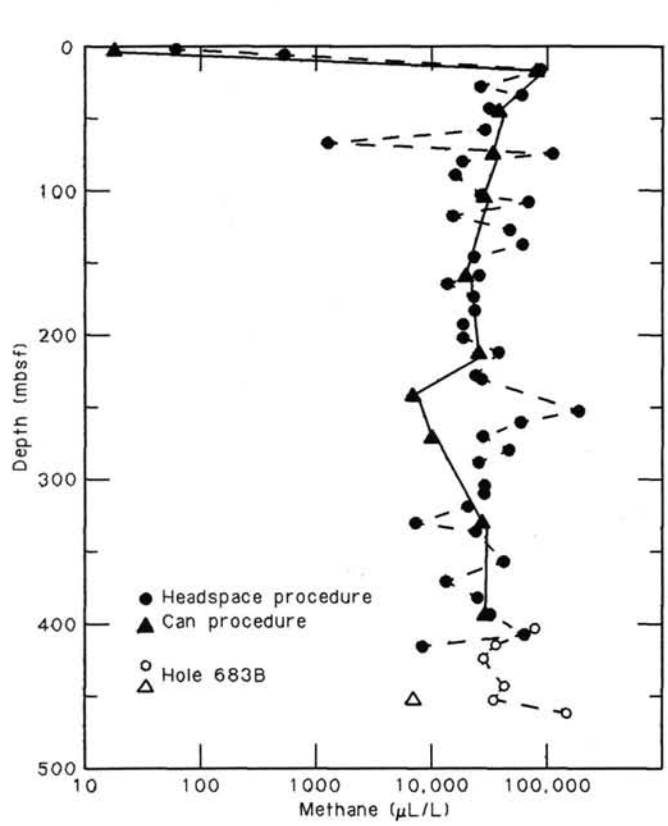

Figure 26. Comparison of methane concentrations (microliters per liter of wet sediment) with depth obtained from headspace and can procedures at Site 683. Data for Hole 683B are indicated with complementary symbols at the bottom of the figure.

dures are presented in Figure 26. The trends in the C_1 data from both procedures are generally similar, except that the headspace procedure produces more detail because of closer sample spacing. The C_1 content of the sediment increases rapidly from the surface. In Core 112-683A-3H at 16 mbsf, the C_1 concentration reaches 88,000 μL/L of wet sediment. In fact, this concentration was the highest that we measured at this site, except for three samples at 74, 252, and 463 mbsf, in which C_1 exceeded 100,000 μL/L. Below 16 mbsf, C_1 concentrations (as measured by both headspace and can procedures) usually remained in the range of 10,000 to 90,000 μL/L. These concentrations apparently represent the limit of the amount of residual C_1 that can be retained by the sediment, as analyzed by these procedures. The rapid increase in C_1 content at the top of Hole 683A correlates inversely with the rapid decrease in sulfate concentrations (see "Inorganic Geochemistry" section, this chapter). The vacutainer data from gas pockets also showed the same inverse correlation.

The changes in the concentrations with depth of C_2 and C_3, as noted in the vacutainer gases (Table 5), were also present in the extracted-gas data (Tables 6 and 7). The change in amounts of extracted C_2 was not abrupt at 126 mbsf, but nevertheless was present. The amounts of extracted C_3 abruptly changed at about 330 mbsf. This change correlates well with the vacutainer gas data. We believe that both of these changes in concentration relate to lithology.

Ethene ($C_{2:1}$) was monitored for the first time at Site 683 (Table 6). We had observed at previous sites that small amounts of $C_{2:1}$ could be detected in gas samples from the headspace procedure, but not from the can procedure or in vacutainer samples (except for those instances where concentrations of $C_{2:1}$ were anomalously high in samples affected by the heat of drilling (see "Organic Geochemistry" section, Site 679 and 682 chapters).

We interpreted these observations to be that $C_{2:1}$ is adsorbed in the sediment and is released during heating at 70°C using the headspace procedure. The amounts of $C_{2:1}$ released are less than 10 μL/L and always at least a factor of 2 less than the amounts of C_2. In Holes 683A and 683B, we did not observe anomalously high concentrations of $C_{2:1}$ as we did at Hole 682A (see "Organic Geochemistry" section, Site 682 chapter). Our attempt to determine if more $C_{2:1}$ could be desorbed from headspace samples by further heating was not successful.

Gas Hydrates

We considered the possibility of gas hydrates at Site 683 because the entire sedimentary column drilled was within the pressure-temperature field that ensures stability of gas hydrates (Kvenvolden and McMenamin, 1980). In addition, the amount of C_1 found in all sediment samples beneath 16 mbsf was commensurate with the existence of gas hydrates (Kvenvolden, 1985). Again, as at Site 682, we did not observe gas hydrates, although each core was inspected carefully. However, the decrease of salinity with depth (from 35.0 to 27.8 g/kg) and chloride content (from 512 to 454 mmol/L) of the pore waters at this site strongly suggests that gas hydrates were present here (see "Inorganic Geochemistry" section, this chapter).

Carbon

Part of each of 17 sediment "squeeze-cakes" from Hole 683A and three from Hole 683B were analyzed for organic carbon and type of organic matter. The results are shown in Tables 8 and 9. The organic carbon profile (Fig. 27) shows three distinct maxima where organic carbon exceeds about 6%. These maxima (at 73, 159, and 241 mbsf) record three periods of high production and/or preservation of organic matter; the maxima do not correlate with any obvious lithologic characteristics, although the wide sample spacing almost precludes our ever making such correlations. Also of interest is the good correlation between organic carbon (OC), as determined by difference from coulometric measurements, and TOC, as measured by Rock-Eval pyrolysis (Fig. 27).

Data from Rock-Eval pyrolysis are listed in Table 9 for the 20 samples from Holes 683A and 683B. To visualize the relationships among the Rock-Eval parameters, we compared a number of these parameters with depth in Figure 28. The depth profiles of S_1, S_2, S_3, TOC, and HI are remarkably similar and show that the amount of hydrocarbons and CO_2 obtained during the programmed pyrolysis was about proportional to the amount of organic matter in the sediments; that is, the more organic-rich the sediment, the more products that are evolved during heating. This result is to be expected where organic matter has not undergone advanced diagenesis. The apparent correlation between TOC and HI showed that an organic matter of higher carbon content also has a higher hydrogen content. Because marine organic matter commonly has higher HI values, we concluded that the more organic-rich material at this site was predominantly of marine origin. T_{max} values ranged from 409 to 433°C. These temperatures indicate that the organic matter is "immature" with respect to considerations of petroleum potential. The apparent inverse relationship between T_{max} and, for example, TOC indicates that the organic matter, which is more organic-rich, is the least mature (i.e., has the lowest T_{max} values). However, T_{max} is not only affected by maturity but also by oxidation and weathering. Similar low OI values for all samples at this site suggest that none of the samples has undergone extensive oxidation. Finally, HI and OI values are plotted in Figure 29. The values cluster between the fields of type II and type III organic matter. The more organic-rich samples fall nearer the type II field, suggesting that the bulk of this organic matter is of marine origin.

Table 8. Profile of organic carbon, carbonate carbon, and total organic carbon for Site 683.

Core/section interval (cm)	Depth (mbsf)	Total carbon (%)	Carbonate carbon (%)	Organic carbon (%)	TOC (%)
112-683A-1H-1, 145-150	1.5	4.16	0.97	3.19	3.12
3H-3, 145-150	44.7	6.19	1.99	4.20	4.53
6H-3, 144-150	16.2	4.24	0.26	3.98	3.72
9H-3, 145-150	73.2	6.56	0.51	6.05	5.96
9H-4, 0-10	73.3	6.43	0.16	6.27	6.61
12X-4, 135-145	103.2	5.09	0.24	4.85	4.90
15X-1, 140-150	127.2	3.32	0.05	3.27	3.22
18X-3, 145-150	158.7	6.17	0.10	6.27	6.37
21X-1, 145-150	184.2	5.62	0.03	5.59	5.54
24X-1, 69-74	211.9	4.49	0.14	4.35	4.29
27X-1, 123-128	241.0	7.36	0.23	7.13	6.95
30X-2, 74-79	270.5	4.41	0.19	4.22	4.18
33X-5, 145-150	304.2	3.62	0.28	3.34	3.35
36X-3, 140-150	329.7	2.46	0.05	2.41	2.34
39X-2, 140-150	356.7	3.14	0.81	2.33	2.15
43X-2, 140-150	393.7	2.73	0.14	2.59	2.43
45X-4, 140-150	415.7	2.04	0.22	1.82	1.72
112-683B-2X-2, 140-150	415.0	3.02	0.02	3.03	3.19
3X-2, 140-150	424.5	3.05	0.60	2.43	2.28
6X-2, 51-63	452.1	2.09	0.03	2.06	1.95

TOC = Total organic carbon from Rock-Eval pyrolysis; organic carbon by difference of total carbon and carbonate carbon.

INORGANIC GEOCHEMISTRY

Introduction and Operation

We collected 20 whole-round, interstitial-water samples from Holes 683A and 683B; nine of these samples were 5-cm-long sections, and the rest were 10-cm-long sections. We collected samples at routine intervals (i.e., Cores 112-683A-1H, 112-683A-3H, and every third core thereafter). Results are listed in Table 10. In addition, two *in-situ* samples were collected from Hole 683A at 230.2 and 363.2 mbsf. Unfortunately, both were contaminated by drill-hole seawater, as shown in Table 11. Problems of contamination by drill-hole seawater are discussed in detail in "Inorganic Geochemistry" section, Site 682 chapter (this volume). In Table 11, the data obtained from neighboring interstitial waters from squeezed sediment samples are compared with data from *in-situ* samples. Values for standard seawater (IAPSO) also are shown. The *in-situ* samples have higher salinity, sulfate, chlorinity, Ca^{2+}, and Mg^{2+} values and lower alkalinity values relative to the squeezed waters, as expected from mixing with seawater. Apparently, in more indurated zones at depths greater than about 200 mbsf (as at this site), the penetration of the probe into the sediments "cracks" the formation, allowing some drill-hole water to penetrate and mix with *in-situ* formation water.

In the more indurated zones, special care was needed during sample preparation before squeezing. The XCB cores from these intervals were composed of small, 2- to 5-cm, almost intact, sediment biscuits floating in a drilling slurry (mixed sediment and drill-water) matrix, as shown in Figure 30. Before squeezing interstitial waters from this type of sediment, the matrix mud should be separated from the biscuits and only the biscuits should be squeezed.

The interstitial-water profiles at Site 683 (as at Site 682) show systematic variations downhole with pronounced minima and maxima. The concentration gradients were generally more extreme than those observed at Site 682 because of higher sedimentation rates (~100 m/m.y.) during the last 2.5 m.y. between 0 and 249 mbsf (see "Biostratigraphy" section, this chapter). At Site 682, the highest sedimentation rates (in the uppermost 100 m) were ~26 m/m.y.

Table 9. Summary of Rock-Eval pyrolysis at Site 683.

Core/section interval (cm)	Depth (mbsf)	Quantity (mg)	T_{max}	S_1	S_2	S_3	PI	S_2/S_3	PC	TOC (%)	HI	OI
112-683A-1H-1, 145-150	1.5	98.7	422	1.31	8.34	1.81	0.14	4.60	0.80	3.12	267	58
3H-3, 145-150	16.2	100.7	429	1.46	13.15	1.95	0.10	6.74	1.21	3.78	347	51
6H-3, 144-150	44.7	103.6	426	1.66	15.62	2.09	0.10	7.47	1.44	4.53	344	46
9H-3, 145-150	73.2	95.5	413	4.18	26.79	2.37	0.14	11.30	2.58	5.96	449	39
9H-4, 0-10	73.3	96.0	409	4.91	30.73	2.25	0.14	13.65	2.97	6.61	464	34
12X-4, 135-145	103.2	99.8	420	2.28	19.76	1.65	0.10	11.97	1.83	4.90	403	33
15X-1, 140-150	127.2	99.7	415	1.29	11.98	0.98	0.10	12.22	1.10	3.22	372	30
18X-3, 145-150	158.7	98.1	413	4.14	30.72	1.98	0.12	15.51	2.90	6.37	482	31
21X-1, 145-150	184.2	101.4	409	3.48	25.92	1.97	0.12	13.15	2.45	5.54	467	35
24X-1, 69-74	211.9	99.6	422	1.62	19.40	1.58	0.08	12.27	1.75	4.29	452	36
27X-1, 123-128	241.0	76.3	404	4.07	35.70	2.68	0.10	13.32	3.31	6.95	513	38
30X-2, 74-79	270.5	100.1	420	1.12	17.57	1.93	0.06	9.10	1.55	4.18	420	46
33X-5, 145-150	304.2	98.8	425	0.71	13.13	1.58	0.05	8.31	1.15	3.35	391	47
36X-3, 140-150	329.7	101.5	424	0.53	7.28	0.95	0.07	7.66	0.65	2.34	311	40
39X-2, 140-150	356.7	92.2	417	1.14	8.25	1.49	0.12	5.53	0.78	2.15	383	69
43X-2, 140-150	393.7	97.9	422	0.54	8.54	1.28	0.06	6.67	0.75	2.43	351	52
45X-4, 140-150	415.7	101.4	433	0.26	4.50	1.08	0.05	4.16	0.39	1.22	261	62
112-683B-2X-2, 140-150	415.0	99.8	433	0.53	12.27	0.63	0.04	19.47	1.06	3.19	384	19
3X-2, 140-150	424.5	92.5	420	0.80	8.57	0.86	0.09	9.96	0.78	2.28	375	37
6X-2, 51-63	452.1	99.0	424	0.37	6.52	0.17	0.05	38.35	0.57	1.95	334	8

Note: Rock-Eval parameters are defined in "Inorganic Geochemistry" section, Site 679 chapter.

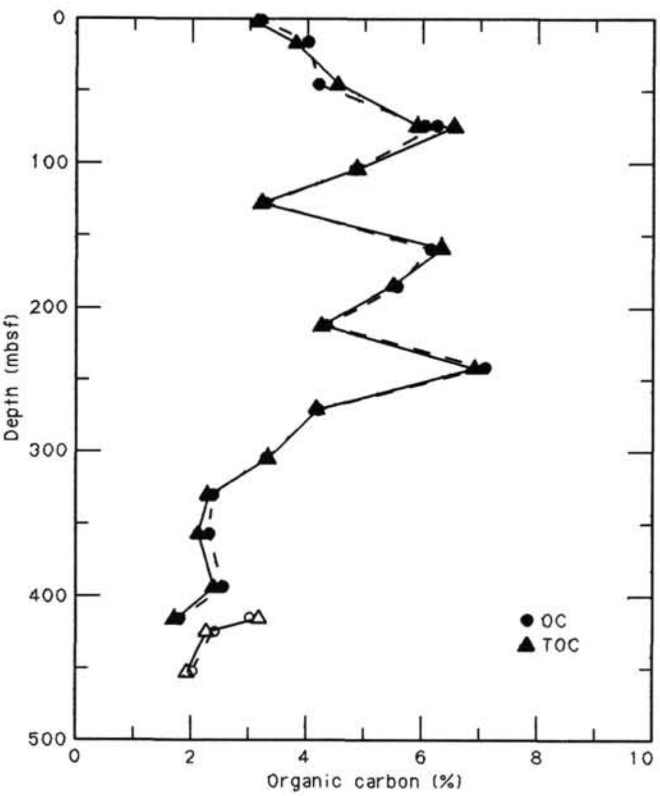

Figure 27. Comparison of organic carbon (OC) and total organic carbon (TOC) wth depth at Site 683. Data for Hole 683B are indicated in complementary open symbols at the bottom of the figure.

The most important systematic downhole variations observed are decreases in salinity, chlorinity, SO_4^{2-}, Mg^{2+}, and Mg^{2+}/Ca^{2+} and increases in alkalinity, NH_4^+, Ca^{2+}, and silica (Figs. 31 through 34). These profiles (except for Ca^{2+} and Mg^{2+}) are most similar to those obtained at Site 682 and during DSDP Leg 57 at Sites 438 and 439; Legs 67 and 84 at Sites 497, 498, 565, 568, and 570 (Moore and Gieskes, 1980; Harrison et al., 1982; Hesse et al., 1985). The similarities between Site 682 and these DSDP sites are discussed in the Site 682 chapter (this volume).

Results

Chloride and Salinity

Both chloride and salinity concentrations generally decrease downhole (Fig. 31 and Table 10). Chloride decreases from ~548 mmol/L near the sediment/seawater interface (1.5 mbsf) to 454 mmol/L at 452 mbsf, a decrease of ~92 mmol/L or 16.9%. Similarly, salinity decreases from 34.2 to 28.8 g/kg, by 16%. Between ~75 and 115 mbsf, small maxima in chloride and salinity are observed, whereas the major concentration decreases were observed below 120 mbsf. Such chloride and salinity profiles (Fig. 31) are the expected, "classical" concentration profiles when marine gas hydrates are present. These two profiles together with the constant methane/ethane ratio below 120 mbsf (see "Organic Geochemistry" section, this chapter; Fig. 31), can indicate the presence of gas hydrates even when they were not obtained because of poor core recovery, as at Site 683. These gas hydrates must have decomposed during coring and core-recovery operations. At Site 683, the cored sediments were found within the pressure-temperature stability field for marine gas hydrates (Kvenvolden and McMenamin, 1980). Decomposition of gas hydrates (which provides a progressive dilution "artifact") was responsible for much of the salinity and chlorinity profiles observed in Fig. 31. The dilution "artifact" by gas hydrates was suggested by Harrison et al. (1982).

The formation of gas hydrates usually causes salinity and chlorinity maxima immediately above these stability fields, as indeed we observed between ~75 and 115 mbsf. Maximum alkalinity was partially responsible for the salinity maximum, but not the chloride maximum. The dilution "artifact" affected all other downhole profiles slightly.

Alkalinity and Sulfate

Sulfate concentrations decreased from 30.7 to 2.5 mmol/L within the uppermost 16 m (Fig. 32 and Table 10). Because of sediment disturbance and slight contamination by drill-hole water, sulfate concentrations were low (between 1 and 4 mmol/L at 16 to ~250 mbsf. Below this depth, sulfate was completely con-

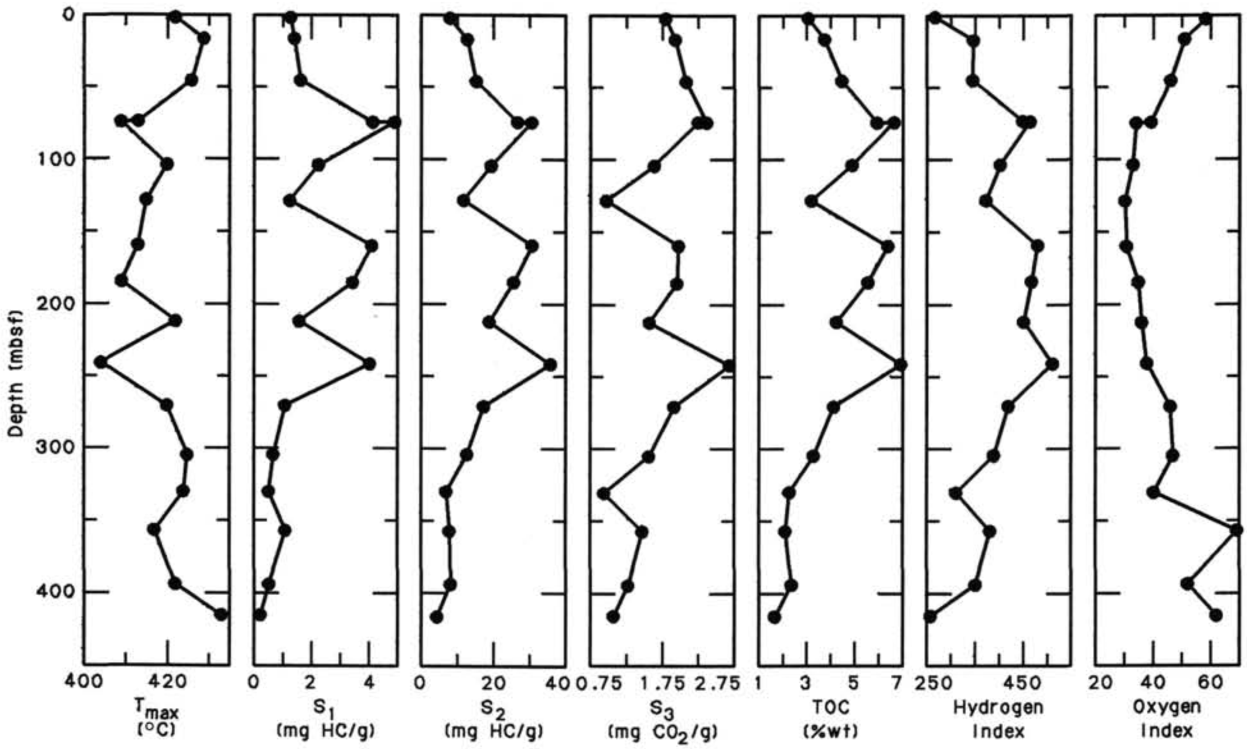

Figure 28. Comparison of Rock-Eval parameters, T_{max}, S_1, S_2, S_3, TOC, HI, and OI at Hole 683A.

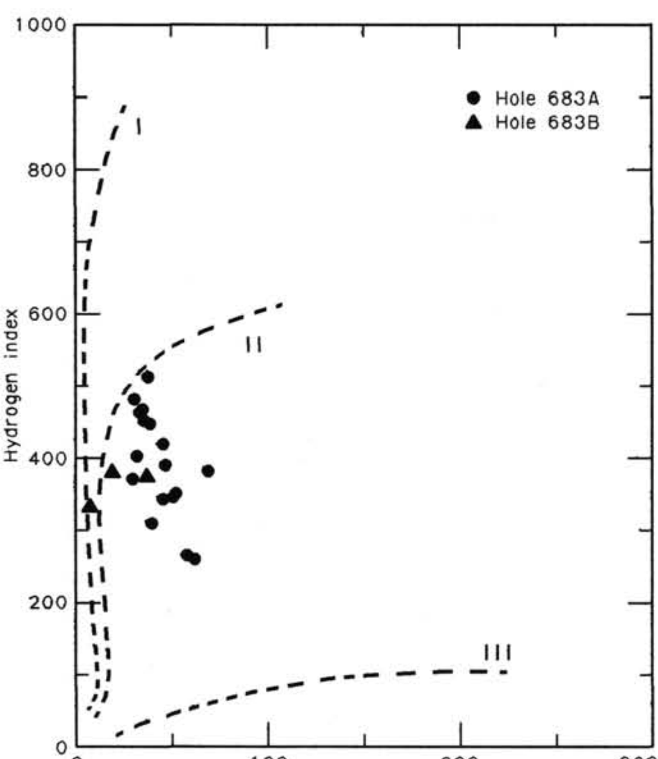

Figure 29. Hydrogen and oxygen indices (HI and OI) obtained from Rock-Eval pyrolysis of sediments from Holes 683A and 683B, plotted on a van Krevelen-type diagram (Tissot and Welte, 1984).

sumed, and the sulfate concentration was zero. This zero sulfate zone correlates well with a slump between the two hiatuses at 250 and 360 mbsf, described in the "Biostratigraphy" section (this chapter).

Alkalinity values also increased rapidly but reached a maximum at a greater depth (~100 mbsf) than the sulfate minimum. Calcite precipitation within the top 80 m consumes alkalinity while it is being produced, as indicated by the pronounced Ca^{2+} minimum and a corresponding Mg^{2+}/Ca^{2+} maximum that we observed in Figure 34. Below about 180 mbsf, carbonate (calcite and dolomite) formation, CO_2 reduction, CH_4 formation, and decreasing NH_4^+ concentrations are primarily responsible for the alkalinity decreases we observed.

Ammonia, Phosphate, and Silica

Similar to the other dissolved compounds, the chemical gradients of ammonia and phosphate were steeper and more extreme at Site 683 than at Site 682 (Fig. 33 and Table 10). Ammonia concentrations increased continuously to a maximum value of 21.5 mmol/L at 159 mbsf. However, at Site 682, the ammonia maximum occurred approximately 150 m deeper (at 308 mbsf) and reached a lower maximum value of only 16 mmol/L. The distinct differences in sedimentation rates at these two sites are responsible for the observed differences in the intensities and depths of maxima and minima in the concentration profiles with depth.

Below about 200 mbsf, ammonia values decrease, probably in part because of ion exchange with clay minerals as well as diffusion.

As at all previous sites, the phosphate maximum occurred at a shallower depth than the ammonia maximum. Below about 100 mbsf, phosphate concentrations decrease markedly with depth. The phosphate profile is a diffusion-reaction profile.

Table 10. Interstitial-water geochemical data from Site 683.

Core/section interval (cm)	Depth (mbsf)	pH	Salinity (g/kg)	Cl^- (mmol/L)	Alkalinity (mmol/L)	SO_4^{2-} (mmol/L)	PO_4^{3-} (μmol/L)	NH_4^+ (mmol/L)	SiO_2 (μmol/L)	Ca^{2+} (mmol/L)	Mg^{2+} (mmol/L)	Mg^{2+}/Ca^{2+}
112-683A-1H-1, 145-150	1.5	7.6	34.2	547.55	4.43	30.68	8.2	0.50	684	9.84	50.93	5.18
3H-3, 145-150	16.2	7.6	34.2	535.15	52.56	2.47	133.3	5.58	980	3.95	51.62	13.07
6H-3, 144-150	44.6	7.2	34.5	525.61	67.52	1.04	160.3	11.22	991	4.09	50.76	12.41
9H-3, 145-150	73.2	7.8	35.5	529.43	85.49	1.72	150.5	15.17	920	6.64	54.31	8.01
9H-4, 0-10	73.2	7.5	35.2	532.29	86.90	3.04	161.6	15.17	914	6.69	54.41	8.13
12X-4, 135-145	103.1	7.6	35.5	523.71	92.21	1.97	149.3	18.97	1023	8.45	51.68	6.12
15X-1, 140-150	127.1	7.6	35.0	512.26	92.32	2.08	118.8	19.90	1015	8.91	47.87	5.37
18X-3, 145-150	158.7	7.6	34.2	505.58	89.44	1.10	132.4	21.45	—	9.16	43.37	4.74
21X-1, 145-150	184.2	7.5	32.9	493.18	77.02	3.97	103.4	21.17	1056	8.06	36.70	4.55
24X-1, 69-74	211.9	—	32.0	488.41	68.37	4.42	46.3	19.79	1184	7.25	33.03	4.56
27X-1, 123-128	240.9	7.6	31.3	483.64	57.90	3.10	39.9	17.22	1227	7.18	29.74	4.14
30X-2, 74-79	270.4	7.7	30.2	477.92	53.22	0.0	25.4	15.98	1229	7.87	27.12	3.45
33X-5, 145-150	304.2	—	29.8	475.06	—	0.0	16.2	13.98	1180	7.62	24.81	3.26
36X-3, 140-150	329.6	7.8	29.8	474.10	40.01	0.0	7.9	10.60	1236	8.84	25.84	2.92
39X-2, 140-150	356.6	7.2	29.4	473.15	35.50	0.0	9.5	10.91	1412	9.19	23.16	2.52
43X-2, 140-150	393.6	7.8	28.2	474.10	26.26	0.95	6.6	9.13	1217	10.79	21.48	1.99
45X-4, 140-150	415.6	7.4	27.8	457.88	28.96	0.0	12.8	7.67	1229	12.75	19.04	1.49
112-683B-2X-2, 140-150	414.9	—	28.8	464.65	—	1.13	6.4	9.73	1295	11.42	20.93	1.83
3X-2, 140-150	424.4	7.4	28.0	455.98	34.90	0.0	5.8	9.76	1337	10.60	18.39	1.73
6X-2, 51-63	452.0	7.7	28.8	454.07	32.28	0.0	4.6	8.49	1252	13.41	16.30	1.22

Table 11. Comparisons of interstitial-water chemical data from squeezed sediment samples with *in-situ* samples contaminated by drill-hole water in Hole 683A

Core/section interval (cm)	Depth (mbsf)	Salinity (g/kg)	Alkalinity (mmol/L)	SO_4^{2-} (mmol/L)	Cl^- (mmol/L)	Ca^{2+} (mmol/L)	Mg^{2+} (mmol/L)
112-683A-24X-1, 69-74	211.9	32.0	68.37	4.42	488.41	7.25	33.03
In situ 1	230.2	33.5	33.66	15.70	515.12	8.90	42.02
27X-1, 123-128	240.9	31.3	57.90	3.10	483.64	7.18	29.74
39X-2, 140-150	356.6	29.4	35.50	0.0	473.15	9.19	23.16
In situ 2	363.2	32.5	18.16	17.17	508.44	12.13	39.84
112-683A-43X-2, 140-150	393.6	28.2	26.26	0.95	474.10	10.79	21.48
Seawater (IAPSO)		~35	~2.5	28.9	559	10.55	53.99

As expected from diatomaceous upwelling sediments, silica concentrations in interstitial water increased rapidly and reached opal-A solubility values at 20 to 50 mbsf. Silica values increased slightly with depth at higher temperatures and pressures to 1412 μmol/L at ~360 m, the depth of the second biostratigraphic hiatus of 2 m.y. duration in the middle Miocene (see "Biostratigraphy" section, this chapter). Below this depth, silica values decreased very slightly with depth.

Calcium and Magnesium (Fig. 34 and Table 10)

Calcium and magnesium concentrations at 1.5 mbsf were lower than the average concentration in seawater, suggesting that the geochemical environment encountered at this site is favorable for carbonate diagenesis (Fig. 34 and Table 10).

The most important systematic downhole variations (shown in Fig. 34) are decreases in Mg^{2+} and Mg^{2+}/Ca^{2+} and increases in Ca^{2+} concentration with depth. The interstitial-water Ca^{2+} profile shows a pronounced minimum at about 16 m and a small but distinct maximum at about 140 mbsf. The minimum is controlled mainly by calcite and some dolomite precipitation. This reaction is also responsible for the apparent alkalinity maximum, which is deeper than the depth of the sulfate minimum zone (shown in Fig. 32).

While calcite precipitates, sulfate reduction and alkalinity production continue. In addition, the Mg^{2+}/Ca^{2+} ratio increases dramatically to a ratio of 13, the highest value ever reported in nonevaporative environments. Consequently, a favorable geochemical environment for rapid dolomitization forms. The depth interval of high rates and intensive dolomitization is between the zone of maximum in Mg^{2+} concentration at 70 to 80 mbsf and about 180 mbsf; below 180 mbsf, the slope of the Mg^{2+} profile is less steep. This depth interval corresponds to the depth of the Ca^{2+} maximum zone, suggesting dolomitization by calcite replacement reaction.

The Mg^{2+}/Ca^{2+} ratio decreases with depth, and the rate of dolomitization should decrease as well. Eventually, at Mg^{2+}/Ca^{2+} ratios of <2 (although still within the stability field of dolomite at the *in-situ* temperatures and pressures), co-precipitation of calcite and dolomite is kinetically favored. Only small amounts of carbonate diagenesis were responsible for the observed strong Ca^{2+} and Mg^{2+} concentration gradients (Fig. 34) at this site relative to high sedimentation rates.

PALEOMAGNETISM

Introduction

Sediments at Site 683 through the first 15 cores (132.5 mbsf) had a magnetization strong enough to be measured with the onboard spinner magnetometer. The demagnetization behavior of these samples is characterized by unidirectional decays of the magnetic vectors with increasing alternating-field demagnetization. The mean destructive field of the samples is between 150 and 200 Oe. These data indicate that the magnetization of these sediments is carried by a medium coercivity phase (or phases). Poor core recovery, specifically the lack of useable samples from Cores 112-683A-10X and 112-683A-13X and limited samples from Core 112-683A-14X, forced us to abandon shipboard sampling.

Results

Hole 683A

Figure 35 shows the declination, inclination, and intensity values vs. depth for the samples measured. The figure shows that all of the upper 65 m of the section is normally magnetized. We believe it was deposited during the Brunhes Chron. We noted the Brunhes-Matuyama boundary at about 65 m (Section 112-

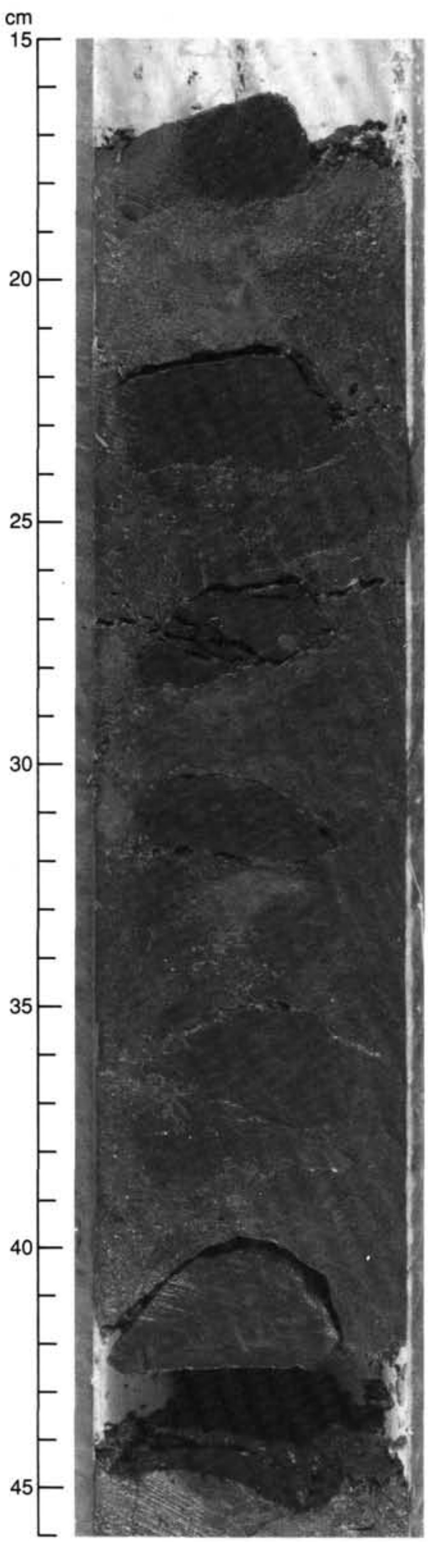

Figure 30. Sediment biscuits floating in drilling-mud matrix.

683A-8H-6). Below this level, all of the samples measured show a reversed magnetization. As stated previously, sampling below 65 mbsf was limited; therefore, we were unable to define this entire lower 70 m as belonging to the Matuyama Chron. Shipboard paleontological studies suggested that portions of this lower section were missing; the section is not entirely all Matuyama in age.

Examination of the declination data from the site (Fig. 35) shows that the measured declinations from the tops of some of the cores are rotated with respect to lower parts of the same core. This rotation was most obvious in Cores 112-683A-2H and 112-683A-3H, where we observed rotations having a declination of as much as 45°. In Core 112-683A-5H, we noted these rotations in the base of the core. These data suggest that there can be rotations of up to 45° or more of the core during HPC coring, which argues for caution in applying the results from oriented cores to tectonic interpretations.

Examination of the intensity vs. depth plot (righthand side of Fig. 35) indicates that the intensity of magnetization of individual samples is cyclic, with perhaps six different maxima occurring during the Brunhes Chron. These cycles suggest a possible correlation with major Quaternary climatic cycles.

PHYSICAL PROPERTIES

After whole-round cores were run through the GRAPE, physical-properties measurements at Site 683 were performed on split cores, generally at an interval of one every two sections (3 m) in good quality APC cores and, wherever possible, in XCB cores. The material recovered with the XCB was generally poor in quality and quantity for physical-property measurements, but samples were carefully selected to ensure maximum data quality. Many cores that did not contain material of acceptable quality were not sampled, which resulted in sparse data coverage over some intervals. No samples were taken from Hole 683B.

Index Properties

The index properties measured at Site 683 include water content (presented as a percentage of dry sample weight), porosity, and bulk and grain densities (Table 12). These were calculated using an assumed salinity of 35‰. Figure 36 illustrates the water-content and porosity profiles for Hole 683A. Both properties show considerable variation through the top 80 m of lithologic Unit I (Subunits IA through IC; Fig. 37) similar to that seen at previous Leg 112 sites. The average values of water content (120%–150%) and porosity (80%) remain approximately constant over this interval. No samples were recovered between 80 and 120 mbsf. However, below 120 m both these properties steadily decreased downhole through Subunits ID and IIA to approximately 300 mbsf (Fig. 36). Below 300 m, which is approximately equivalent to the Subunit IIA/IIB boundary, water content and porosity appear to increase slightly to 65% and 64%, respectively, at 418 m near the bottom of the hole.

The bulk-density profile for Hole 683A (Fig. 38), based on both GRAPE and measured values, shows a similar variability in the upper 80 m with values oscillating between 1.3 and 1.6 g/cm^3. Both GRAPE and measured values of bulk density decrease below 80 mbsf to an apparent minimum between 160 and 175 mbsf. This zone corresponds closely to a decrease of $CaCO_3$ concentration in the sediments downhole. Below 175 mbsf, the bulk density increases with depth through Subunits ID and IIA. At the Subunit IIA/IIB boundary, the bulk density shows a stepwise increase from values of less than 1.6 g/cm^3 to values greater than 1.9 g/cm^3. These values then appear to decrease slightly to the bottom of the hole. The GRAPE profile for Hole 683B (Fig. 39) indicates another significant step in bulk density below 430 m, which corresponds approximately to the boundary between Units II and III, a major unconformity.

Compressional-Wave Velocity

Velocity measurements in Hole 683A were conducted on APC cores using the *P*-wave logger mounted adjacent to the GRAPE. As at previous sites, XCB cores were not good enough to transmit sound waves through the sediment; thus all measurements in XCB cores had to be discounted. Furthermore, the presence of gas in most APC cores also limited the amount of useful ve-

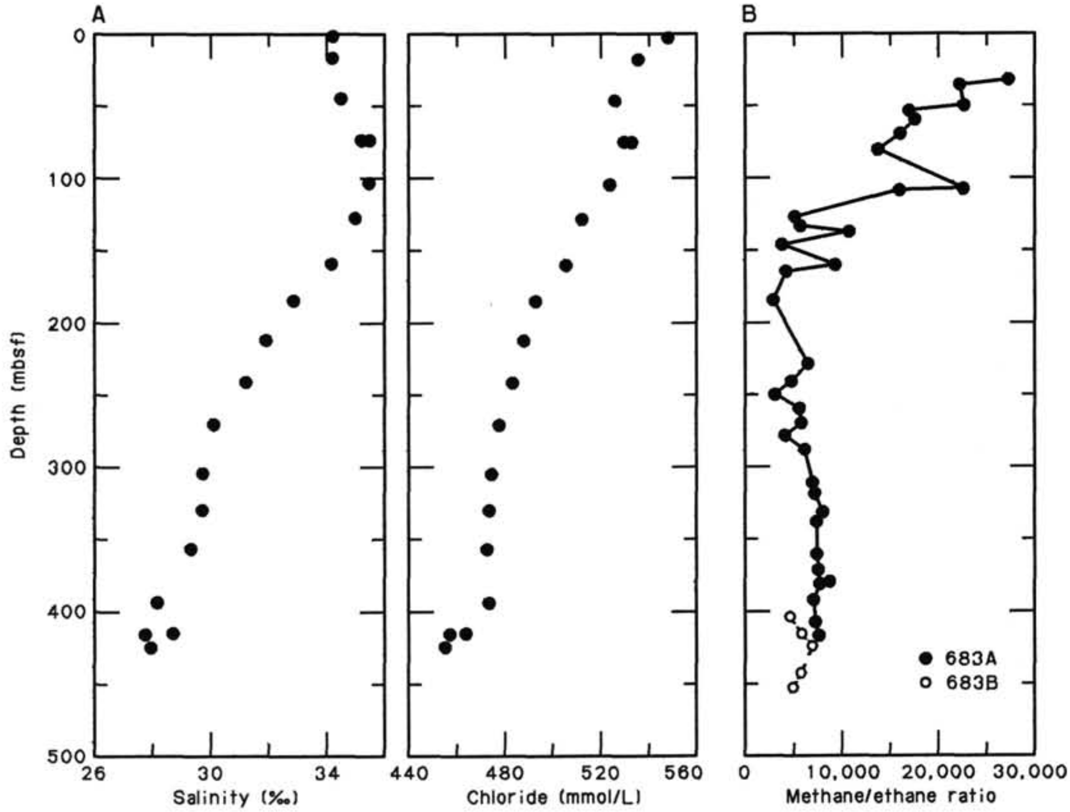

Figure 31. A. Interstitial salinity and chloride profiles. B. Methane/ethane ratio at Site 683.

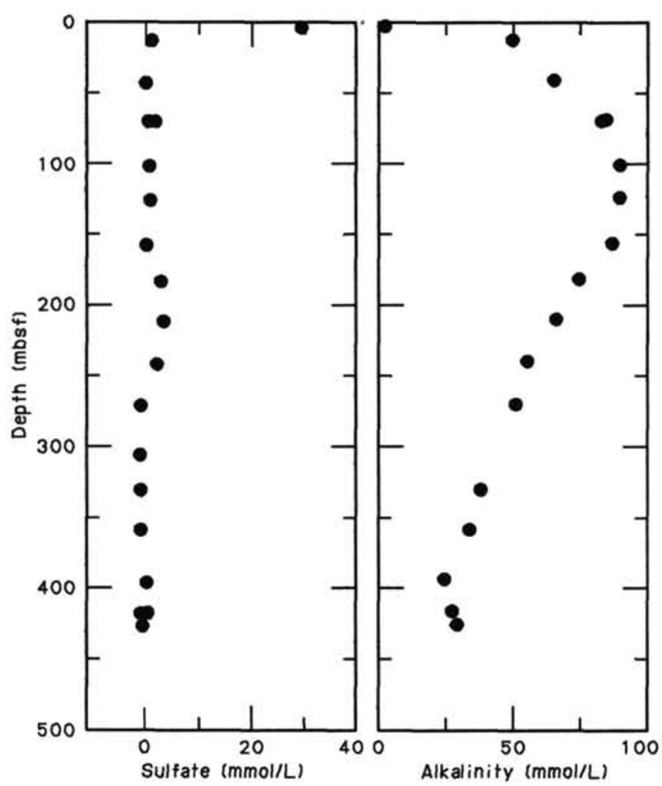

Figure 32. Interstitial sulfate and alkalinity profiles at Site 683.

locity data that could be obtained. The few valid measurements that we were able to get for Hole 683A are summarized in Figure 40. Velocities in the top 50 m of the hole range from 1483 to 1532 m/s. Our attempts to measure velocities on unlithified sediment with the Hamilton Frame were unsuccessful owing to the friability of the sediment recovered in XCB cores. Two velocity measurements on a cemented limestone bed in Section 112-683B-6X, CC gave values of 3.24 and 3.26, respectively.

Vane Shear Strength

The undrained vane shear strength measurements for Site 683 were performed with the Wykham Farrance vane apparatus and are listed in Table 13. Measurements were conducted in Hole 683A down to Core 112-683A-10X, after which core material was too disturbed for valid measurements. Subunit IA shows a relatively uniform shear strength profile (Fig. 41) with values between 30 and 50 kPa. Below 50 mbsf, the strength increases sharply with depth in Subunits IB and IC.

Total Overburden Stress

The total overburden stress was calculated for Site 683 using bulk-density measurements and assuming hydrostatic pore-pressure conditions. The total stress profile (Fig. 42) shows a slight deviation from a linear increase with depth at approximately 110–135 mbsf, which is slightly below the lithologic Unit IC/ID boundary. A second change in slope of the total stress profile occurs at approximately 270–290 mbsf, just above the Subunit IIA/IIB boundary.

Thermal Conductivity

Thermal conductivity was measured using the needle-probe method on Cores 112-683A-2H through 112-683A-10X. Below

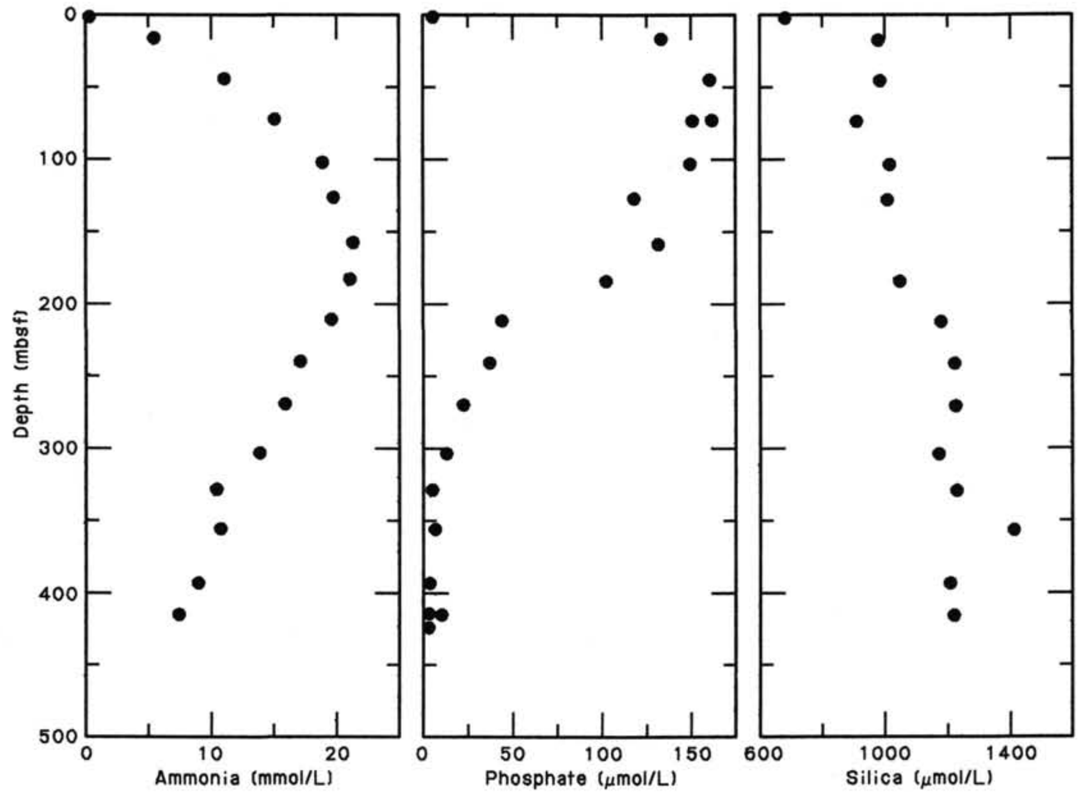

Figure 33. Interstitial ammonia, phosphate, and silica profiles at Site 683.

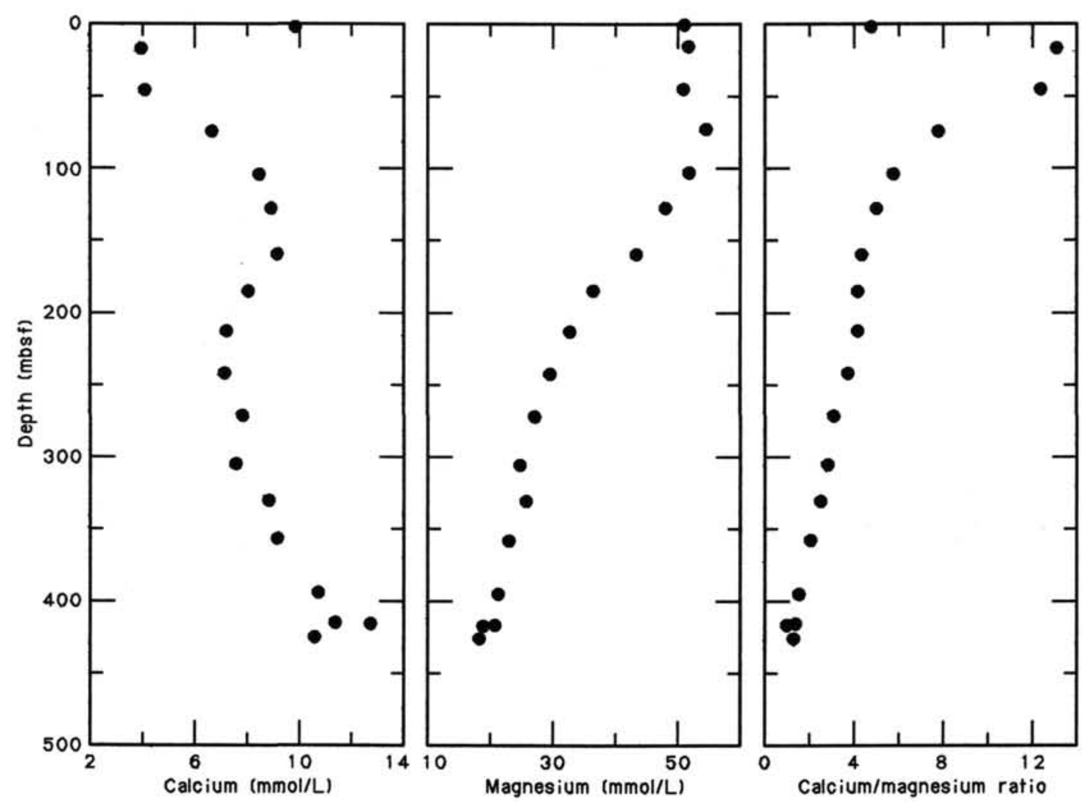

Figure 34. Interstitial calcium, magnesium, and Mg^{2+}/Ca^{2+} profiles at Site 683.

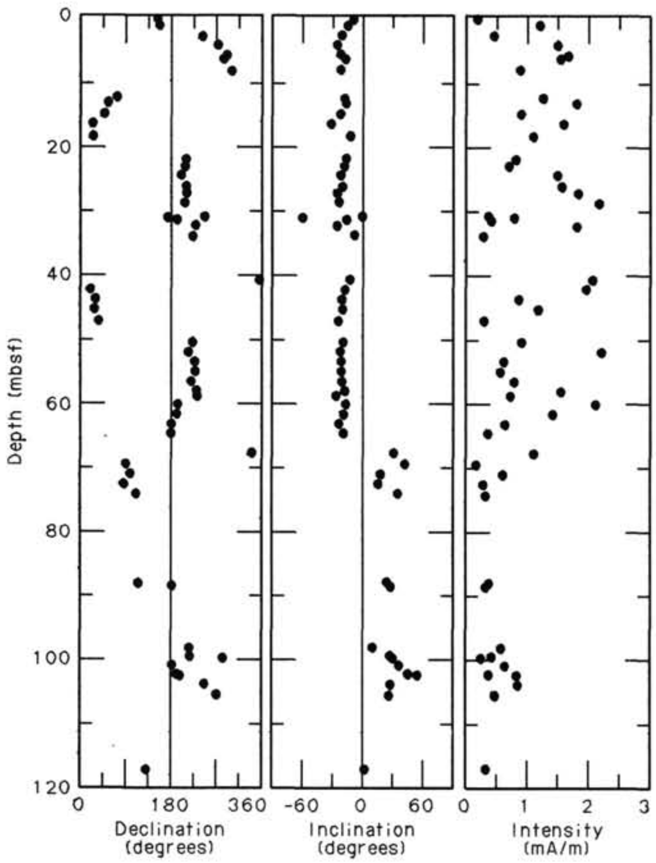

Figure 35. Declination, inclination, and magnetic intensity plots vs. depth below seafloor. Note that the Brunhes Matuyama boundary occurs at 65 mbsf. Rotations are observed in the declination values from the two uppermost cores. A cyclicity of intensity values also is suggested in the upper 75 m of the section.

this depth, samples were too disturbed by drilling for reliable measurements. The obtained values are listed in Table 14 and plotted vs. depth in Figure 43.

The thermal conductivity shows variation in oscillations of lithologic Subunits IA and IB. This variation is consistent with the variation of index properties. Figure 44 shows the relation between thermal conductivity and water content for the data that were measured at almost the same points. It is obvious that thermal conductivity correlates well with the water content for APC samples.

Thermal conductivity is relatively low in Subunit IC. However, some of these low values could possibly result from disturbance of the core. This may be supported by our observation that thermal conductivity is too low when compared with the water content at the same depth (indicated by pluses in Fig. 44).

Discussion

The physical-properties data from Site 683 show some interesting trends similar to those found at other Leg 112 sites. The variability of index properties at Site 683 (Figs. 36 and 37) is common to most of the sites where a continuous Quaternary sequence was recovered. The index properties are sensitive to lithological variations and appear to be related to subtle differences in composition or degree of bioturbation. In contrast to other sites (compare, for example, Site 682, Fig. 39), the vane shear strength through this sequence remains low, although minor variations are seen.

Table 12. Summary of index-properties data from Hole 683A

Core/section interval (cm)	Depth (mbsf)	Water contents (% dry wt)	Porosity (%)	Bulk density (g/cm^3)	Grain density (g/cm^3)
112-683A-1-1, 119	1.19	167.82	82.47	1.35	2.46
2-2, 82	4.52	180.27	83.02	1.32	2.33
2-4, 71	7.41	149.66	81.94	1.40	2.45
3-2, 71	13.91	152.45	83.18	1.41	2.58
3-2, 56	16.76	129.67	79.72	1.45	2.57
4-2, 64	23.34	112.55	75.01	1.45	2.41
4-4, 55	26.25	126.01	77.96	1.43	2.52
4-6, 78	29.48	131.17	79.27	1.43	2.38
5-2, 83	33.03	126.90	78.27	1.43	2.48
5-3, 83	34.53	168.91	82.52	1.35	2.42
6-2, 75	42.45	134.53	79.32	1.42	2.39
6-3, 62	43.82	138.99	80.82	1.42	2.33
6-6, 79	47.24	109.26	76.69	1.50	2.59
7-2, 72	51.92	112.98	77.36	1.49	2.61
7-4, 84	55.04	105.64	73.88	1.47	2.40
7-6, 93	58.13	130.01	79.92	1.45	2.57
8-2, 91	61.61	118.97	77.61	1.46	1.98
8-6, 33	67.03	198.93	86.88	1.34	2.21
9-2, 79	70.99	208.67	83.85	1.27	1.94
9-5, 17	74.87	176.11	85.17	1.37	2.27
9-5, 75	75.45	169.94	83.91	1.37	2.38
9-6, 67	76.87	130.94	80.14	1.45	2.56
10-1, 63	78.83	92.52	74.26	1.58	2.54
16-1, 133	136.53	145.19	81.06	1.40	2.47
18-3, 71	157.91	139.75	78.57	1.38	2.29
18-4, 11	158.81	178.42	83.28	1.33	2.12
21-2, 65	184.85	119.44	75.18	1.42	2.23
24-1, 59	211.79	79.04	66.93	1.55	2.38
26-1, 33	230.53	104.44	72.12	1.45	2.09
30-1, 36	268.56	69.93	65.42	1.63	2.46
30-1, 126	269.46	81.65	67.68	1.54	2.25
34-4, 99	311.69	37.28	50.81	1.92	2.61
40-2, 141	366.11	51.85	60.55	1.82	2.58
40-4, 80	368.50	63.26	63.03	1.67	2.34
45-5, 25	415.95	56.25	60.07	1.71	2.55
45-6, 58	417.78	65.21	63.95	1.66	2.48

The decrease in bulk density in Unit ID (Fig. 38) appears to correlate with mineralogic and geochemical data that indicate a decrease in total carbonate content (Fig. 15, "Lithostratigraphy" section, this chapter). Calcium carbonate contents in Subunits IA and IB (down to 75 mbsf) are generally high, averaging about 10%. Smear slides indicate that much of the carbonate in these sediments is authigenic calcite. Below 75 mbsf, the carbonate content is reduced drastically in a zone where pore waters show an increase in Ca^{2+} and a corresponding decrease in Mg^{2+}. This significant reduction in the relatively dense carbonate probably results in the decreased bulk density of the sediments in this unit.

It is also possible that dissolution of calcite and replacement by rather smaller volumes of dolomite could be accompanied by increased porosity with a resultant decrease in bulk density. Unfortunately, porosity data are sparse in this region. The few data points at the base of the sequence do not indicate anomalously high porosity. However, at Site 682 a similar pattern is seen in Unit IA, where low bulk densities are associated with carbonate dissolution. At Site 682, an increase in porosity is associated with this zone of low bulk density.

The bulk-density data also show significant changes at depths of 300 mbsf in Hole 683A and at 430 m in Hole 683B. The latter value correlates well with the unconformity between Eocene and middle Miocene sediments, but the former value occurs almost 60 m below a middle Miocene–Pliocene hiatus. In the absence of major lithological differences between the two units, this sudden increase in bulk density at 300 m may indicate another unconformity at this level. Isolated dolomitic intervals are re-

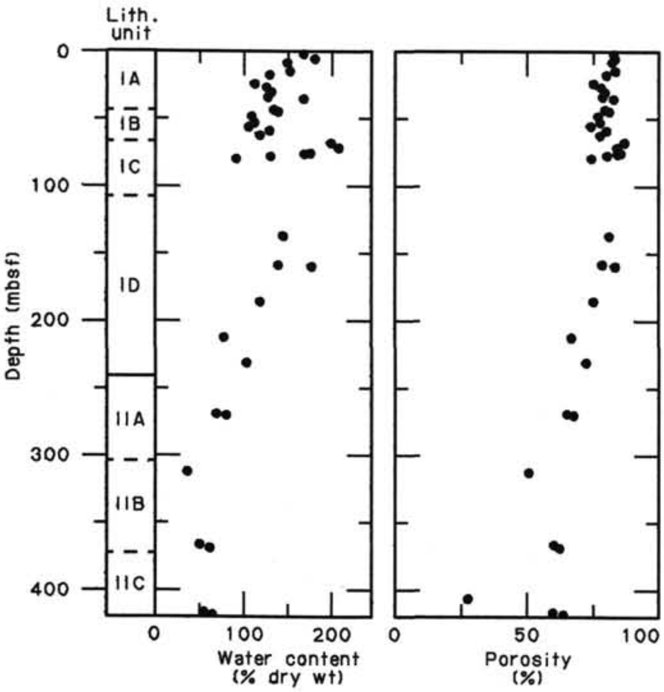

Figure 36. Water-content and porosity profiles for Hole 683A. Lithologic units are shown schematically.

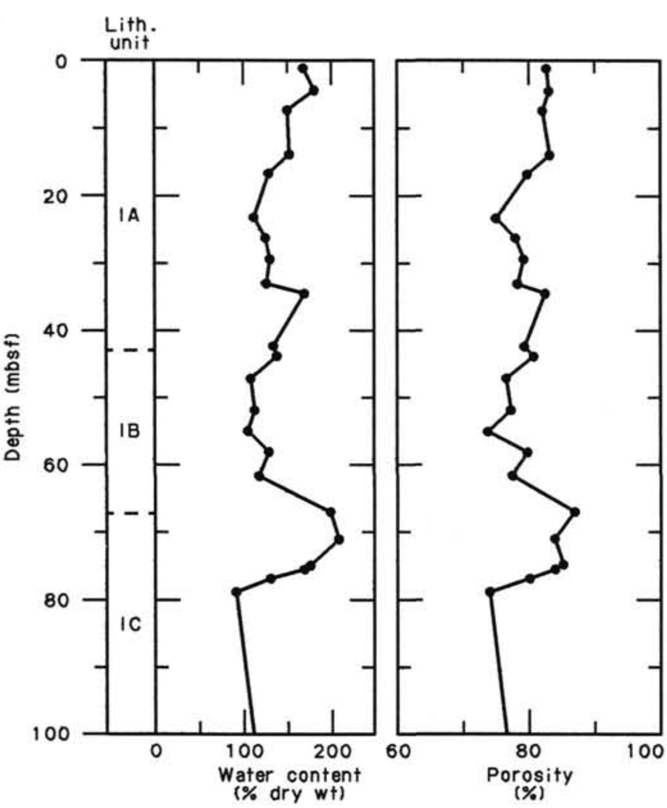

Figure 37. Details of water-content and porosity profiles for the top 100 m of Hole 683A. Lithologic units are shown schematically.

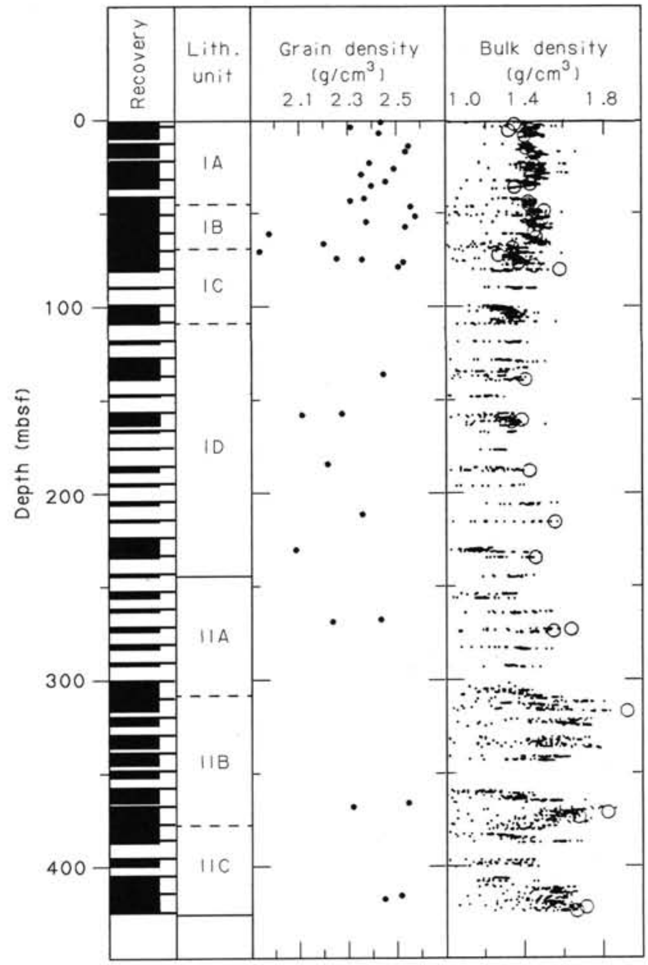

Figure 38. Bulk- and grain-density profiles for Hole 683A. Small dots indicate GRAPE-derived bulk densities; open circles shows bulk densities measured from samples.

corded in Core 112-683A-34 (see "Lithostratigraphy" section, this chapter), but dolomitization does not appear to be pervasive enough to cause this major change in bulk density.

GEOPHYSICS

Seismic Reflection

The sites along the northern of the two corridors of geophysical information across the Peru margin are located on seismic record CDP-2 (also Peru-2), which was shot across the continental slope, across the trench, and onto the floor of the Pacific Basin. These data were recorded by Seiscom-Delta for the Nazca Plate Project on a DFS-3 system using a sound source of two 300-in.^{3} and two 1000-in.^{3} air guns. The returning signals were detected on a 1600-m hydrophone streamer with 24 hydrophone groups. The processing performed for the Nazca Plate Project was only 12-fold and did not include migration. Copies of the field tapes were used for reprocessing data at the U.S. Geological Survey facility in Denver, Colorado (von Huene et al., 1985; Kulm et al., in press). The processing sequence included migration before stacking, which was applied in a manner developed especially for deep-water data (Miller and von Huene, 1986). A major part of the line is shown in Figure 45.

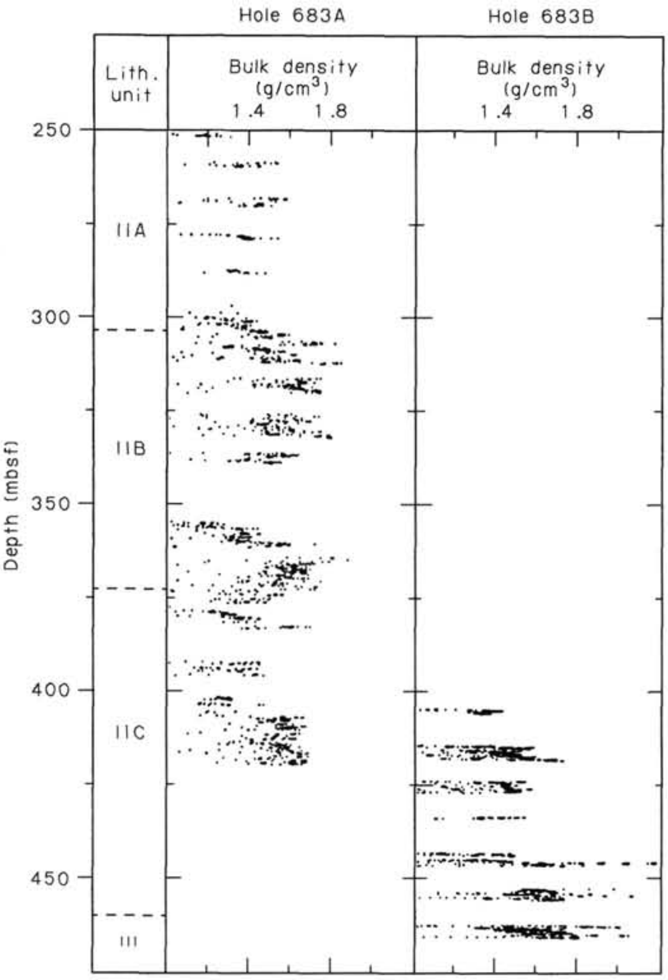

Figure 39. GRAPE bulk densities for the lower part of Hole 683A and all of 683B. Note the distinct stepwise increases at 300 m in Hole 683A and at 440 m in Hole 683B.

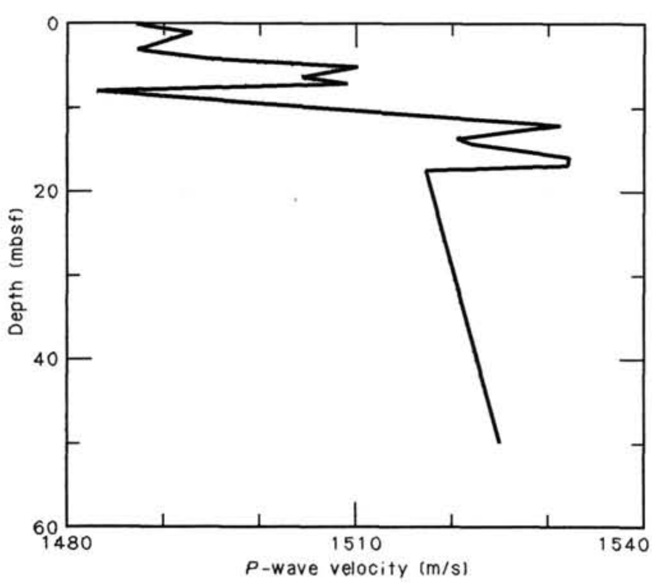

Figure 40. *P*-wave velocity data for Hole 683A.

Table 13. Summary of vane-shear-strength data from Hole 683A.

Core/section interval (cm)	Depth (mbsf)	Undrained vane strength (kPa)
112-683A-1H-1, 117	1.17	33.22
2H-2, 80	4.50	35.52
2H-4, 75	7.45	42.45
3H-2, 65	13.87	52.13
3H-4, 54	16.76	47.52
4H-2, 62	23.34	51.67
4H-4, 60	26.25	47.98
4H-6, 75	29.48	40.60
5H-2, 80	33.03	40.60
5H-3, 80	34.53	45.21
6H-2, 80	42.45	45.21
7H-2, 72	51.92	34.60
7H-4, 88	55.04	47.98
7H-6, 94	58.14	55.82
8H-2, 93	61.63	48.44
8H-4, 58	64.28	70.59
8H-7, 33	67.03	62.28
9H-2, 79	70.99	60.90
9H-5, 17	74.87	89.04
9H-5, 75	75.45	114.88
9H-6, 67	76.87	77.05
10X-1, 63	78.83	61.82

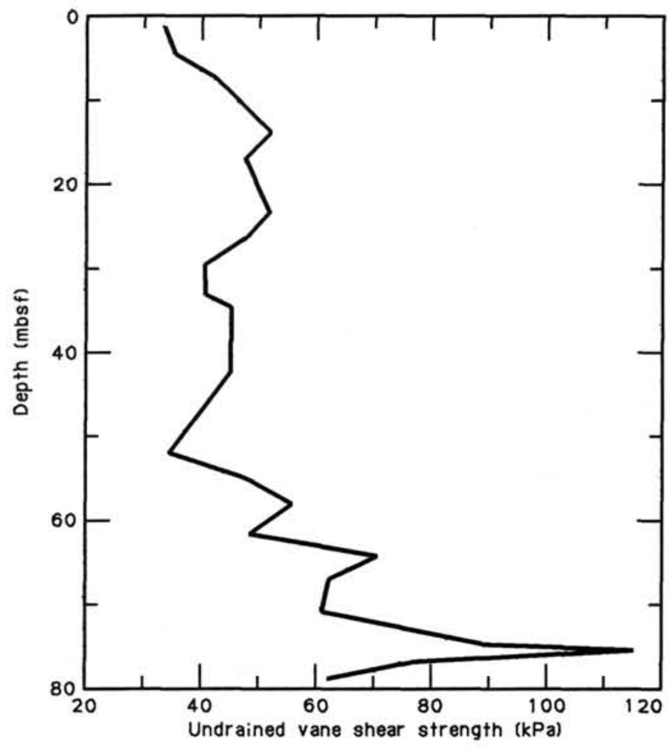

Figure 41. Vane-shear-strength profile for the top 80 m of Hole 683A.

A series of sites was selected for drilling along seismic record CDP-2, which crossed the transition between the continental crust and the accretionary complex. Site 683 was selected to provide a landward reference section that characterizes crust of continental affinity. This reference section was compared with other sites in the transitional and accreted sections. The most seaward part of the continental crust underlies Yaquina Basin, which is represented by the landward part of the seismic record (Fig. 45) and is located beneath the upper slope. At the base of

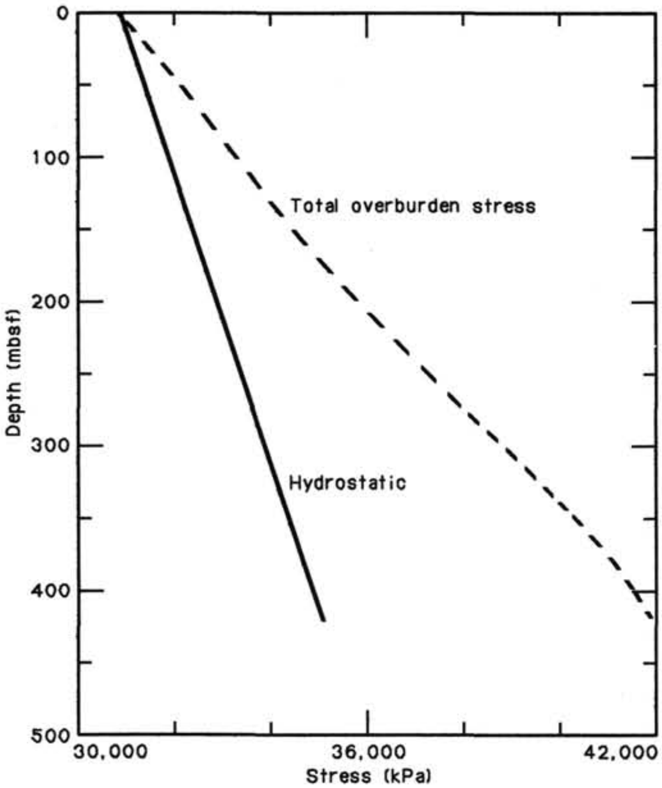

Figure 42. Hydrostatic and total overburden stress profiles for Site 683. Total overburden stress was calculated from bulk-density measurements by assuming hydrostatic pore-pressure conditions.

the Yaquina Basin sediment sequence, the basement is identified by a lack of structure, except for rare weak reflections. Some strong but irregular reflections occur at the top of the basement surface. These surface reflections are overlain by a unit having a strong upper reflective boundary but little internal structure. This unit is overlain in turn by a well-stratified sequence having considerable sedimentary and tectonic structure (Ballesteros et al., this volume).

This basement has an accoustic velocity of around 5.6 km/s, and it probably represents metamorphic rock similar to that recovered at the Delphin drill hole about 30 km to the east (Thornburg, 1985). The overlying sedimentary unit having little internal structure corresponds in position to a unit with a seismic velocity of 3.6 km/s in an adjacent seismic refraction section (Jones, 1981). Eocene rock in the Delphin drill hole is in a similar stratigraphic position and has a seismic velocity of 3.0 km/s. An earlier study interpreted this unit having little structure as Eocene (von Huene et al., 1985). The upper, well-stratified unit has a great deal of structure, including an antiform, normal faults, and bedding that has various dips (Ballesteros et al., this volume). Sedimentary units have lateral changes in thickness, indicate local unconformities, and are locally truncated at the seafloor. This basic structure is cut by many normal faults. Because of the dissimilarity between the structure of the upper unit and the structure of the reflections beneath it, von Huene et al. (1985) attributed this internal structure to sedimentation rather than tectonics (Fig. 45).

Site 683 was located on the seaward flank of Yaquina Basin, where the upper sequence of sediment thins to provide ready access to the older sequences below, but this lower sequence is not as severely faulted as it is in the midslope area (Fig. 45). Below a possible thin distal wedge of the upper stratified unit that is hidden in the seafloor reverberation, the lower unit is characterized by few internal reflections and extends for about 0.4 s. This corresponds to about 600 or 700 m at a refraction velocity between 3.0 and 3.6 km/s. Drilling proved many of our geophysical hypotheses to be incorrect. Instead of being Eocene, the lower, poorly reflective unit corresponded to a sequence of massive diatomaceous strata of middle Miocene to Quaternary age. The high-amplitude reflections at the base of the unit are rocks of middle Eocene age that unconformably underlie the Neogene section. The question then becomes "What is the source of error?"

Table 14. Thermal-conductivity data for Hole 683A.

Core/section interval (cm)	Depth (m)	Thermal conductivity (W/m·K)
112-683A-2H-3, 90	6.10	0.870
2H-4, 70	7.40	0.809
2H-4, 120	7.90	0.868
2H-5, 40	8.60	0.802
3H-1, 70	12.40	0.715
3H-2, 70	13.90	0.808
3H-3, 70	15.40	0.800
3H-4, 70	16.90	0.848
3H-5, 40	18.10	0.868
3H-5, 120	18.90	0.882
4H-1, 70	21.90	0.854
4H-2, 70	23.40	0.884
4H-3, 70	24.90	0.903
4H-4, 70	26.40	0.813
4H-5, 70	27.90	0.945
4H-6, 70	29.40	0.852
5H-1, 70	31.40	0.831
5H-2, 70	32.90	0.885
5H-3, 70	34.40	0.799
6H-1, 70	40.90	0.766
6H-2, 70	42.40	0.821
6H-3, 50	43.70	0.838
6H-6, 40	46.62	0.910
6H-7, 40	48.12	0.886
7H-2, 70	51.90	0.871
7H-4, 70	54.90	0.933
7H-5, 70	56.40	0.912
7H-6, 47	57.77	0.875
8H-1, 58	59.78	0.806
8H-5, 25	65.19	0.900
8H-6, 75	67.19	0.752
8H-7, 35	68.29	0.730
9H-2, 70	70.73	0.729
9H-4, 79	73.82	0.789
9H-5, 41	74.94	0.776
9H-6, 47	76.50	0.684
10X-1, 67	78.87	0.726

A review of the refraction velocity data shows that the boundaries were highly generalized and similar to earlier interpretations of CDP-2 (Jones, 1981). An overlapping pair of stations, sonobuoys 6 and 9, were shot downdip across the entire slope. The variations in thickness of sediment sequences as well as the major tectonic boundary occurring between this pair of stations are complexities that analysis of these data cannot resolve. Thus the velocity measured was probably from the weathered zone of the metamorphic basement. The differences in the velocity models of Jones (1981) and Hussong et al. (1976) for the same transect (but using different refraction methods and the two points on which the 3.6 km/s velocity is based) further suggest that these data provide only a raw estimate. It now seems that a more appropriate velocity for the Eocene rocks beneath the slope, which is still in the appropriate stratigraphic position, is the 2.5 km/s layer (Jones, 1981; Dang, 1985).

Another problem with previous interpretations of seismic record CDP-2 stems from an incorrect age for the greater part of

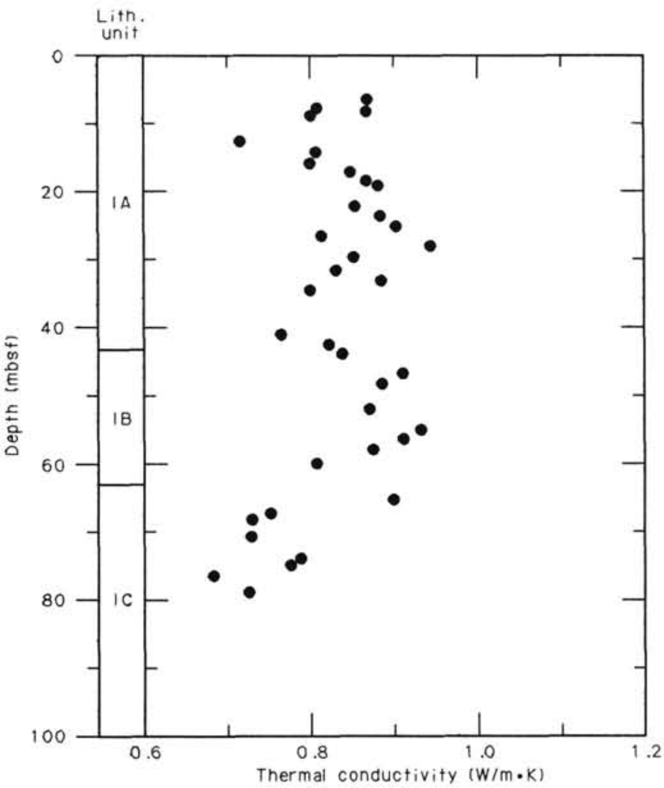

Figure 43. Thermal conductivity vs. depth below seafloor for Hole 683A.

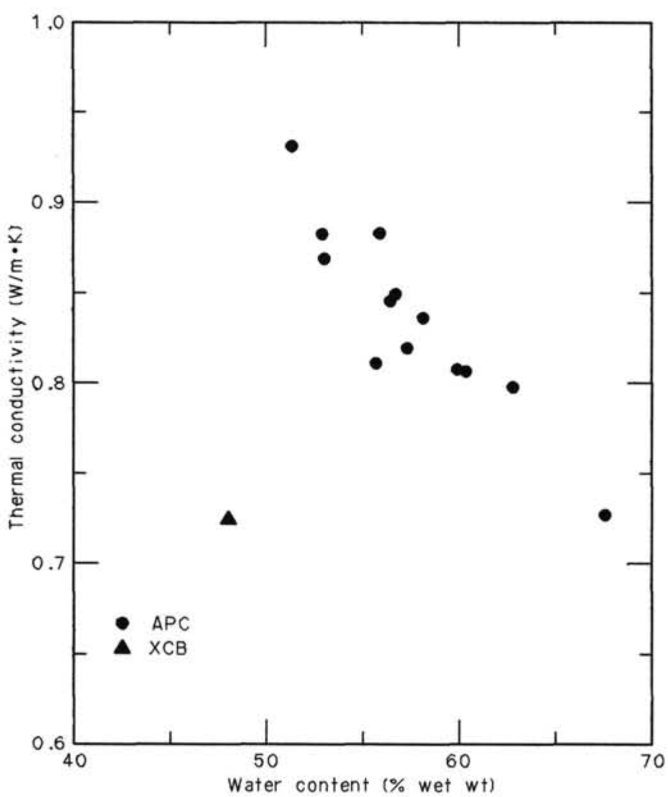

Figure 44. Thermal conductivity vs. water content for Hole 683A.

the section penetrated by the Delphin drill hole. Further paleontological work (both pre-cruise and on board the *Resolution*) indicated that samples from this hole were Miocene instead of Oligocene (Schrader and Cruzado, 1987).

At Site 683, only the top 50 m of core measurements provided reliable velocity data (see "Physical Properties" section, this chapter), which required us to estimate the depths to various reflections from a general velocity curve of data obtained at other Leg 112 sites, such as the logging data (Site 679) and the 2.5-km/s refraction point (Fig. 46). Applying a velocity gradient so constructed to the time intercepts of the reflection record provided results consistent with the character of the lithologies drilled. A low-angle discordance at 0.14 s corresponds to 110 m (Fig. 47), which is about the depth of the boundary between Quaternary and Pliocene sediments. That boundary can be followed upslope, where it becomes increasingly deeper, which suggests a major Quaternary depocenter in Yaquina Basin. The Pliocene and Miocene are represented by weakly reflective landward-dipping events. These events merge with the series of high-amplitude reflections that are just below the bottom depth of Hole 683A.

At Hole 683B, the high-amplitude reflection begins at about 0.54 s, which corresponds to a depth of about 485 mbsf. This depth is about 35 m deeper than the major hiatus between the middle Miocene and the middle Eocene. Considering the uncertainty of the velocity and the time intercepts, agreement between the depth of these high-amplitude reflections and the recovered Eocene rocks is reasonable. The base of the zone of high-amplitude reflections is at about 710 m, which indicates a middle Eocene or older sedimentary section of about 225 m thick. At the Delphin drill hole, the Eocene is shown to be 480 m thick and separated from the overlying sediment section by a profound hiatus that probably eliminated the Oligocene rock (Schrader and Cruzado, 1987). In the seismic record, the top of the middle Eocene or older sediment section had a rough upper surface and appeared to be an erosional unconformity that extends about 15 km landward from the site. Considering that we found the same hiatus at both the Delphin drill hole and Site 682, the unconformity is probably a feature of regional extension.

The significance of this unconformity to the tectonic history of the Peruvian margin may lie in its correspondence in time to the first andesitic and dacitic tuffs of the arc volcanism in the Cordillera Occidental and probably also to the great lowering of sea level in the Oligocene. The time of the first arc volcanism is thought to mark the beginning of the rapid uplift of today's Andes. This orogeny, coupled with lowered sea levels, may have profoundly affected the continental shelf at that time.

Heat Flow

Temperature Measurements

Temperatures were measured three times at Site 683 using the APC tool. The tool was first run while recovering Core 112-683A-5H. The temperature record indicates typical frictional heating and decay curves (Fig. 48) that give an extrapolated temperature of 4.0 ± 0.2°C at 40.2 mbsf. We were unable to conduct further measurements during APC coring owing to hard sediments.

The other two runs of the APC tool were made with the pore-water sampler following Cores 112-683A-25X and 112-683A-39X. The temperature recorded just before we pulled out of the hole can be regarded as the lower limits of the true formation temperature. These limits are 7.2°C at 230.2 mbsf and 10.0°C at 363.2 mbsf.

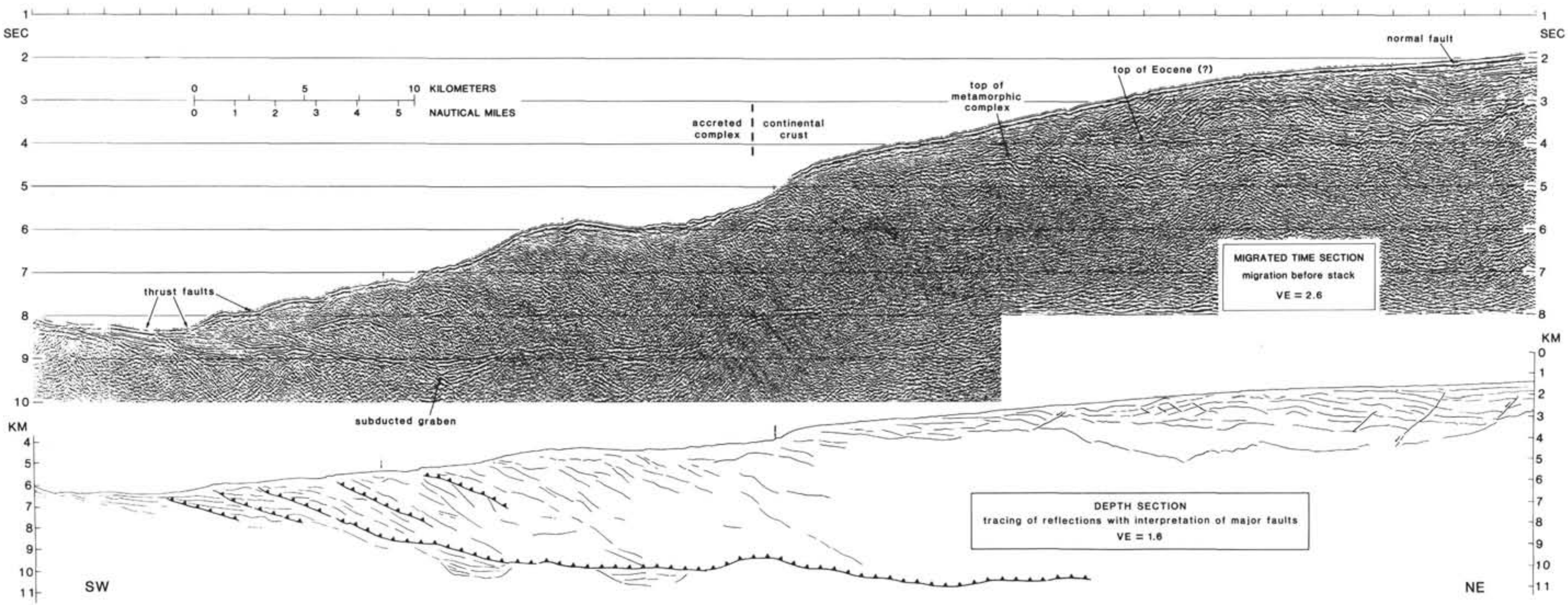

Figure 45. Migrated time section and line drawing of the corresponding depth section of CDP-2 (from Kulm et al., 1986).

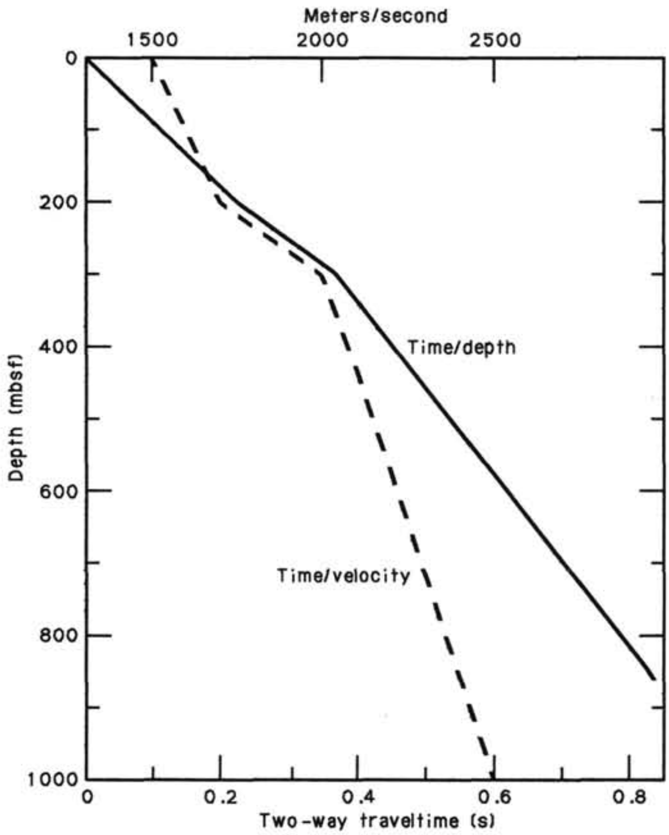

Figure 46. Estimated curve of velocity and the corresponding curve of intercept time with depth.

Heat-Flow Estimation

The temperature gradient between the seafloor and 40.2 mbsf was calculated from the bottom-water and the equilibrium temperatures extrapolated from the APC tool record. According to our oceanographic data, the bottom-water temperature was about 1.8°C, thus we estimated the gradient to be 50×10^{-3} K/m, correcting for the characteristic of the APC tool (see "Explanatory Notes," this volume). From thermal-conductivity data corrected to *in-situ* temperature and pressure conditions, the heat flow from 0 to 40.2 mbsf was calculated to be 39 mW/m^2. This value is consistent with the 32–45 mW/m^2 value measured by ordinary surface heat flow probes on the midslope of the Peru Trench near Site 683 (Yamano, 1986).

Based on this heat-flow value, we estimated the temperature vs. depth profile in Hole 683A, a plot of which is shown in Figure 49. Temperatures between the seafloor and 80 mbsf (indicated by a solid line) were determined from heat-flow and thermal-conductivity data obtained at Hole 683A. Below 80 mbsf (indicated by a broken line), we estimated temperature using the thermal-conductivity values inferred from water-content data, based on the relationship of thermal conductivity vs. water content for Leg 112 samples (see "Physical Properties" section, Site 688 chapter). In Figure 49, this equilibrium temperature is indicated by a circle, and lower limit temperatures obtained from our records using the APC tool are represented by triangles.

SUMMARY AND CONCLUSIONS

A major objective at Site 683 was to establish a reference section for the upper part of the continental crust that could be compared with that for the accreted complex at the foot of the Peruvian margin. Thus, this site was selected at the most seaward area, where geophysical characteristics of the continental section could be observed as they are displayed at the Delphin drill hole, about 30 km landward. In addition, water depths during the Cenozoic should have been sufficient at this site to record fluctuations of coastal upwelling without the major hiatuses found in the sediment sequence located on the shelf.

At the Delphin drill hole, Paleozoic metamorphic basement is unconformably overlain by about 60 m of sandy micaceous sediment containing megafossils and reworked basement rock. This in turn is overlain by a clastic sequence mixed with carbonate beds deposited during Eocene time. The early submergence that allowed deposition of this proximal marine sediment probably continued through at least part of the Neogene Andean orogeny. The unconformity is presently located at a depth of about 2.7 km. If such subsidence is regional, then it must be related to the plate convergence that accompanied Neogene tectonism. This requires some form of tectonic erosion in the subduction zone. Although we did not sample basement at Site 683, the microfossils and lithology of the uppermost part of a 250-m-thick Eocene section suggests subsidence at the site in agreement with such a concept.

The Neogene lithology at Site 683 is dominated by diatomaceous mud and mudstone and which was deposited at a lower-bathyal depth (2 to 4 km) and which correlates to a modern depth of about 3 km. A major unconformity separates the section into two lithological units. The upper is a 240-m-thick upper Pliocene to Quaternary diatomaceous mud and mudstone with a calcareous sequence beginning at about 30 m and extending to 67 m, followed by a silt-rich sequence that grades to a poorly recovered section containing mostly mud. Overall rates of sediment accumulation are 100 m/m.y., which is greater than most of the rates measured on the shelf and upper slope during Leg 112. Apparently, much of the sediment was swept from the continental shelf because the diatoms are mixed assemblages of oceanic and near-shore upwelling genera, while 50% to 90% of the benthic foraminifers were transported from the shelf. The seismic record shows that the upper 70 m of the section at Site 683 is at the distal end of a wedge-shaped body that becomes 800 to 900 m thick at the depositional center of Yaquina Basin, about 18 km upslope. Here, the unit contains irregular beds and laps down onto a flat reflection (Ballesteros et al., this volume). The underlying unit is distinguished by numerous turbidite beds and corresponds to seismic reflections of uniform thickness upslope to the edge of the shelf. Indication of abundant downslope transportation continues deeper in the section to the unconformity at the base of the Pliocene.

A hiatus of about 6.5 m.y. separates the Pliocene section from that of the middle Miocene. This hiatus corresponds to an angular unconformity in the seismic record at the site but becomes conformable about 15 km upslope. Middle Miocene lithologies are principally indurated diatomaceous mudstones marked by increased amounts of volcanic glass, sparse calcareous interbeds, and rare turbidites. Some of the mixed microfossil assemblages continue into this unit, but the sediment records hemipelagic sedimentation with sparse, transported clastic interbeds. The mudstones attain fissility with increasing consolidation and minor extensional microfaults.

In the Neogene sequence, diagenesis produces many of the same products seen in samples from the shelf, except in smaller amounts, which we also noted at Site 682. Calcite and dolomite are the main products of carbonate diagenesis. Generation of micritic dolomite layers and authigenic calcite cements throughout the sequence follows reaction pathways controlled by organic-matter diagenesis. The gradients of dissolved chemical species are steeper than at Site 682: the maxima and minima of calcium, magnesium, and alkalinity (all involved in carbonate mineral diagenesis) are more pronounced. The sulfate-reduction zone is compressed toward the sediment/water interface (<20

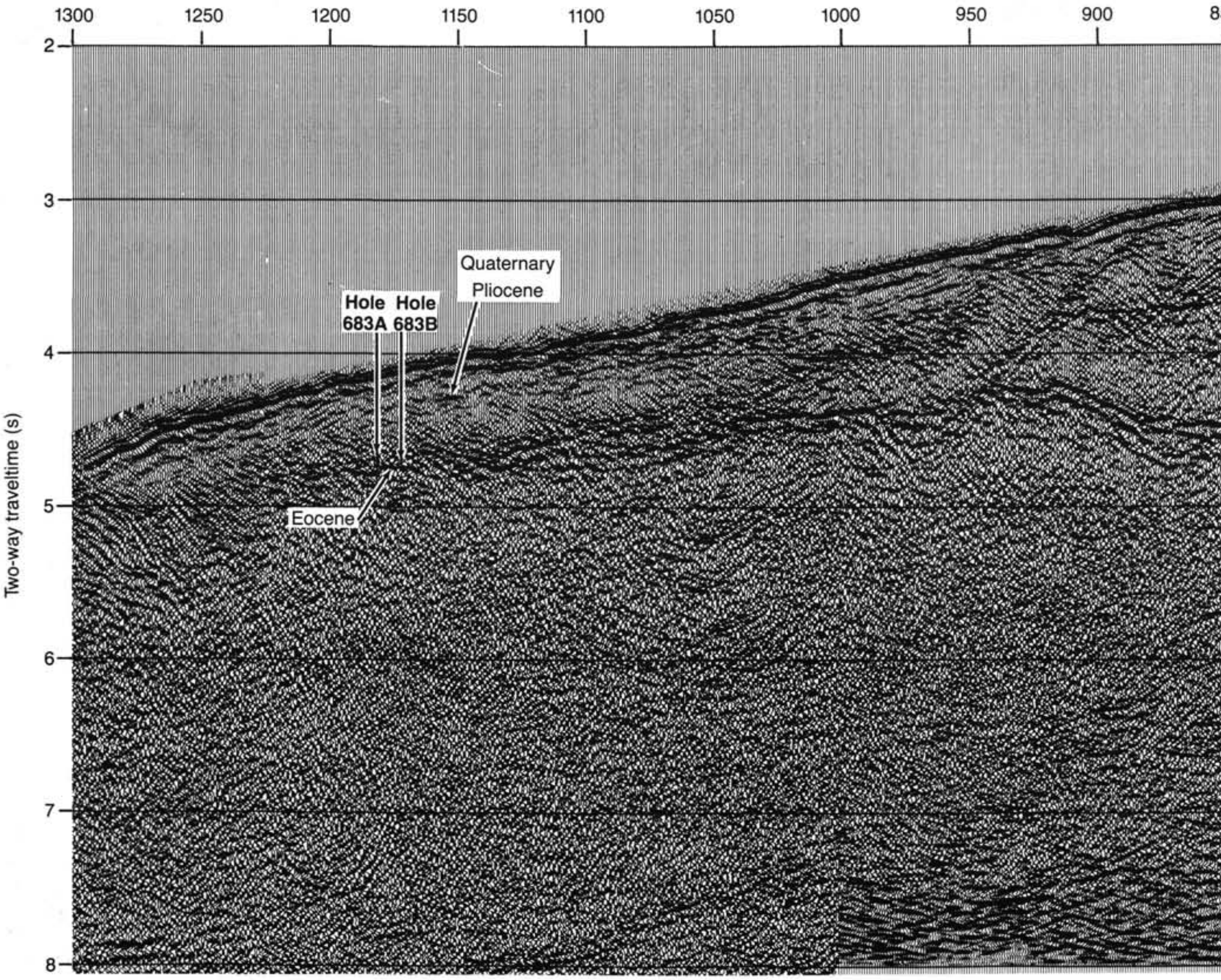

Figure 47. Large-scale seismic section for the area of Site 683.

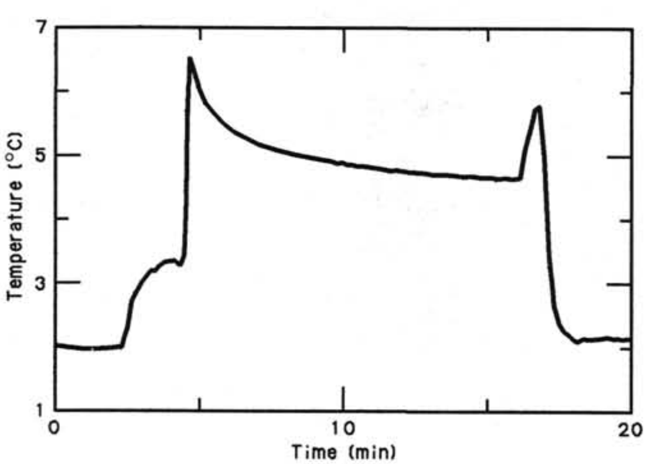

Figure 48. Temperature vs. time records obtained during recovery of Core 112-683A-5H using the APC tool.

mbsf), which is typical for rapidly accumulating sediments rich in organic carbon. Methanogenesis dominates throughout the remainder of the hole. Calcite precipitates first near the base of the sulfate-reduction zone. This causes the Mg^{2+}/Ca^{2+} molar ratio to increase dramatically to around 13, the highest value ever reported for nonevaporitive environments. Consequently, highly favorable conditions for rapid dolomitization prevail. With increasing dolomitization at depth, the Mg^{2+}/Ca^{2+} ratio decreases to a value <2, again favoring the development of calcite.

The middle Eocene sediment is delineated in seismic records as a unit with irregular reflections of low frequency and high amplitude bounded above and below by unconformities. The hiatus having the overlying Neogene sequence probably occurred for about 25 m.y., and the Eocene sediment contains more sand, volcanic glass, and lithic fragments, which contrasts with the ubiquitous diatoms of the Neogene. A well-indurated mudstone with good fissility contains some dolomicrite and micritic limestone breccias. As at Site 682, this unit contains shallow-water nannofossils and upper-bathyal and upper-middle-bathyal

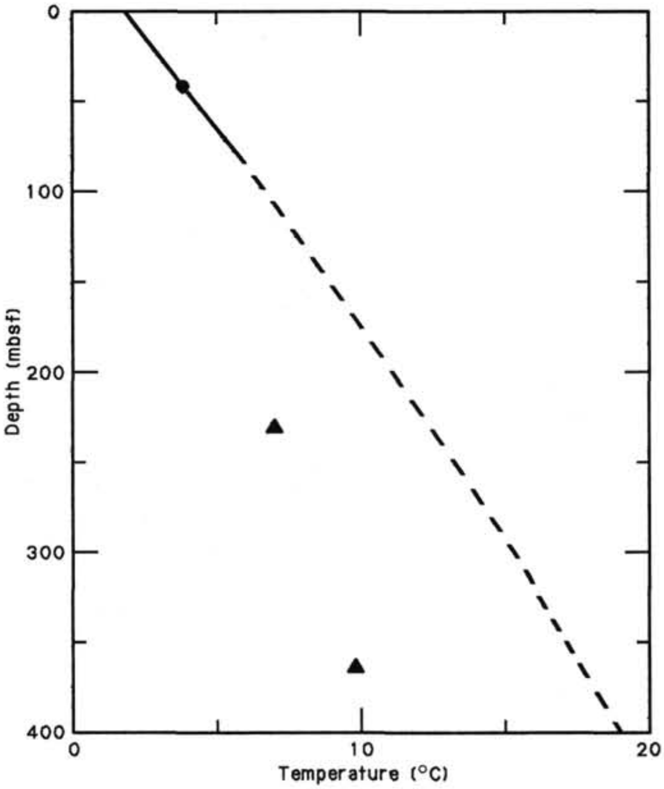

Figure 49. Temperature vs. depth plot for Hole 683A. Circle and triangles indicate the extrapolated equilibrium temperature and the lower limit temperatures, respectively. Solid line represents the temperature profile based on the heat-flow and thermal-conductivity data (0–40.2 mbsf) in Hole 683A. Broken line indicates the profile calculated using the estimated thermal conductivity.

benthic foraminifers, but the latter may have been transported. The seismic record indicates a thickness of about 250 m, with the underlying unconformity lying on the basement.

Organic matter at this site is primarily of marine origin. The Pliocene and Miocene sections have high organic-carbon contents (4–7 wt% of organic carbon), high hydrogen indices, and are immature. The Eocene and upper Quaternary organic matter has slightly higher oxygen indices and appears more mature. This peculiar maturity of organic matter in the oldest and youngest sediments may be explained by the greater age of the Eocene samples and a stronger reworking of the Quaternary sediment. The methane/ethane ratio decreased rapidly from $>25,000$ to <5000 at 126 m and remained about the same from there to the bottom of the hole. This change corresponds to the depth where salinity also begins to decrease, suggesting the presence of gas hydrates. We suspect that the essentially constant methane/ethane ratio may be linked to the containment of methane in a hydrated form, although the mechanism remains unclear. The decrease in chloride content with depth and the increase in alkalinity are similar to those values obtained at previous DSDP sites, where gas hydrates were usually observed visually. At Site 683, the upward diffusion of a residual brine, probably from the formation of gas hydrates, was observed for the first time in the anomalously high concentrations of salinity and chloride at about 100 m, only 26 m above the first indication of gas hydrates.

We noted an interesting stratigraphic similarity between Site 682 on the southern transect and Site 683 on the northern one, despite their separation by about 200 km. Both display a hiatus between approximately 8 and 12 m.y. and another major one above the Eocene sections, although the hiatuses at Site 683 appear to be of a longer duration. Both show similar stratigraphies, the greatest differences being the thick Pliocene–Quaternary section and the shorter Oligocene break at Site 683. We now believe that the same basic tectonic history exists in the revised stratigraphy of the Delphin drill hole (Schrader and Cruzado, in press). The similar tectonic histories at these three holes suggest a regional subsidence of the continental crust between Eocene and Miocene time.

REFERENCES

Anderson, R. N., Hobart, M. A., and Langseth, M. G., 1979. Convective heat transfer in oceanic crust and sediment in the Indian Ocean. *Science*, 204:828–832.

Baldauf, J. G., 1985. A high-resolution late Miocene–Pliocene diatom biostratigraphy for the eastern equatorial Pacific. *In* Meyer, L., Thayer, F., Thomas, E., et al., *Init. Repts. DSDP*, 85: Washington (U.S. Govt. Printing Office), 457–475.

Barron, J., 1985. Late Eocene to Holocene diatom biostratigraphy of the equatorial Pacific Ocean, Deep Sea Drilling Project Leg 85. *In* Meyer, L., Thayer, F., Thomas, E., et al., *Init. Repts. DSDP*, 85: Washington (U.S. Govt. Printing Office), 413–456.

Berggren, W. A., 1977. Atlas of Palaeogene planktonic foraminifera. Some species of the genera, *Subbotina, Planorotalites, Morozovella, Acarinina* and *Truncorotaloides*. *In* Ramsay, A.T.S. (Ed.), *Oceanic Micropaleontol.*, 1: 205–300.

Berggren, W. A., Aubry, M. P., and Hamilton, N., 1983. Neogene magnetobiostratigraphy of DSDP Site 516 (Rio Grande Rise, south Atlantic). *In* Barker, P. F., Carlson, R. L., Johnson, D. A., et al., *Init. Repts. DSDP*, 72: Washington (U.S. Govt. Printing Office), 675–706.

Blow, W. H., 1969. Late middle Eocene to Recent planktonic foraminiferal biostratigraphy. *In* Bronnimann, P., and Renz, H. H. (Eds.), *Proc. First Int. Conf. Planktonic Microfossils*, 1:199–421.

Bolli, H. M., and Saunders, J. B., 1985. Oligocene to Holocene low latitude planktic foraminifera. *In* Bolli, H. M., Saunders, J. B., Perch-Nielsen, K., (Eds.), *Plankton Stratigraphy*: London (Cambridge Univ. Press), 155–256.

Bourgois, J., Pautot, G., Bandy, W., Boinet, T., Chotin, P., Huchon, P., Lepinay, B., Monge, F., Monlaü, J., Pelletier, B., Sosson, M., and von Huene, R., in press. Tectonic regime of the Andean convergent margin off Peru (SeaPERC cruise of the R/V *Jean Charcot*, July, 1986). *C. R. Acad. Sci. Paris*.

Bullard, E. C., 1954. The flow of heat through the floor of the Atlantic Ocean. *Proc. R. Soc. London*, A-222:408–429.

Burckle, L. H., 1977. Pliocene and Pleistocene diatom datum levels from the equatorial Pacific. *Quat. Res.*, 7:330–340.

Claypool, G. E., and Kaplan, I. R., 1974. The origin and distribution of methane in marine sediments. *In* Kaplan, I. R. (Ed.), *Natural Gases in Marine Sediments*: New York (Plenum Press), 94–129.

Claypool, G. E., and Kvenvolden, K. A., 1938. Methane and other hydrocarbon gases in marine sediment. *Annu. Rev. Earth Planet. Sci. 1983*, 11:299–327.

Dang, S. P., 1985. Seismic refraction velocity structure. *In* Hussong, D. M., et al. (Eds.), *Atlas of the Ocean Margin Drilling Program, Peru Continental Margin, Region VI*: Woods Hole (Marine Science Int.).

De Wever, P., Riedel, W. R., et al., 1979. Recherches actuelles sur les Radiolaires en Europe. *Annu. Soc. Géol. Nord*, 98:205–222.

De Wever, P., 1982. Radiolaires du Trias et du Lias de la Tethys (taxonomie, stratigraphie). *Annu. Soc. Géol. Nord*, 7:

Douglas, R. G., 1973. Benthonic foraminiferal biostratigraphy in the Central North Pacific, Leg 17, Deep Sea Drilling Project. *In* Winterer, E. L., Ewing, J. I., et al., *Init. Repts. DSDP*, 17: Washington (U.S. Govt. Printing Office), 607–671.

Harrison, W. E., Hesse, R., and Gieskes, J. M., 1982. Relationship between sedimentary facies and interstitial water chemistry of slope, trench and Cocos Plate sites from the Middle America Trench transect, active margin off Guatemala, Deep Sea Drilling Project, Leg 67. *In* Aubouin, J., von Huene, R., et al., *Init. Repts. DSDP*, 67: Washington (U.S. Govt. Printing Office), 603–613.

Hesse, R., Lebel, J. and Gieskes, J. M., 1985. Interstitial water chemistry of gas-hydrate-bearing sections on the Middle America Trench slope, Deep Sea Drilling Project, Leg 84. *In* von Huene, R., Aubouin, J., et al., *Init. Repts. DSDP*, 84: Washington (U.S. Govt. Printing Office), 727-737.

Hussong, D. M., Edwards, P. B., Johnson, S. H., Campbell, J. F., and Sutton, G. H., 1976. Crustal structure of the Peru-Chile Trench: 8°S—12°S latitude. *Am. Geophys. Union Mono.*, 19:71-86.

Jones, P. R., 1981. Crustal structure of the Peru continental margin and adjacent Nazca plate, 9°S latitude. *In* Kulm, L. D., Dymond, J., Dasch, E. J., and Hussong, D. M. (Eds.), *Nazca Plate: Crustal Formation and Andean Convergence.* Geol. Soc. Am. Mem., 154:423-443.

Kennett, J. P., and Srinivasan, M. S., 1983. *Neogene Planktonic Foraminifera:* Stroudsburg, PA (Hutchison Ross).

Kling, S. A., 1978. Radiolaria. *In* Haq B. U., and Boersma, A. (Eds.), *Introduction to Marine Micropaleontology*: Amsterdam (Elsevier), 203-244.

Koizumi, I., 1986. Pliocene and Pleistocene diatom datum levels related with paleoceanography in the northwest Pacific. *Mar. Micropaleontol.*, 10:309-325.

Kulm, L. D., Schrader, H., Resig, J. M., Thornburg, T. M., Masias, A., and Johnson, L., 1981. Late Cenozoic carbonates on the Peru continental margin: lithostratigraphy, biostratigraphy, and tectonic history. *In* Kulm, L. D., Dymond, J., Dasch, E. J., and Hussong, D. M. (Eds.). *Nazca Plate: Crustal Formation and Andean Convergence.* Geol. Soc. Am. Mem., 154:469-508.

Kulm, L. D., Miller, J., and von Huene, R., 1986. The Peru Continental Margin Record, Section 2. *In* von Huene, R. (Ed.), *Seismic Images of Modern Convergent Margins.* AAPG Stud. in Geol., 26:39-40.

Kulm, L. D., Thornburg, T., and Resig, J., in press. Final Report of conduct of the Peru-Chile site survey.

Kvenvolden, K. A., 1985. Comparison of marine gas hydrates in sediments of an active and passive continental margin. *Mar. Petrol. Geol.*, 2:65-71.

Kvenvolden, K. A., and McMenamin, M. A., 1980. Hydrates of natural gas: A review of their geologic occurrence. *U.S. Geol. Surv. Cir. 825.*

Miller, J., and von Huene, R., 1986. Processing techniques for multichannel seismic data in deep water. *In* von Huene, R. (Ed.), *Seismic Images of Modern Convergent Margins.* AAPG Spec. Studies in Geol., 26.

Moore, G. W., and Gieskes, J. M., 1980. Interaction between sediment and interstitial water near the Japan Trench, Leg 57, Deep Sea Drilling Project. *In* Scientific Party, *Init. Repts. DSDP*, 56, 57 (Pt. 2): Washington (U.S. Govt. Printing Office), 1269-1275.

Nigrini, C., 1977. Tropical Cenozoic Artostrobiidae (Radiolaria). *Micropaleontol.*, 23:241-269.

Poore, R. Z., 1979. Oligocene through Quaternary planktonic foraminiferal biostratigraphy of the north Atlantic: DSDP Leg 49. *In* Luyendyk, B. P., Cann, J. R., et al., *Init. Repts. DSDP*, 49: Washington (U.S. Govt. Printing Office), 447-517.

Resig, J. M., 1976. Benthic foraminiferal stratigraphy, eastern margin, Nazca Plate. *In* Yeats, R. S., Hart, S. R., et al., *Init. Repts. DSDP*, 34: Washington (U.S. Govt. Printing Office), 743-759.

Riedel, W.R., and Sanfilippo, A., 1978. Stratigraphy and evolution of tropical Cenozoic radiolarians. *Micropaleontology*, 24:61-96.

Schrader, H., and Cruzado, J., 1987. A revised biostratigraphy of the Delphin and Ballena wells, central Peruvian shelf. *Proc., Latin Am. Cong.*, Lima, July, 1987.

Schuette, G. and Schrader, H., 1979. Diatom taphocoenoses in the coastal upwelling area off western South America. *Nova Hedwigia, Beihefte*, 64:359-378.

________, 1981. Diatoms in surface sediments: A reflection of coastal upwelling. *In* Richards, A. (Ed.), *Coastal Upwelling*: Washington (Am. Geophys. Union), 372-380.

Srinivasan, M. S., and Kennett, J. P., 1981. Neogene planktonic foraminiferal biostratigraphy and evolution: Equatorial to Subantarctic, South Pacific. *Mar. Micropaleontol.*, 6:499-533.

Stone, B., 1946. *Stichocassidulina*, a new genus of foraminifera from northwestern Peru. *J. Paleontol.*, 20:59-61.

Thornburg, T. M., 1985. Seismic stratigraphy of Peru forearc basins. *In* Hussong, D. M., et al. (Eds.), *Atlas of the Ocean Margin Drilling Program, Peru Continental Margin, Region VI*: Woods Hole (Marine Science Int.).

Tissot, B. P., and Welte, D. H., 1984. *Petroleum Formation and Occurrence* (2nd Ed.): Berlin-Heidelberg (Springer-Verlag).

von Huene, R., Kulm, L. D., and Miller, J., 1985. Structure of the frontal part of the Andean convergent margin. *J. Geophys. Res.*, 90(B7): 5429-5442.

Yamano, M., 1986. Heat flow studies of the circum-Pacific subduction zones [D.Sc. dissert.]. Tokyo (Univ. of Tokyo).

Ms 112A-114

SITE 683 HOLE A CORE 1H CORED INTERVAL 3071.8-3074.0 mbsl; 0.0-2.2 mbsf

TIME-ROCK UNIT	FORAMINIFERS	NANNOFOSSILS	RADIOLARIANS	DIATOMS		PALEOMAGNETICS	PHYS. PROPERTIES	CHEMISTRY	SECTION	METERS	GRAPHIC LITHOLOGY	DRILLING DISTURB.	SED. STRUCTURES	SAMPLES
QUATERNARY	* N23 Quaternary	* NN20	* Quaternary	*	*Pseudoeunotia doliolus* Zone		● γ=1.35 ϕ=82.47	OC: 3.19 IC: 0.97	1, 2, CC	0.5, 1.0				*, *, IW KVE *, *

BIOSTRAT. ZONE/FOSSIL CHARACTER: FORAMINIFERS, NANNOFOSSILS, RADIOLARIANS, DIATOMS

LITHOLOGIC DESCRIPTION

DIATOMACEOUS MUD

Major lithology: diatomaceous mud, dark olive gray to olive gray (5Y 3.5/2). Homogeneous to mottled, extensively bioturbated, with rare shell fragments and small irregular patches of black pyrite 2-mm long. Section 1, 0 cm, to CC, 7 cm.

Minor lithology: feldspathic spicule sand, white (5Y 8/1). Peloids 1–3 mm.

SMEAR SLIDE SUMMARY (%):

	1, 0 D	1, 10 D	1, 40 M	2, 9 M	2, 41 M
TEXTURE:					
Sand	10	5	5	55	2
Silt	40	35	40	25	30
Clay	50	60	55	20	68
COMPOSITION:					
Quartz	Tr	10	Tr	Tr	
Feldspar	10	10	5	20	3
Rock fragments	5	—	5	5	—
Clay	40	50	45	15	45
Volcanic glass	Tr	Tr	Tr	—	—
Calcite/dolomite	Tr	Tr	Tr	Tr	Tr
Accessory minerals	Tr	—	—	—	—
Pyrite	Tr	Tr	Tr	—	10
Fe oxides?	2	—	—	—	—
Glauconite	Tr	Tr	—	—	—
Gypsum?	Tr	—	Tr	—	—
Apatite?	Tr	—	Tr	—	—
Foraminifers	—	—	5	Tr	Tr
Nannofossils	—	—	Tr	—	Tr
Diatoms	40	30	40	5	40
Radiolarians	2	Tr	Tr	5	Tr
Sponge spicules	2	—	—	50	—
Silicoflagellates	Tr	—	Tr	—	—
Fish remains	Tr	—	—	—	—

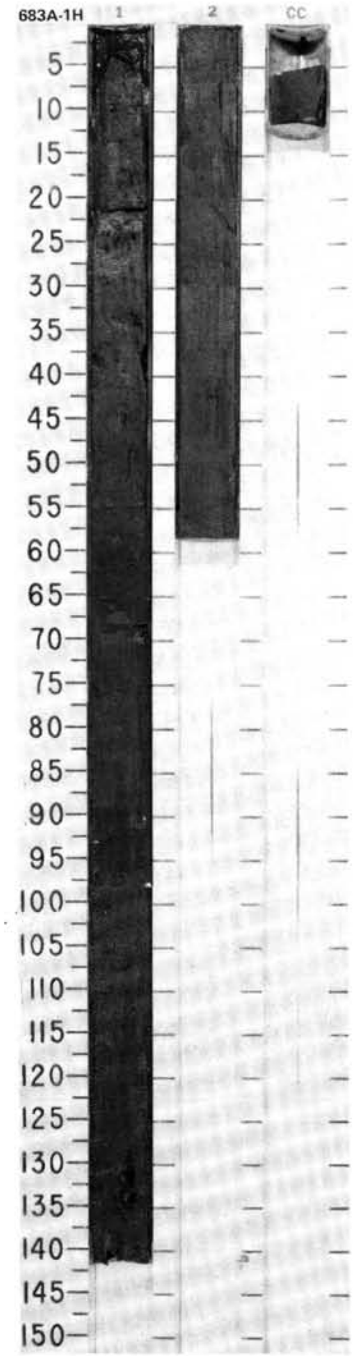

SITE 683 HOLE A CORE 2H CORED INTERVAL 3074.0-3083.5 mbsl; 2.2-11.7 mbsf

TIME-ROCK UNIT	FORAMINIFERS	NANNOFOSSILS	RADIOLARIANS	DIATOMS	PALEOMAGNETICS	PHYS. PROPERTIES	CHEMISTRY	SECTION	METERS	GRAPHIC LITHOLOGY	DRILLING DISTURB.	SED. STRUCTURES	SAMPLES
QUATERNARY	*Quaternary N23	*NN20	*Quaternary	*Pseudoeunotia doliolus Zone	Brunhes	• γ=1.32 φ=83.02; • γ=1.40 φ=81.94		1, 2, 3, 4, 5, CC	0.5, 1.0				

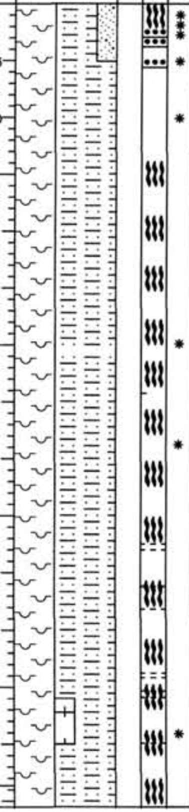

LITHOLOGIC DESCRIPTION

CALCAREOUS DIATOMACEOUS MUD

Major lithology: calcareous diatomaceous mud, olive gray to dark olive gray (5Y 3.5/2, 5Y 3/2). Extensively to moderately bioturbated with thin graded interbeds of dark olive gray sandy and silty mud. Regular color changes from lighter to darker mud at Section 1, 10–30 cm, reflect slight variations in diatomaceous, terrigenous, and calcareous components. Section 1, 0 cm, to CC.

Minor lithologies:
1. foraminiferal feldspathic sand, olive gray (5Y 4/2). Sharp-based graded bed. Section 1, 17 cm.
2. feldspathic diatomaceous sandy mud, dark olive gray (5Y 3.5/2). Sharp-based graded bed. Section 1, 52 cm.
3. feldspathic spicule sand, white (5Y 8/1). Peloids 1–3 mm.
4. diatom-nannofossil mud, Section 5, 33 cm.

SMEAR SLIDE SUMMARY (%):

	1, 8 D	1, 17 M	1, 20 M	1, 52 M	1, 102 M	3, 3.5 D
TEXTURE:						
Sand	5	90	40	20	60	Tr
Silt	45	10	30	40	20	45
Clay	50	—	30	40	20	55
COMPOSITION:						
Quartz	—	5	Tr	Tr	—	Tr
Feldspar	5	30	20	20	20	10
Rock fragments	Tr	10	10	—	Tr	5
Clay	35	—	30	30	15	27
Volcanic glass	—	—	5	—	—	—
Calcite/dolomite	3	—	—	—	—	3
Accessory minerals	—	2	—	—	—	—
Pyrite	2	—	5	5	Tr	5
Glauconite	—	Tr	—	—	—	—
Foraminifers	5	50	20	10	5	5
Nannofossils	Tr	—	Tr	Tr	—	—
Diatoms	48	—	10	35	10	38
Radiolarians	Tr	—	—	—	—	—
Sponge spicules	2	—	Tr	—	50	3
Fish remains	Tr	3	Tr	Tr	—	4
Bivalve shells	—	—	Tr	—	—	—

	3, 81 D	5, 33 M
TEXTURE:		
Sand	5	5
Silt	30	55
Clay	65	40
COMPOSITION:		
Quartz	Tr	—
Feldspar	10	5
Rock fragments	—	Tr
Clay	30	20
Volcanic glass	Tr	—
Calcite/dolomite	Tr	10
Accessory minerals		
Pyrite	5	3
Foraminifers	5	5
Nannofossils	5	15
Diatoms	45	37
Radiolarians	—	5
Silicoflagellates	—	Tr

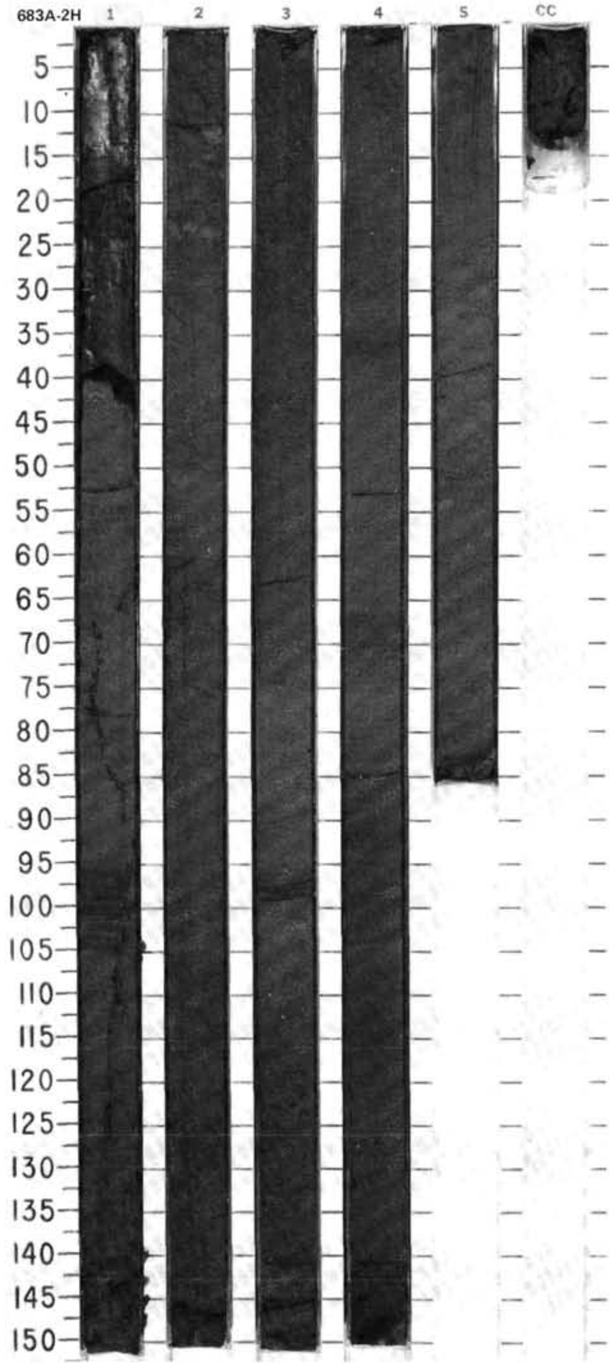

SITE 683 HOLE A CORE 3H CORED INTERVAL 3083.5-309.3 mbsl; 11.7-21.2 mbsf

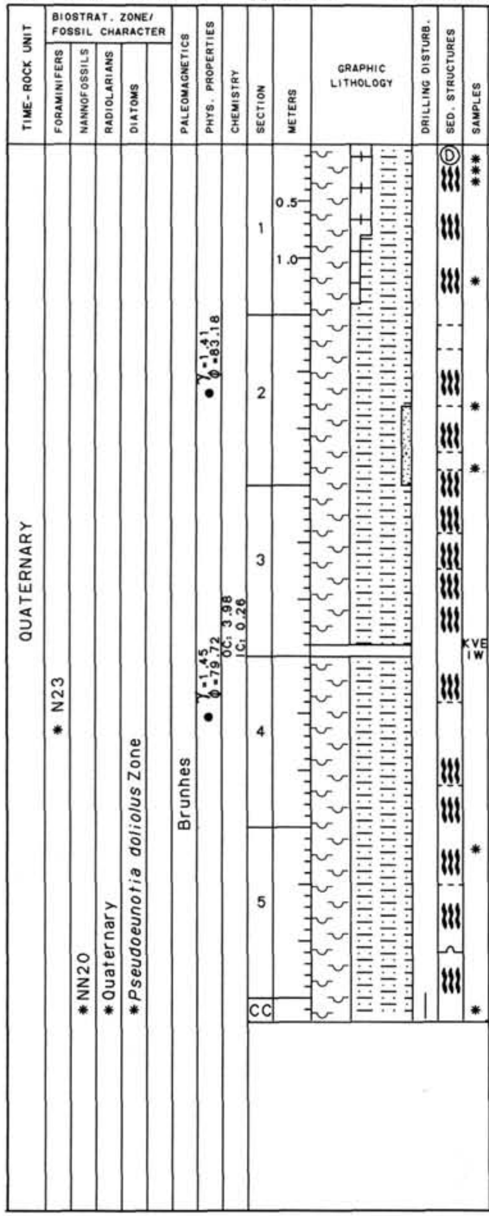

LITHOLOGIC DESCRIPTION

NANNOFOSSIL-BEARING, DIATOMACEOUS MUD, grading downward into DIATOMACEOUS MUD

Major lithology: Section 1, 0–140 cm: nannofossil-bearing, diatomaceous mud, olive gray to dark olive gray (5Y 3.5/2, 5Y 3/2). Bioturbated. Degassing voids with black pyrite concentrations. Section 1, 140 cm, to CC: diatomaceous mud, dark olive gray to olive gray (5Y 3.5/2, 5Y 3/2). Bioturbated, white spicule peloids.

Minor lithology: feldspathic lithic silty sand: dark olive gray (5Y 3.5/2). Thin bed, Section 2, 83 cm.

SMEAR SLIDE SUMMARY (%):

	1, 12 M	1, 21 D	1, 30.5 M	1, 124 D	2, 83 M	2, 129 M
TEXTURE:						
Sand	10	5	10	10	40	60
Silt	45	55	45	45	30	15
Clay	45	40	45	45	30	15
COMPOSITION:						
Quartz	Tr	—	Tr	—	5	Tr
Feldspar	5	5	5	5	22	85
Rock fragments	Tr	Tr	Tr	Tr	22	Tr
Clay	35	27	30	35	15	13
Volcanic glass	—	—	Tr	—	Tr	Tr
Calcite/dolomite	10	10	10	5	5	—
Accessory minerals						
Pyrite	10	3	3	3	3	2
Gypsum	—	—	—	Tr	—	—
Glauconite	—	—	—	—	3	—
Foraminifers	10	10	5	5	10	Tr
Nannofossils	—	10	10	—	Tr	—
Diatoms	30	35	37	47	15	Tr
Radiolarians	—	—	Tr	Tr	Tr	—
Sponge spicules	—	—	Tr	Tr	Tr	Tr
Silicoflagellates	—	—	Tr	Tr	—	—

	5, 19 M	CC, 16 M
TEXTURE:		
Sand	5	5
Silt	40	45
Clay	55	50
COMPOSITION:		
Quartz	5	Tr
Feldspar	5	5
Rock fragments	10	Tr
Clay	25	42
Calcite/dolomite	10	3
Accessory minerals		
Pyrite	10	3
Glauconite	Tr	—
Dolomite rhombs.	2	—
Foraminifers	Tr	5
Nannofossils	Tr	5
Diatoms	30	37
Sponge spicules	3	—

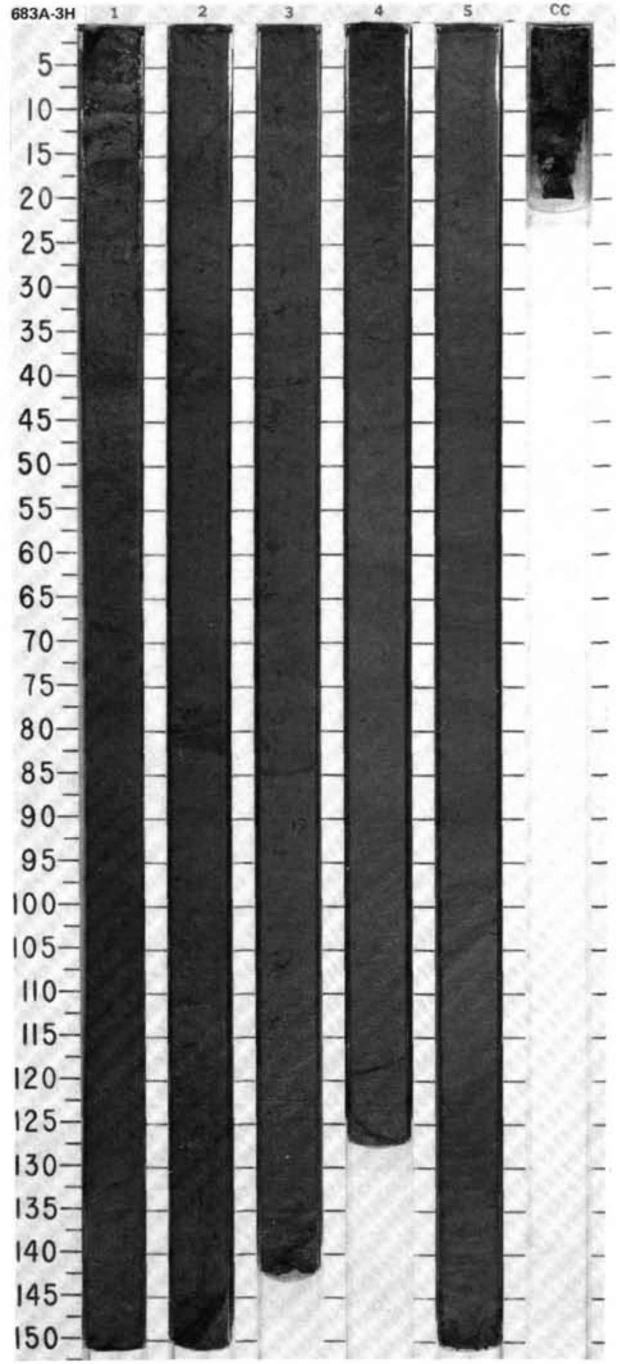

SITE 683 HOLE A CORE 4H CORED INTERVAL 3093.0-3102.5 mbsl; 21.2-30.7 mbsf

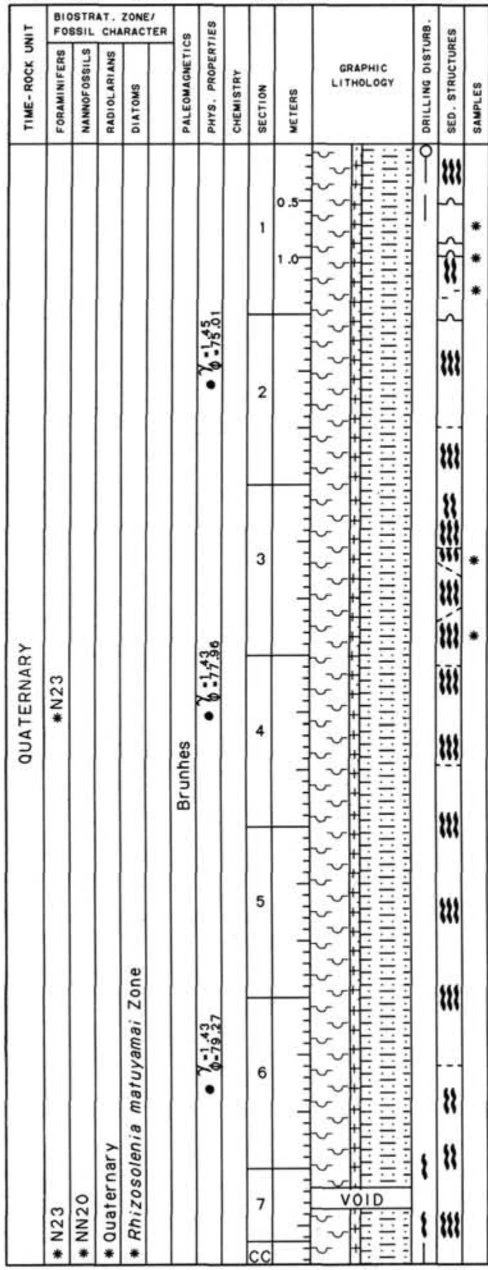

LITHOLOGIC DESCRIPTION

DIATOMACEOUS FORAMINIFER-BEARING MUD

Major lithology: diatomaceous foraminifer-bearing mud, olive, olive gray, and dark olive gray (5Y 3.5/2, 5Y 4/2, 5Y 3/2). Bioturbated (including *Chondrites*), with slump folds and sharp inclined contacts throughout; gas voids in upper 60 cm. Scattered black pyrite streaks. Section 1, 0 cm, to CC.

Minor lithology: spicule-bearing ash, white peloid, Section 3, 131.5 cm.

SMEAR SLIDE SUMMARY (%):

	1, 71 D	1, 98 D	1, 127 D	3, 53 M	3, 131.5 M
TEXTURE:					
Sand	15	10	5	10	15
Silt	55	50	50	50	55
Clay	30	40	45	40	30
COMPOSITION:					
Quartz	Tr	Tr	Tr	—	—
Feldspar	5	5	5	10	5
Rock fragments	Tr	5	Tr	Tr	Tr
Clay	30	35	40	30	—
Volcanic glass	—	—	—	—	60
Calcite/dolomite	5	3	10	10	—
Accessory minerals					
Pyrite	3	2	3	3	—
Gypsum	—	Tr	—	Tr	—
Foraminifers	10	5	7	5	—
Nannofossils	2	Tr	Tr	5	—
Diatoms	42	45	35	37	15
Radiolarians	3	—	—	—	—
Sponge spicules	—	—	—	—	20

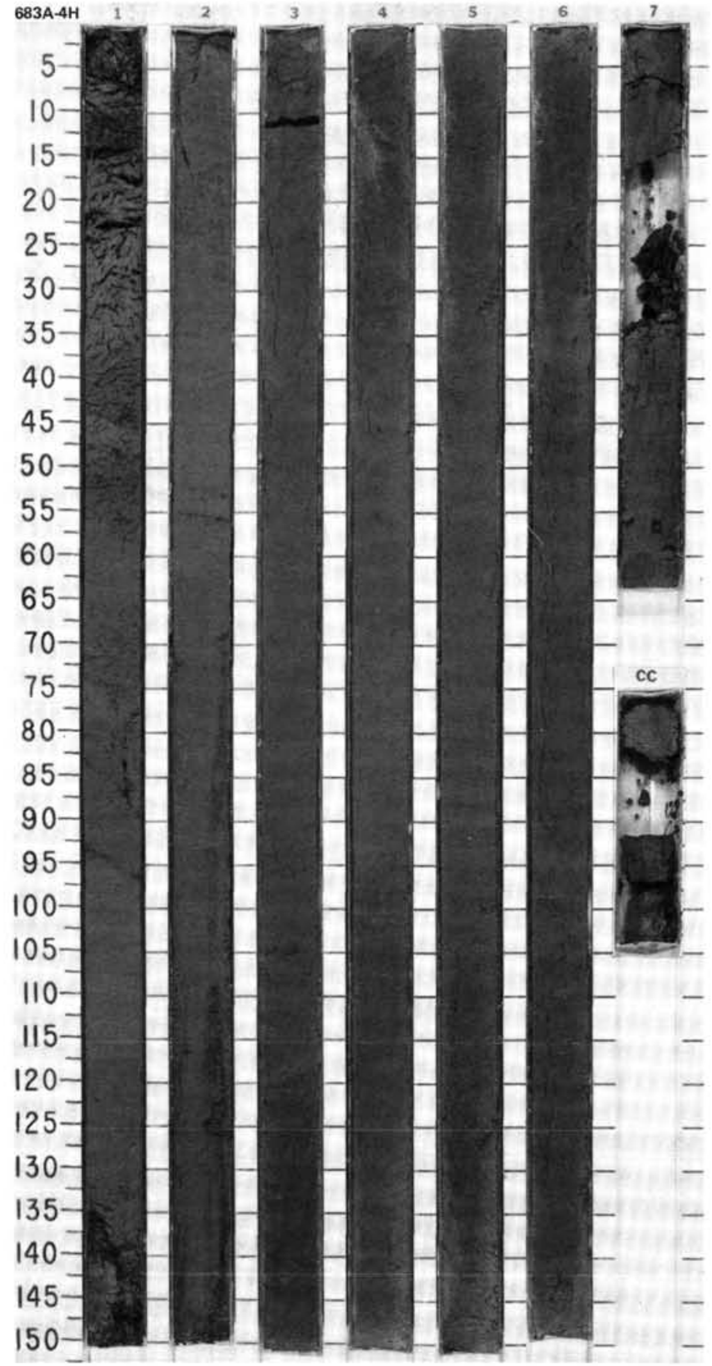

SITE 683 HOLE A CORE 5H CORED INTERVAL 3102.5-3112.0 mbsl; 30.7-40.2 mbsf

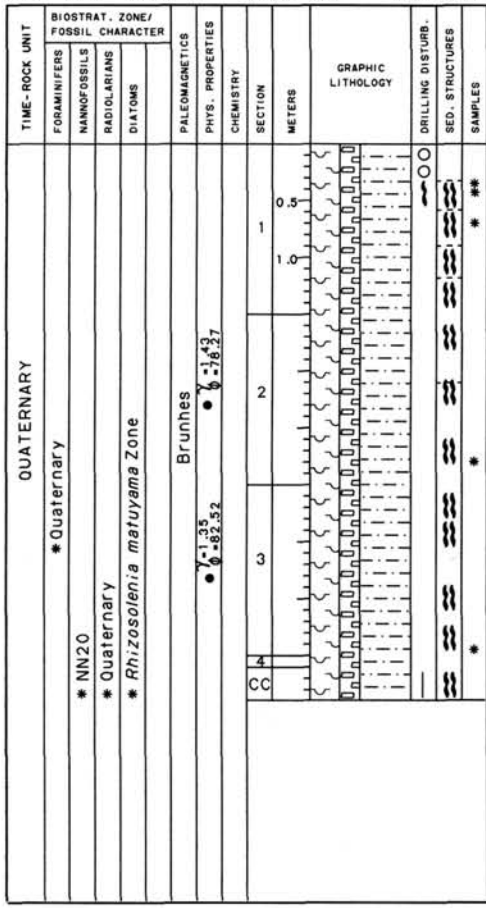

LITHOLOGIC DESCRIPTION

CALCAREOUS DIATOMACEOUS MUD

Major lithology: calcareous diatomaceous mud, dark olive gray to olive (5Y 3/2, 5Y 4.5/2). Bioturbated, cyclic color changes at 20–40-cm spacing. Section 1, 0 cm, to CC.

Minor lithologies:
1. pyrite-bearing diatomaceous mud, black (5Y 2.5/2); interbed, Section 2, 128 cm.
2. calcareous diatomaceous mud, light olive green to dark olive green (5Y 4.5/2), interbedded laminae.

SMEAR SLIDE SUMMARY (%):

	1, 37 M	1, 38 M	1, 69 D	2, 128 D	4, 6 D
TEXTURE:					
Sand	10	10	10	10	15
Silt	50	55	50	45	45
Clay	40	35	40	45	40
COMPOSITION:					
Quartz	Tr	—	—	—	—
Feldspar	5	10	15	10	10
Rock fragments	Tr	5	—	5	5
Clay	25	30	35	40	25
Volcanic glass	—	—	5	Tr	—
Calcite/dolomite	10	20	10	5	20
Accessory minerals					
Pyrite	2	3	5	10	5
Gypsum	—	Tr	Tr	—	Tr
Glauconite	—	—	Tr	—	—
Foraminifers	5	Tr	Tr	Tr	3
Nannofossils	15	5	Tr	—	7
Diatoms	38	33	30	30	—
Radiolarians	—	—	—	Tr	25
Sponge spicules	—	—	Tr	—	—
Silicoflagellates	—	—	—	Tr	—

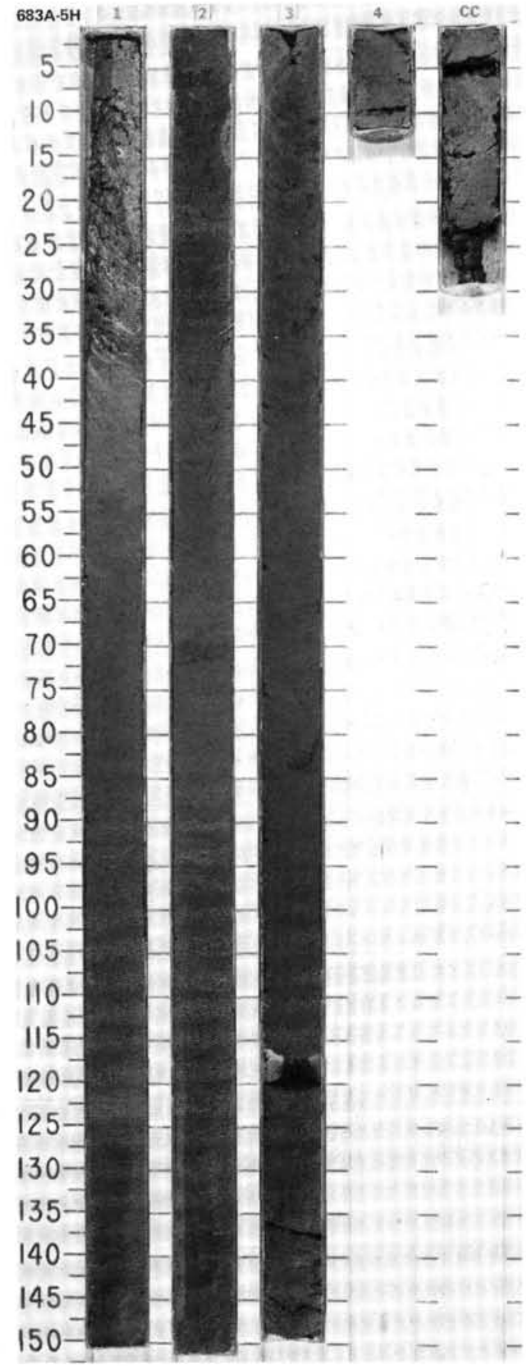

SITE 683 HOLE A CORE 6H CORED INTERVAL 3112.0-3121.5 mbsl; 40.2-49.7 mbsf

TIME-ROCK UNIT	BIOSTRAT. ZONE/ FOSSIL CHARACTER: FORAMINIFERS	NANNOFOSSILS	RADIOLARIANS	DIATOMS	PALEOMAGNETICS	PHYS. PROPERTIES	CHEMISTRY	SECTION	METERS
QUATERNARY	* N23	* NN20	* Quaternary	* *Rhizosolenia matuyama* Zone	Brunhes	• γ=1.42 φ=79.32; • γ=1.42 φ=80.82; • γ=1.50 φ=76.69	OC: 4.20 IC: 1.99	1, 2, 3, 4, 5, 6, 7	0.5, 1.0

GRAPHIC LITHOLOGY

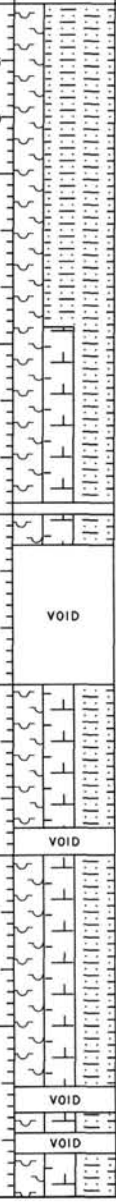

DRILLING DISTURB. | SED. STRUCTURES | SAMPLES

KVE
IW

LITHOLOGIC DESCRIPTION

DIATOMACEOUS MUD, CALCAREOUS DIATOMACEOUS MUD, and NANNOFOSSIL-DIATOM MUD

Major lithology: Section 1, 0 cm, to Section 2, 145 cm: diatomaceous mud and calcareous diatomaceous mud, dark olive gray, very dark gray, and olive (5Y 3/2, 5Y 4/3, 5Y 3/1); moderate bioturbation. Section 2, 145 cm, to Section 7, 150 cm: nannofossil-diatom mud, olive gray (5Y 5/2, 5Y 4/2); moderate bioturbation; below Section 7, 42 cm: incipient fissility and parting (not scaly cleavage). Section 8, 0 cm, to CC: diatomaceous mud, dark olive gray (5Y 3/2); bioturbated.

SMEAR SLIDE SUMMARY (%):

	2, 54 M	3, 69 D	5, 17 D	6, 52 D	6, 145 M
TEXTURE:					
Silt	10	20	20	50	45
Clay	90	80	80	50	55
COMPOSITION:					
Quartz	—	4	5	3	2
Feldspar	Tr	3	—	2	2
Rock fragments	—	3	—	—	1
Clay	50	45	25	20	30
Volcanic glass	3	2	—	—	Tr
Calcite/dolomite	5	3	—	10	5
Accessory minerals	—	—	—	—	5
Glauconite	—	Tr	—	—	—
Pyrite	—	2	—	—	—
Gypsum	—	Tr	—	—	—
Foraminifers	—	Tr	Tr	5	5
Nannofossils	5	Tr	40	30	25
Diatoms	35	35	28	30	25
Radiolarians	—	—	—	Tr	—
Sponge spicules	2	3	2	Tr	—

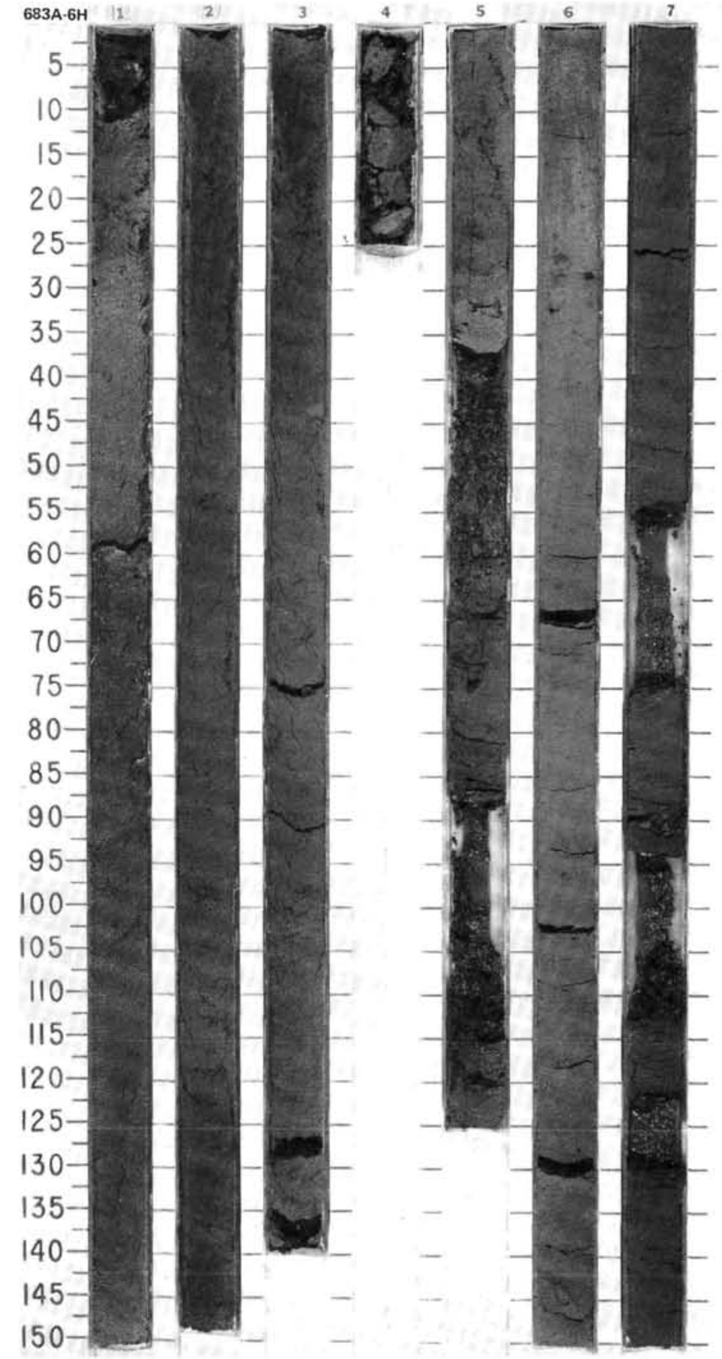

SITE 683 HOLE A CORE 6H CORED INTERVAL 3112.0-3121.5 mbsl; 40.2-49.7 mbsf

TIME-ROCK UNIT	FORAMINIFERS	NANNOFOSSILS	RADIOLARIANS	DIATOMS	PALEOMAGNETICS	PHYS. PROPERTIES	CHEMISTRY	SECTION	METERS	GRAPHIC LITHOLOGY	DRILLING DISTURB.	SED. STRUCTURES	SAMPLES	LITHOLOGIC DESCRIPTION
QUATERNARY		*NN20	*Quaternary	* *Rhizosolenia matuyama* Zone		Brunhes		8	0.5					
								CC	1.0		×			

SITE 683 HOLE A CORE 7H CORED INTERVAL 3121.5-3131.0 mbsl; 49.7-59.2 mbsf

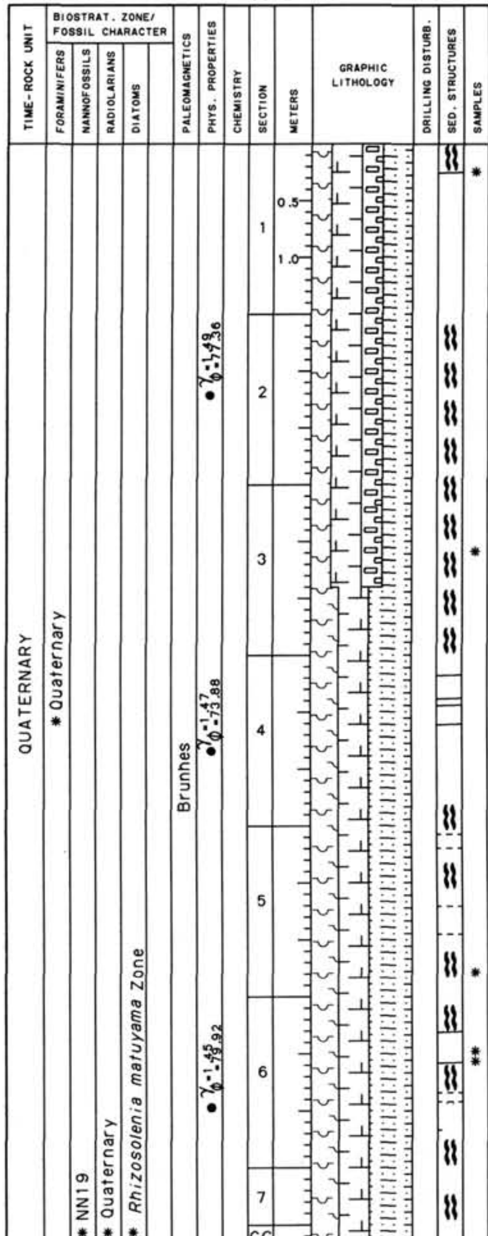

LITHOLOGIC DESCRIPTION

CALCAREOUS DIATOM- AND NANNOFOSSIL-RICH MUD

Major lithology: calcareous diatom- and nannofossil-rich mud, dark olive gray to olive (5Y 3/2, 5Y 4/3). Massive to moderately bioturbated, with sharp-based cyclic color changes in lower part of core. Section 1, 0 cm, to CC.

SMEAR SLIDE SUMMARY (%):

	1, 21 D	3, 56 M	5, 130 D	6, 57 D	6, 59 D
TEXTURE:					
Sand	5	—	—	5	—
Silt	50	35	55	25	50
Clay	45	65	45	70	50
COMPOSITION:					
Quartz	5	3	5	5	4
Feldspar	—	2	5	—	3
Rock fragments	—	—	5	—	3
Clay	20	15	35	—	30
Volcanic glass	Tr	—	5	Tr	—
Calcite/dolomite	20	5	5	—	5
Accessory minerals					
Pyrite	5	—	—	Tr	—
Glauconite	—	—	—	—	Tr
Foraminifers	Tr	5	Tr	5	5
Nannofossils	30	50	10	50	20
Diatoms	20	20	30	40	30
Radiolarians	Tr	—	—	—	—
Sponge spicules	Tr	Tr	—	—	—
Silicoflagellates	Tr	Tr	—	Tr	Tr

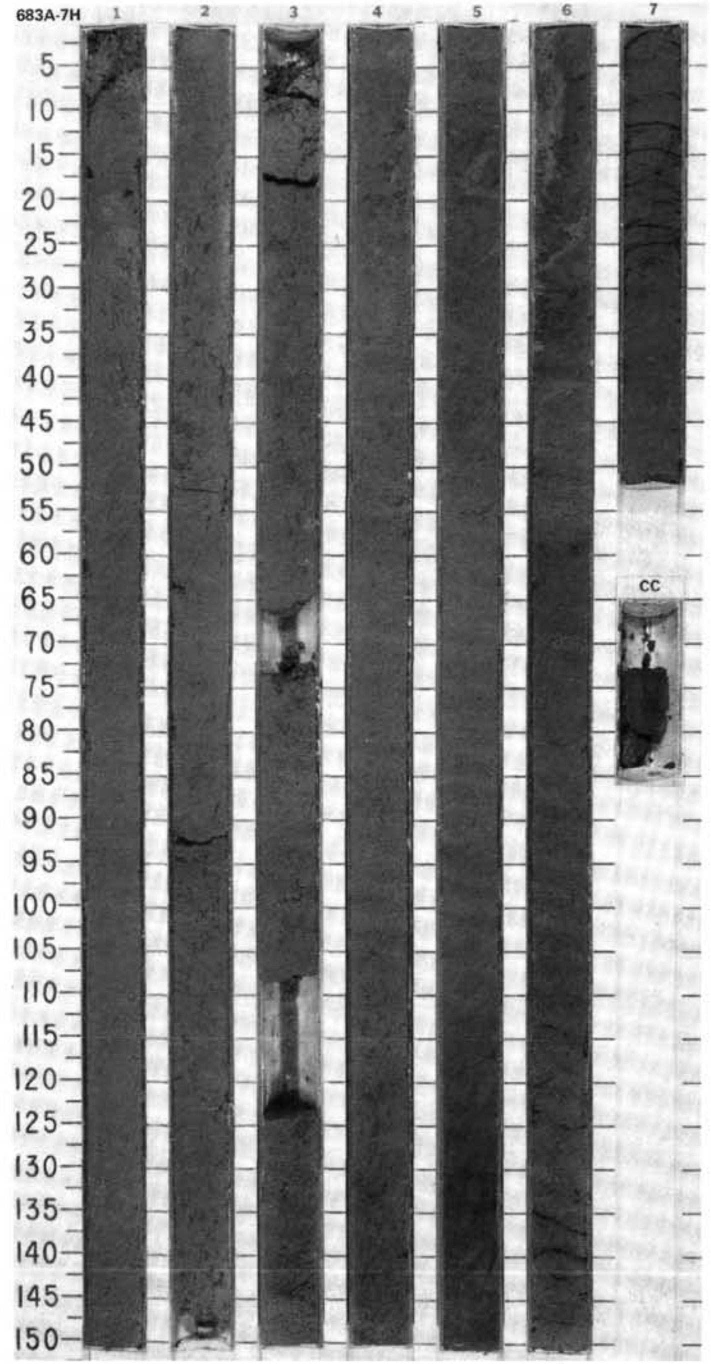

SITE 683 HOLE A CORE 8H CORED INTERVAL 3131.0-3140.5 mbsl; 59.2-68.7 mbsf

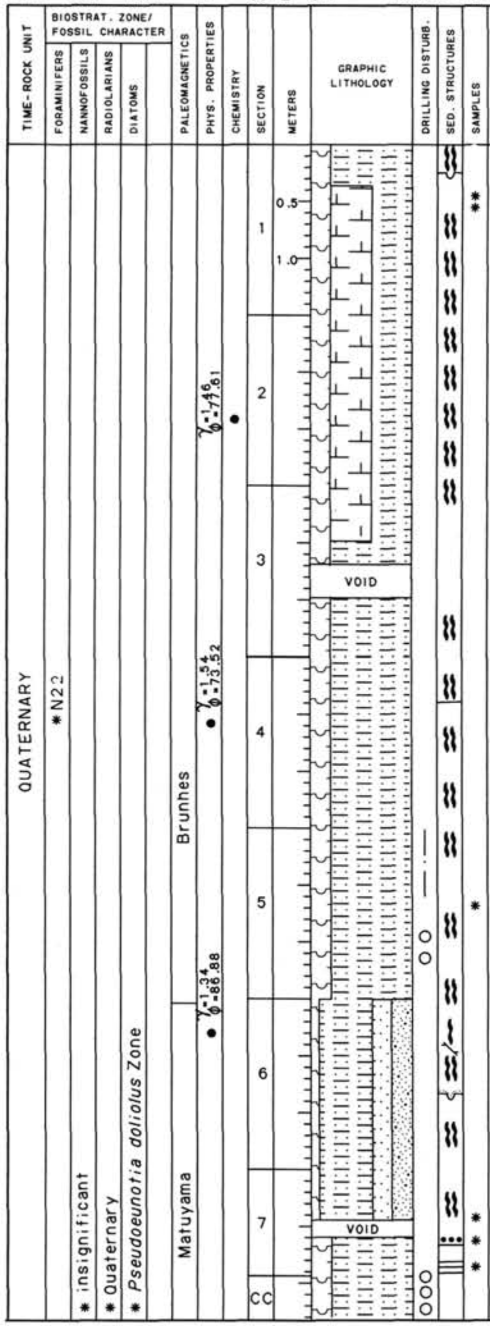

LITHOLOGIC DESCRIPTION

DIATOMACEOUS NANNOFOSSIL MUD, grades downward into DIATOM-BEARING MUD, DIATOM-BEARING MUD interbedded with QUARTZO-FELDSPATHIC SAND AND SILT, and DIATOMACEOUS MUD

Major lithology: Section 1, 0 cm, to Section 3, 50 cm: diatomaceous nannofossil mud, dark green, olive, and very dark gray (10Y 4/2, 5Y 4/3, 5Y 3/1); moderate bioturbation, color darkens downward. Section 3, 50 cm, to Section 5, 150 cm: diatom-bearing mud, dark olive gray, very dark gray (5Y 3/2, 5Y 3/1); moderate bioturbation. Section 5, 150 cm, to Section 7, 45 cm: diatom-bearing mud, dark olive gray (5Y 3/2), interbedded with quartzo-feldspathic sand and silt, very dark gray (5Y 3/1), in sharp-based graded beds as large as 5-cm thick; moderate bioturbation. Section 7, 45 cm, to CC: diatomaceous mud, dark olive gray (5Y 3/2); moderate bioturbation.

Minor lithology:
1. diatomaceous mud, olive gray (5Y 4/2), thin interbeds; Section 3, 50 cm, to Section 5, 150 cm.
2. foraminiferal silt, very dark gray (5Y 3/1); Section 5, 150 cm, to Section 7, 45 cm. Sharp-based graded bed, Section 7, 60 cm.

SMEAR SLIDE SUMMARY (%):

	1, 39 D	1, 50 D	5, 65 D	7, 40 M	7, 59 M	7, 66 D
TEXTURE:						
Sand	5	5	5	40	25	—
Silt	20	15	35	50	45	45
Clay	75	80	60	10	30	55
COMPOSITION:						
Quartz	5	4	5	35	10	5
Feldspar	10	2	5	35	10	5
Rock fragments	—	2	3	10	5	—
Mica	Tr	—	—	—	—	—
Clay	45	15	60	10	30	55
Volcanic glass	—	—		7	Tr	—
Calcite/dolomite	7	5	Tr	Tr	—	—
Accessory minerals						
Pyrite	3	3	—	—	—	—
Glauconite	—	—	Tr	—	5	Tr
Opaques	—	—	—	—	—	Tr
Foraminifers	2	—	5	—	30	Tr
Nannofossils	3	40	—	—	—	—
Diatoms	25	25	15	10	10	35
Radiolarians	—	—	—	—	—	Tr
Sponge spicules	Tr	2	—	—	—	—
Silicoflagellates	Tr	2	—	—	—	—

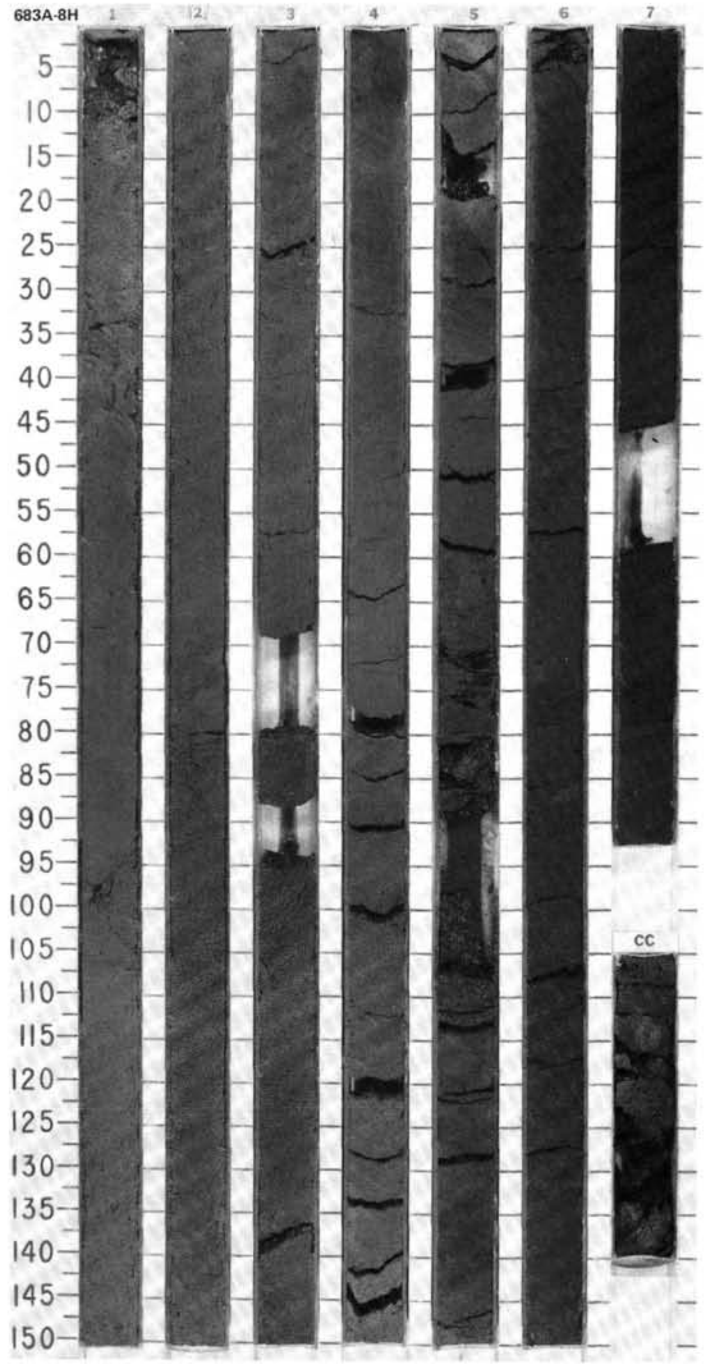

SITE 683 HOLE A CORE 9H CORED INTERVAL 3140.5-3150.0 mbsl; 68.7-78.2 mbsf

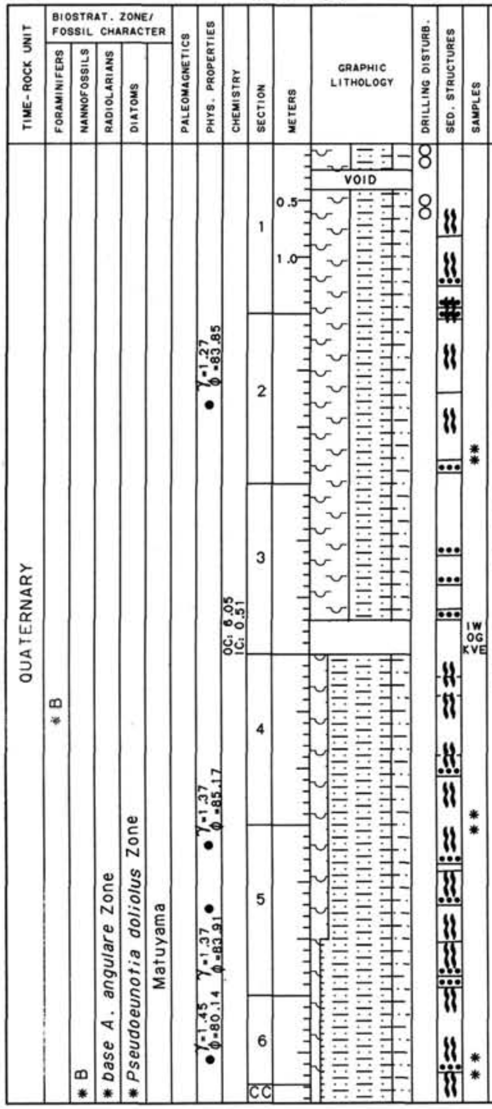

LITHOLOGIC DESCRIPTION

DIATOMACEOUS MUD interbedded with DIATOM-BEARING SANDY or SILTY MUD

Major lithology: diatomaceous mud, very dark gray to olive (5Y 3/1, 5Y 4/3), interbedded with diatom-bearing sandy or silty mud, very dark gray to dark gray (5Y 3/1, 10 Y 3/1), in sharp-based graded layers to 3-mm thick. Moderate bioturbation, especially at tops of graded interbeds. Section 1, 0 cm, to CC.

Minor lithology: nannofossil ooze, dark gray (5Y 4/1). Section 5, 2 cm.

SMEAR SLIDE SUMMARY (%):

	2, 123 D	2, 130 D	4, 147 D	5, 2 M	6, 58 D	6, 64 D
TEXTURE:						
Sand	—	10	5	—	—	—
Silt	10	20	30	15	35	35
Clay	90	70	65	85	65	65
COMPOSITION:						
Quartz	4	5	5	—	5	5
Feldspar	4	10	20	—	5	5
Rock fragments	—	5	5	—	—	5
Mica	Tr	—	2	—	Tr	Tr
Clay	35	35	25	—	65	65
Volcanic glass	2	3	—	—	5	—
Calcite/dolomite	3	2	8	—	Tr	Tr
Accessory minerals						
Pyrite	3	3	2	—	—	—
Apatite	—	Tr	—	—	—	—
Glauconite	—	Tr	5	—	—	—
Foraminifers	—	Tr	8	Tr	5	5
Nannofossils	2	—	—	85	—	—
Diatoms	45	35	20	15	15	15
Radiolarians	—	Tr	—	—	—	Tr
Sponge spicules	2	Tr	—	—	—	Tr
Silicoflagellates	Tr	2	—	Tr	—	Tr

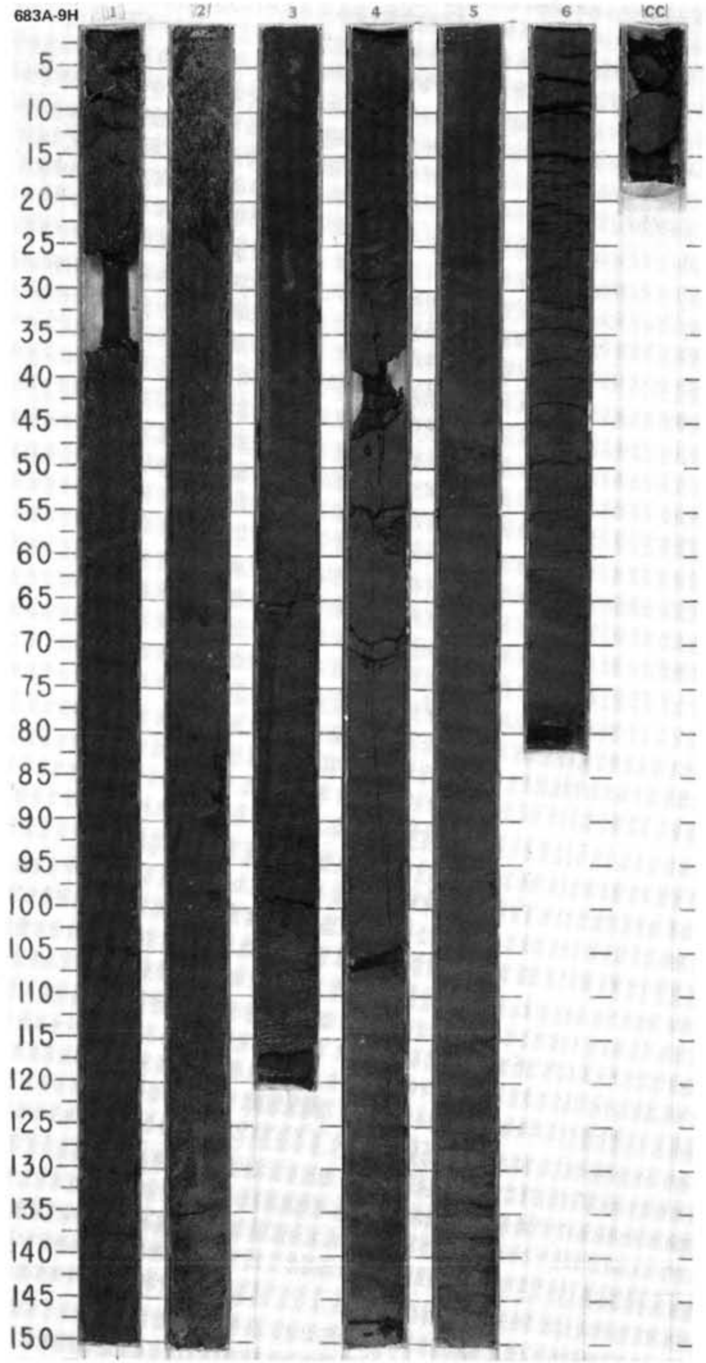

SITE 683 HOLE A CORE 10X CORED INTERVAL 3150.0-3159.5 mbsl; 78.2-87.7 mbsf

TIME-ROCK UNIT	FORAMINIFERS	NANNOFOSSILS	RADIOLARIANS	DIATOMS	PALEOMAGNETICS	PHYS. PROPERTIES	CHEMISTRY	SECTION	METERS	GRAPHIC LITHOLOGY	DRILLING DISTURB.	SED. STRUCTURES	SAMPLES
QUATERNARY	* N22	B *	base *A. angulare* Zone *	*Pseudoeunotia doliolus* Zone *		γ=1.58 ● φ=74.26		1, CC	0.5, 1.0	VOID			*

LITHOLOGIC DESCRIPTION

CALCAREOUS DIATOMACEOUS MUD

Major lithology: calcareous diatomaceous mud, very dark gray to dark olive gray (5Y 3/1, 5Y 3/2). Moderately bioturbated, with rare sharp-based graded siltier interbeds. Section 1, 0 cm, to CC.

SMEAR SLIDE SUMMARY (%):

	1, 57 D
TEXTURE:	
Sand	5
Silt	10
Clay	85
COMPOSITION:	
Quartz	5
Feldspar	15
Rock fragments	5
Clay	35
Calcite/dolomite	8
Accessory minerals	
Glauconite	Tr
Pyrite	3
Foraminifers	2
Nannofossils	2
Diatoms	25
Sponge spicules	Tr

SITE 683 HOLE A CORE 11X CORED INTERVAL 3159.5-3169.0- mbsl; 87.7-97.2 mbsf

TIME-ROCK UNIT	FORAMINIFERS	NANNOFOSSILS	RADIOLARIANS	DIATOMS	PALEOMAGNETICS	PHYS. PROPERTIES	CHEMISTRY	SECTION	METERS	GRAPHIC LITHOLOGY	DRILLING DISTURB.	SED. STRUCTURES	SAMPLES
QUATERNARY		insignificant *	base *A.angulare* Zone *	*Rhizosolenia matuyama* Zone *				1	0.5, 1.0				*

LITHOLOGIC DESCRIPTION

DIATOMACEOUS MUD

Major lithology: diatomaceous mud, black (5Y 2.5/2). Minor bioturbation. Section 1, 0-118 cm.

Minor lithology: diatom-bearing terrigenous mud: very dark gray (5Y 3/1). Thin, sharp-based, graded beds at Section 1, 87 and 100 cm.

SMEAR SLIDE SUMMARY (%):

	1, 101 D
TEXTURE:	
Sand	15
Silt	35
Clay	50
COMPOSITION:	
Quartz	10
Feldspar	10
Rock fragments	5
Clay	50
Volcanic glass	5
Calcite/dolomite	5
Accessory minerals	
Glauconite	Tr
Foraminifers	5
Diatoms	10
Sponge spicules	Tr

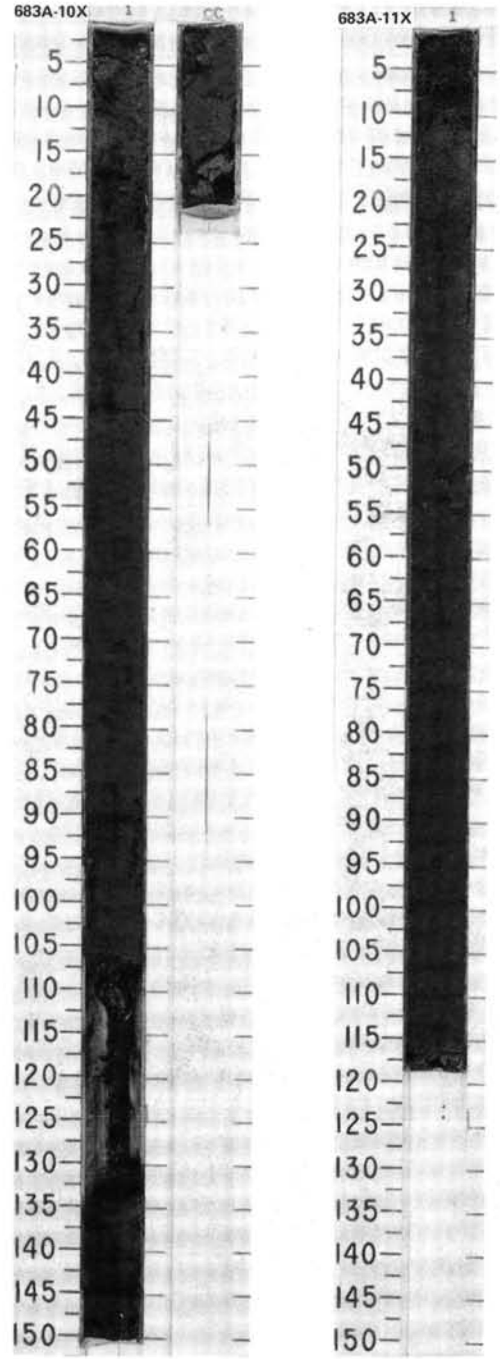

SITE 683 HOLE A CORE 12X CORED INTERVAL 3169.0-3178.5 mbsl; 97.2-106.7 mbsf

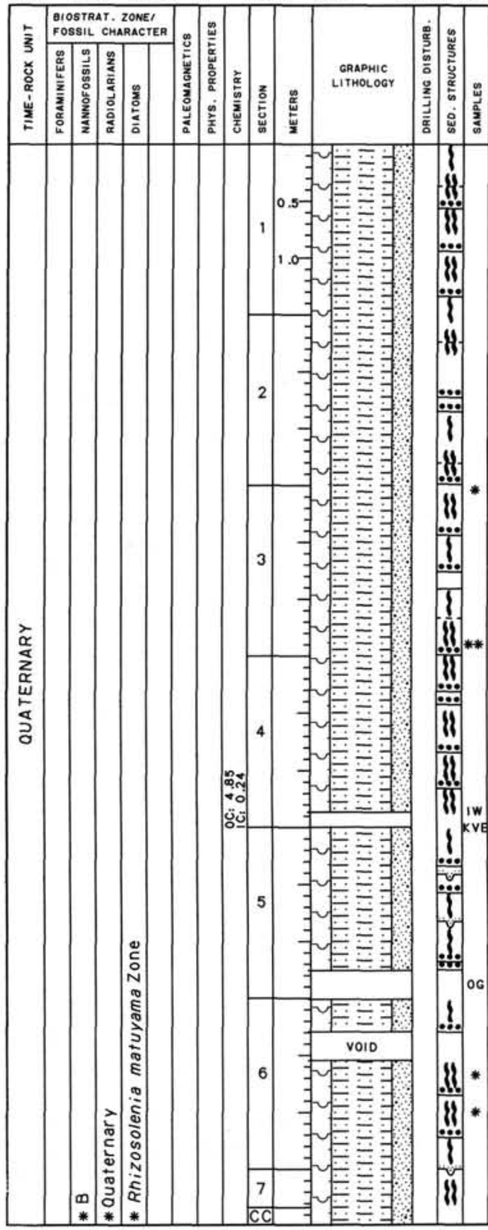

LITHOLOGIC DESCRIPTION

DIATOMACEOUS MUD interbedded with DIATOMACEOUS SANDY SILT AND MUD

Major lithology: diatomaceous mud, dark olive gray (5Y 3/2). Bioturbated, especially at tops of beds. Interbedded with diatomaceous sandy silt and mud, very dark gray (5Y 3/1), in sharp-based, graded beds. Section 1, 0 cm, to CC.

SMEAR SLIDE SUMMARY (%):

	3, 10 D	3, 142 D	3, 142 D	6, 62 D	6, 99 D
TEXTURE:					
Sand	5	20	15	10	5
Silt	30	50	50	50	40
Clay	65	30	35	40	55
COMPOSITION:					
Quartz	5	10	5	10	5
Feldspar	10	25	20	15	10
Rock fragments	5	3	5	15	—
Mica	2	—	2	—	2
Clay	35	25	35	40	40
Volcanic glass	3	5	5	5	2
Calcite/dolomite	—	5	5	5	3
Accessory minerals					
Pyrite	3	—	5	—	3
Glauconite	2	5	3	5	Tr
Foraminifers	—	2	—	—	—
Diatoms	35	20	15	5	35
Radiolarians	—	Tr	Tr	Tr	—
Sponge spicules	Tr	Tr	Tr	—	Tr
Silicoflagellates	Tr	—	Tr	Tr	—

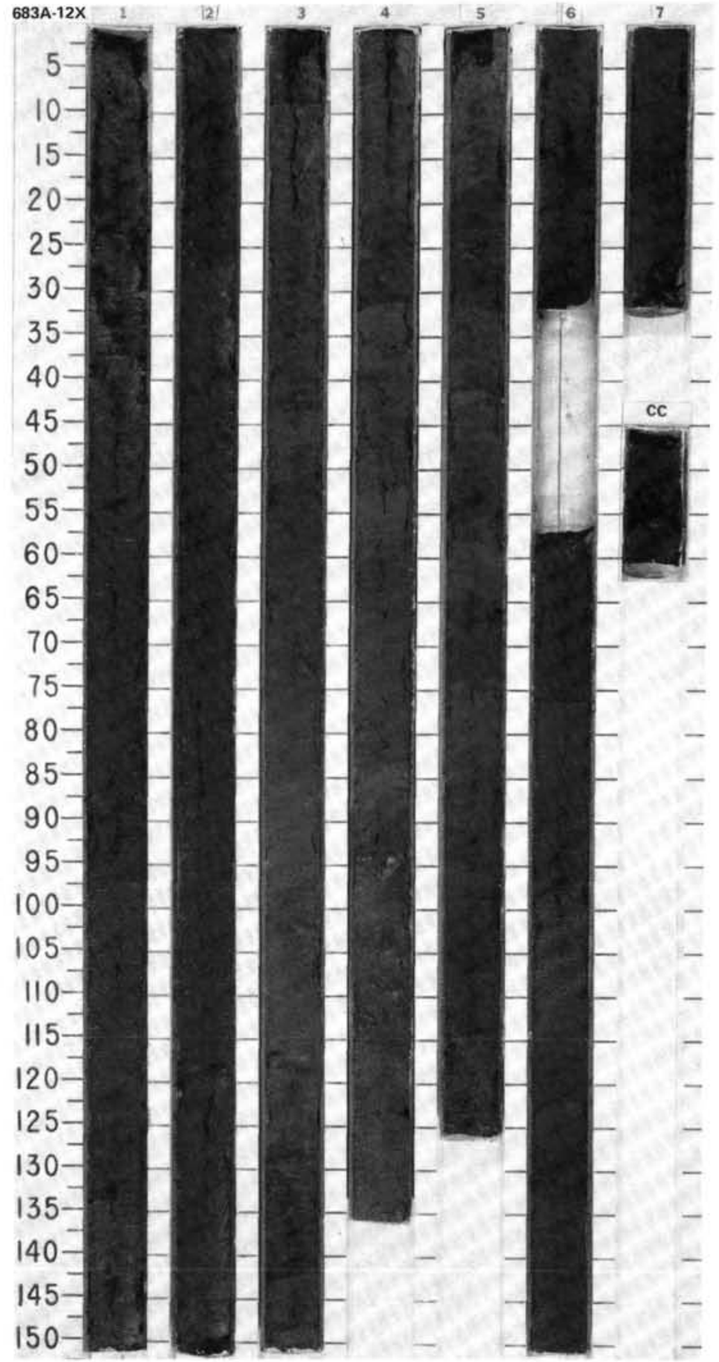

SITE 683 HOLE A CORE 13X CORED INTERVAL 3178.5-3188.0 mbsl; 106.7-116.2 mbsf

TIME-ROCK UNIT	FORAMINIFERS	NANNOFOSSILS	RADIOLARIANS	DIATOMS	PALEOMAGNETICS	PHYS. PROPERTIES	CHEMISTRY	SECTION	METERS	GRAPHIC LITHOLOGY	DRILLING DISTURB.	SED. STRUCTURES	SAMPLES
QUATERNARY		B *	*A. angulare* Zone *	*Rhizosolenia matuyama* Zone *				1, CC	0.5	VOID			*

LITHOLOGIC DESCRIPTION

DIATOM-BEARING SILTY MUD and DIATOMACEOUS MUD

Major lithology: diatom-bearing silty mud and diatomaceous mud, very dark gray (5Y 3/1). Section 1, 0 cm, to CC.

SMEAR SLIDE SUMMARY (%):

	1, 45
	D
TEXTURE:	
Silt	30
Clay	70
COMPOSITION:	
Quartz	10
Feldspar	15
Rock fragments	3
Mica	Tr
Clay	40
Volcanic glass	Tr
Calcite/dolomite	5
Accessory minerals	
Pyrite	2
Nannofossils	Tr
Diatoms	25
Radiolarians	Tr
Sponge spicules	Tr
Silicoflagellates	Tr

SITE 683 HOLE A CORE 14X CORED INTERVAL 3188.0-3197.5 mbs; 116.2-125.7 mbsf

TIME-ROCK UNIT	FORAMINIFERS	NANNOFOSSILS	RADIOLARIANS	DIATOMS	PALEOMAGNETICS	PHYS. PROPERTIES	CHEMISTRY	SECTION	METERS	GRAPHIC LITHOLOGY	DRILLING DISTURB.	SED. STRUCTURES	SAMPLES
QUATERNARY	N21-N22 *	insignificant *	*A. angulare* Zone *	*Pseudoeunotia doliolus* Zone *				1, CC	0.5, 1.0				*, *

LITHOLOGIC DESCRIPTION

DIATOMACEOUS MUD

Major lithology: diatomaceous mud, dark olive gray (5Y 3/2). Moderate to extensive bioturbation. Section 1, 0 cm, to CC.

Minor lithology: diatomaceous silty mud, very dark gray (5Y 3/1). Sharp-based graded turbidite bed at CC, 5 cm.

SMEAR SLIDE SUMMARY (%):

	1, 49	CC, 3
	D	D
TEXTURE:		
Sand	—	10
Silt	30	30
Clay	70	60
COMPOSITION:		
Quartz	5	10
Feldspar	15	15
Rock fragments	2	2
Mica	—	Tr
Clay	40	30
Volcanic glass	3	3
Calcite/dolomite	5	5
Accessory minerals		
Pyrite	3	2
Zircon	Tr	Tr
Foraminifers	—	3
Diatoms	25	30
Sponge spicules	Tr	—
Silicoflagellates	2	Tr

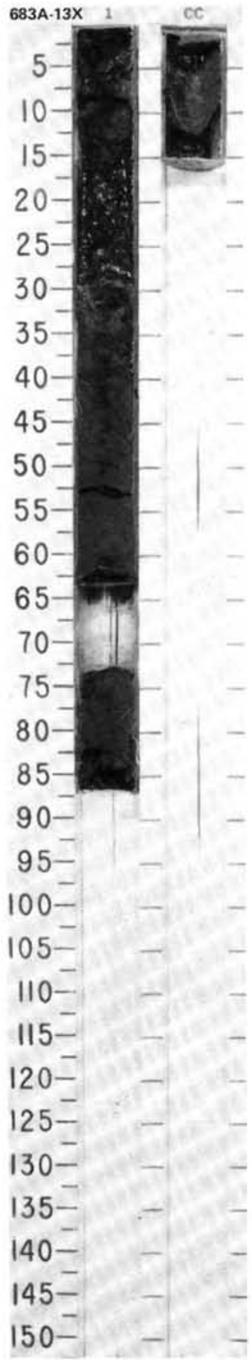

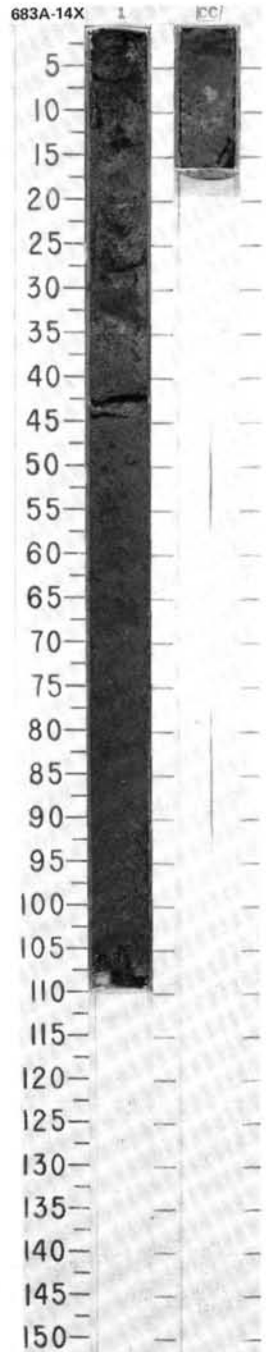

SITE 683 HOLE A CORE 15X CORED INTERVAL 3197.5-3207.0 mbsl; 125.7-135.2 mbsf

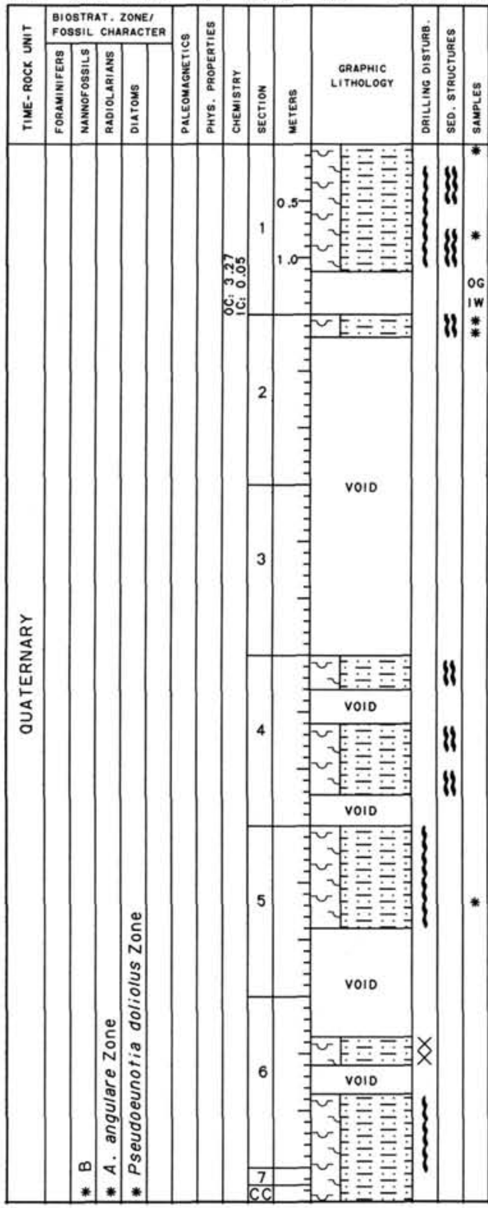

LITHOLOGIC DESCRIPTION

DIATOMACEOUS SILTY MUD

Major lithology: diatomaceous silty mud, dark olive gray to very dark gray (5Y 3/2, 10Y 3/1). Moderate bioturbation. Drilling-induced hackly parting in top 30 cm. Section 1, 0 cm, to CC.

Minor lithology: nannofossil ooze, pale olive (5Y 5.5/4). Clast 0.5–2-cm diameter, Section 1, 0–2 cm.

SMEAR SLIDE SUMMARY (%):

	1, 2 M	1, 79 D	2, 9 D	2, 9 D	5, 62 D
TEXTURE:					
Silt	30	30	20	30	50
Clay	70	70	80	70	50
COMPOSITION:					
Quartz	5	—	4	5	Tr
Feldspar	10	10	4	10	—
Rock fragments	Tr	—	—	—	—
Mica	Tr	—	—	Tr	—
Clay	10	50	60	50	—
Volcanic glass	3	—	—	—	—
Calcite/dolomite	10	3	Tr	3	15
Accessory minerals					
Pyrite	2	Tr	2	2	Tr
Glauconite	—	2	—	—	—
Foraminifers	Tr	—	—	—	—
Nannofossils	50	—	—	—	—
Diatoms	10	35	30	30	85
Sponge spicules	—	Tr	Tr	—	—
Silicoflagellates	—	Tr	—	—	Tr

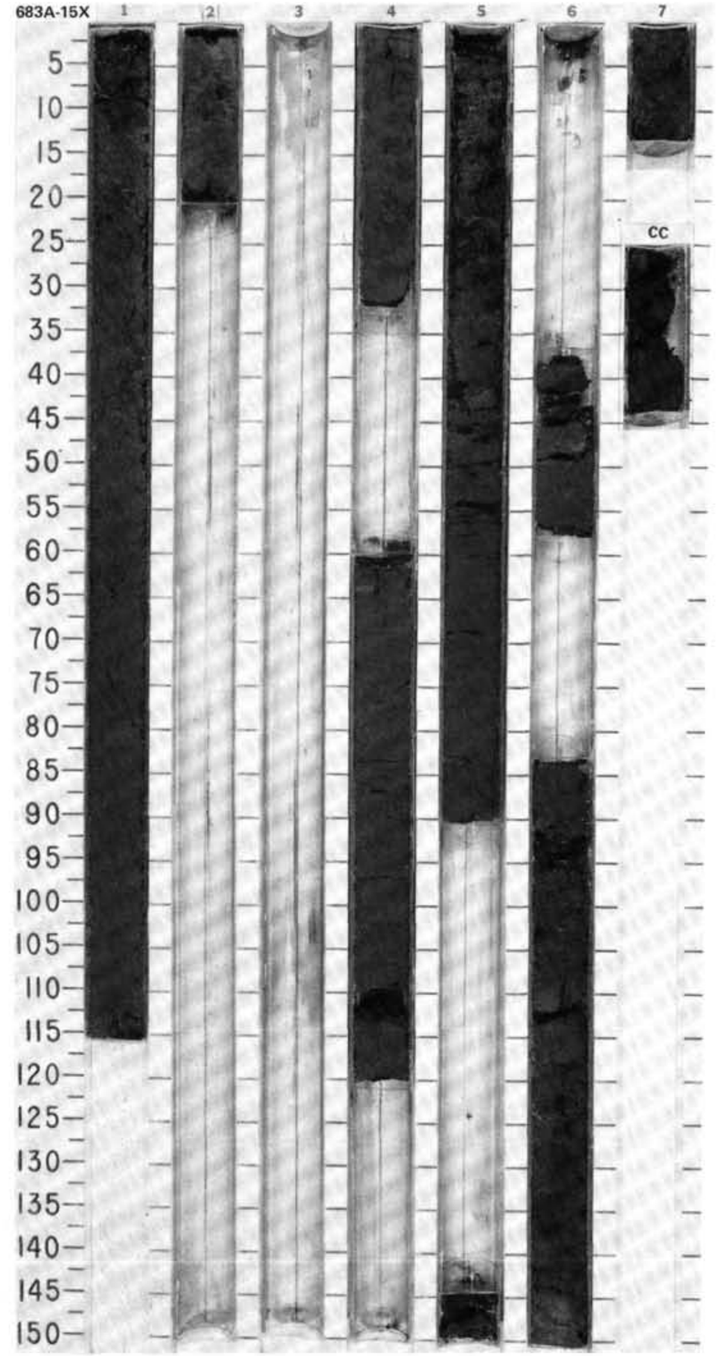

SITE 683 HOLE A CORE 16X CORED INTERVAL 3207.0-3216.5 mbsl; 135.2-144.7 mbsf

TIME-ROCK UNIT	BIOSTRAT. ZONE/ FOSSIL CHARACTER: FORAMINIFERS	NANNOFOSSILS	RADIOLARIANS	DIATOMS	PALEOMAGNETICS	PHYS. PROPERTIES	CHEMISTRY	SECTION	METERS	GRAPHIC LITHOLOGY	DRILLING DISTURB.	SED. STRUCTURES	SAMPLES	LITHOLOGIC DESCRIPTION
QUATERNARY		B *	A. angulare Zone *	Pseudoeunotia doliolus Zone *		● γ=1.40 φ=81.06		1 2	0.5 1.0	VOID VOID			* * *	

FELDSPATHIC DIATOMACEOUS MUD and SANDY MUD

Major lithology: feldspathic diatomaceous mud and sandy mud, very dark olive gray to black (5Y 2.5/2). Extensive bioturbation. Section 1, 0 cm, to CC.

SMEAR SLIDE SUMMARY (%):

	1, 26 D	1, 81 D	1, 83 D
TEXTURE:			
Sand	10	15	15
Silt	40	45	35
Clay	50	40	50
COMPOSITION:			
Quartz	Tr	—	Tr
Feldspar	20	20	10
Rock fragments	10	5	5
Clay	30	30	40
Volcanic glass	—	5	Tr
Calcite/dolomite	Tr	Tr	2
Accessory minerals			
Glauconite	Tr	—	—
Pyrite	2	2	3
Foraminifers	—	Tr	10
Nannofossils	—	—	Tr
Diatoms	35	35	30
Radiolarians	—	—	Tr
Sponge spicules	3	3	—
Silicoflagellates	—	Tr	—

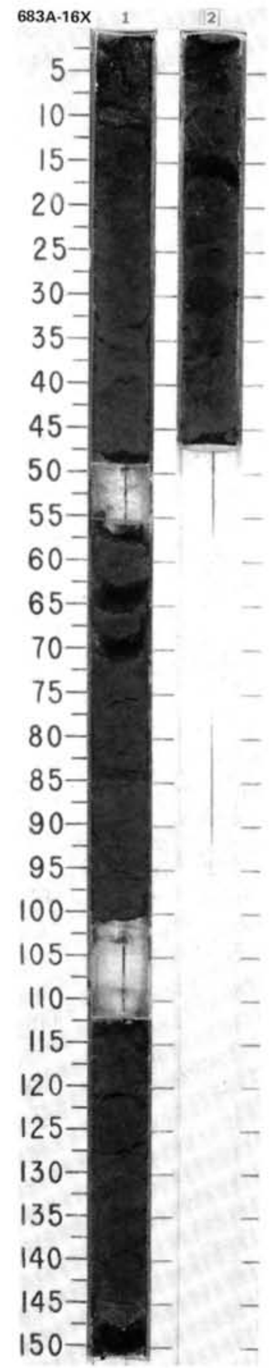

SITE 683 HOLE A CORE 17X CORED INTERVAL 3216.5-3226.0 mbsl; 144.7-154.2 mbsf

TIME-ROCK UNIT	FORAMINIFERS	NANNOFOSSILS	RADIOLARIANS	DIATOMS	PALEOMAGNETICS	PHYS. PROPERTIES	CHEMISTRY	SECTION	METERS	GRAPHIC LITHOLOGY	DRILLING DISTURB.	SED. STRUCTURES	SAMPLES
PLEISTOCENE/PLIOCENE		B *	base *A. angulare* to top *P. prismatium* Zone *	*Nitzschia reinholdii* Zone *				1 CC	0.5				* ***

BIOSTRAT. ZONE/FOSSIL CHARACTER

LITHOLOGIC DESCRIPTION

DIATOMACEOUS MUD and DIATOMACEOUS OOZE

Major lithology: diatomaceous mud and diatomaceous ooze, dark olive gray to olive gray (5Y 3/2, 5Y 4/2). Moderate bioturbation, faint bedding. Section 1, 0 cm, to CC.

Minor lithologies:
1. sandy diatomaceous mud, very dark gray (5Y 3/1) burrow fills.
2. feldspathic spicular silt, olive gray (5Y 4/2). Probably a collapsed sponge.

SMEAR SLIDE SUMMARY (%):

	1, 10 D	1, 42 D	1, 46 D	1, 51 M	1, 94 M
TEXTURE:					
Sand	10	5	2	15	20
Silt	50	65	43	55	35
Clay	40	30	55	30	45
COMPOSITION:					
Quartz	—	—	Tr	Tr	5
Feldspar	15	10	5	40	15
Rock fragments	5	—	Tr	—	5
Mica	—	—	—	—	Tr
Clay	20	20	45	25	35
Volcanic glass	—	Tr	Tr	—	—
Calcite/dolomite	Tr	Tr	2	—	5
Accessory minerals					
Pyrite	3	3	2	2	5
Gypsum	—	—	Tr	—	—
Glauconite	—	—	—	—	Tr
Foraminifers	—	—	Tr	—	—
Nannofossils	—	Tr	—	—	—
Diatoms	50	65	45	20	30
Sponge spicules	5	2	1	13	Tr
Silicoflagellates	2	Tr	—	—	—
Fish remains	—	—	—	—	Tr

683A-17X 1 CC

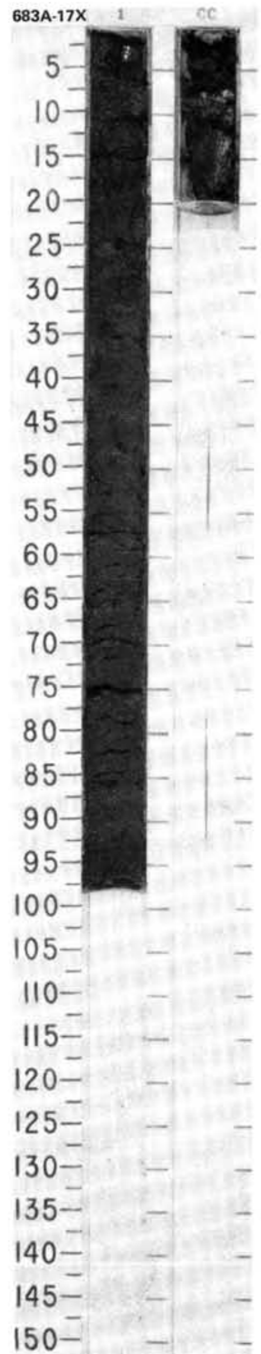

SITE 683 HOLE A CORE 18X CORED INTERVAL 3226.0-3235.5 mbsl; 154.2-163.7 mbsf

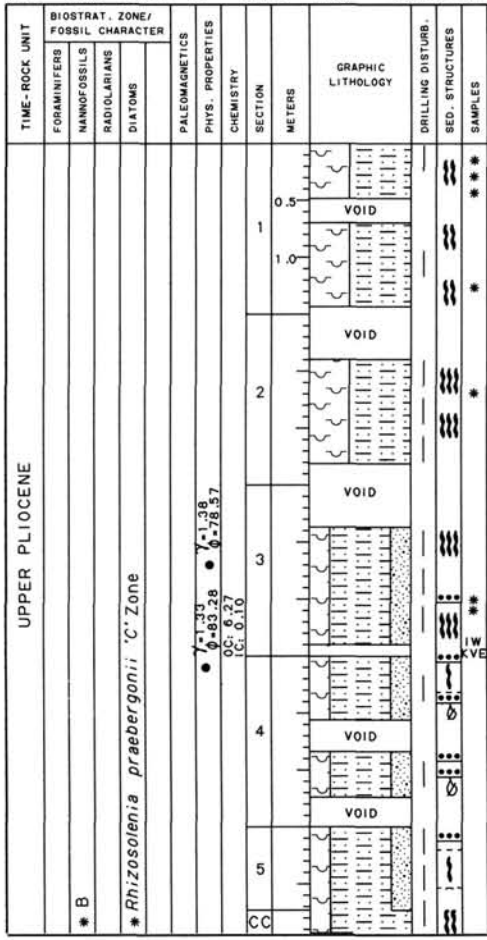

LITHOLOGIC DESCRIPTION

DIATOMACEOUS MUD

Major lithology: diatomaceous mud, dark olive gray (5Y 3/2). Moderate to extensive bioturbation, with graded turbidite interbeds and sponge fragments.

Minor lithologies:
1. diatom- and spicule-rich feldspathic silt, light olive gray (5Y 6/2). Collapsed sponges.
2. pyritiferous diatom-bearing mud, dark gray (5Y 4/1). Sharp-based graded turbidite beds, Section 3, 105 cm, to Section 4, 108 cm. One turbidite contains a collapsed sponge within its coarser grained base.

SMEAR SLIDE SUMMARY (%):

	1, 22 M	1, 28 D	1, 38 M	1, 132 D	2, 70 M	3, 105 M	3, 108 M
TEXTURE:							
Sand	100	5	10	10	100	—	20
Silt	—	35	60	50	—	15	70
Clay	—	60	30	40	—	85	10
COMPOSITION:							
Quartz	—	Tr	—	10	—	—	—
Feldspar	—	5	35	5	—	5	10
Rock fragments	—	Tr	—	5	—	Tr	Tr
Clay	—	50	30	30	—	20	10
Volcanic glass	—	1	—	—	—	—	—
Calcite/dolomite	—	2	—	—	—	—	5
Accessory minerals							
Pyrite	—	2	2	5	—	60	3
Glauconite	—	—	—	3	—	—	2
Foraminifers	—	—	3	2	—	—	20
Nannofossils	—	—	—	3	—	—	—
Diatoms	—	40	15	35	—	15	45
Radiolarians	—	Tr	—	—	—	—	—
Sponge spicules	—	—	15	2	—	—	5
Silicoflagellates	—	—	Tr	—	—	—	—
Fish remains (bone)	100	—	—	—	100	—	—

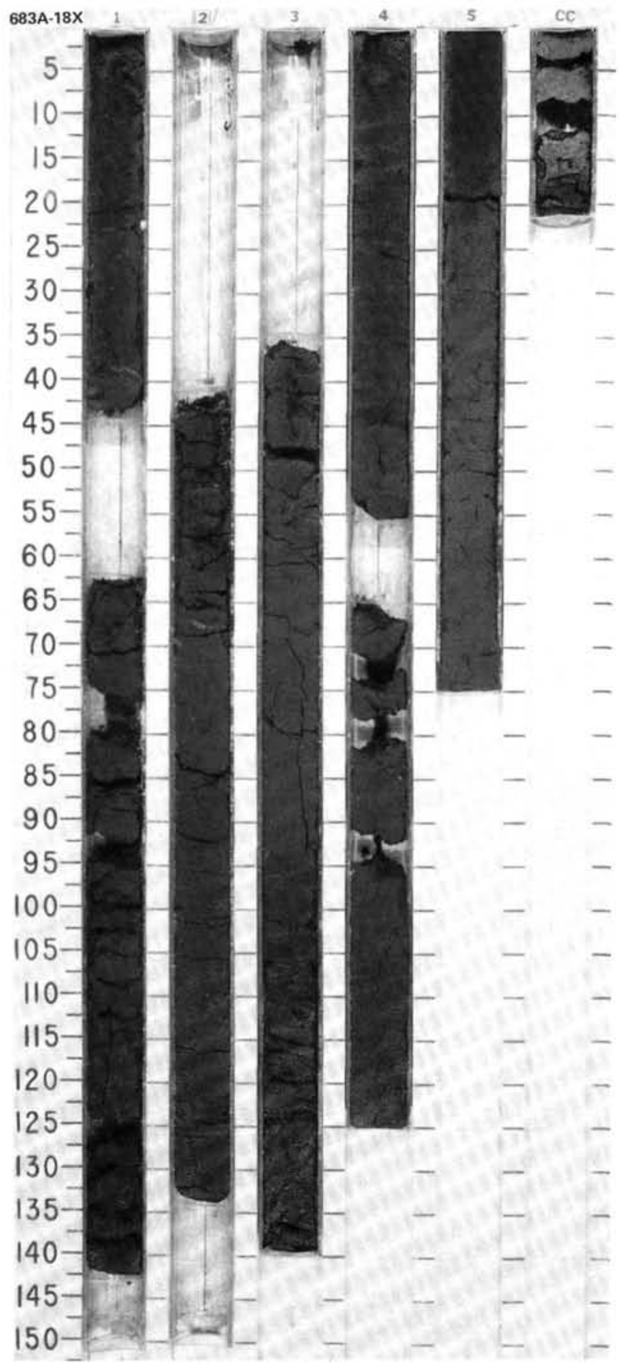

SITE 683 HOLE A CORE 19X CORED INTERVAL 3235.5-3245.0 mbsl; 163.7-173.2 mbsf

TIME-ROCK UNIT	BIOSTRAT. ZONE/ FOSSIL CHARACTER: FORAMINIFERS	NANNOFOSSILS	RADIOLARIANS	DIATOMS	PALEOMAGNETICS	PHYS. PROPERTIES	CHEMISTRY	SECTION	METERS	GRAPHIC LITHOLOGY	DRILLING DISTURB.	SED. STRUCTURES	SAMPLES
UPPER PLIOCENE	N18-N19 *	NN18 *		*Rhizosolenia praebergonii* Zone *				1 CC	0.5	VOID			* * *

LITHOLOGIC DESCRIPTION

DIATOMACEOUS MUD AND SANDY MUD

Major lithology: diatomaceous mud and sandy mud, locally foraminifer-bearing, black (5Y 2.5/2). Moderate bioturbation, with minor shell fragments and collapsed sponge fragments. Section 1, 0 cm, to CC.

SMEAR SLIDE SUMMARY (%):

	1, 15 D	1, 69 D	CC, 18 M
TEXTURE:			
Sand	5	30	5
Silt	35	30	35
Clay	60	40	60
COMPOSITION:			
Quartz	Tr	5	Tr
Feldspar	5	15	5
Rock fragments	Tr	5	Tr
Clay	50	35	50
Volcanic glass	Tr	1	Tr
Calcite/dolomite	2	2	Tr
Accessory minerals			
Pyrite	3	2	3
Glauconite	—	Tr	Tr
Foraminifers	—	15	1
Nannofossils	—	Tr	—
Diatoms	40	20	40
Sponge spicules	—	Tr	1
Fish remains	—	Tr	—

SITE 683 HOLE A CORE 20X CORED INTERVAL 3245.0-3254.5 mbsl; 173.2-182.7 mbsf

TIME-ROCK UNIT	BIOSTRAT. ZONE/ FOSSIL CHARACTER: FORAMINIFERS	NANNOFOSSILS	RADIOLARIANS	DIATOMS	PALEOMAGNETICS	PHYS. PROPERTIES	CHEMISTRY	SECTION	METERS	GRAPHIC LITHOLOGY	DRILLING DISTURB.	SED. STRUCTURES	SAMPLES
UPPER PLIOCENE		B *	*Spongaster pentas* Zone *	*Rhizosolenia praebergonii* Zone *				1 CC	1.0				*

LITHOLOGIC DESCRIPTION

DIATOMACEOUS MUD

Major lithology: diatomaceous mud, black to dark olive gray (5Y 2.5/2, 5Y 3/2). Slightly bioturbated, with minor collapsed sponge fragments. Section 1, 0 cm, to CC.

SMEAR SLIDE SUMMARY (%):

	1, 26
TEXTURE:	
Silt	40
Clay	60
COMPOSITION:	
Feldspar	5
Rock fragments	Tr
Clay	45
Volcanic glass	Tr
Calcite/dolomite	Tr
Accessory minerals	
Pyrite	3
Foraminifers	1
Diatoms	45
Sponge spicules	1

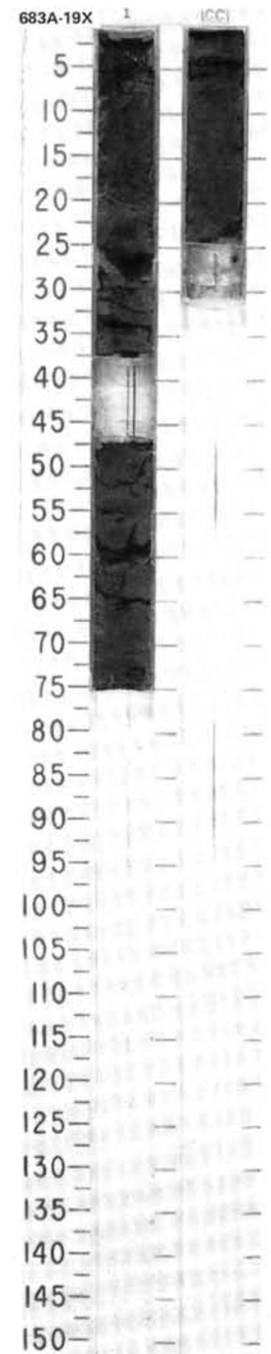

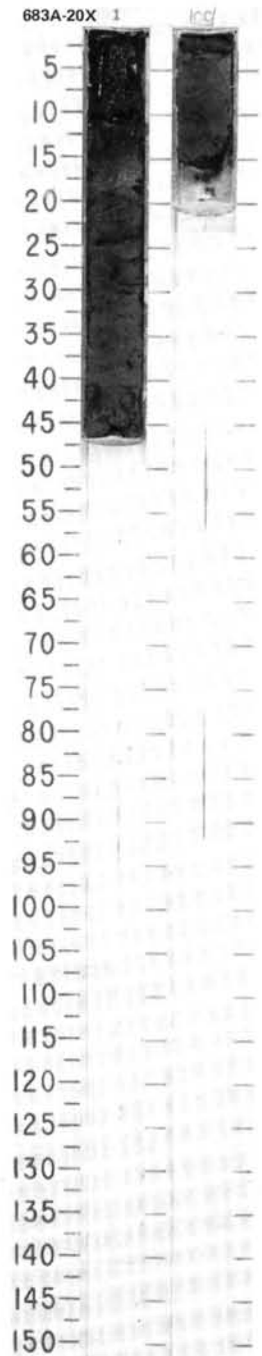

SITE 683 HOLE A CORE 21X CORED INTERVAL 3254.5-3264.0 mbsl; 182.7-192.2 mbsf

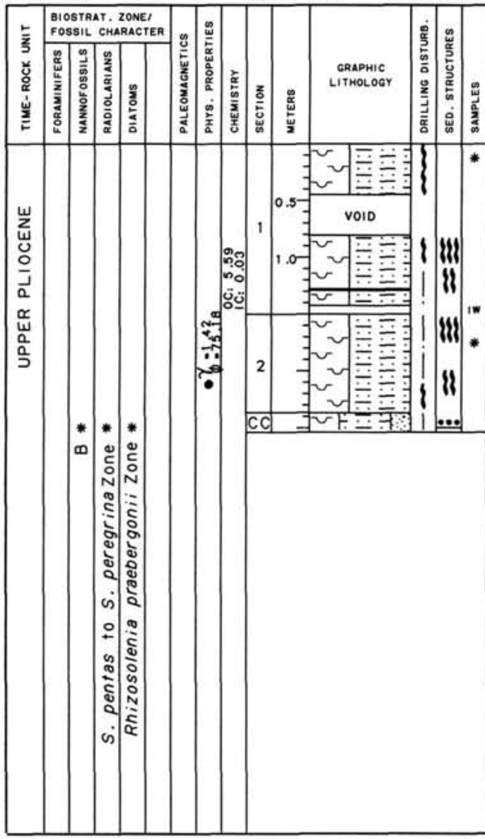

LITHOLOGIC DESCRIPTION

DIATOMACEOUS MUD

Major lithology: diatomaceous mud, black to dark olive gray (5Y 2.5/2, 5Y 3/2). Extensive to moderate bioturbation (including *Chondrites*), sparse sponge fragments. Section 1, 0 cm, to CC.

Minor lithology: diatomaceous sandy mud, dark olive gray (5Y 3/2), sharp-based graded turbidite bed, at CC, 5 cm.

SMEAR SLIDE SUMMARY (%):

	1, 19	2, 26
TEXTURE:		
Silt	40	35
Clay	60	65
COMPOSITION:		
Quartz	—	Tr
Feldspar	5	5
Rock fragments	—	10
Clay	50	45
Calcite/dolomite	—	Tr
Pyrite	—	3
Diatoms	45	37
Fish remains	Tr	—

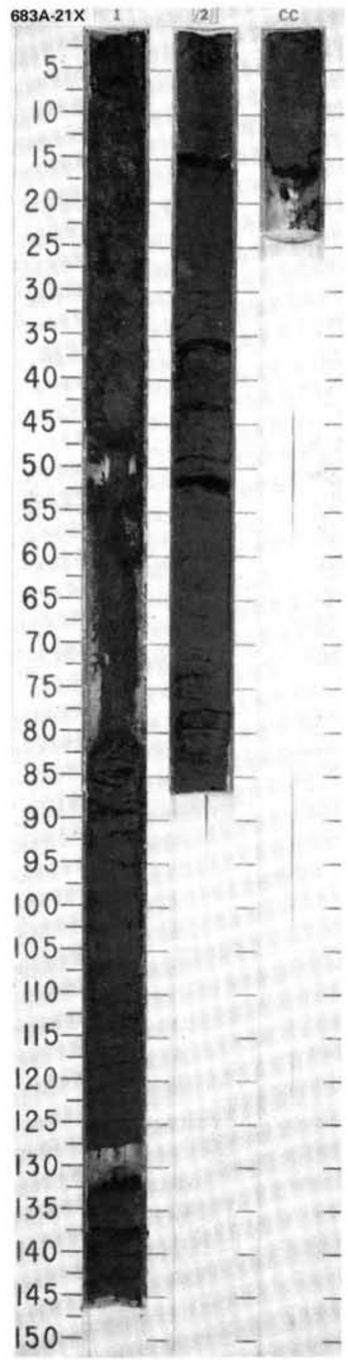

SITE 683 HOLE A CORE 22X CORED INTERVAL 3264.0-3273.5 mbsl; 192.2-201.7 mbsf

TIME-ROCK UNIT	FORAMINIFERS	NANNOFOSSILS	RADIOLARIANS	DIATOMS	PALEOMAGNETICS	PHYS. PROPERTIES	CHEMISTRY	SECTION	METERS	GRAPHIC LITHOLOGY	DRILLING DISTURB.	SED. STRUCTURES	SAMPLES
UPPER PLIOCENE		B *	*upper S. pentas* Zone *	*Rhizosolenia praebergonii* Zone *				1 CC	0.5				* **

LITHOLOGIC DESCRIPTION

DIATOMACEOUS MUD

Major lithology: diatomaceous mud, black to dark olive gray (5Y 3/1, 5Y 3/2). Massive, with rare collapsed sponge fragments. No obvious bioturbation. Section 1, 0 cm, to CC.

Minor lithology: diatomaceous sandy mud, dark olive gray (5Y 3/2). Sharp-based graded turbitite bed containing collapsed sponge fragments at CC, 8.5 cm.

SMEAR SLIDE SUMMARY (%):

	1, 40 D	CC, 5 M	CC, 8 M
TEXTURE:			
Sand	—	—	15
Silt	30	30	35
Clay	70	70	50
COMPOSITION:			
Quartz	5	Tr	10
Feldspar	—	Tr	—
Clay	60	58	45
Calcite/dolomite	—	Tr	5
Accessory minerals			
Pyrite	5	2	10
Foraminifers	—	—	Tr
Diatoms	30	40	30
Sponge spicules	—	—	Tr

SITE 683 HOLE A CORE 23X CORED INTERVAL 3273.5-3283.0 mbsl; 201.7-211.2 mbsf

TIME-ROCK UNIT	FORAMINIFERS	NANNOFOSSILS	RADIOLARIANS	DIATOMS	PALEOMAGNETICS	PHYS. PROPERTIES	CHEMISTRY	SECTION	METERS	GRAPHIC LITHOLOGY	DRILLING DISTURB.	SED. STRUCTURES	SAMPLES
UPPER PLIOCENE		B *	*S. pentas* top *S. peregrina* Zone *	*Rhizosolenia praebergonii* Zone *				1 CC	0.5 1.0				* * ** **

LITHOLOGIC DESCRIPTION

DIATOMACEOUS MUD

Major lithology: diatomaceous mud, black to dark olive gray (5Y 2.5/1, 5Y 3/2). Massive to fissile; no obvious bioturbation. Section 1, 0 cm, to CC.

SMEAR SLIDE SUMMARY (%):

	1, 11 D	1, 40 D	1, 91 D	1, 100 D	CC, 8 D	CC, 20 D
TEXTURE:						
Sand	—	—	5	5	—	—
Silt	15	25	20	35	25	35
Clay	85	75	75	60	75	65
COMPOSITION:						
Quartz	—	—	1	—	—	—
Feldspar	5	5	5	5	5	5
Rock fragments	Tr	Tr	1	5	Tr	Tr
Clay	75	65	Tr	50	65	50
Volcanic glass	—	—	—	Tr	—	1
Calcite/dolomite	Tr	Tr	—	Tr	Tr	1
Accessory minerals						
Pyrite	5	5	5	5	5	3
Gypsum	—	—	Tr	—	—	—
Glauconite	—	—	Tr	—	—	—
Diatoms	15	25	28	35	25	40
Radiolarians	—	—	—	Tr	—	—
Sponge spicules	—	—	1	Tr	—	—

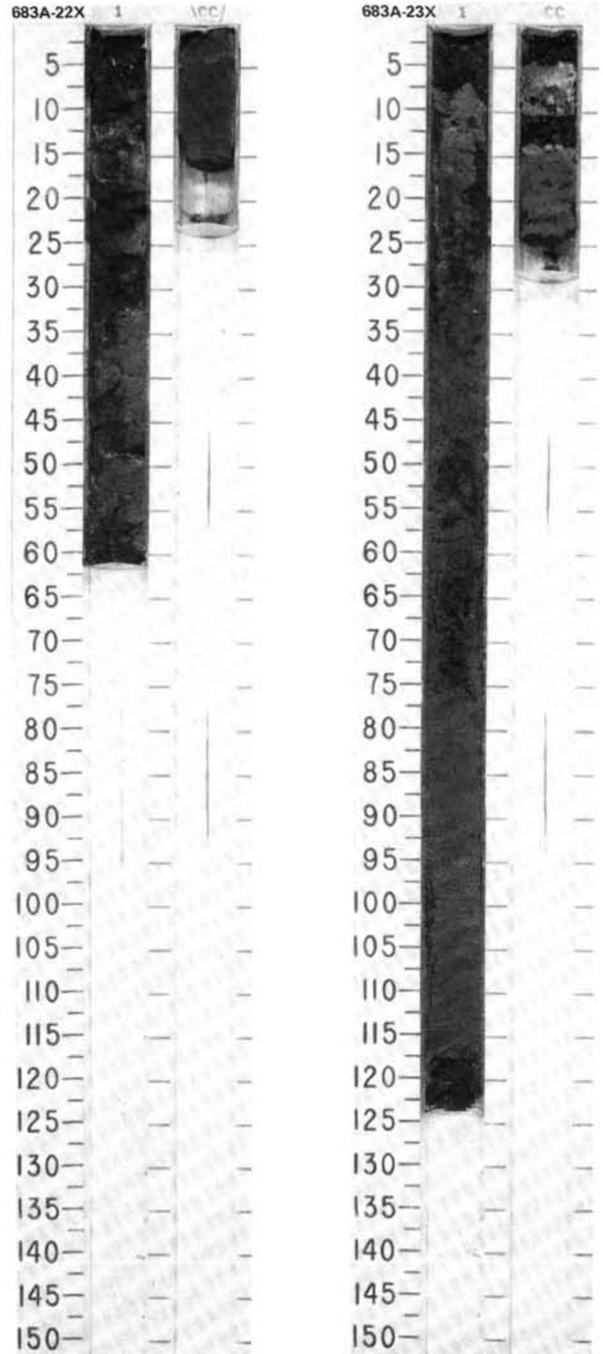

SITE 683 HOLE A CORE 24X CORED INTERVAL 3283.0-3292.5 mbsl; 211.2-220.7 mbsf

TIME-ROCK UNIT	FORAMINIFERS	NANNOFOSSILS	RADIOLARIANS	DIATOMS	PALEOMAGNETICS	PHYS. PROPERTIES	CHEMISTRY	SECTION	METERS	GRAPHIC LITHOLOGY	DRILLING DISTURB.	SED. STRUCTURES	SAMPLES
UPPER PLIOCENE		B *	*S. pentas* top *S. peregrina* Zone *	*Rhizosolenia praebergonii* Zone *		γ=1.55 ● φ=66.93	OC: 4.35 IC: 0.14	1	0.5				* * * IW KVE
								CC					

BIOSTRAT. ZONE/ FOSSIL CHARACTER

LITHOLOGIC DESCRIPTION

DIATOMACEOUS MUD to SOFT MUDSTONE

Major lithology: diatomaceous mud to soft mudstone, dark olive gray (5Y 3/2). Slightly fissile, minor bioturbation. Section 1, 0 cm, to CC.

Minor lithology: glauconitic sand, black (5Y 2.5/2) sharp-based graded turbidite bed 6-mm thick, at Section 1, 46 cm.

SMEAR SLIDE SUMMARY (%):

	1, 23 D	1, 45 M	1, 60 D
TEXTURE:			
Sand	10	85	15
Silt	45	10	40
Clay	45	5	45
COMPOSITION:			
Quartz	—	5	5
Feldspar	10	15	15
Rock fragments	5	5	5
Clay	40	6	40
Volcanic glass	1	—	—
Calcite/dolomite	1	5	Tr
Accessory minerals	—	1	—
Pyrite	3	3	3
Glauconite	—	60	—
Diatoms	40	—	30
Sponge spicules	—	—	1
Silicoflagellates	—	—	1
Fish remains	—	Tr	—

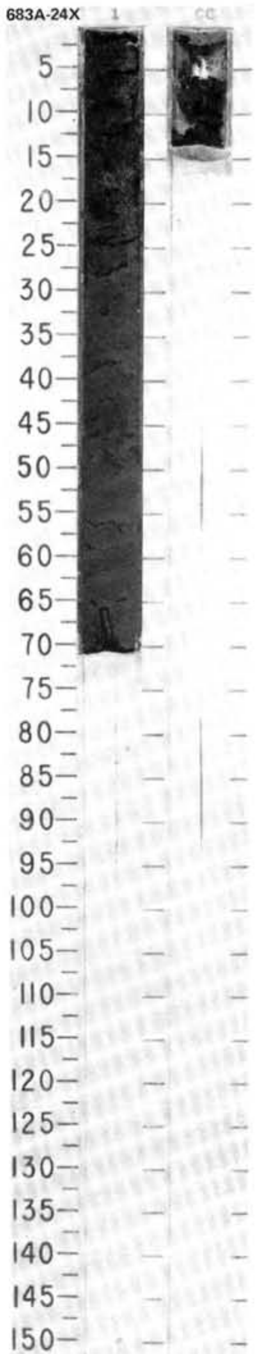

SITE 683 HOLE A CORE 25X CORED INTERVAL 3292.5-3302.0 mbsl; 220.7-230.2 mbsf

TIME-ROCK UNIT	FORAMINIFERS	NANNOFOSSILS	RADIOLARIANS	DIATOMS	PALEOMAGNETICS	PHYS. PROPERTIES	CHEMISTRY	SECTION	METERS	GRAPHIC LITHOLOGY	DRILLING DISTURB.	SED. STRUCTURES	SAMPLES
UPPER PLIOCENE		* B	* upper *S. pentas* Zone	* *Rhizosolenia praebergonii* Zone				1, 2, 3, 4, 5, 6, CC	0.5, 1.0	HOLE FILL FROM WIPER TRIP; VOID; VOID			*

LITHOLOGIC DESCRIPTION

DIATOMACEOUS MUD AND MUDDY DIATOMACEOUS OOZE

Section 1, 0 cm, to Section 5, 75 cm: recycled material from upper part of hole.

Major lithology: Section 5, 75 cm, to CC: diatomaceous mud and muddy diatomaceous ooze, dark olive gray (5Y 3/2). Massive, locally bioturbated.

SMEAR SLIDE SUMMARY (%):

	1, 120 D	2, 123 M	5, 138 D	6, 10 D
TEXTURE:				
Sand	10	10	5	5
Silt	45	30	40	45
Clay	45	60	55	50
COMPOSITION:				
Quartz	—	—	10	—
Feldspar	5	5	5	5
Rock fragments	Tr	Tr	—	Tr
Clay	40	35	40	45
Volcanic glass	Tr	—	—	Tr
Calcite/dolomite	5	15	Tr	—
Accessory minerals				
Pyrite	3	2	2	2
Foraminifers	10	3	—	—
Nannofossils	2	5	—	—
Diatoms	35	30	43	45
Radiolarians	Tr	—	Tr	Tr
Sponge spicules	—	2	—	3
Silicoflagellates	Tr	2	—	Tr
Fish remains	—	1	—	—

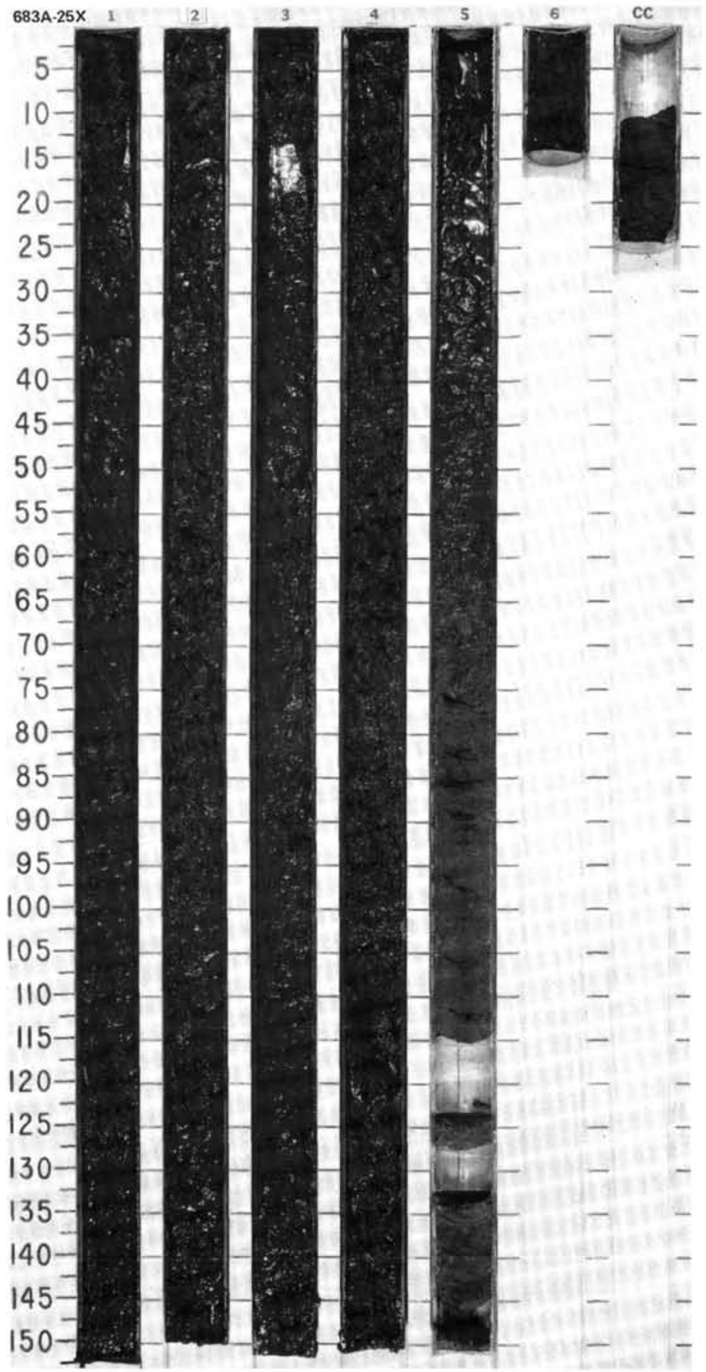

SITE 683 HOLE A CORE 26X CORED INTERVAL 3302.0-3311.5 mbsl; 230.2-239.7 mbsf

TIME-ROCK UNIT	FORAMINIFERS	NANNOFOSSILS	RADIOLARIANS	DIATOMS	PALEOMAGNETICS	PHYS. PROPERTIES	CHEMISTRY	SECTION	METERS	GRAPHIC LITHOLOGY	DRILLING DISTURB.	SED. STRUCTURES	SAMPLES	LITHOLOGIC DESCRIPTION
MIOCENE (LOWER UPPER-UPPER MIDDLE) / UPPER PLIOCENE		B *	D. pettersoni Zone *	Rhizosolenia praebergonii Zone *		γ=1.45 ● φ=72.1 ●		1, CC					* *	see below

BIOSTRAT. ZONE/ FOSSIL CHARACTER

LITHOLOGIC DESCRIPTION

DIATOMACEOUS MUD

Major lithology: diatomaceous mud, dark olive gray to black (5Y 3/2, 5Y 3/1). Moderately bioturbated. Section 1, 0 cm, to CC.

Minor lithology: glass-rich diatom-bearing silty mud, olive (5Y 5/4) patches.

SMEAR SLIDE SUMMARY (%):

	1, 18 M	1, 26 D
TEXTURE:		
Sand	5	15
Silt	40	20
Clay	55	65
COMPOSITION:		
Quartz	3	5
Feldspar	10	5
Rock fragments	2	—
Mica	Tr	—
Clay	25	35
Volcanic glass	30	—
Calcite/dolomite	Tr	10
Accessory minerals		
Pyrite	5	5
Glauconite	Tr	2
Micrite	7	—
Diatoms	18	35
Sponge spicules	Tr	3

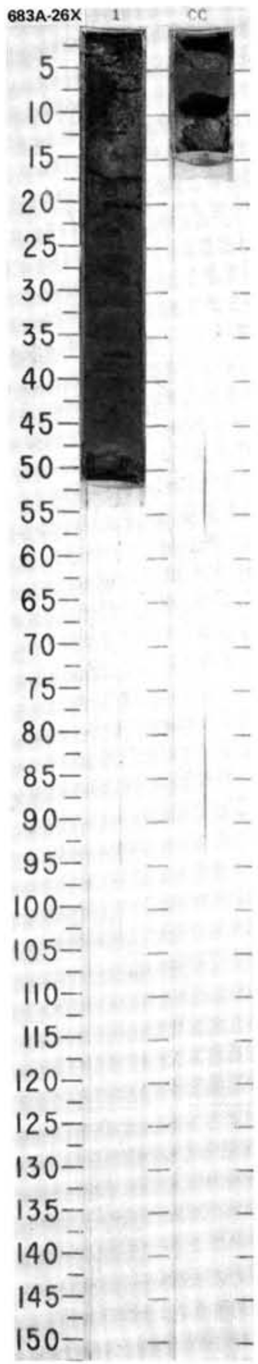

SITE 683 HOLE A CORE 27X CORED INTERVAL 3311.5-3321.0 mbsl; 239.7-249.2 mbsf

TIME-ROCK UNIT	FORAMINIFERS	NANNOFOSSILS	RADIOLARIANS	DIATOMS	PALEOMAGNETICS	PHYS. PROPERTIES	CHEMISTRY	SECTION	METERS	GRAPHIC LITHOLOGY	DRILLING DISTURB.	SED. STRUCTURES	SAMPLES
MIDDLE MIOCENE		insignificant *	*D. pettersoni* Zone *	*Rhizosolenia praebergonii* Zone *			OC: 7.13 IC: 0.23	1	0.5 1.0	VOID			* * IW KVE
								CC					

LITHOLOGIC DESCRIPTION

DIATOMACEOUS SANDY and SILTY MUDSTONE

Major lithology: diatomaceous sandy and silty mudstone, dark olive gray to black (5Y 3/2, 5Y 2.5/2). Partially indurated, fissile to fractured. Section 1, 0 cm, to CC.

Minor lithologies:
1. diatom-bearing, ash-rich mud, olive (5Y 4/3) clast, at Section 1, 26 cm. 2. dolomite nodule, olive (5Y 4/3), at Section 1, 107 cm.
3. dolomicrite, olive gray (5Y 5/2) breccia with dark olive gray fracture fill (5Y 3/2) at CC, 10 cm.

SMEAR SLIDE SUMMARY (%):

	1, 2 M	1, 91 D
TEXTURE:		
Sand	5	20
Silt	40	30
Clay	5	50
COMPOSITION:		
Quartz	5	5
Feldspar	10	3
Rock fragments	5	2
Mica	2	Tr
Clay	30	40
Volcanic glass	30	3
Calcite/dolomite	—	3
Accessory minerals		
Pyrite	3	2
Glauconite	—	Tr
Diatoms	15	40
Sponge spicules	—	2

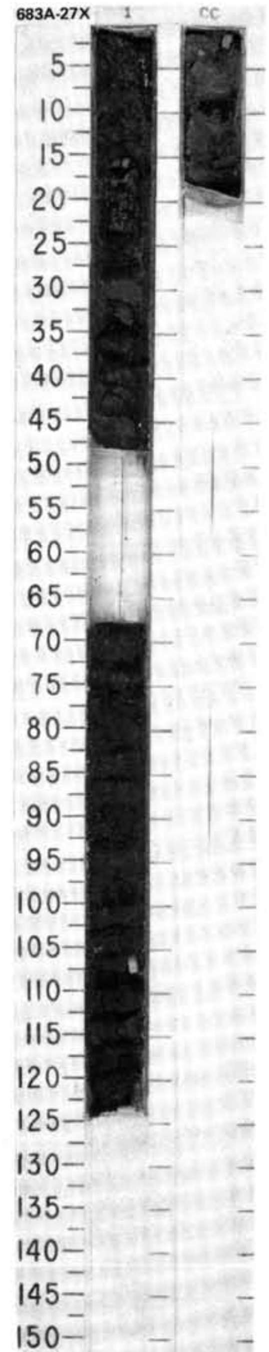

SITE 683 HOLE A CORE 28X CORED INTERVAL 3321.0-3330.5 mbsl; 249.2-258.7 mbsf

TIME-ROCK UNIT	BIOSTRAT. ZONE/FOSSIL CHARACTER: FORAMINIFERS	NANNOFOSSILS	RADIOLARIANS	DIATOMS	PALEOMAGNETICS	PHYS. PROPERTIES	CHEMISTRY	SECTION	METERS	GRAPHIC LITHOLOGY	DRILLING DISTURB.	SED. STRUCTURES	SAMPLES
MIDDLE MIOCENE		insignificant *	*D. pettersoni* Zone *	undifferentiated *				1, 2, CC	0.5, 1.0	VOID			* * ***

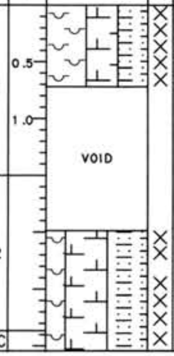

LITHOLOGIC DESCRIPTION

CLAY-RICH NANNOFOSSIL-DIATOM OOZE and DIATOM- AND SPICULE-BEARING MUD AND SILICEOUS NANNOFOSSIL-OOZE

Major lithology: Section 1, 0–55 cm: clay-rich nannofossil-diatom ooze, olive to dark olive gray (5Y 4/3/5, 5Y 3/2). Massive, brecciated by drilling. Section 2, 50 cm, to CC: diatom- and spicule-bearing mud and siliceous nannofossil-ooze, very dark gray to olive (5Y 3/1, 5Y 4/3.5).

SMEAR SLIDE SUMMARY (%):

	1, 61 D	2, 82 D	2, 130 M	CC, 9 M	CC, 12 D
TEXTURE:					
Sand	5	—	—	—	—
Silt	15	15	20	45	30
Clay	80	85	80	55	70
COMPOSITION:					
Quartz	2	2	5	5	—
Feldspar	2	2	10	5	—
Rock fragments	1	1	5	—	—
Mica	—	Tr	Tr	5	Tr
Clay	20	25	35	—	65
Volcanic glass	—	3	3	5	—
Calcite/dolomite	—	3	—	Tr	—
Accessory minerals					
Pyrite	2	2	2	—	5
Glauconite	—	—	Tr	—	—
Micrite	3	Tr	2	—	—
Foraminifers	Tr	—	—	Tr	Tr
Nannofossils	30	40	3	55	5
Diatoms	40	20	25	10	10
Radiolarians	—	—	—	Tr	—
Sponge spicules	Tr	2	10	15	15
Silicoflagellates	Tr	—	—	Tr	Tr

SITE 683 HOLE A CORE 29X CORED INTERVAL 3330.5-3340.0 mbsl; 258.7-268.2 mbsf

TIME-ROCK UNIT	BIOSTRAT. ZONE/FOSSIL CHARACTER: FORAMINIFERS	NANNOFOSSILS	RADIOLARIANS	DIATOMS	PALEOMAGNETICS	PHYS. PROPERTIES	CHEMISTRY	SECTION	METERS	GRAPHIC LITHOLOGY	DRILLING DISTURB.	SED. STRUCTURES	SAMPLES
MIDDLE MIOCENE		insignificant*	*D. pettersoni* Zone *	undifferentiated *				1, CC	0.5, 1.0	VOID			* *

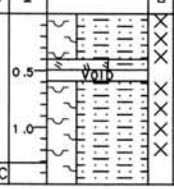

LITHOLOGIC DESCRIPTION

DIATOMACEOUS MUD

Major lithology: diatomaceous mud, dark olive gray (5Y 3/2). Slightly bioturbated, minor foraminifers. Section 1, 0 cm, to CC.

Minor lithology: volcanic ash (dacite or rhyodacite?) interbed at Section 1, 40–45 cm.

SMEAR SLIDE SUMMARY (%):

	1, 43 M	1, 119 D
TEXTURE:		
Sand	10	5
Silt	90	20
Clay	—	75
COMPOSITION:		
Quartz	5	2
Feldspar	5	10
Rock fragments	—	2
Mica	Tr	—
Clay	—	40
Volcanic glass	90	5
Dolomite	—	3
Accessory minerals		
Glauconite	—	Tr
Pyrite	—	2
Nannofossils	—	3
Diatoms	—	30
Sponge spicules	—	3

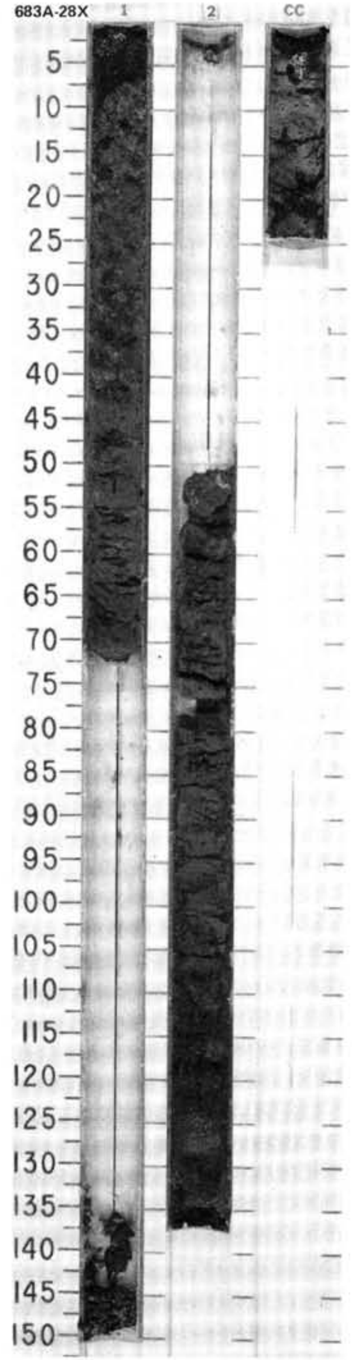

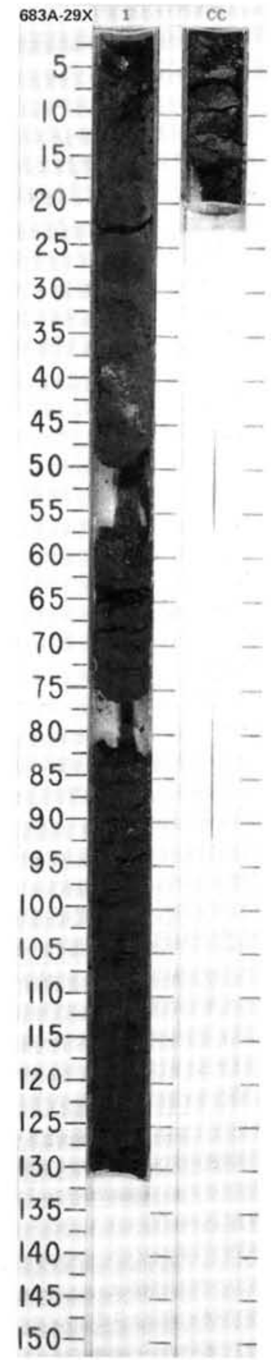

SITE 683 HOLE A CORE 30X CORED INTERVAL 3340.0-3349.5 mbsl; 268.2-277.7 mbsf

TIME-ROCK UNIT	BIOSTRAT. ZONE/FOSSIL CHARACTER: FORAMINIFERS	NANNOFOSSILS	RADIOLARIANS	DIATOMS	PALEOMAGNETICS	PHYS. PROPERTIES	CHEMISTRY	SECTION	METERS	GRAPHIC LITHOLOGY	DRILLING DISTURB.	SED. STRUCTURES	SAMPLES
MIDDLE MIOCENE	*N9-N14; N16-N18*	NN8*	*D. alata* Zone*	*Craspedodiscus cosinodiscus* Zone*		γ=1.83 ● φ=65.42; γ=1.54 ● φ=67.68	OC: 4.22 IC: 0.19	1; 2; CC	0.5; 1.0	VOID			*; *; KVE OG IW; *

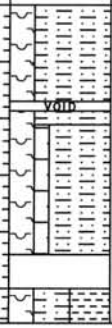

LITHOLOGIC DESCRIPTION

DIATOMACEOUS MUD, DIATOMACEOUS NANNOFOSSIL MUD, and DIATOMACEOUS CLAY-RICH MUD

Major lithology: Section 1, 0–104 cm: diatomaceous mud, black (5Y 2.5/2). Slightly bioturbated. Section 1, 104 cm, to Section 2, 70 cm: diatomaceous nannofossil mud, dark olive gray to olive gray (5Y 3/2, 5Y 4/2). Moderately bioturbated. CC: diatomaceous clay-rich mud, dark olive gray (5Y 3/2).

SMEAR SLIDE SUMMARY (%):

	1, 37 D	2, 4 D	CC, 10 D
TEXTURE:			
Sand	5	—	—
Silt	20	45	20
Clay	75	55	80
COMPOSITION:			
Quartz	5	—	3
Feldspar	15	—	10
Rock fragments	5	—	2
Mica	Tr	—	Tr
Clay	40	30	50
Volcanic glass	5	—	3
Dolomite	—	Tr	3
Accessory minerals			
Opaques	—	5	—
Pyrite	2	—	Tr
Glauconite	Tr	—	Tr
Foraminifers	Tr	—	1
Nannofossils	Tr	25	Tr
Diatoms	25	25	25
Radiolarians	—	—	Tr
Sponge spicules	3	15	3
Silicoflagellates	—	Tr	—

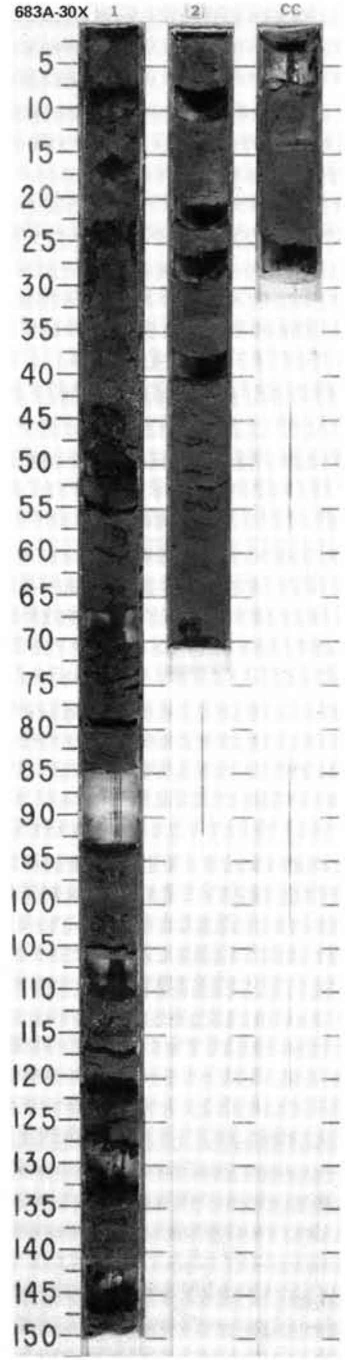

SITE 683 HOLE A CORE 31X CORED INTERVAL 3349.5-3359.0 mbsl; 277.7-287.2 mbsf

TIME-ROCK UNIT	FORAMINIFERS	NANNOFOSSILS	RADIOLARIANS	DIATOMS	PALEOMAGNETICS	PHYS. PROPERTIES	CHEMISTRY	SECTION	METERS	GRAPHIC LITHOLOGY	DRILLING DISTURB.	SED. STRUCTURES	SAMPLES	LITHOLOGIC DESCRIPTION
MIDDLE MIOCENE		insignificant *	*D. alata* Zone *	*Craspedodiscus coscinodiscus* Zone *				1, 2, CC	0.5, 1.0		X		*	see below

DIATOMACEOUS SPICULE-BEARING MUD

Major lithology: diatomaceous spicule-bearing mud, dark olive gray (5Y 3/2). Slightly to moderately bioturbated, with scattered foraminifers throughout. Section 1, 0 cm, to CC.

SMEAR SLIDE SUMMARY (%):

	1, 81
	D
TEXTURE:	
Silt	60
Clay	40
COMPOSITION:	
Quartz	5
Feldspar	5
Clay	37
Calcite/dolomite	1
Accessory minerals	
Pyrite framboids	2
Nannofossils	Tr
Diatoms	25
Sponge spicules	25
Silicoflagellates	Tr
Fish remains	Tr

SITE 683 HOLE A CORE 32X CORED INTERVAL 3359.0-3368.5 mbsl; 287.2-296.7 mbsf

TIME-ROCK UNIT	FORAMINIFERS	NANNOFOSSILS	RADIOLARIANS	DIATOMS	PALEOMAGNETICS	PHYS. PROPERTIES	CHEMISTRY	SECTION	METERS	GRAPHIC LITHOLOGY	DRILLING DISTURB.	SED. STRUCTURES	SAMPLES	LITHOLOGIC DESCRIPTION
MIDDLE MIOCENE		insignificant *	*D. alata* Zone *	undifferentiated *				1, CC	0.5, 1.0		O, X		*	see below

DIATOMACEOUS SPICULAR NANNOFOSSIL-BEARING MUD

Major lithology: diatomaceous spicular nannofossil-bearing mud, black, dark olive gray, and olive (5Y 2.5/2, 5Y 3/2, 5Y 4/3). Moderately bioturbated in CC. Section 1, 0 cm, to CC.

SMEAR SLIDE SUMMARY (%):

	1, 74
	D
TEXTURE:	
Silt	40
Clay	60
COMPOSITION:	
Clay	55
Foraminifers	Tr
Nannofossils	5
Diatoms	20
Radiolarians	Tr
Sponge spicules	20

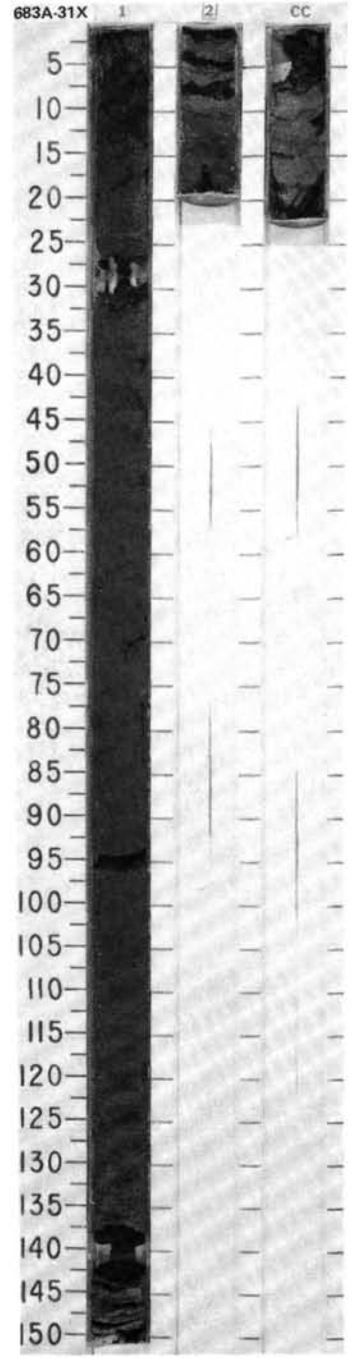

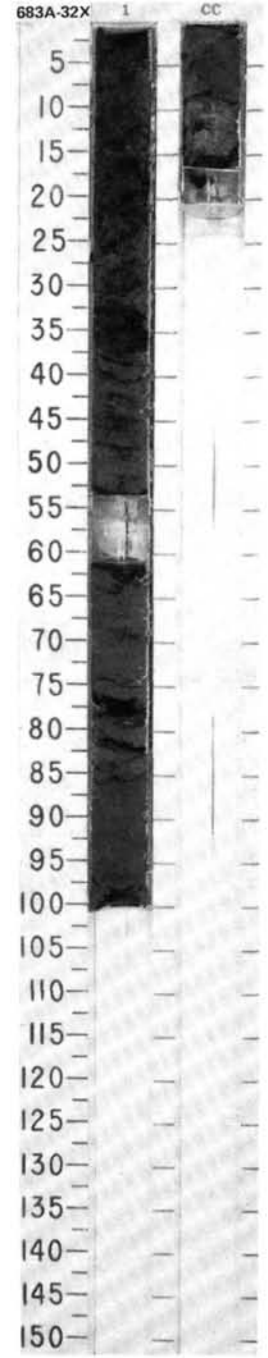

SITE 683 HOLE A CORE 33X CORED INTERVAL 3368.5-3378.0 mbsl; 296.7-306.2 mbsf

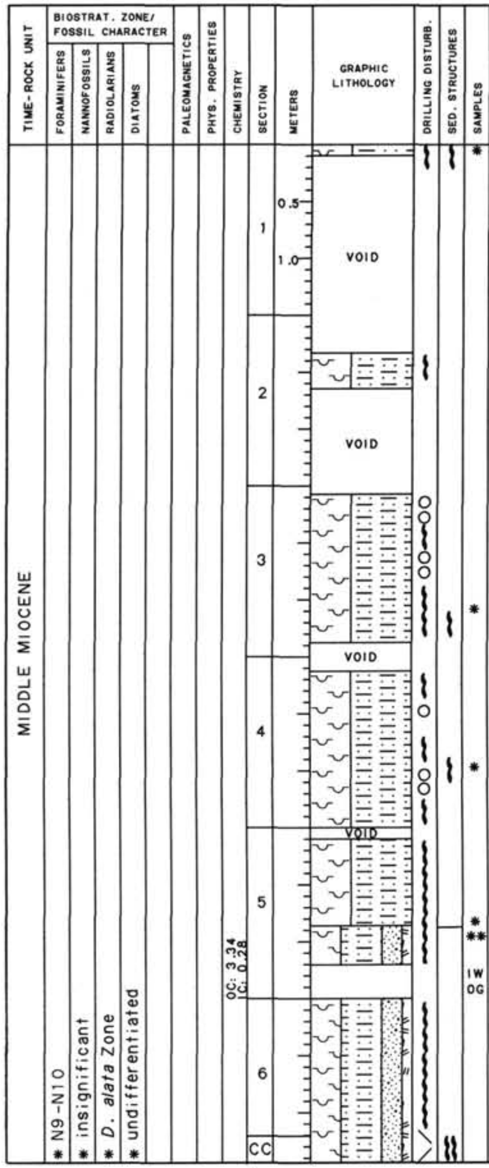

LITHOLOGIC DESCRIPTION

DIATOMACEOUS MUD, grading downward into DIATOM-BEARING ASH-RICH SILTY MUD

Major lithology: Section 1, 0 cm, to Section 5, 85 cm: diatomaceous mud, dark olive gray (5Y 3/2); locally bioturbated. Section 5, 85 cm, to CC: diatom-bearing, ash-rich silty mud, olive gray (5Y 5/2), interbedded with diatomaceous mud, dark olive gray (5Y 3/2); bioturbated.

Minor lithology: ash-bearing diatomaceous mud, olive gray (5Y 5.2). Thin interbed, Section 6, 43 cm.

SMEAR SLIDE SUMMARY (%):

	1, 4 D	3, 106 D	4, 93 D	5, 80 D	5, 85 M	5, 85 D
TEXTURE:						
Sand	—	—	—	—	—	10
Silt	40	30	40	30	60	50
Clay	60	70	60	70	40	40
COMPOSITION:						
Quartz	5	—	1	—	—	—
Feldspar	—	—	1	—	3	5
Rock fragments	—	—	—	—	—	2
Clay	55	56	52	40	30	30
Volcanic glass	Tr	Tr	—	—	—	—
Dolomite	Tr	—	Tr	Tr	Tr	—
Accessory minerals						
Pyrite	—	2	5	5	2	3
Zircon	—	—	Tr	—	—	—
Foraminifers	—	—	—	—	—	10
Nannofossils	Tr	2	1	20	—	20
Diatoms	40	40	40	35	65	30
Radiolarians	Tr	Tr	Tr	Tr	—	—

	5, 96 M	6, 43 M
TEXTURE:		
Sand	10	5
Silt	70	50
Clay	20	45
COMPOSITION:		
Quartz	20	5
Feldspar	40	5
Clay	—	40
Volcanic glass	38	20
Dolomite	—	Tr
Accessory minerals		
Pyrite	2	Tr
Nannofossil	Tr	—
Diatoms	Tr	30

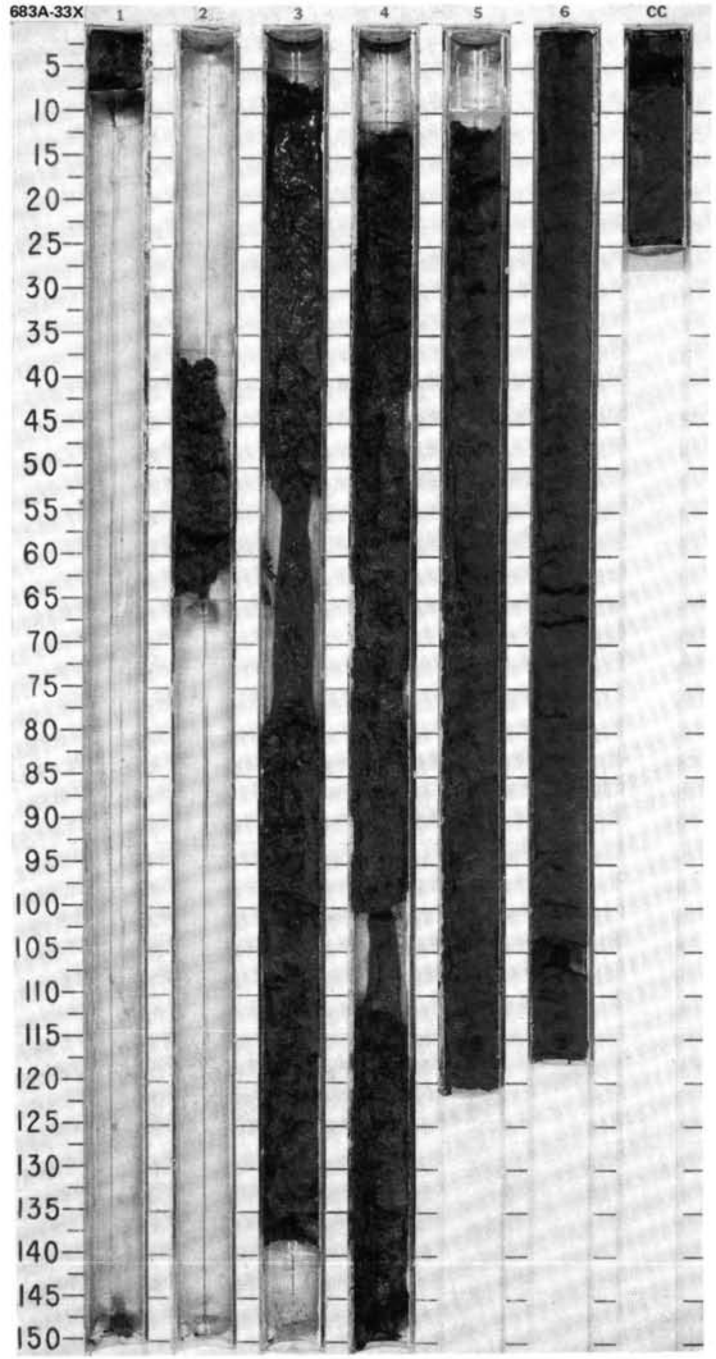

SITE 683 HOLE A CORE 34X CORED INTERVAL 3378.0-3387.5 mbsl; 306.2-315.7 mbsf

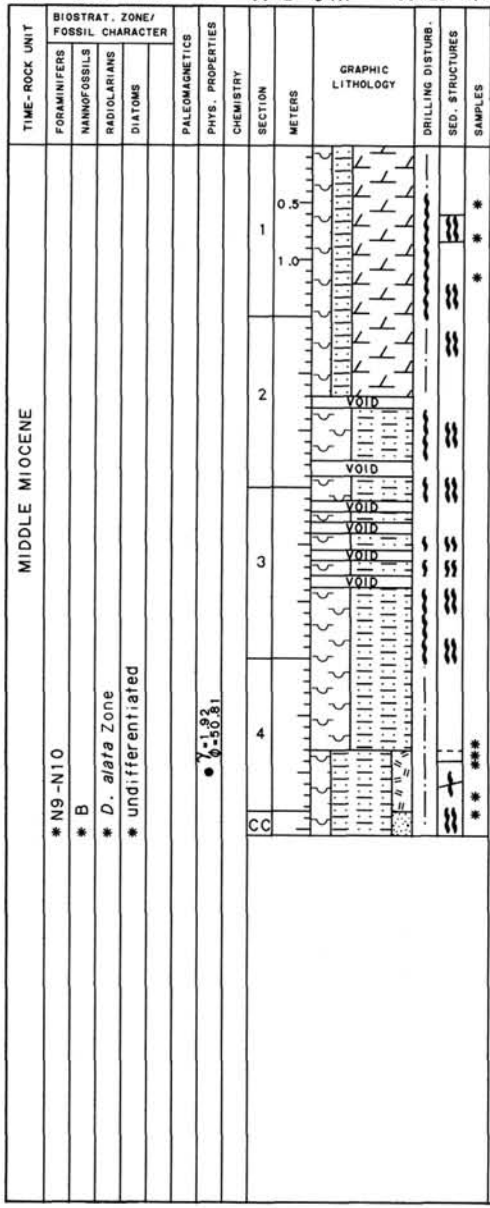

LITHOLOGIC DESCRIPTION

DOLOMITIC MUD interbedded with minor DIATOMACEOUS MUD, DIATOMACEOUS MUD grading rapidly down into ASH AND DIATOM-BEARING ASHY MUD, and DIATOMACEOUS SANDY MUD

Major lithology: Section 1, 0 cm, to Section 2, 70 cm: dolomitic mud, olive (5Y 5/3), interbedded with minor diatomaceous mud, dark olive gray to olive gray (5Y 5/2, 5Y 4/2); moderate bioturbation. Section 2, 70 cm, to Section 4, 82 cm: diatomaceous mud, dark olive gray to olive gray (5Y 3/2, 5Y 4/2): moderate bioturbation, severely disturbed by drilling. Section 4, 82–145 cm: ash and diatom-bearing ashy mud, dark gray to dark olive gray (5Y 4/1, 5Y 3/2); minor bioturbation, rare irregular subparallel laminations. CC: diatomaceous sandy mud, dark olive gray (5Y 3/2); moderate bioturbation.

Minor lithologies:
Section 1, 0 cm, to Section 2, 70 cm: dolomite, olive (5Y 5/3). Thin hard interbed, Section 1, 76–81 cm; hard base of dolomitic mud layer, Section 1, 0–60 cm.
Section 4, 82–145 cm:
1. volcanic ash or ash-bearing sand, light olive gray (5Y 6/2). Thin sharp-based interbed at Section 4, 85–90 cm.
2. sandy diatomaceous mud, very dark gray (5Y 3/1); moderate bioturbation. Section 4, 87 cm.

SMEAR SLIDE SUMMARY (%):

	1, 50 D	1, 82 M	1, 116 D	3, 49 D	4, 79 D	4, 87 M
TEXTURE:						
Sand	5	—	—	—	3	60
Silt	70	70	50	30	37	30
Clay	25	30	50	70	60	10
COMPOSITION:						
Quartz	—	Tr	—	3	—	—
Feldspar	5	—	3	5	Tr	35
Rock fragments	—	—	—	—	—	5
Clay	20	20	40	62	55	10
Volcanic glass	—	—	—	Tr	Tr	45
Dolomite rhombs.	55	70	10	—	—	Tr
Accessory minerals						
Pyrite	5	—	2	Tr	5	—
Diatoms	15	10	45	30	40	5
Radiolarians	—	—	—	Tr	—	—
Sponge spicules	Tr	Tr	—	—	—	—

	4, 120 M	CC, 1 D
TEXTURE:		
Sand	—	25
Silt	40	25
Clay	60	50
COMPOSITION:		
Quartz	10	—
Feldspar	10	15
Rock fragments	—	5
Clay	53	45
Volcanic glass	10	2
Dolomite rhombs.	—	Tr
Accessory minerals		
Pyrite	2	3
Glauconite	—	Tr
Zeolites	—	Tr
Diatoms	15	25
Sponge spicules	—	5
Silicoflagellates	—	Tr

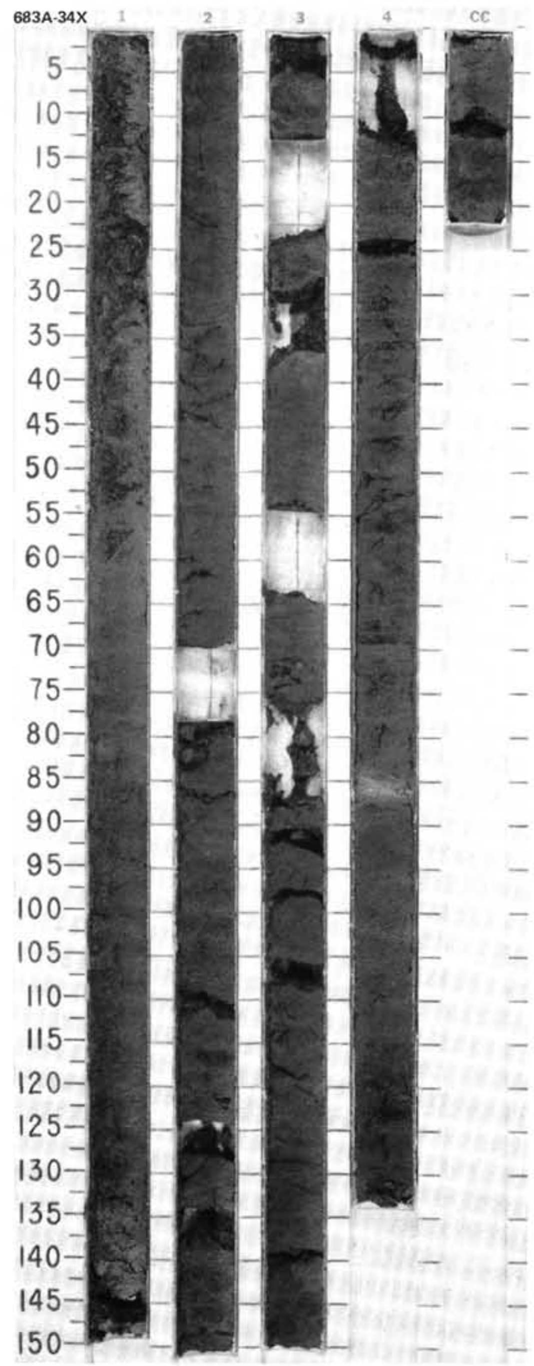

SITE 683 HOLE A CORE 35X CORED INTERVAL 3387.5-3397.0 mbsl; 315.7-325.2 mbsf

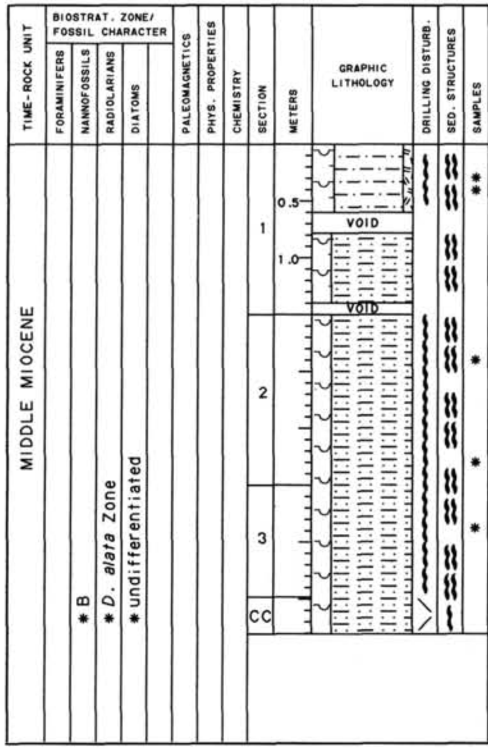

LITHOLOGIC DESCRIPTION

DIATOMACEOUS MUD, grading downward into DIATOMACEOUS AND DIATOM-BEARING PYRITE-RICH MUDSTONE

Major lithology: Section 1, 0–60 cm: diatomaceous mud, greenish gray to dark olive gray (10Y 4/2, 5Y 3/2), interbedded with volcanic ash and ash-bearing mud, gray (5Y 5/2); moderately bioturbated. Section 1, 60 cm, to CC: diatomaceous and diatom-bearing pyrite-rich mudstone, dark olive gray to black (5Y 3/2, 5Y 2.5/2); moderately to slightly bioturbated.

SMEAR SLIDE SUMMARY (%):

	1, 23 M	1, 37 D	2, 40 D	2, 137 M	3, 44 D
TEXTURE:					
Sand	80	5	—	—	—
Silt	20	30	40	30	30
Clay	—	65	60	70	70
COMPOSITION:					
Quartz	—	—	—	Tr	Tr
Feldspar	15	7	5	—	—
Rock fragments	10	—	Tr	—	—
Clay	—	65	60	65	70
Volcanic glass	75	—	—	5	5
Dolomite	—	—	—	Tr	—
Accessory minerals					
Pyrite	—	3	5	10	10
Diatoms	—	25	25	20	15
Radiolarians	—	—	—	Tr	—
Sponge spicules	—	—	—	Tr	—
Fish remains	—	—	5	—	—

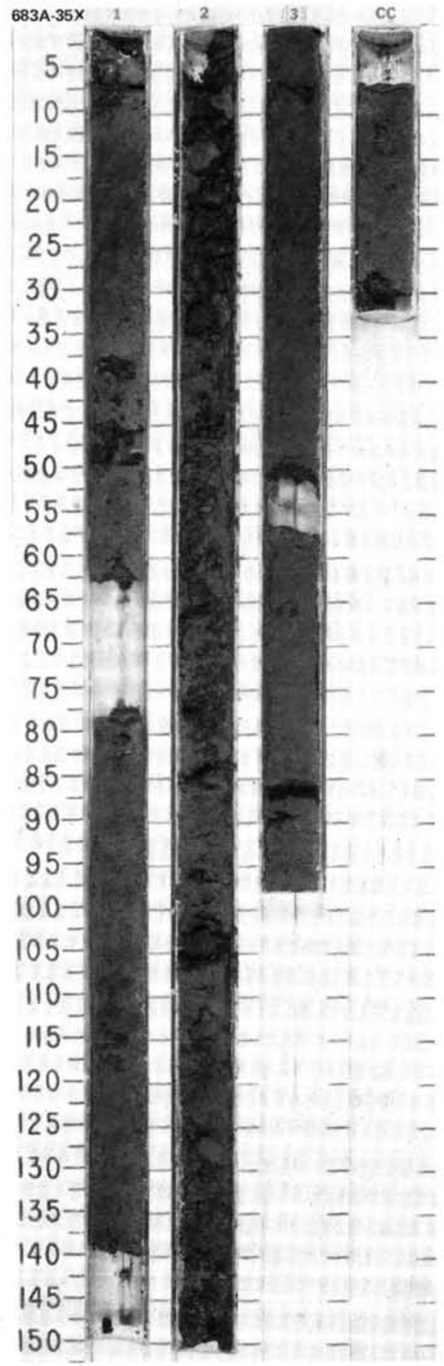

SITE 683 HOLE A CORE 36X CORED INTERVAL 3397.0-3406.5 mbsl; 325.2-334.7 mbsf

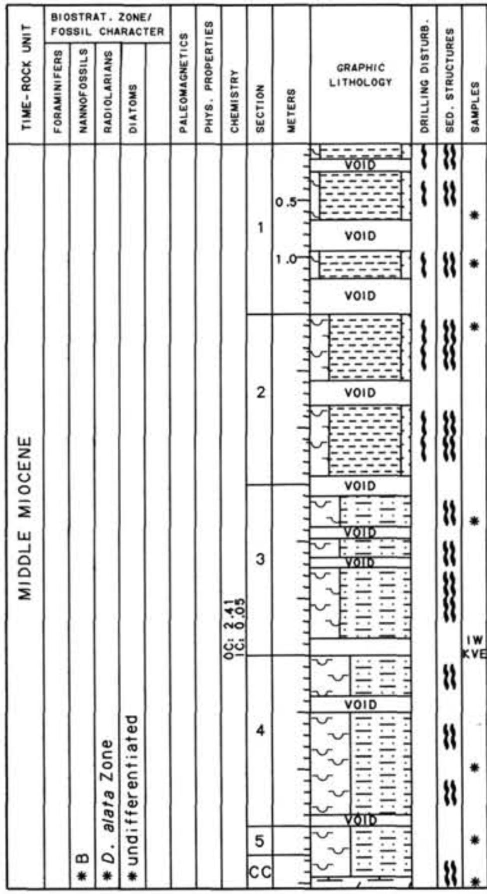

LITHOLOGIC DESCRIPTION

DIATOM-BEARING to DIATOMACEOUS MUD

Major lithology: diatom-bearing to diatomaceous mud, dark olive gray and olive gray to dark gray (5Y 3/2, 5Y 5/2, 5Y 4/1). Moderately bioturbated, pyrite-rich. Section 1, 0 cm, to CC.

Minor lithologies:
1. pyritiferous diatom-bearing mud, dark gray (5Y 4/2); Section 1, 115 cm.
2. ashy diatomaceous mud, olive gray (5Y 4/2); Section 4, 95–100 cm.
3. dolomicrite, light olive gray (5Y 6/2); CC, 30 cm.

SMEAR SLIDE SUMMARY (%):

	1, 64 M	1, 114 D	2, 15 D	3, 38 M	4, 98 M	5, 12 D	CC, 29 M
TEXTURE:							
Sand	—	—	—	5	—	—	—
Silt	25	20	25	45	25	40	—
Clay	75	80	75	50	75	60	100
COMPOSITION:							
Quartz	5	5	—	—	Tr	—	—
Feldspar	5	—	Tr	10	Tr	5	Tr
Rock fragments	—	—	—	5	—	5	—
Clay	60	80	70	40	45	55	15
Volcanic glass	Tr	Tr	Tr	—	10	—	—
Dolomite	Tr	—	Tr	Tr	Tr	—	85
Accessory minerals							
Pyrite	20	5	10	5	5	5	Tr
Glauconite	—	—	—	—	—	Tr	—
Nannofossils	—	—	—	—	—	—	Tr
Diatoms	10	10	20	40	40	30	—
Radiolarians	—	Tr	—	—	—	—	—
Sponge spicules	—	Tr	—	—	—	Tr	—
Silicoflagellates	—	—	—	—	—	Tr	—

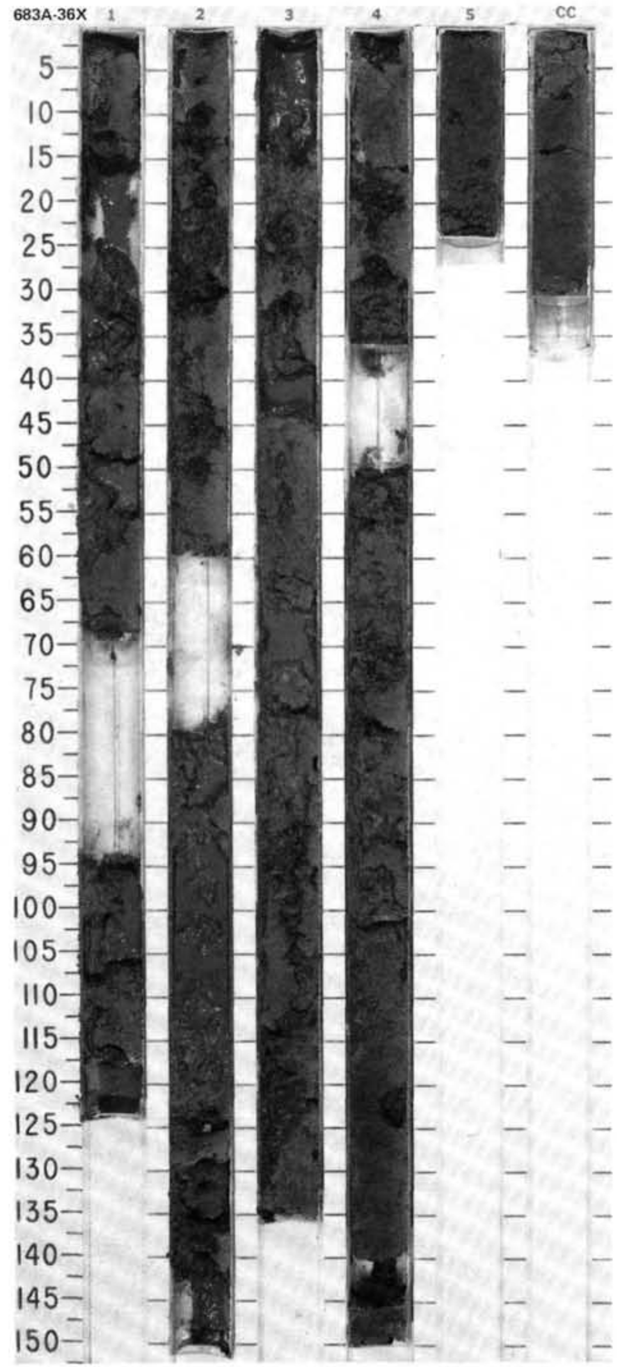

SITE 683 HOLE A CORE 37X CORED INTERVAL 3406.5-3416.0 mbsl; 334.7-344.2 mbsf

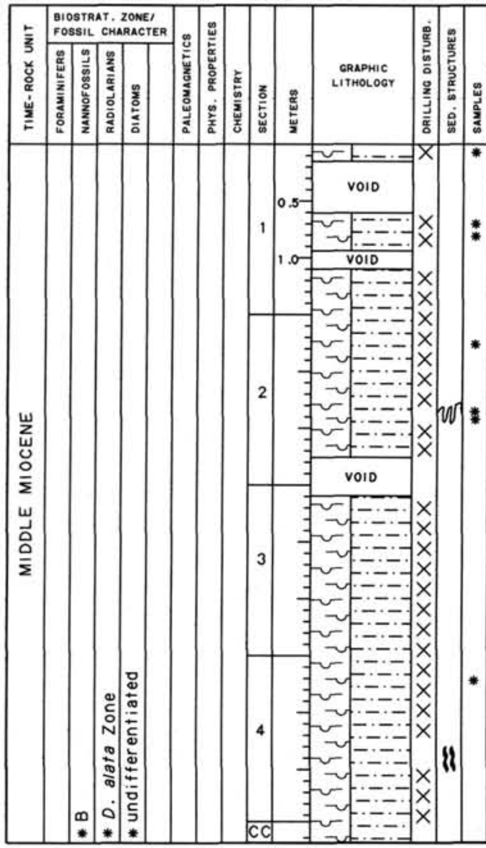

LITHOLOGIC DESCRIPTION

DIATOMACEOUS OOZE and DIATOMACEOUS MUD to MUDSTONE

Major lithology: diatomaceous ooze and diatomaceous mud to mudstone, dark olive gray to dark greenish gray (5Y 3/2, 10Y 3.5/2, 10Y 3/1). Highly disrupted by drilling, some fissility. Rare soft sediment deformation and microfaults; rare bioturbation (including *Chondrites*). Pyritiferous. Section 1, 0 cm, to CC.

Minor lithologies:
1. muddy nannofossil-bearing diatom ooze, greenish gray (10Y 3.5/2), Section 1, 10 cm.
2. volcanic ash (vitric tuff) clast in feldspathic ashy volcanic sand, white to dusky green (10Y 8/1, 10Y 5/2), Section 2, 90–95 cm.

SMEAR SLIDE SUMMARY (%):

	1, 10 D	1, 71 D	1, 75 M	2, 32 D	2, 87 M	2, 90 M	4, 30 D
TEXTURE:							
Sand	3	10	5	15	70	60	—
Silt	57	30	35	35	30	30	50
Clay	40	60	60	50	—	10	50
COMPOSITION:							
Feldspar	5	5	10	10	40	30	5
Rock fragments	Tr	Tr	Tr	5	—	Tr	Tr
Clay	35	50	50	40	—	10	45
Volcanic glass	—	—	—	—	60	50	—
Calcite/dolomite	—	Tr	Tr	—	—	—	—
Accessory minerals							
Pyrite	5	5	5	10	Tr	Tr	5
Glauconite	—	—	Tr	Tr	—	—	Tr
Zeolites	—	—	Tr	—	—	—	—
Foraminifers	Tr	—	—	—	—	—	—
Nannofossils	5	—	—	—	—	—	—
Diatoms	50	40	35	35	Tr	10	45
Radiolarians	—	—	Tr	—	—	—	—
Sponge spicules	—	Tr	Tr	Tr	—	—	—
Fish remains	—	—	Tr	—	—	—	—

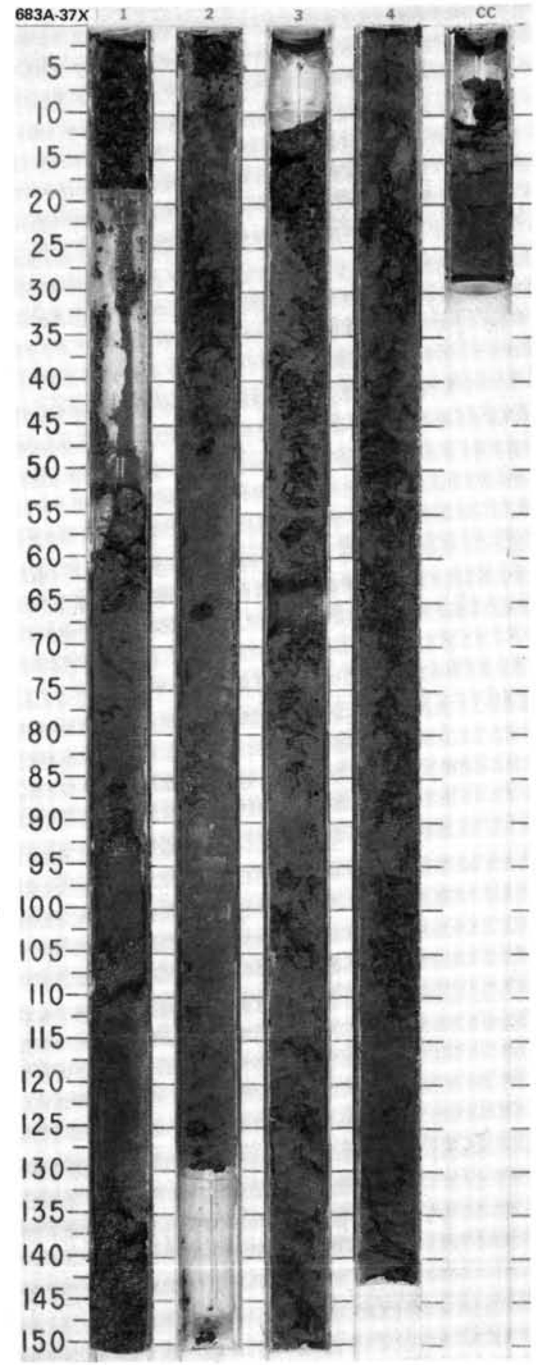

SITE 683 HOLE A CORE 38X CORED INTERVAL 3416.0-3425.5 mbsl; 344.2-353.7 mbsf

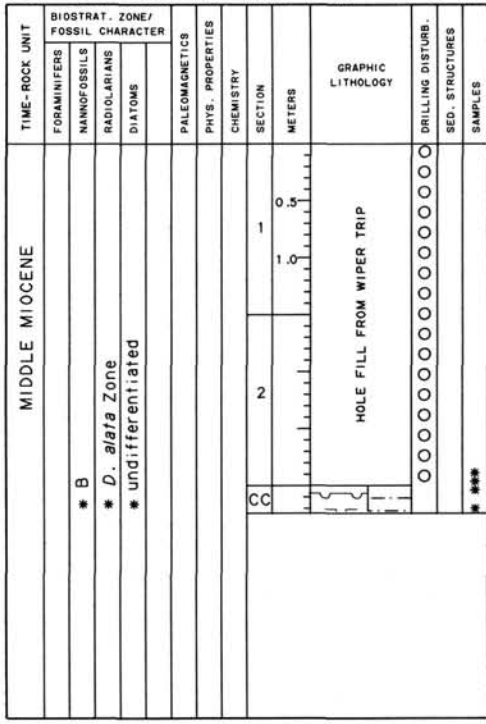

LITHOLOGIC DESCRIPTION

MUDDY DIATOMITE and PYRITIFEROUS FELDSPATHIC SAND

Major lithology: CC, 0–22 cm: muddy diatomite, olive (5Y 4/3), and pyritiferous feldspathic sand, dark gray (N 4/). Bent and necked clasts in drilling biscuit.

Section 1, 0 cm, to Section 2, 150 cm: recycled debris from top of hole.

SMEAR SLIDE SUMMARY (%):

	CC, 4 D	CC, 10 M	CC, 12 M	CC, 16 D
TEXTURE:				
Sand	—	50	—	—
Silt	50	40	60	—
Clay	50	10	40	—
COMPOSITION:				
Feldspar	5	65	Tr	5
Rock fragments	Tr	15	—	Tr
Mica	—	Tr	—	—
Clay	40	5	35	35
Calcite/dolomite	2	—	Tr	2
Accessory minerals				
Pyrite	3	15	5	3
Nannofossils	—	—	Tr	—
Diatoms	50	Tr	60	55
Radiolarians	Tr	—	—	—

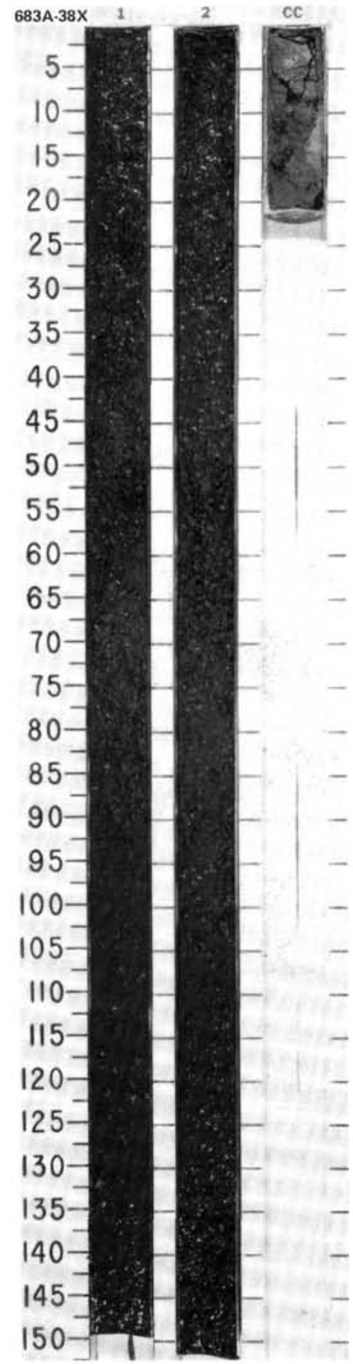

SITE 683 HOLE A CORE 39X CORED INTERVAL 3425.5-3435.0 mbsl; 353.7-363.2 mbsf

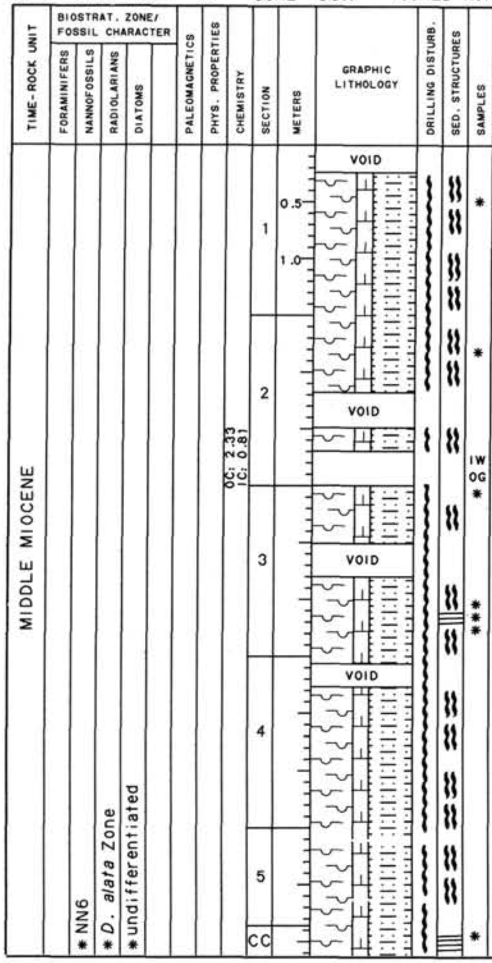

LITHOLOGIC DESCRIPTION

NANNOFOSSIL-BEARING DIATOMACEOUS MUD AND MUDSTONE, interbedded with DIATOMACEOUS OOZE AND DIATOMITE

Major lithology: Section 1, 0 cm, to CC: nannofossil-bearing diatomaceous mud and mudstone, olive gray (5Y 4/2), moderate bioturbation, pyrite-bearing; interbedded with diatomaceous ooze and diatomite, greenish gray to olive gray (10Y 6/2, 5Y 4/2), thin laminae and lenses.

SMEAR SLIDE SUMMARY (%):

	1, 61 D	2, 40 M	3, 8 D	3, 118 M	3, 119 M	3, 121 M	CC, 6 M
TEXTURE:							
Sand	—	20	—	—	5	—	—
Silt	60	40	40	40	50	45	60
Clay	40	40	60	60	45	55	40
COMPOSITION:							
Quartz	—	—	Tr	—	—	—	Tr
Feldspar	3	10	Tr	—	10	5	—
Rock fragments	—	5	—	5	5	Tr	—
Clay	30	25	50	35	35	45	45
Volcanic glass	—	—	Tr	—	—	—	Tr
Calcite/dolomite	2	10	Tr	Tr	5	3	Tr
Accessory minerals							
Pyrite	Tr	10	5	5	5	5	5
Zeolites	—	—	—	Tr	—	—	—
Foraminifers	Tr	Tr	—	—	—	—	—
Nannofossils	15	10	5	5	5	2	—
Diatoms	50	25	40	50	35	40	50
Radiolarians	Tr	Tr	—	Tr	Tr	Tr	Tr
Sponge spicules	—	5	—	—	—	—	—
Silicoflagellates	—	Tr	—	Tr	—	—	—

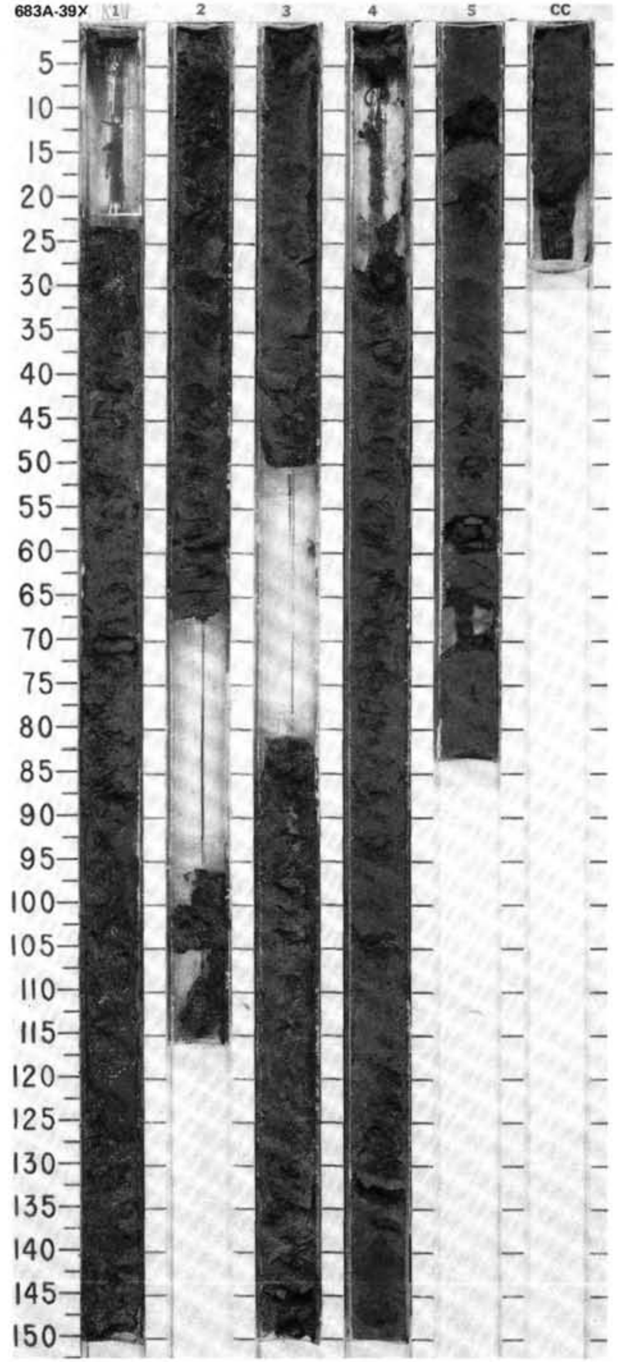

SITE 683 HOLE A CORE 40X CORED INTERVAL 3435.0-3444.5 mbsl; 363.2-372.7 mbsf

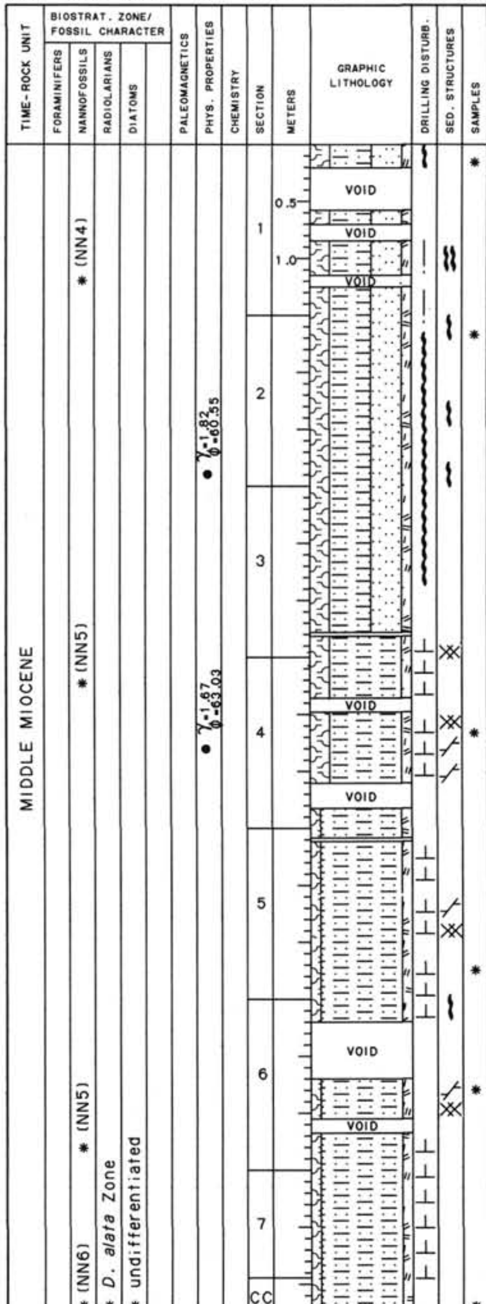

LITHOLOGIC DESCRIPTION

VOLCANIC ASH-BEARING SILICEOUS MUDSTONE, interbedded with DIATOMACEOUS SILTSTONE and MUDSTONE

Major lithology: volcanic ash-bearing siliceous mudstone interbedded with diatomaceous siltstone and mudstone, dark gray to dark greenish gray (5Y 3/1, 5GY 3/1). Fissile, highly shattered by drilling. Sparsely burrowed, with extensional microfaults. Section 1, 0 cm, to CC.

Minor lithology: glassy crystal-lithic tuff, gray (2.5Y 6/0), at CC, 28–31 cm.

SMEAR SLIDE SUMMARY (%):

	1, 17 D	2, 23 D	1, 23 D	4, 69 D	5, 128 D	6, 76 D	CC, 30 M
TEXTURE:							
Sand	—	—	—	—	—	—	60
Silt	20	70	70	30	50	25	35
Clay	80	30	30	70	50	75	5
COMPOSITION:							
Quartz	5	3	5	—	20	—	25
Feldspar	—	4	15	—	5	—	30
Rock fragments	—	3	5	Tr	—	—	20
Mica	—	—	—	—	—	—	5
Clay	65	22	30	55	50	75	—
Volcanic glass	10	25	—	5	10	10	15
Calcite/dolomite	—	Tr	Tr	—	—	—	—
Accessory minerals	2	5	—	Tr	5	—	3
Pyrite	5	3	3	Tr	—	3	—
Opaques	—	—	—	—	—	—	2
Micrite	—	—	2	—	Tr	—	—
Nannofossils	—	Tr	—	—	—	2	—
Diatoms	3	15	25	25	5	3	Tr
Sponge spicules	10	20	15	15	5	7	—

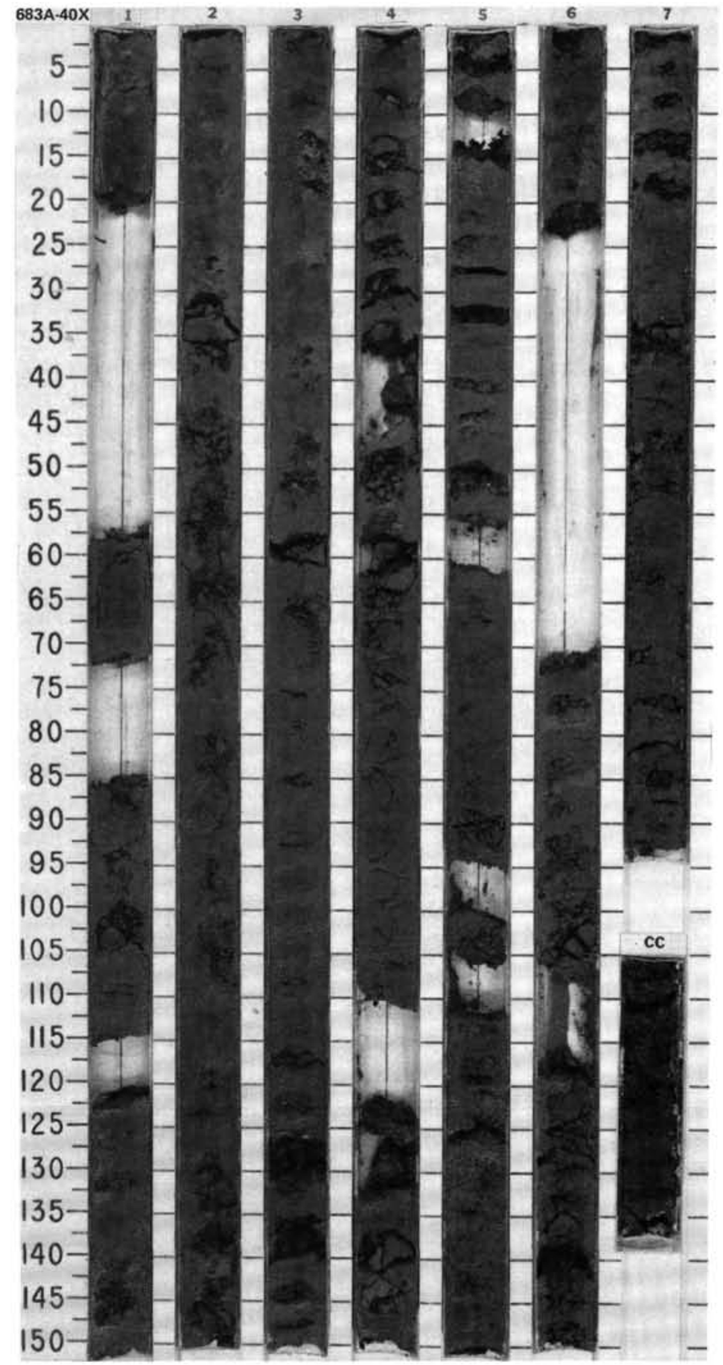

SITE 683 HOLE A CORE 41X CORED INTERVAL 3444.5-3454.0 mbsl; 372.7-381.2 mbsf

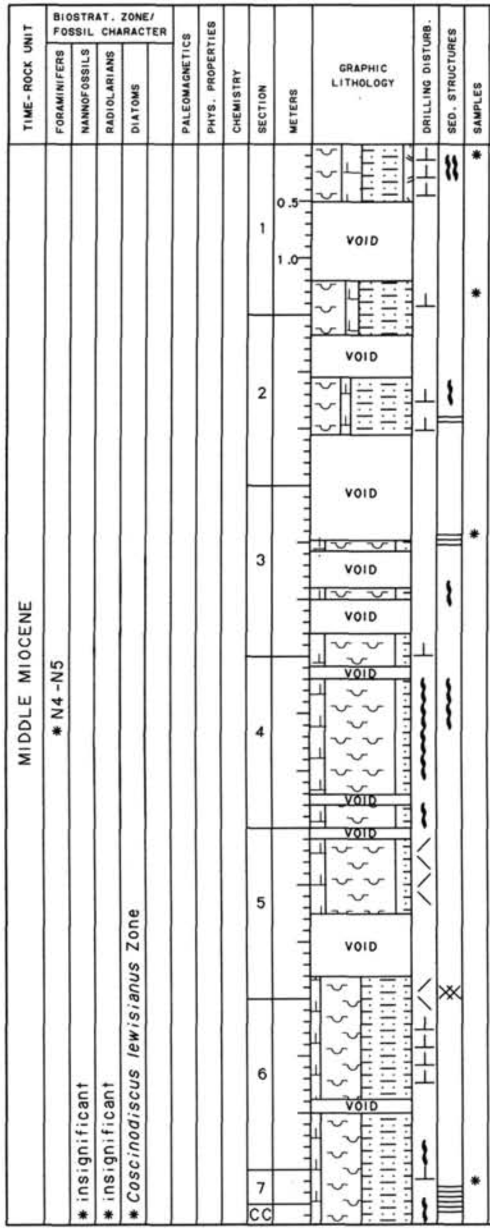

LITHOLOGIC DESCRIPTION

GLASS-BEARING DIATOM OOZE AND DIATOMACEOUS MUDSTONE, SPONGE SPICULE-BEARING DIATOM-NANNOFOSSIL MUDSTONE, DIATOM-BEARING MUDSTONE, and NANNOFOSSIL DIATOM OOZE

Major lithology: Section 1, 0–50 cm: glass-bearing diatom ooze and diatomaceous mudstone, dark gray to dark greenish gray (5GY 3/1, 5GY 4/1); minor bioturbation. *Section 1, 120 cm, to Section 2, 20 cm: sponge spicule-bearing diatom-nannofossil* mudstone, dark gray (5GY 3/1): minor bioturbation. Section 2, 55–105 cm: diatom-bearing mudstone, dark olive gray (5Y 3/2); minor bioturbation. Section 3, 47 cm, to CC: nannofossil diatom ooze, dark olive gray to olive gray (5Y 3/2, 5Y 4/2); faintly laminated and bioturbated.

SMEAR SLIDE SUMMARY (%):

	1, 5 D	1, 135 D	3, 52 D	7, 21 D
TEXTURE:				
Silt	85	30	87	40
Clay	15	70	13	60
COMPOSITION:				
Feldspar	5	—	—	—
Rock fragments	5	—	—	—
Mica	—	—	Tr	—
Clay	15	50	13	50
Volcanic glass	10	—	—	—
Calcite/dolomite	Tr	—	—	—
Accessory minerals	Tr	—	—	—
Pyrite	—	—	2	—
Micrite	—	5	—	—
Nannofossils	Tr	10	15	10
Diatoms	50	10	50	15
Sponge spicules	15	25	20	25

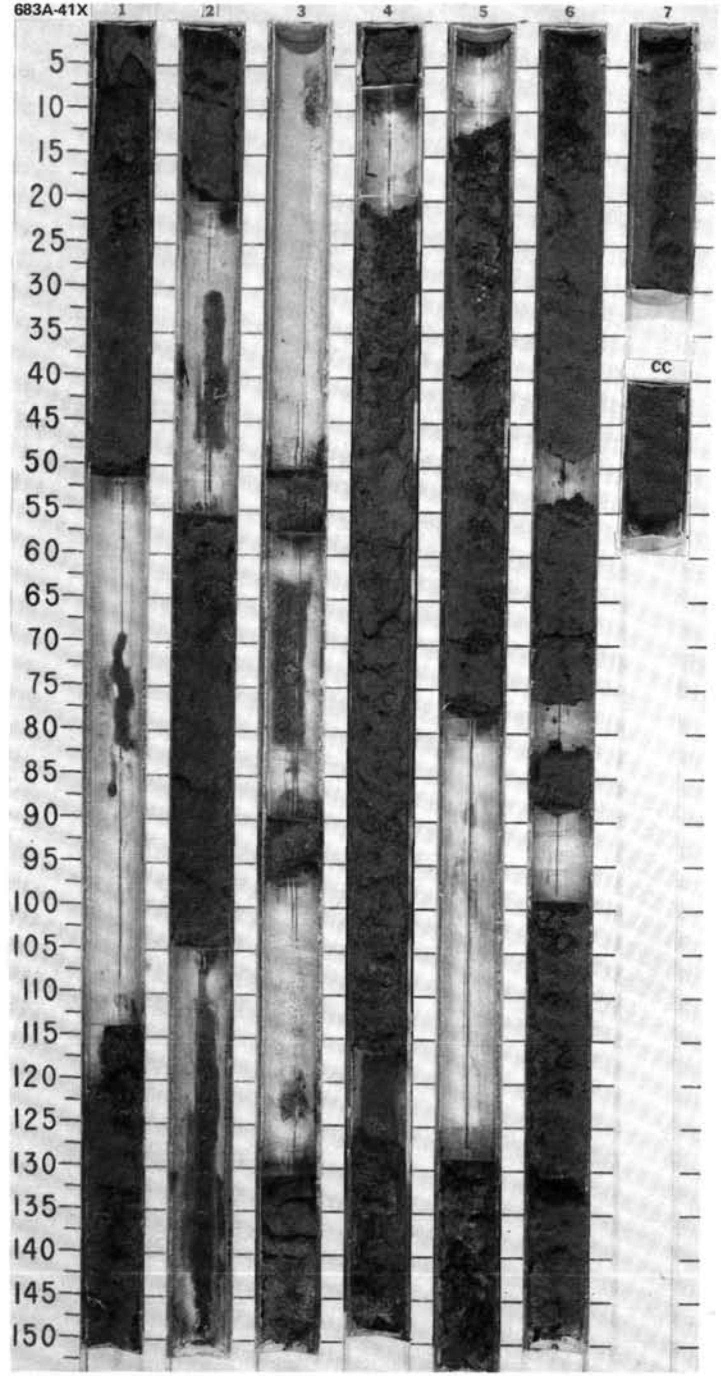

SITE 683 HOLE A CORE 42X CORED INTERVAL 3454.0-3463.5 mbsl; 381.2-390.7 mbsf

TIME-ROCK UNIT	FORAMINIFERS	NANNOFOSSILS	RADIOLARIANS	DIATOMS	PALEOMAGNETICS	PHYS. PROPERTIES	CHEMISTRY	SECTION	METERS	GRAPHIC LITHOLOGY	DRILLING DISTURB.	SED. STRUCTURES	SAMPLES
MIDDLE MIOCENE		insignificant *	insignificant *	*Cestodiscus peplum* Zone *				1	0.5				*
								CC					*

BIOSTRAT. ZONE/ FOSSIL CHARACTER

LITHOLOGIC DESCRIPTION

DIATOM- AND SPICULE-BEARING SILTY MUD and MUDSTONE

Major lithology: diatom- and spicule-bearing silty mud and mudstone, olive gray, olive, and dark olive gray (5Y 4/2, 5Y 4/3, 5Y 3/2). Highly fractured by drilling, locally laminated, compressional microfaults. Section 1, 0 cm, to CC.

Minor lithology: dolomite, hard loose pebble with internal laminations and fractures. Section 1, 3–4 cm.

SMEAR SLIDE SUMMARY (%):

	1, 25 D	CC, 8 D
TEXTURE:		
Sand	5	—
Silt	30	35
Clay	65	65
COMPOSITION:		
Quartz	5	—
Feldspar	10	Tr
Rock fragments	5	—
Mica	Tr	—
Clay	45	50
Volcanic glass	3	—
Calcite/dolomite	2	—
Accessory minerals		
Pyrite	3	4
Micrite	5	6
Nannofossils	—	5
Diatoms	20	5
Sponge spicules	2	30

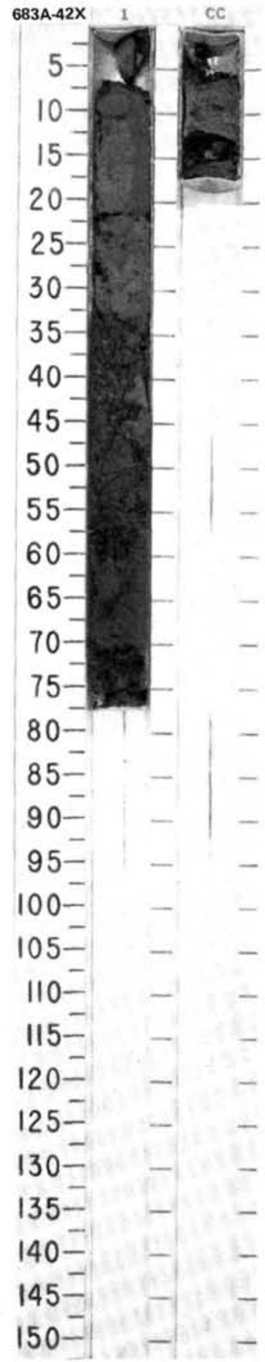

SITE 683 HOLE A CORE 43X CORED INTERVAL 3463.5-3473.0 mbsl; 390.7-400.2 mbsf

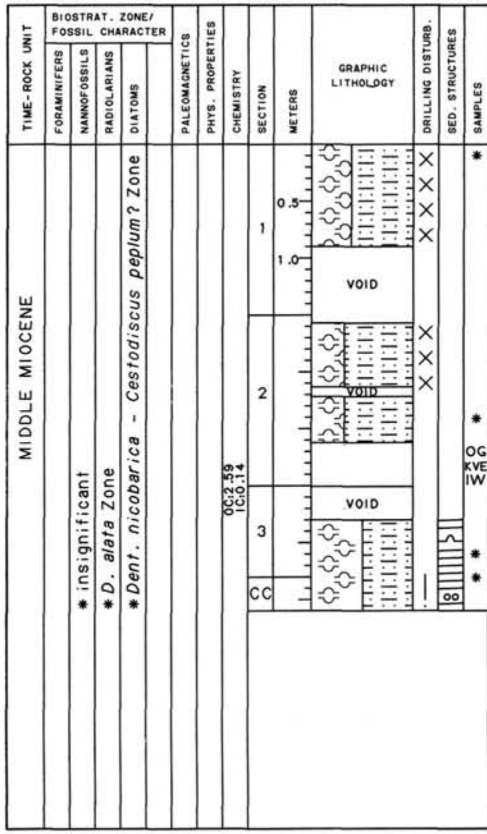

LITHOLOGIC DESCRIPTION

DIATOMACEOUS MUD AND MUDSTONE, and DIATOMACEOUS OOZE AND CHLORITIC DIATOMACEOUS MUD

Major lithology: Section 1, 0 cm, to Section 2, 107 cm: diatomaceous mud and mudstone, black (5Y 2.5/2); fissile, severely disturbed by drilling. Section 3, 30 cm, to CC: diatomaceous ooze and chloritic diatomaceous mud, olive gray (5Y 4/2); finely laminated, slump folds and microfaults.

SMEAR SLIDE SUMMARY (%):

	1, 14 D	2, 92 D	3, 58 M	3, 69 M
TEXTURE:				
Sand	—	—	10	—
Silt	45	45	20	85
Clay	55	55	70	15
COMPOSITION:				
Quartz	5	—	—	—
Feldspar	—	5	12	5
Rock fragments	—	—	—	2
Mica	Tr	—	5	—
Clay	55	55	30	10
Volcanic glass	—	Tr	3	3
Calcite/dolomite	Tr	Tr	—	—
Accessory minerals	—	5	—	2
Pyrite	—	—	2	3
Chlorite	—	—	10	—
Micrite	—	—	3	—
Foraminifers	—	—	2	—
Nannofossils	—	Tr	3	Tr
Diatoms	35	35	25	70
Radiolarians	Tr	Tr	—	—
Sponge spicules	5	Tr	10	5
Silicoflagellates	Tr	—	—	—

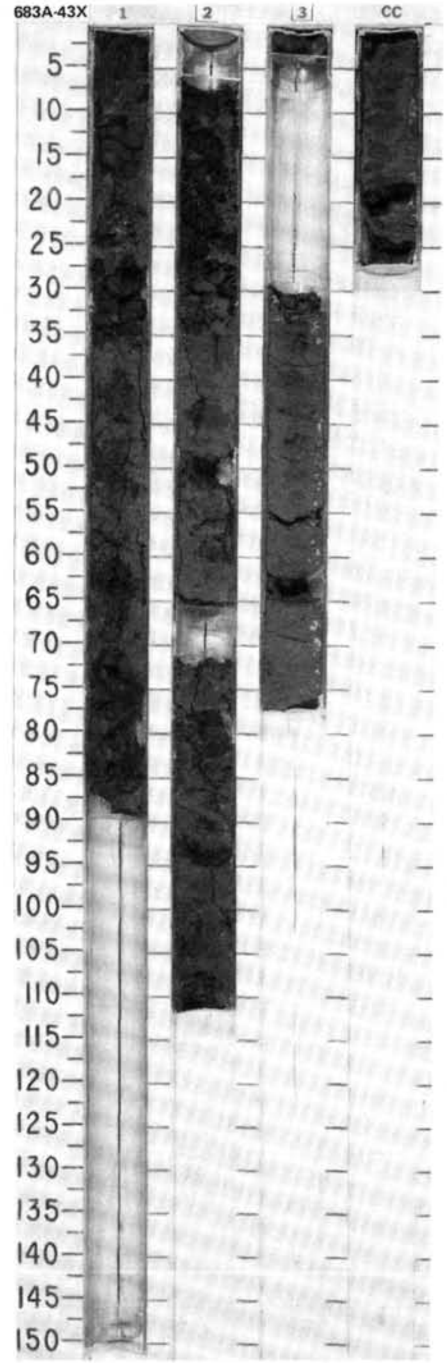

SITE 683 HOLE A CORE 44X CORED INTERVAL 3473.0-3482.5 mbsl; 400.2-409.7 mbsf

TIME-ROCK UNIT: MIDDLE MIOCENE

BIOSTRAT. ZONE/FOSSIL CHARACTER:
- FORAMINIFERS: * N4-N5
- NANNOFOSSILS: * B; * (NN5)
- RADIOLARIANS: * *D. alata* to *C. costata* Zone
- DIATOMS: * *Coscinodiscus lewisianus* Zone

PALEOMAGNETICS | PHYS. PROPERTIES | CHEMISTRY | SECTION | METERS | GRAPHIC LITHOLOGY | DRILLING DISTURB. | SED. STRUCTURES | SAMPLES

Sections: 1, 2, 3, 4, 5, 6, CC — Meters: 0.5, 1.0 — VOID, VOID, VOID, VOID, VOID, VOID

LITHOLOGIC DESCRIPTION

DIATOMACEOUS AND SILICEOUS SILTSTONE and MUDSTONE

Major lithology: diatomaceous and siliceous siltstone and mudstone, dark olive gray to olive (5Y 3/2, 5Y 3.3). Locally nannofossil-rich; finely laminated; highly fractured by drilling. Both extensional and compressional faults. Local minor bioturbation, some fissility. Section 1, 0 cm, to CC.

Minor lithology: volcanic ash, light gray (2.5Y 7/0). Section 6, 16–18 cm.

SMEAR SLIDE SUMMARY (%):

	1, 7 D	2, 23 D	3, 86 D	4, 84 M	4, 147 M	5, 14 D
TEXTURE:						
Sand	—	—	5	—	5	—
Silt	55	35	30	70	45	80
Clay	45	65	65	30	50	20
COMPOSITION:						
Quartz	—	—	—	—	2	2
Rock fragments	—	—	—	—	2	—
Clay	42	40	40	25	50	16
Volcanic glass	—	—	—	—	1	2
Calcite/dolomite	—	—	—	2	—	—
Accessory minerals	—	—	—	—	—	3
Pyrite	2	2	Tr	—	—	2
Opaques	—	—	—	3	—	—
Micrite	1	3	3	—	Tr	—
Nannofossils	3	25	25	—	—	—
Diatoms	52	17	29	65	40	70
Sponge spicules	—	13	3	5	5	5

	5, 16 M	5, 18 M
TEXTURE:		
Silt	70	—
Clay	30	—
COMPOSITION:		
Quartz	—	3
Mica	—	2
Clay	28	—
Volcanic glass	5	90
Accessory minerals	—	5
Pyrite	2	—
Diatoms	60	Tr
Sponge spicules	5	—

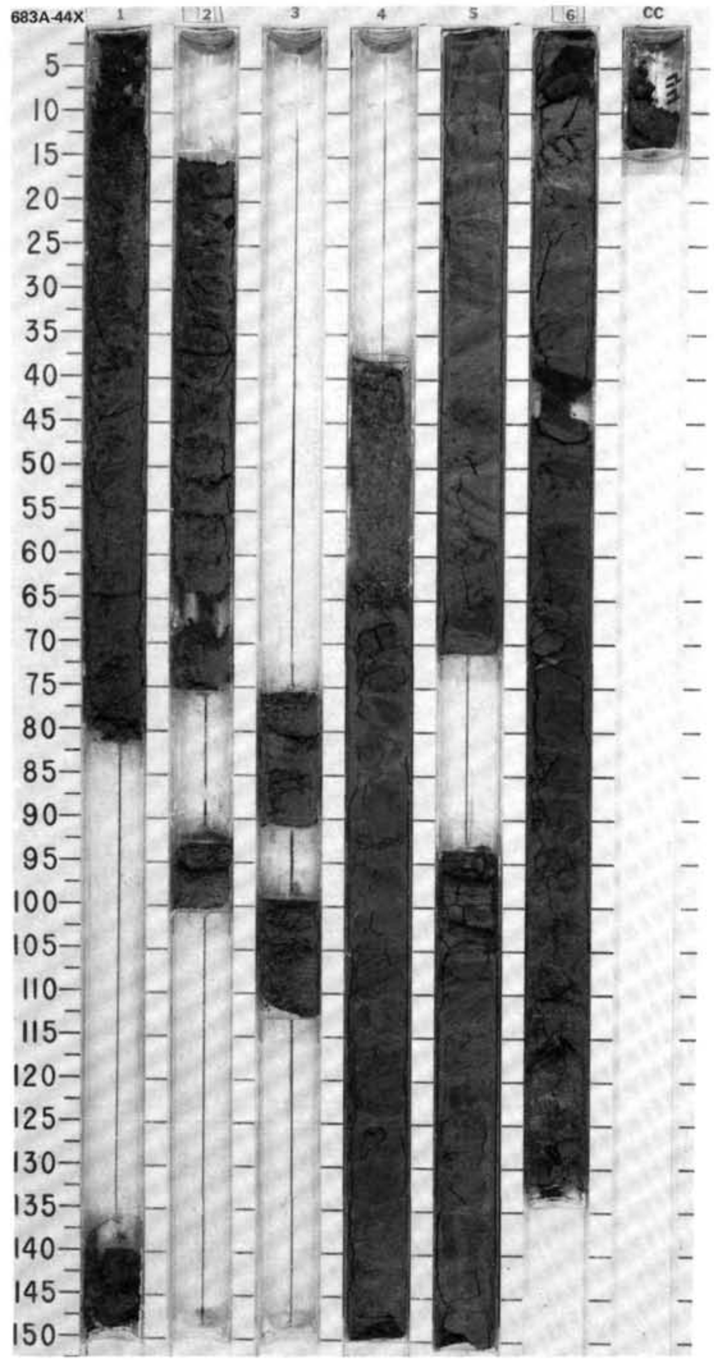

SITE 683 HOLE A CORE 45X CORED INTERVAL 3482.5-3492.0 mbsl; 409.7-419.2 mbsf

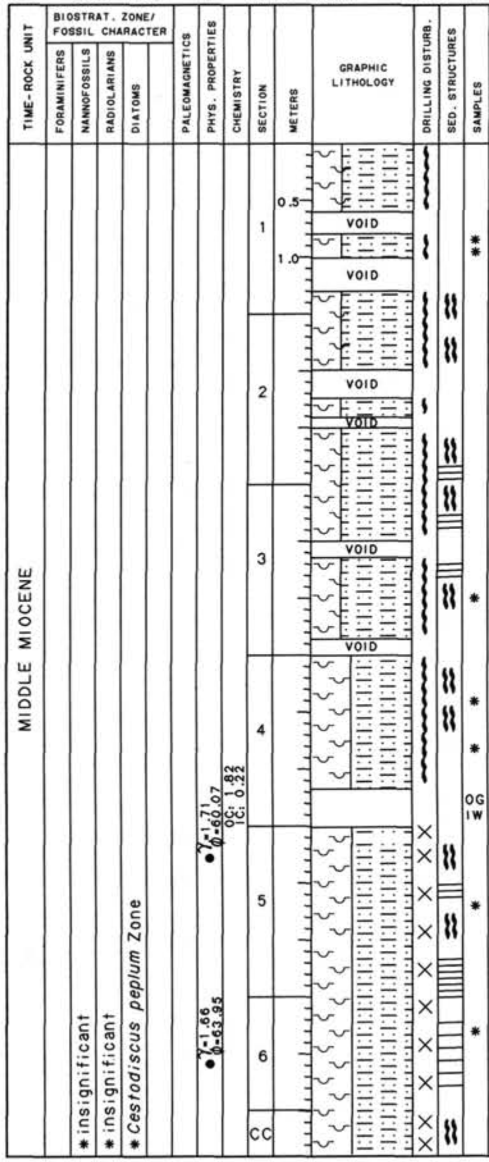

LITHOLOGIC DESCRIPTION

DIATOM-BEARING TO DIATOMACEOUS MUDSTONE

Major lithology: diatom-bearing to diatomaceous mudstone, dark olive gray to greenish gray (5Y 3/2, 5Y 4/2). Well-developed fissility, locally finely laminated. Section 1, 0 cm, to CC.

Minor lithology: pyritiferous diatom ooze, greenish gray (5GY 5/1). Section 6, 30–35 cm.

SMEAR SLIDE SUMMARY (%):

	1, 86 D	1, 100 D	3, 103 D	4, 45 M	4, 77 M	5, 71 M	6, 32 D
TEXTURE:							
Sand	—	—	—	—	—	—	5
Silt	20	35	35	65	25	25	70
Clay	80	65	65	35	75	75	25
COMPOSITION:							
Quartz	Tr	—	Tr	—	—	—	—
Feldspar	5	—	5	3	—	—	4
Rock fragments	—	—	5	5	—	—	5
Clay	70	50	55	55	40	38	15
Volcanic glass	Tr	5	—	—	—	—	—
Calcite/dolomite	Tr	Tr	Tr	Tr	Tr	—	Tr
Accessory minerals							
Pyrite	5	5	3	2	5	2	10
Unidentified	10	5	2	2	5	5	Tr
Glauconite	–	–	Tr	–	–	–	–
Pyroxene	–	–	–	–	–	5	–
Nannofossils	Tr	Tr	—	Tr	—	—	—
Diatoms	10	30	30	30	50	50	65
Radiolarians	—	—	Tr	1	—	—	—
Sponge spicules	—	5	Tr	2	—	—	1
Silicoflagellates	—	—	Tr	Tr	—	—	—
Fish remains	—	—	Tr	Tr	—	—	—

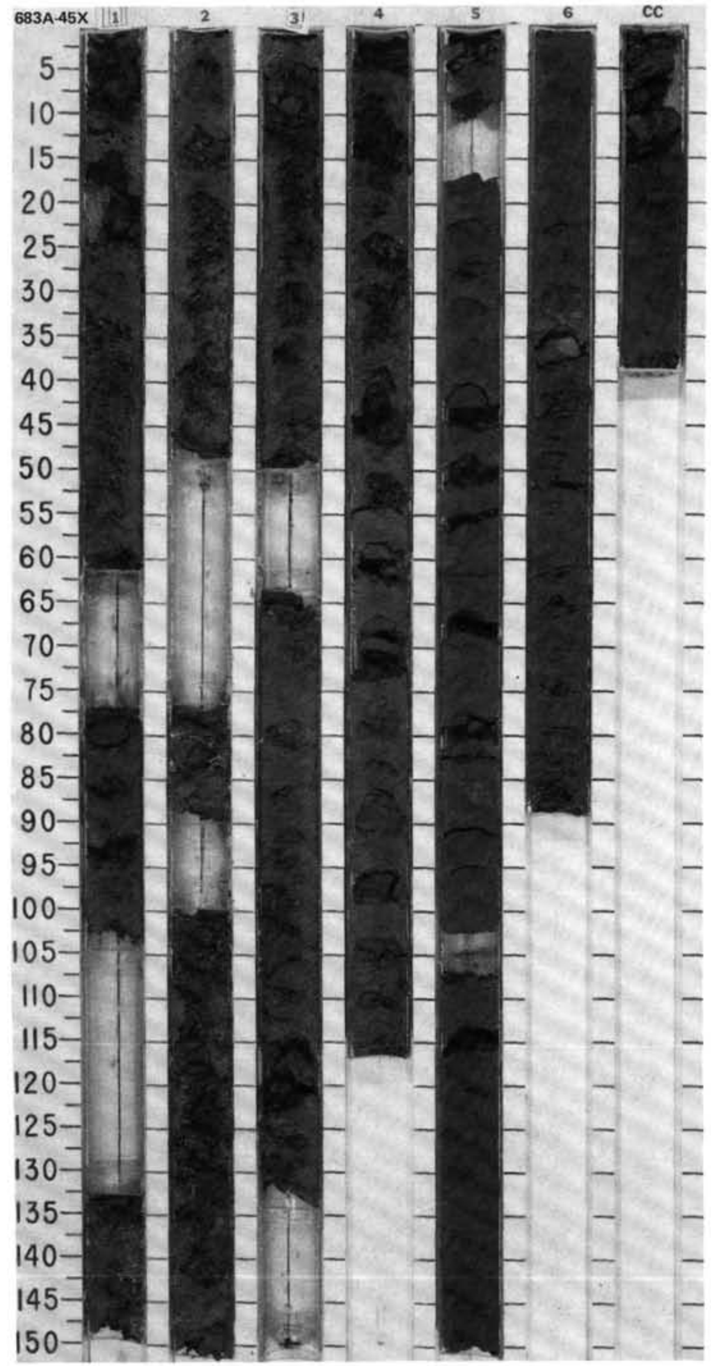

SITE 683 HOLE B CORE 1X CORED INTERVAL 3474.0-3483.5 mbsl; 402.5-412 mbsf

TIME-ROCK UNIT: MIDDLE MIOCENE

BIOSTRAT. ZONE/FOSSIL CHARACTER: NANNOFOSSILS: * NN5; DIATOMS: undifferentiated *

SECTION: 1, CC

LITHOLOGIC DESCRIPTION

DIATOMACEOUS MUDSTONE and DIATOMACEOUS OOZE

Major lithology: diatomaceous mudstone and diatomaceous ooze, locally nannofossil-bearing, with rare foraminifers, gray to dark gray (5Y 4/1, 5Y 3/1). Faintly laminated, extensively fractured by drilling. Section 1, 0 cm, to CC.

SMEAR SLIDE SUMMARY (%):

	1, 13 M	1, 93 D	1, CC D
TEXTURE:			
Silt	100	20	50
Clay	—	80	50
COMPOSITION:			
Quartz	—	2	—
Feldspar	—	3	—
Rock fragments	—	3	—
Mica	—	Tr	—
Clay	Tr	50	50
Volcanic glass	Tr	2	—
Dolomite	Tr	3	—
Accessory minerals	—	Tr	—
Pyrite	2	1	Tr
Micrite	—	—	Tr
Nannofossils	—	11	Tr
Diatoms	98	25	25
Sponge spicules	—	Tr	25
Silicoflagellates	Tr	—	—

SITE 683 HOLE B CORE 2X CORED INTERVAL 3483.5-3493.0 mbsl; 412.0-421.5 mbsf

TIME-ROCK UNIT: MIDDLE MIOCENE

BIOSTRAT. ZONE/FOSSIL CHARACTER: FORAMINIFERS: * B, * B; RADIOLARIANS: * D. pettersoni Zone; DIATOMS: * Denticula nicobarica Zone

PHYS. PROPERTIES: • γ=1.73 φ=59.1

CHEMISTRY: OC: 3.03 IC: 0.02

SECTION: 1, 2, 3, CC

VOID

VOID

VOID

LITHOLOGIC DESCRIPTION

DIATOMACEOUS MUDSTONE AND DIATOMACEOUS OOZE

Major lithology: diatomaceous mudstone and diatomaceous ooze, olive gray to dark olive gray (5Y 3.5/2). Locally pyritiferous. Fissile, with rare soft sediment deformation and minor bioturbation. Section 1, 0 cm, to CC.

Minor lithology: muddy diatom ooze, greenish gray (5Y 5/1). Small patches <0.5-cm diameter, in Section 3, 10–30 cm.

SMEAR SLIDE SUMMARY (%):

	1, 90 D	2, 82 M	3, 19 M	3, 25 D
TEXTURE:				
Sand	3	3	—	5
Silt	37	42	40	45
Clay	60	55	60	50
COMPOSITION:				
Quartz	—	—	Tr	—
Feldspar	5	5	Tr	5
Rock fragments	Tr	—	—	5
Clay	55	35	40	40
Volcanic glass	—	5	5	—
Dolomite	Tr	Tr	Tr	2
Accessory minerals	2	5	—	2
Pyrite	2	15	Tr	5
Phosphate peloids	Tr	—	—	—
Diatoms	35	35	55	40
Radiolarians	1	—	Tr	1
Sponge spicules	Tr	—	—	Tr
Fish remains	—	—	—	Tr

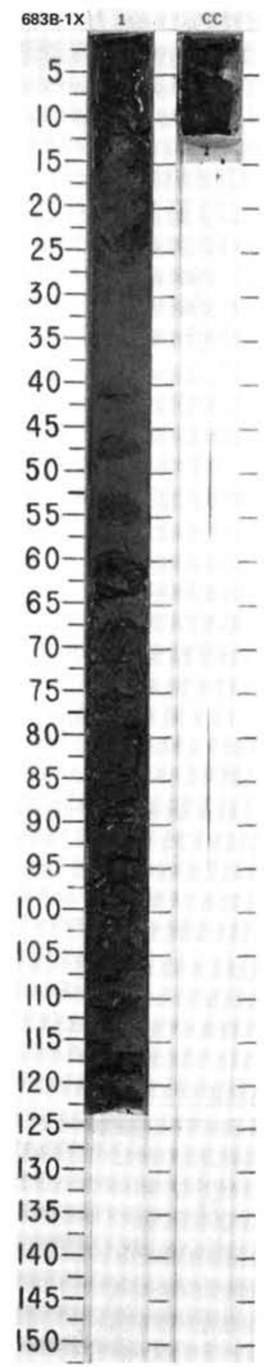

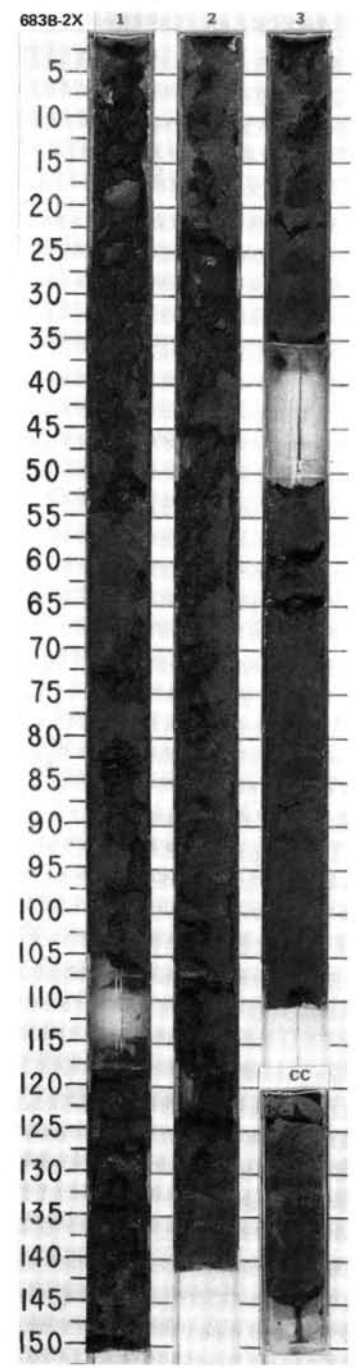

SITE 683 HOLE B CORE 3X CORED INTERVAL 3493.0-3502.5 mbsl; 421.5-431.0 mbsf

TIME-ROCK UNIT: MIDDLE MIOCENE

BIOSTRAT. ZONE/FOSSIL CHARACTER: NANNOFOSSILS: *NN6 *NN6; RADIOLARIANS: *D. pettersoni Zone; DIATOMS: *undifferentiated

CHEMISTRY: OC: 2.43 IC: 0.06

SECTION: 1, 2, CC; METERS: 0.5, 1.0

VOID

LITHOLOGIC DESCRIPTION

DIATOMACEOUS MUDSTONE and MUDDY DIATOM OOZE

Major lithology: diatomaceous mudstone and muddy diatom ooze, olive gray (5Y 4/2). Highly disrupted by drilling. Mottled, with contorted laminae due to soft sediment deformation. Section 1, 0 cm, to CC.

Minor lithology: micritic limestone, olive gray (5Y 5/2). Hard fragment, Section 1, 9–12 cm.

SMEAR SLIDE SUMMARY (%):

	1, 10 M	2, 115 D	2, 123 M
TEXTURE:			
Sand	—	5	—
Silt	100	45	40
Clay	—	50	60
COMPOSITION:			
Quartz	—	Tr	5
Feldspar	—	5	—
Rock fragments	—	Tr	—
Clay	—	40	30
Calcite/dolomite	100	2	5
Accessory minerals	—	Tr	5
Pyrite	—	3	Tr
Zircon	—	—	Tr
Foraminifers	—	—	Tr
Nannofossils	—	5	5
Diatoms	Tr	45	50
Radiolarians	—	Tr	Tr
Silicoflagellates	—	Tr	—

SITE 683 HOLE B CORE 4X CORED INTERVAL 3502.5-3512.0 mbsl; 431.0-440.5 mbsf

TIME-ROCK UNIT: MIDDLE MIOCENE

BIOSTRAT. ZONE/FOSSIL CHARACTER: NANNOFOSSILS: NN5 * *NN6; DIATOMS: C. lewisianus Zone *

SECTION: 1, CC; METERS: 0.5

LITHOLOGIC DESCRIPTION

DIATOMACEOUS MUDSTONE

Major lithology: diatomaceous mudstone, olive gray (5Y 4/2). Highly disturbed by drilling. Section 1, 0 cm, to CC.

Minor lithology: dolomicrite, olive (5Y 5/3), Section 1, 0–6 cm.

SMEAR SLIDE SUMMARY (%):

	1, 7 M	CC, 13 D	CC, 9.5 M
TEXTURE:			
Sand	—	5	2
Silt	100	55	53
Clay	—	40	45
COMPOSITION:			
Quartz	—	Tr	Tr
Feldspar	—	5	5
Rock fragments	—	Tr	Tr
Clay	—	30	35
Dolomite rhombs.	90	—	—
Accessory minerals			
Auth. carbonate	—	Tr	10
Pyrite	—	1	—
Unidentified	—	—	Tr
Nannofossils	—	2	10
Diatoms	10	60	40
Radiolarians	—	2	—
Silicoflagellates	—	Tr	—
Fish remains	—	Tr	—

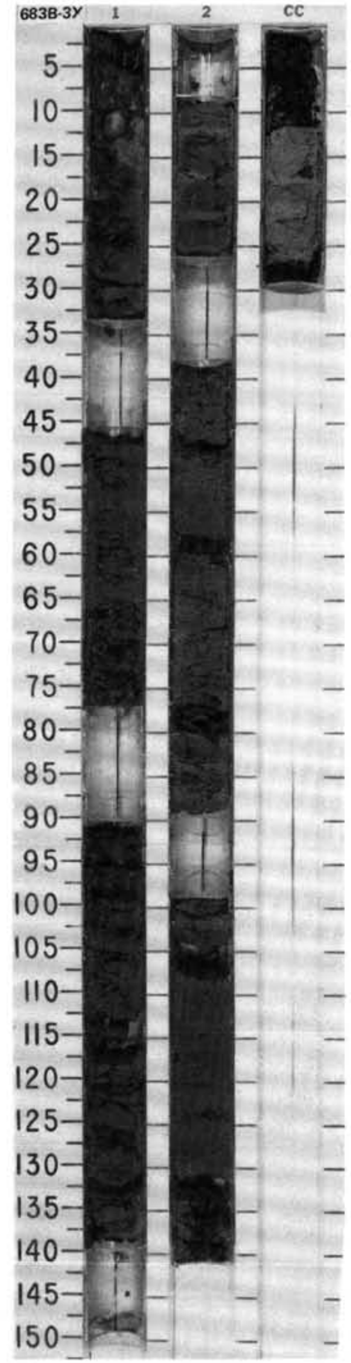

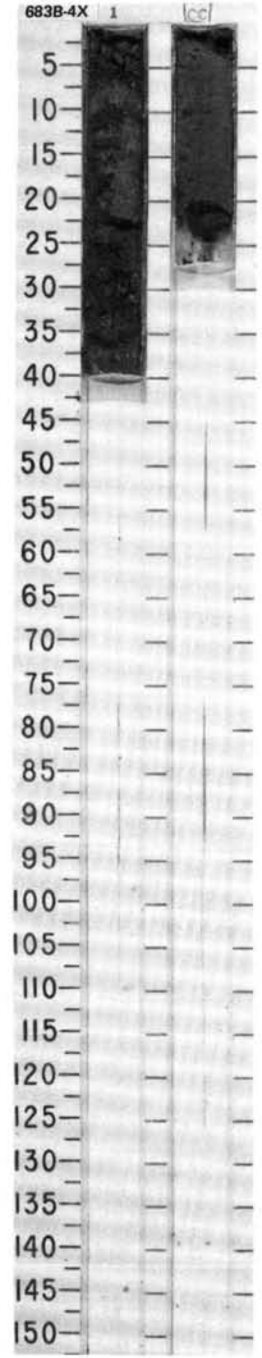

SITE 683 HOLE B CORE 5X CORED INTERVAL 3512.0-3521.5 mbsl; 4405.5-450.0 mbsf

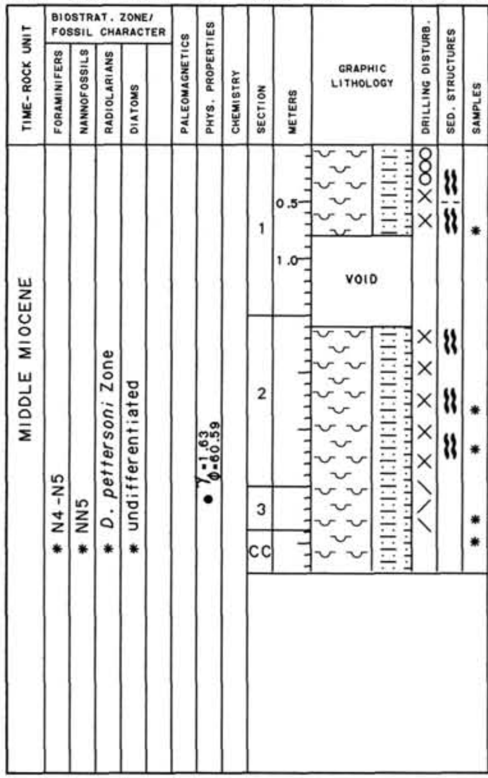

LITHOLOGIC DESCRIPTION

MUDDY DIATOMACEOUS OOZE and DIATOMACEOUS MUD TO MUDSTONE

Major lithology: muddy diatomaceous ooze and diatomaceous mud to mudstone, dark olive gray (5Y 3/2). Faintly bedded to laminated; moderate bioturbation. Section 1, 0 cm, to CC.

Minor lithology: nannofossil-bearing diatomaceous mud, greenish gray (5Y 5/1), Section 3, 29 cm.

SMEAR SLIDE SUMMARY (%):

	1, 74 D	2, 85 D	2, 115 M	3, 29 M	CC, 15 D
TEXTURE:					
Sand	5	—	—	5	—
Silt	60	80	55	45	50
Clay	35	20	45	50	50
COMPOSITION:					
Quartz	—	—	Tr	Tr	Tr
Feldspar	—	Tr	5	5	Tr
Rock fragments	Tr	—	Tr	Tr	Tr
Clay	35	20	40	40	45
Volcanic glass	5	5	—	—	—
Calcite/dolomite	—	—	—	3	3
Accessory minerals					
Pyrite	5	5	2	2	2
Foraminifers	Tr	—	—	Tr	—
Nannofossils	3	Tr	—	15	5
Diatoms	50	70	53	35	45
Radiolarians	—	—	—	—	Tr
Sponge spicules	2	Tr	—	Tr	Tr

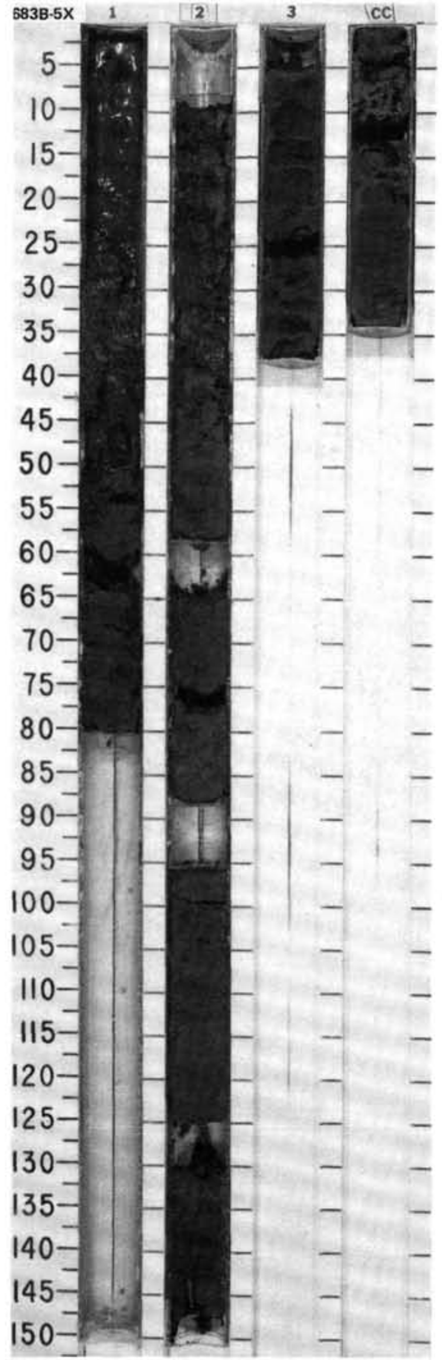

SITE 683 HOLE B CORE 6X CORED INTERVAL 3521.5-3531.0 mbsl; 450.0-459.5 mbsf

TIME-ROCK UNIT	BIOSTRAT. ZONE/FOSSIL CHARACTER: FORAMINIFERS	NANNOFOSSILS	RADIOLARIANS	DIATOMS	PALEOMAGNETICS	PHYS. PROPERTIES	CHEMISTRY	SECTION	METERS	GRAPHIC LITHOLOGY	DRILLING DISTURB.	SED. STRUCTURES	SAMPLES
MIDDLE MIOCENE		* insignificant	* D. pettersoni Zone	* Coscinodiscus gigas var. diorama? Zone		γ=1.81 φ=63.41	OC: 2.06 IC: 0.03	1, 2, 3, CC	0.5, 1.0	VOID, VOID, VOID			IW KVE

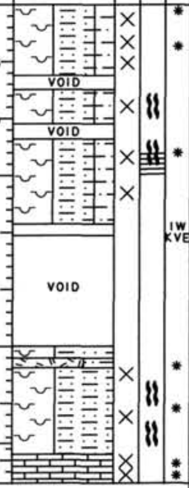

LITHOLOGIC DESCRIPTION

MUDDY DIATOMACEOUS OOZE AND DIATOMACEOUS MUD TO MUDSTONE and MICRITIC LIMESTONE BRECCIA

Major lithology: Section 1, 0 cm, to CC, 12 cm: diatomaceous sandy mudstone and muddy diatomaceous ooze, dark olive gray (5Y 3/2); locally bioturbated and laminated. CC, 12–45 cm: micritic limestone breccia, greenish gray (5GY 6/1), with white calcite veins; well-lithified sedimentary breccia.

Minor lithologies:
1. dolomitic micritic limestone, black with light olive brown layers (5Y 2.5/2, 2.5Y 5/4)), Section 3, 10–30 cm. Hard fragment, Section 1, 0–3 cm.
2. volcanic ash, gray (5Y 6/1), Section 3, 10–30 cm. Layer dispersed by drilling disturbance.

SMEAR SLIDE SUMMARY (%):

	1, 2 M	1, 36 D	1, 136 M	3, 15 M	3, 62 D	CC, 41 M	CC, 45 M
TEXTURE:							
Sand	—	20	—	50	2	10	—
Silt	50	30	40	45	53	20	50
Clay	50	50	60	5	45	70	50
COMPOSITION:							
Quartz	—	5	Tr	8	Tr	—	—
Feldspar	Tr	10	Tr	10	5	—	—
Rock fragments	—	5	—	—	Tr	—	—
Clay	—	40	40	—	45	—	—
Volcanic glass	—	—	Tr	70	—	—	—
Calcite/dolomite	100	2	—	—	Tr	100	100
Accessory minerals							
Pyrite	—	3	Tr	10	5	—	—
Unidentified	—	5	—	2	Tr	—	—
Glauconite	—	—	—	—	Tr	—	Tr
Foraminifers	—	Tr	—	—		—	—
Nannofossils	Tr	—	—	—	Tr	—	Tr
Diatoms	—	30	60	—	45	—	—
Sponge spicules	—	—	—	—	Tr	—	—

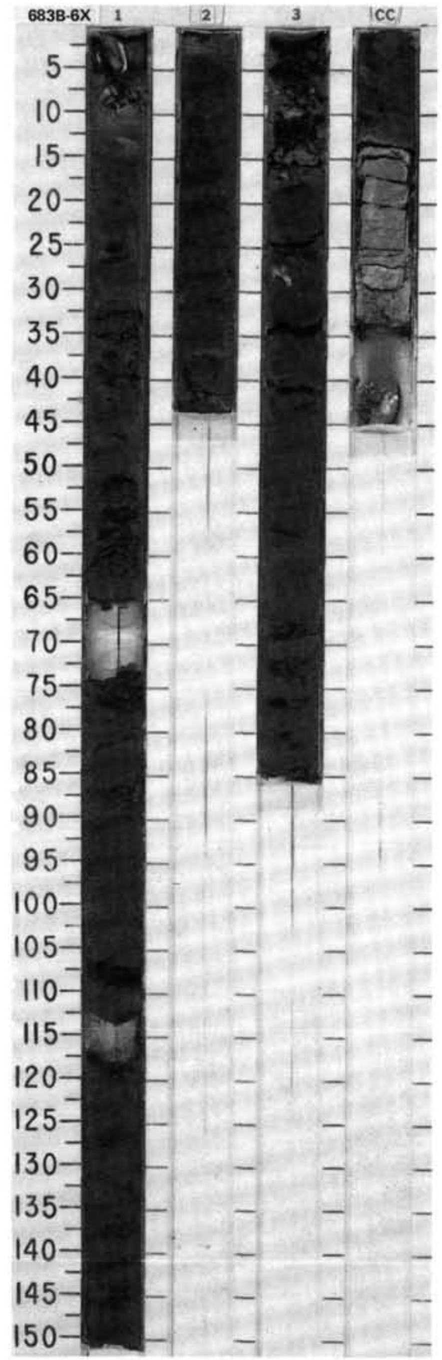

SITE 683 HOLE B CORE 7X CORED INTERVAL 3531.0-3540.5 mbsl; 459.5-469.0 mbsf

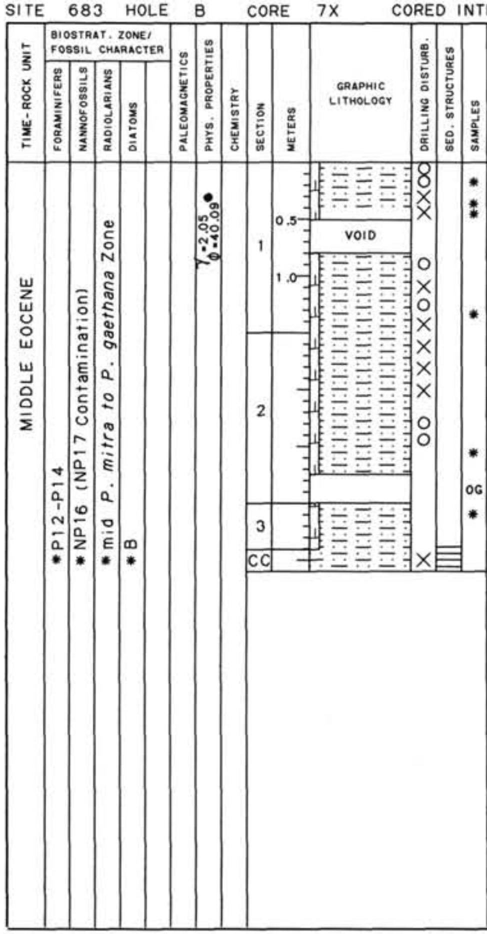

LITHOLOGIC DESCRIPTION

MUDSTONE FRAGMENTS in a drill slurry of FELDSPATHIC LITHIC SILT

Major lithology: mudstone fragments in a drill slurry of feldspathic lithic silt, black to dark olive gray (5Y 2.5/2, 5Y 3/2). Highly disrupted by drilling, but locally 2-mm-thick laminae are preserved. Section 1, 0 cm, to CC.

Minor lithology: dolomitic micrite, pinkish gray (5Y 6/2), interbeds. Section 1, 45–47 and 80–82 cm.

SMEAR SLIDE SUMMARY (%):

	1, 19 M	1, 35 D	1, 45 M	1, 139 M	2, 106 M	3, 14 D
TEXTURE:						
Sand	—	20	—	5	15	20
Silt	5	60	20	10	10	15
Clay	95	20	80	85	75	65
COMPOSITION:						
Quartz	Tr	10	—	Tr	5	5
Feldspar	Tr	40	—	5	10	10
Rock fragments	5	30	—	Tr	5	5
Mica	—	Tr	—	—	—	—
Clay	95	10	—	90	75	65
Volcanic glass	—	Tr	—	—	—	—
Calcite/dolomite	—	—	85	—	—	2
Accessory minerals						
Pyrite	Tr	5	—	3	3	8
Glauconite	—	Tr	—	—	—	—
Unidentified	—	—	—	2	2	3
Nannofossils	—	5	15	—	Tr	5

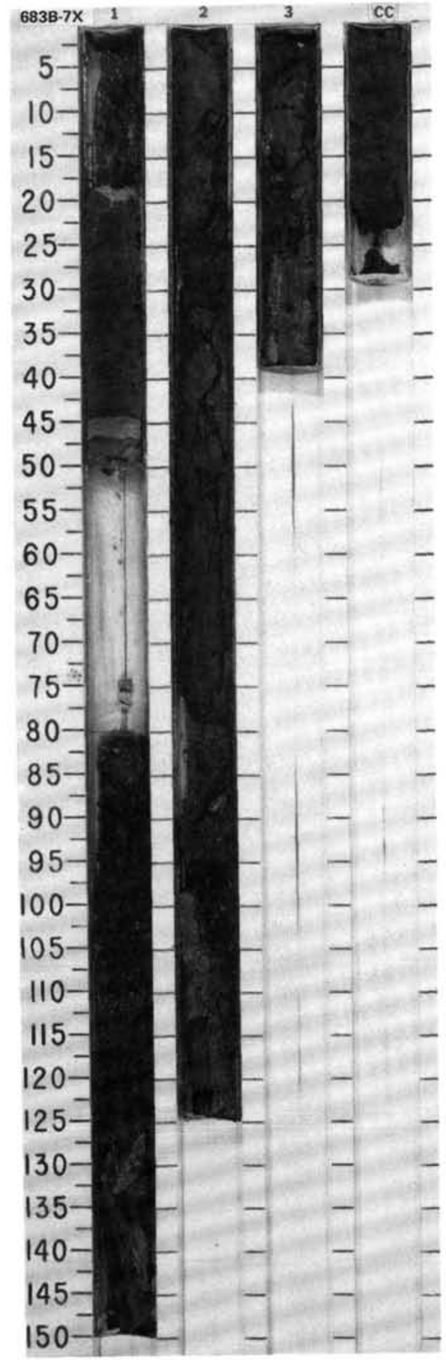

SITE 683 HOLE B CORE 8X CORED INTERVAL 3540.5-3550.0 mbsl; 469.0-478.5 mbsf

TIME-ROCK UNIT	FORAMINIFERS	NANNOFOSSILS	RADIOLARIANS	DIATOMS	PALEOMAGNETICS	PHYS. PROPERTIES	CHEMISTRY	SECTION	METERS	GRAPHIC LITHOLOGY	DRILLING DISTURB.	SED. STRUCTURES	SAMPLES
MIDDLE EOCENE	P4 - P6 *	NP16 / NP16 NP17 (Contamination)*	P. chalara Zone to P. mitra Zone *	downhole contamination *				1 / CC					* * ****

BIOSTRAT. ZONE/ FOSSIL CHARACTER

LITHOLOGIC DESCRIPTION

Drilling breccia containing MUDSTONE, SILTY MUDSTONE, AND SAND; sedimentary breccia of MUDSTONE, and DIATOMACEOUS MUDSTONE AND BRECCIATED MICRITIC LIMESTONE

Major lithology: Section 1, 0–55 cm: mudstone, silty mudstone, and sand, dark gray (5Y 4/1). Sparse bioturbation. CC, 0–33 cm: sedimentary breccia of mudstone, black to greenish gray (5Y 2.5/2, 5GY 5/1). Bedded, with some faulting perpendicular to bedding, fluid escape structures. CC, 33–50 cm: diatomaceous mudstone, dark olive gray to black (5Y 3/2, 5Y 2.5/2), and brecciated micritic limestone, burrowed.

SMEAR SLIDE SUMMARY (%):

	1, 9 M	1, 47 M	CC, 5 M	CC, 6 M	CC, 13 D	CC, 18 M
TEXTURE:						
Sand	10	—	—	—	—	—
Silt	—	65	80	60	45	55
Clay	90	35	20	40	55	45
COMPOSITION:						
Quartz	2	5	1	Tr	—	5
Feldspar	5	25	1	Tr	—	—
Rock fragments	3	5	—	—	—	5
Mica	—	5	Tr	Tr	—	—
Clay	90	35	28	40	55	45
Volcanic glass	Tr	5	Tr	Tr	—	Tr
Calcite/dolomite	—	3	Tr	5	10	1
Accessory minerals	Tr	—	3	5	5	—
Pyrite	—	1	2	—	—	3
Rutile	—	—	Tr	—	—	1
Nannofossils	—	1	Tr	—	—	—
Diatoms	—	15	65	50	30	40
Radiolarians	—	—	—	—	Tr	Tr
Sponge spicules	—	Tr	—	Tr	Tr	—
Silicoflagellates	—	—	Tr	—	—	Tr
Fish remains	—	—	—	—	—	Tr

SITE 683 HOLE B CORE 9X CORED INTERVAL 3550.0-3559.5 mbsl; 478.5-488.0 mbsf

TIME-ROCK UNIT	FORAMINIFERS	NANNOFOSSILS	RADIOLARIANS	DIATOMS	PALEOMAGNETICS	PHYS. PROPERTIES	CHEMISTRY	SECTION	METERS	GRAPHIC LITHOLOGY	DRILLING DISTURB.	SED. STRUCTURES	SAMPLES
MIDDLE EOCENE		NP16 *		B *				CC					***

BIOSTRAT. ZONE/ FOSSIL CHARACTER

LITHOLOGIC DESCRIPTION

Drilling breccia containing DIATOMACEOUS MUDDY SILT, DOLOMITE, and MUDDY VOLCANIC ASH

Major lithology: diatomaceous muddy silt, dark olive gray to dusky yellow green (5Y 3/2, 5GY 5/1); laminated, similar to laminated clasts in 112-683B-8X-CC (Mid-Miocene, NN5). Dolomite, olive (5Y 4/2), hard fragment, burrowed. Muddy volcanic ash, dark greenish gray (5GY 3/1), Eocene. CC, 0–32 cm.

SMEAR SLIDE SUMMARY (%):

	CC, 13 D	CC, 14 D	CC, 23 D
TEXTURE:			
Silt	60	60	60
Clay	40	40	40
COMPOSITION:			
Quartz	2	3	5
Feldspar	15	10	—
Rock fragments	3	2	40
Mica	Tr	—	—
Clay	38	38	—
Volcanic glass	3	3	40
Calcite/dolomite	2	—	15
Accessory minerals			
Pyrite	2	2	—
Glauconite	—	Tr	—
Micrite	—	2	—
Nannofossils	Tr	Tr	Tr
Diatoms	35	40	—
Sponge spicules	Tr	Tr	—